# Studies on Oman Meteorites

Inauguraldissertation
der Philosophisch-naturwissenschaftlichen Fakultät
der Universität Bern

vorgelegt von

**Ali Faraj Ahmed Al-Kathiri**

von Oman

Leiter der Arbeit:

PD Dr. Edwin Gnos

Dr. Beda Hofmann

Institut für Geologie, Universität Bern

# Studies on Oman Meteorites

Inauguraldissertation
der Philosophisch-naturwissenschaftlichen Fakultät
der Universität Bern

vorgelegt von

**Ali Faraj Ahmed Al-Kathiri**

von Oman

Leiter der Arbeit:

PD Dr. Edwin Gnos

Dr. Beda Hofmann

Institut für Geologie, Universität Bern

Von der Philosophisch-naturwissenschaftlichen Fakultät angenommen

Der Dekan

Bern, 9. Februar 2006 Prof. Dr. P. Messerli

## Acknowledgments

I thank to the Swiss National Foundation for funding this project (grants 2100-064929 and 200020-107681) and the Ministry of Commerce and Industry of the Sultanate of Oman for assistance and permitting fieldwork in Oman.

Special thanks to the following:

All my family members and relatives for their patience and the love they gave me through the period of my study.

His Highness Maqbool Bin Ali Sultan, Minister of Commerce and Industry, for his support and granting me a study leave to conduct my PhD thesis at the University of Bern.

Drs. Beda Hofmann and Edwin Gnos for their direct supervision and their unlimited scientific and technical assistance. They are also thanked for their transfer of knowledge and experience through the period of my PhD study and during the meteorite search campaigns.

Prof. Martin Engi for his scientific guiding and supervision. His is thanked for his care, hospitality and creating very friendly working atmosphere.

Akram Al-Muraza, Khalid Al-Rawas, and Sami Al-Zubaidi and all my colleagues from the Ministry of Commerce and Industry, Salalah, for their logistic and administrative support during the project.

Dr. Hilal Al-Azri, Directorate general of Minerals, Ministry of Commerce and Industry, Muscat, for his support in initiating the project, and permission to search for meteorite in Oman.

Prof. Tjerk Peters for presenting the research proposal to the Ministry of Commerce and Industry to initiate a joint Omani-Swiss meteorite search project and his recommendation to include me as member of the search team.

Dr. Timothy Jull, NSF lab, University of Arizona, for providing the $^{14}C$ terrestrial ages of a large number of meteorites recovered during the joint Omani-Swiss meteorite search project including those used for the study of weathering of meteorites from Oman.

Prof. Otto Eugster for his noble gas isotope measurements and his field support during one meteorite search campaign in Oman.

Prof. Urs Krähenbühl for his chemical analyses on the iron meteorite Shisr 043 and the lunar meteorite SaU 169, and his field support during one meteorite search campaign in Oman.

Dr. Kees Welten for his determination of the cosmic ray exposure age for the Shisr 043 iron meteorite.

Manuel Eggimann and Dr. Sylvio Lorenzetti for their assistance and joining us during various periods of meteorite search in Oman.

Profs. Rainer Wieler and Ingo Leya, Dr. Salim Al-Busaidi, Ali Al-Rajihi, Mohamed Al-Batashi, Dr. Niklaus Waber, Mohamed Ishaq, Jürg Bühler, Lorenz Moser and Mark Hauser for joining us during some meteorite searching periods.

Ulli Linden and Werner Zaugg for passing on their computing experience and helping whenever it is needed.

Vreni Jakob and Jürg Megert for preparing petrographic thin sections of the meteorites recovered during our search program, and Ruth Mäder for analysis of water content in meteorites.

Peter Vollenweider for making additional photographs of meteorites used in this study.

Isabelle Jobin, Sarah Antenen, Barbara Grose and Brigitte Schneiter for always having been very helpful with any administrative work or question during my stay in Bern.

Many thanks to all professors, assistants, post doctors, colleges and employees at the Institute of Geological Science and the Museum of Natural History at Bern for their hospitality and kind help.

# Abstract

A large number of meteorites have been recovered during the joint Omani-Swiss meteorite search project (2001-2005). This made meteorites from Oman available to scientists around the world as well as to Omani researchers and students to perform scientific research on different aspects of the science of meteoritics.

This PhD thesis consists of five independent sections prepared for publication in peer-reviewed journals, in which I am the first author in the first three papers and a co-author in the last two papers.

During this PhD thesis most of the work was directed to study the terrestrial weathering of meteorites, starting in the field by measuring fragmentation, dispersion of fragments on the soil and taking soil samples to compare the effect of soil chemistry on the meteorites. At the University of Bern sample preparations were done on a large number of meteorites and soil samples for chemical analysis and petrographic investigations. In addition, studies were also performed on rare and unique meteorites such as the KREEP-rich lunar meteorite SaU 169, the only iron meteorite so far found in Oman (Shisr 043) and the Martian meteorite SaU 094.

Results from the weathering study showed that the chemical composition of the desert soil in the interior of Oman is very homogeneous and the influence of soil geochemistry on meteorite weathering can therefore be assumed to be nearly constant over the whole study area. The investigation of weathering-related parameters (fragmentation, dispersion of fragments on the soil, alteration mineralogy, color of powdered meteorites, bulk chemistry) as a function of $^{14}C$ terrestrial ages showed an accumulation of Sr, Ba and $H_2O$, and a loss of S with increasing terrestrial age. Fast iron metal oxidation is correlated with rapid rates of water absorption. The slower oxidation of troilite releases sulfate, allowing the steady precipitation of Ba and Sr sulfates over time. Cementation of pores with weathering products gradually decreases the weathering rate over time, however the rate of purely physical weathering will remain constant. Meteorite powders exhibit a color change as a function of weathering grade. Fresh unweathered meteorites have a dark grey color, with increasing amounts of weathered metal and troilite, the powder commonly grades to dusky brown, grayish brown, moderate brown, and finally light brown for strongly weathered meteorites. The local surface topography (hard/soft soil, depressions and small hills) also has a marked influence on the weathering of meteorites.

The iron meteorite Shisr 043 is a single mass not paired with any of the other eight known iron meteorites from the Arabian Peninsula. Based on the mean kamacite bandwidth and the chemical composition of the meteorite it is classified as a medium octahedrite belonging to the chemical group IIIAB. Cosmic ray exposure data yielded an age of 290 ± 20 Ma, and a terrestrial age of <10,000 years.

Sayh al Uhaymir 169 is the first known KREEP-rich lunar meteorite. The study on the regolith part of the lunar meteorite showed that it contains clasts of Ti-poor to Ti-rich basalts, gabbros to granulites, and regolith breccias, and that the regolith formed in two stages. The younger regolith additionally contains a highland gabbronorite clast with anorthite $An_{96-97}$, forsteritic ($Fo_{85}$) and fayalitic ($Fo_{12}$) mineral clasts, and impact melt shards. Based on the regolith chemistry, the comparison of Fe-Ti-Th-K concentrations with remote sensing data from the lunar surface, the KREEP clast contained in the regolith, and the volcanic clast types and its $TiO_2$ content, the regolith source area can be assigned to the vicinity of the Apollo 12 and 14 landing sites. In combination with data on the impact melt part of SaU 169 the complex history of the

meteorite could be reconstructed registering impact events on the Moon at 3909 ± 13 Ma, ~2800 Ma, ~200 Ma, <340000 years, and a delivery to Earth <10000 years ago.

Sayh al Uhaymir 094 is classified as a strongly-shocked melanocratic olivine-porphyric Martian rock belonging to the shergottite group with affinities to lherzolitic shergottites. Its model composition is very similar to the Dar al Gani 476/489/670/735/876 shergottites from the Libyan Desert. The meteorite is now recognized to be paired with SaU 005/008/051/060/090/120/125/130/131/150 making it the largest known strewnfield produced by a Martian meteorite.

All meteorites found during this project were classified using optical methods and electron microprobe. These results are listed in the appendix 1.

## Contents

# Introduction

## Meteorites

Meteorites are extraterrestrial rocks fallen on Earth. Their origin is mainly the asteroid belt located between Mars and Jupiter, and a few are derived from Mars and the Earth's Moon. Meteorites pass through the Earth's atmosphere at a velocity between 10 to 30 km/s (McSween, 1999). Only a small number of meteoroids survive the atmospheric abrasion during their short transit to arrive to the Earth's surface as meteorites. Meteorites that finally arrive on the ground may have lost up to 99% of their volume (Norton, 2002). Recovered meteorites have variable masses ranging from less than one gram to approx. 60 tons (Hoba). However, only large meteorites of at least several meters diameter with a mass of 100's of tons can produce impact craters.

Meteorites are divided into three main groups: (i) iron meteorites, (ii) stony meteorites and (iii) stony-iron meteorites, which are subsequently divided to subgroups of different types (Figure 1). Within observed and recovered falls, stony meteorites are the most abundant type (Figure 2) with 86% of chondrites and 8% of achondrites (McSween, 1999). The iron meteorites constitute 5% of the observed and recovered falls whereas the stony-irons make up only about 1% (McSween, 1999).

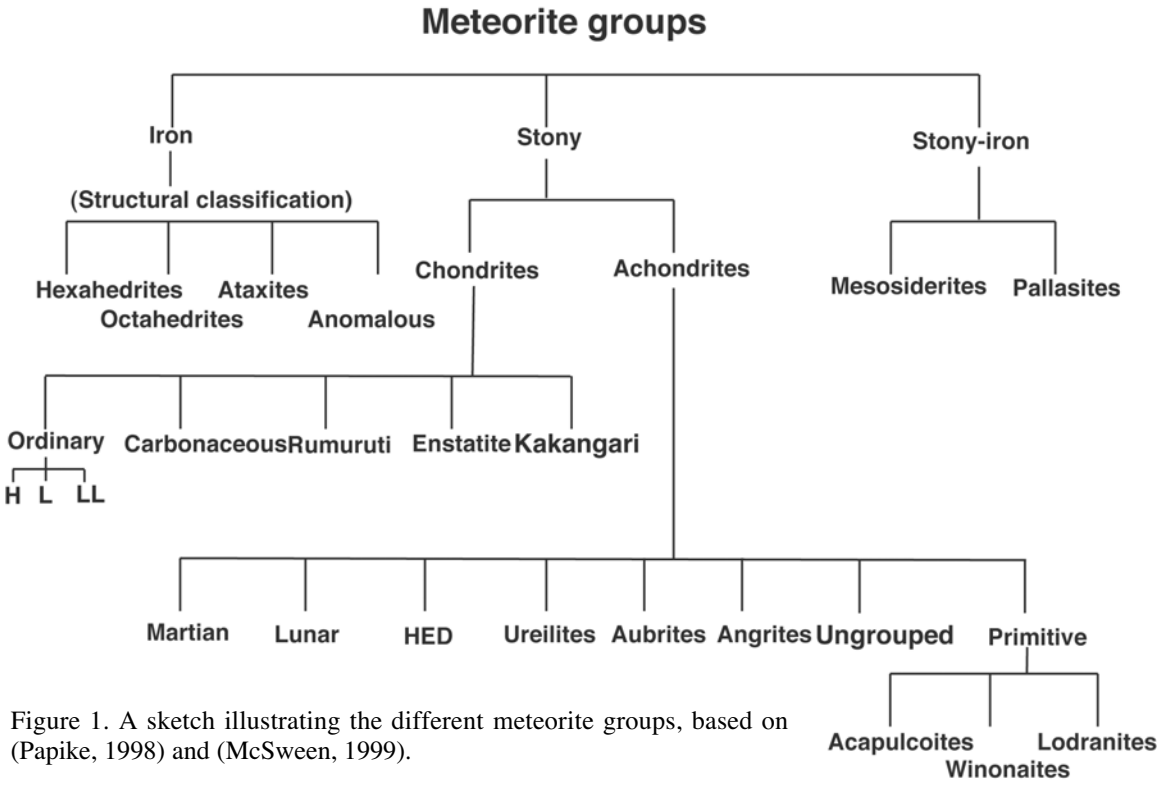


Figure 1. A sketch illustrating the different meteorite groups, based on (Papike, 1998) and (McSween, 1999).

The flux of meteorites to the earth is estimated to be between 36 and 116 falls over 10 g per $10^6$ $km^2$ $yr^{-1}$ (Bland, 2001). Applying this estimate to Oman, with an area of about 309 thousand $km^2$ (Ministry of Information, Sultanate of Oman: www.omanet.om/english/home.asp) we expect about 11 to 36 meteorite falls over 10 g per year.

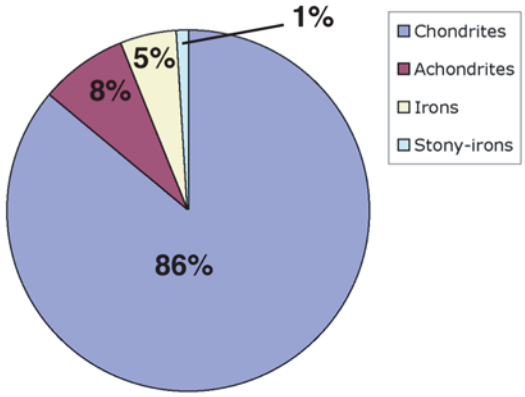


Figure 2. Distribution of observed and recovered meteorite fall (McSween 1999).

**Meteorite Searching in Oman**

Even though hot deserts have become an important source for meteorite recoveries during the last 20 years, only a few meteorites have been found in the Sultanate of Oman before 1999. Since the publication in the Meteoritical Bulletin No 84, August 2000, of 39 meteorites found in Oman in 1999 and 2000 (Grossman, 2000), a total of 1439 meteorites found 1999-2004 have been published in the Meteoritical Bulletin. To illustrate the importance of Oman as a source for meteorites it can be noted that Omani meteorites constitute 15.7% of all newly described meteorites since 2000.

Building up on the existing collaborations (since more than 30 years), between the Directorate General of Minerals, Ministry of Commerce and Industry, Muscat (DGM) and the University of Bern, the Natural History Museum Bern together with the Institute of Geological Sciences of the University of Bern took the initiative to explore possibilities to conduct a scientifically motivated meteorite search in Oman. The first joint Omani-Swiss meteorite search program was conducted in January-February 2001. Three subsequent searches were conducted during this PhD program in January-February 2002, September 2002-January 2003 and February-March 2005. These expeditions were supported by the Swiss National Science Foundation (grants 2100-064929 and 200020-107681) and the Ministry of Commerce and Industry, Sultanate of Oman. The official title of the project is “Distribution, classification and terrestrial weathering of meteorites in the Sultanate of Oman”.

For safety reasons, searching for meteorites is conducted by at least two 4WD cars especially when searching areas more than 10 km away from a main road. Geological maps (scale 1:250 000), satellite images, GPS and compass are used to locate meteorites and find areas with geological potential for meteorite accumulations. Meteorite finds are carefully documented in the field. The procedure includes assigning a field number, taking photographs (for individual meteorites), taking coordinates using GPS and counting number of fragments and their distance and direction to the largest fragment. Additionally, daily temperature and humidity are measured three times a day at early morning (just before or at sun-rise), at mid-day and at the evening (after sun-set).

**Aims of the Project**

The aims of the meteorite search project in Oman were: i) to survey all favorable areas of Oman for the potential of meteorite recovery under consideration of geological background (type of soil, age and type of surface rock, climate factors); ii) to carefully document all meteorites (location, orientation of fragmentation with reference to each other); iii) to obtain terrestrial ages of finds from different regions from Oman desert and compare them with chemical and mineralogical weathering proxies to determine the relationship between weathering of meteorites and their terrestrial ages; iv) to carry out a regional survey on the distribution of meteorites in the Oman desert; v) to provide a basis for the preservation of Omani meteorites for scientific research before they end up in the hands of professional meteorite hunters. All meteorites were described and classified according to their petrology and mineral chemistry (optical transmitted and reflected light microscopy, electron microprobe on petrographic thin sections) as a basis for publication in the Meteoritical Bulletin and in order to identify strewnfields, meteorite pairing and relationships to earlier findings.

**Importance of Meteorite Finds During this Project for Oman**

It is known among geologists that Oman contains a mountain belt that includes one of the best exposed segments of oceanic crust (Ophiolite) in the world, if not the best. The recovery of a large number of meteorites including rare species allows Oman to contribute in meteorite research, thus meteorites will bring a further attraction to many geologists, universities, and scientific organizations worldwide. The recovered meteorites will be preserved as a natural heritage of Oman. There will be a transfer of knowledge from qualified Swiss meteorite experts to Omani geologists in the frame of PhD research. In future, qualified Omani researchers will be able to perform their own meteorite research. Finally some of the recovered meteorites will be exhibited in museums in Oman to educate the public about meteorites, and some answers to the formation of the solar system and beyond the solar system that meteorites carry with them.

**Geology of the Searched Area**

The meteorites search area is confined to the central plains of the Oman desert (Figure 3), which comprises more than 50% of the area of the country (Le Métour et al., 1995). This essentially flat area lies at an altitude of between 50 and 250 m and is underlain by limestone, predominantly Miocene in age (minor Oligocene and Eocene). The horizontal bedding has remained largely undisturbed since marine deposition, with the exception of local salt tectonics. The area forms a vast peneplain partially covered by a layer of rocky debris. The Jiddat Al Harasis is the largest of these limestone plains. It crops out extensively around Hayma and has almost no drainage network. These limestone plains are partially covered by aeolian sand dunes, which are still being shaped by the desert winds. These dune fields (Figure 3) constitute the immense Rub al Khali desert and dunes accumulate locally to form ramlats (dune fields) in the north of Dhofar. A vast inland depression is located to the northeast of the central plains, the Umm as Samim sabkhah. Vast alluvial fans form a transitional belt to the Oman Mountains.

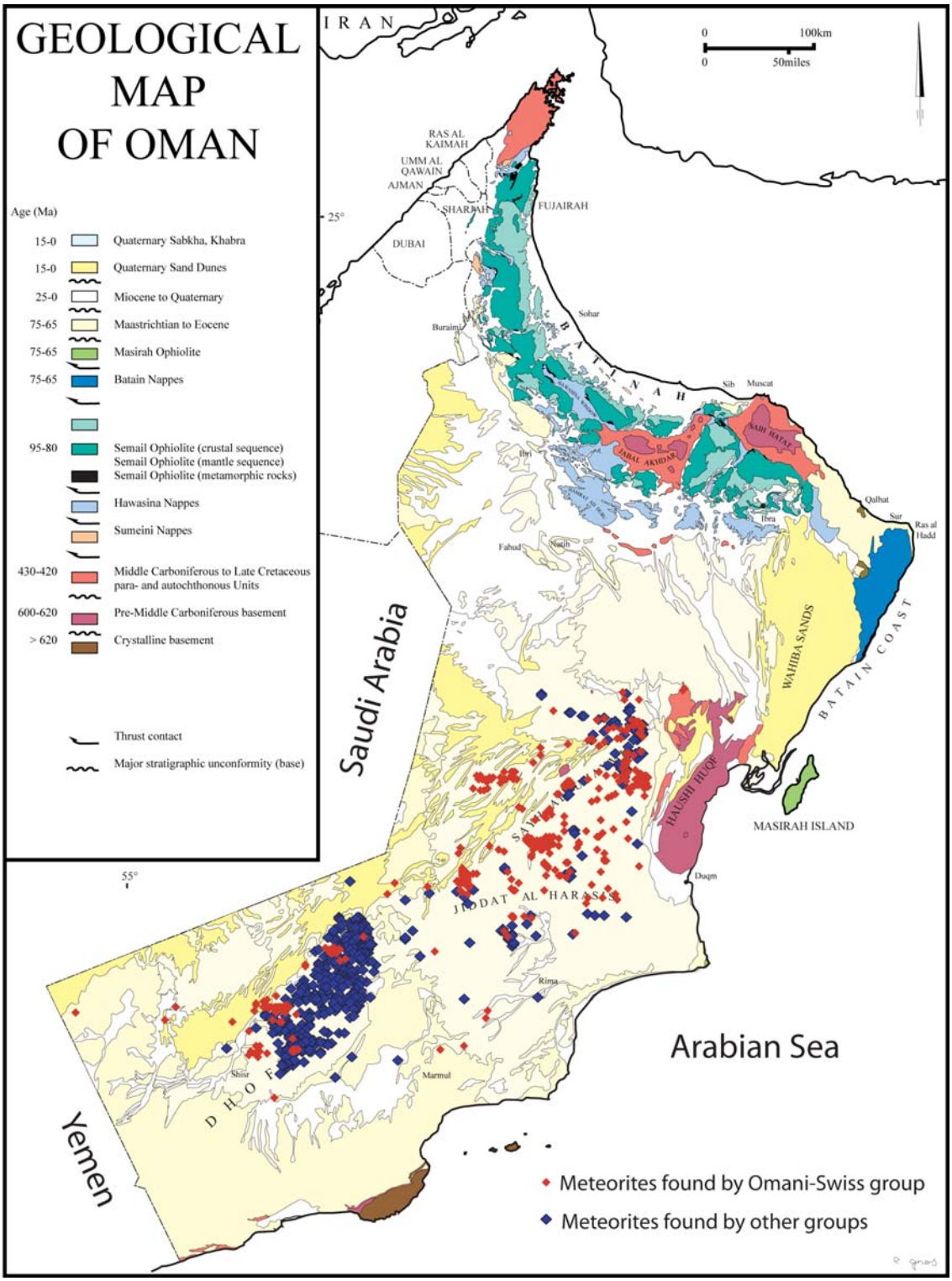


Figure 3. Meteorite finds by the Omani-Swiss searching group during this project and those found by other searching groups, plotted on a geological of Oman based on Glennie et al., (1974), Le Métour et al., (1993), Peters et al., (1995) and Peters et al., (2001).

Erosion and deposition since the end of marine deposition in the Tertiary have been limited in this area and meteorites have had a chance to accumulate over prolonged periods of time. The color/brightness contrast between the dark meteorites and the light carbonate surfaces facilitates identification of the meteorites (Figure 4). The data of this study however showed that the bulk of the meteorites preserved on surfaces fell only during the last 50,000 years. The fate of older meteorites remains unclear, as weathering of silicates in the oldest examples is still only minor.

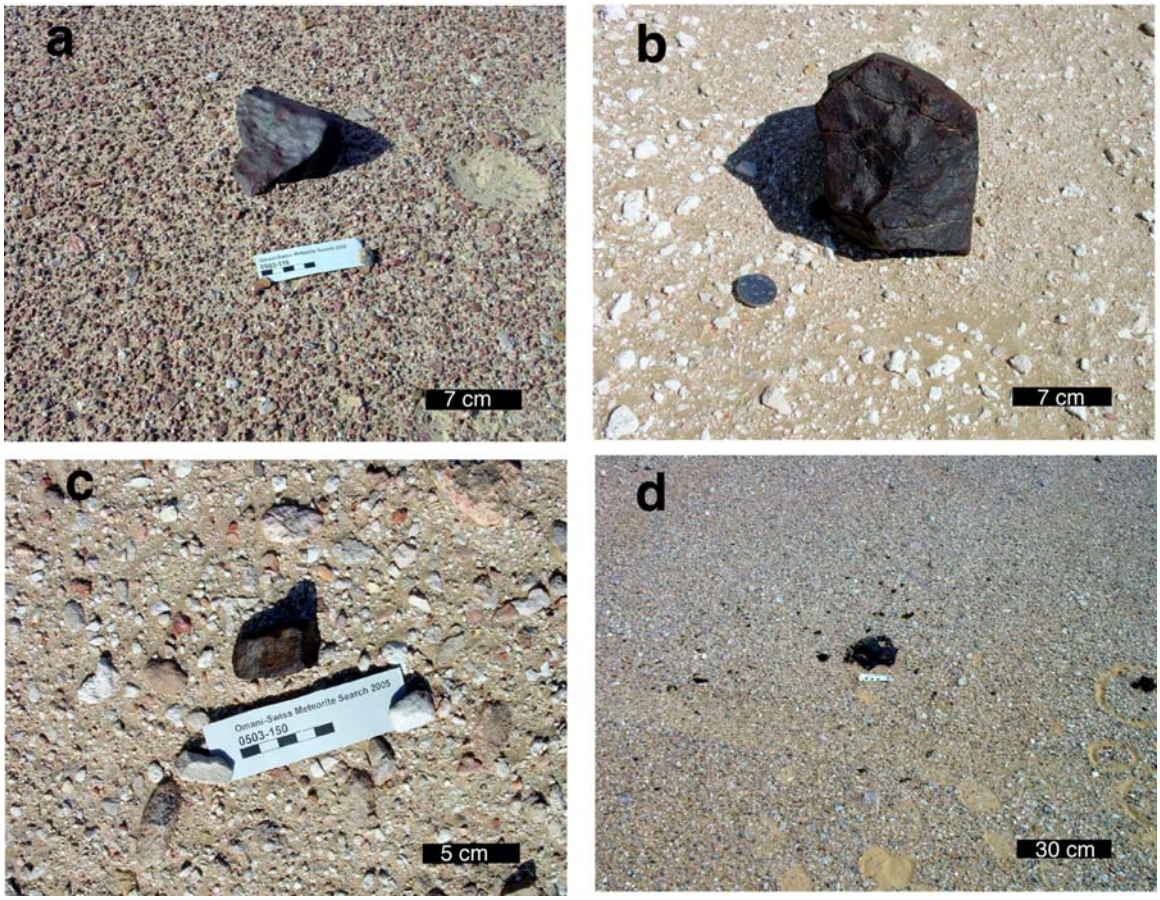


Figure 4. Images of meteorites from Oman: a) meteorite from Sayh al Uhaymir; b) meteorite from Jidat al Harasis showing strong color contrast to the light colored background; c) a small meteorite from Jiddat Al Harasis; d) meteorite from Sayh al Uhaymir with dispersed fragments.

**Meteorite Finds**

Soon after the publication of 39 meteorite finds from Oman in the Meteoritical Bulletin No 84, August 2000 (Grossman, 2000), the number of published meteorite finds increased rapidly to >1400 until 2005 (Grossman, 2000; Grossman and Zipfel, 2001; Russell et al., 2004; Russell et al., 2003; Russell et al., 2002; Russell et al., 2005).

During four periods of meteorite search between early 2001 and 2005 (see above) more than 3500 meteorite fragments representing ~200-300 fall events were found (Figure 3), totalling about 1485 kg. This includes many meteorite fragments from strewnfields (e.g. JaH 073, SaU 001, Dho 020, Dho 005 and JaH 055) reaching more than 3000 pieces from JaH 073 alone. Out of those finds we published 266 meteorites in the Meteoritical Bulletin No. 87, 2003, and No. 88, 2004, (Russell et al., 2004; Russell et al., 2003) (Appendix 1). The recovered meteorites were partly transported to the Natural History Museum Bern for Curation and Research, in case of obvious pairings were deposited at the Department of Minerals in Salalah, Oman.

From the recovered meteorites, chemical analyses were obtained by a combination of INAA, ICP-MS and ICP-OES on 47 samples from ordinary chondrites representing 39 individual falls (Appendix 2). Also a CV3 carbonaceous chondrite was analyzed. Terrestrial ages ($^{14}C$) were determined on samples from 56 ordinary chondrite pieces, a CV3 carbonaceous chondrite, a lunar meteorite (SaU 169) and a Martian meteorite (SaU 094). Out of the dated samples, five were from the JaH 073 strewnfield, and three from the Dho 005 strewnfield. Studied ordinary chondrites were selected from different areas from Oman interior desert representing as large a spread of weathering as possible. Even more detailed studies were made on the lunar meteorite (SaU 169), the Martian meteorite (SaU 094) and the iron meteorite (Shisr 043).

Below are the most interesting meteorites within the long list of recoveries:

1- Unique KREEP-rich lunar (Moon) meteorite (SaU 169); see sections 3 and 4
2- Martian meteorite SaU 094 (shergottite); see section 5
3- Several carbonaceous chondrites; (two CV3's, one CR, one CO)
4- A small strewnfield of a Rumuruti chondrite
5- A strewnfield of a mesosiderite
6- About 8 LL chondrites
7- An iron meteorite (Shisr 043); see section 2
8- A L-chondritic impact-melt breccia (JaU 089)
9- An ureilite (achondrite)
10- Two enstatite chondrites, types EL4 (SaU 188) and EH4
11- About 6 chondrites of low-metamorphic grade (<4)
12- High-grade metamorphic L chondrite (probably 7)
13- Strewnfield of ordinary chondrite (JaH 073) where more than 3000 pieces were collected weighing more than 550 kg (under investigation)

**Soil Samples**

For the weathering study, in addition to the meteorites, two types of soil samples were collected: 1) 97 samples of soil under meteorites, and 2) 48 reference soil samples. Samples of soils under meteorite were collected from beneath meteorites that were sufficiently large (>200g) and firmly embedded in the soil to test if there is an input of meteoritic components to the underlaying soil as a result of weathering of meteorites. Reference soil samples are typically taken from the top 5 cm of the soil at a distance of about 10 m from meteorite finds (including 2 calcrete samples from 20 cm depth). Reference soil samples were collected from all major collection areas to represent all the different lithological formations and types of soil. In strewnfields comprising several to hundreds of meteorite fragments, only a few representative

soil samples were collected. Both soil types were sieved to obtain the <0.15 mm fraction, then representative samples from different areas were selected for bulk chemical analysis using a combination of INAA, ICP-MS and ICP-OES (Appendices 3 and 4). Also, all sieved 145 soils samples were analyzed without further treatment by ICP-OES following aqua regia extraction (Appendices 5 and 6).

# PhD Thesis Content

**Section 1**

In the first paper, we investigate weathering-induced mineralogical and chemical changes of meteorites recovered from various areas in the central Oman desert, compare weathering-related parameters (fragmentation, dispersion of fragments on the soil, alteration mineralogy, color of powdered meteorites, bulk chemistry) with $^{14}C$ terrestrial ages, and put these findings into the context of the geological and climatic history. We show that intensity of weathering in meteorites generally increases with their terrestrial age. The major geochemical influences of weathering are an accumulation of Sr, Ba and $H_2O$, and a loss of S. Fragmentation of meteorites is believed to be a result of the combined effects of volume increase, diurnal thermal cycling and infiltration of soil material into cracks due to wind and water. Soils from the interior Oman desert are very homogeneous in bulk chemistry, their influence on meteorite weathering can therefore be assumed to be nearly constant over the whole study area. Soils under meteorites are contaminated with Ni and Co mobilized from the meteorite to the under-laying soil as result of terrestrial weathering of meteorites. Ni/Co ratios in soil under meteorite are generally higher than chondritic values, indicating a higher mobility of Ni than of Co.

**Section 2**

The second paper is about the first iron meteorite recovered from Oman (Shisr 043). It is the only iron meteorite among >1400 finds reported from Oman until 2005, even though iron meteorite constitute about 5% of observed falls. This statistical anomaly may be due to collecting by ancients, as iron meteorites are easily recognized, or to preferential sinking of heavy irons into the soil.

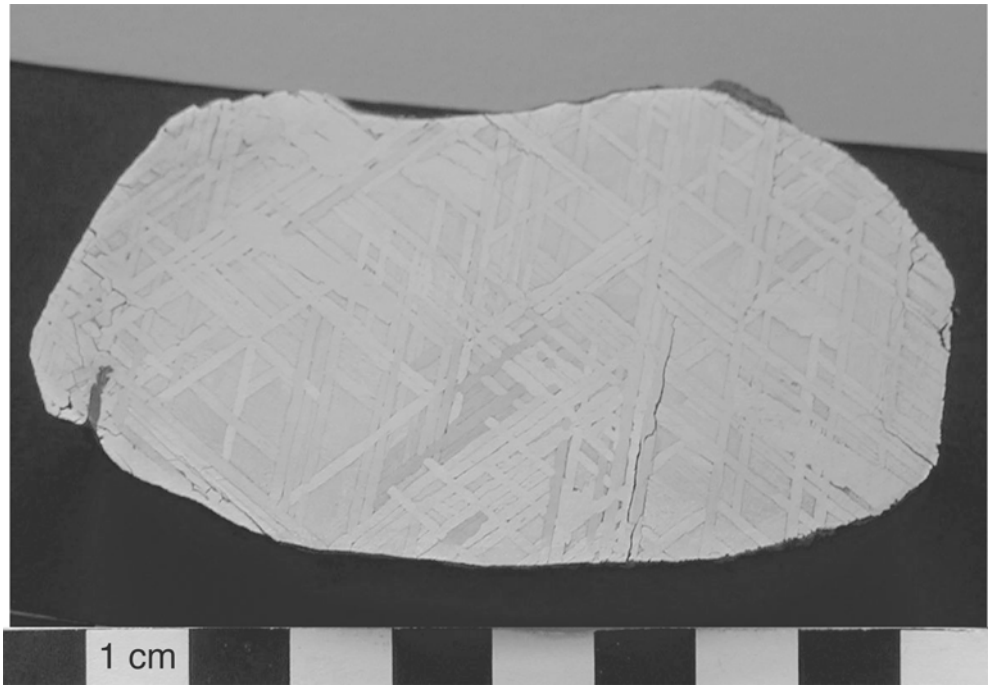


Figure 5. Image of an etched end-piece of the Shisr 043 iron meteorite (medium octahedrite) displaying typical Widmanstätten pattern.

The kamacite bandwidth (Figure 5), the chemical composition, the cosmic-ray exposure (CRE) age, and the Vickers hardness (HV) all are consistent with a strongly shocked IIIAB medium octahedrite classification for Shisr 043. Cosmogenic isotope ratios indicate that Shisr 043 had a small pre-atmospheric mass, its CRE age of 290 ± 20 Ma is characteristic for irons of the IIIAB group, and the $^{41}$Ca saturation as well as the low degree of weathering point to a sub-recent fall. Shisr 043 seems not to be paired with any of the other iron meteorite finds from the Arabian Peninsula.

**Section 3**

In the third paper the mineralogy and classification of the regolith part of the SaU 169 lunar meteorite is discussed including a description of the different minerals and rock clasts contained in the regolith (Figure 6). The regolith is mainly made up of mineral fragments (commonly pyroxene and plagioclase), rock fragments (breccia, wide range of basalts, and mafic granulites), and yellow and orange glass beads all embedded on a fine-grained ground mass. The basalt rocks are very small fragments reaching a maximum size of approx. 2.0 mm x 0.9 mm, whereas the largest clast is a grey KREEP breccia (approx. 7.5 mm x 4.0 mm).

A lunar origin is proven by typically lunar elemental ratios of Fe/Mn (moon 60-80; average regolith: 80; KREEP clast: 74) and K/U (moon 1700; average regolith: 1682; KREEP clast: 1253). The chemical composition of the bulk regolith breccia falls between that of the soil and of the regolith breccia of the Apollo 14 and Apollo 12 landing sites. Also, the largest (KREEP) clast has a chemical composition and total REE content identical to the ITE-rich high-K KREEP of the Apollo 14 landing site. This indicates that the SaU 169 regolith possibly is derived from the Apollo 14 landing site region in the Fra Mauro crater area near 17°W 4°S. The chemical composition of SaU 169 is clearly different from that of any other known lunar meteorite.

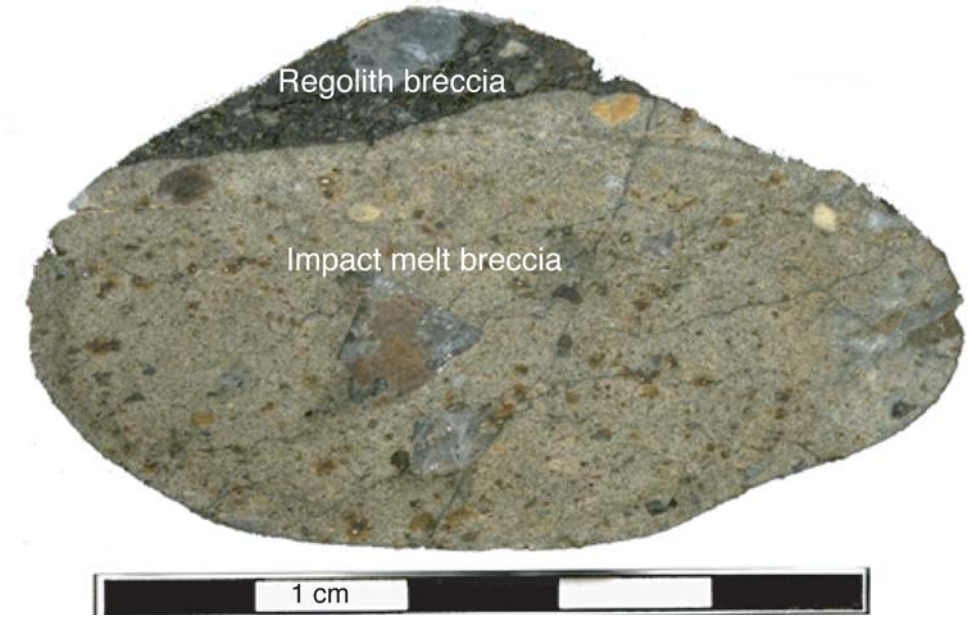


Figure 6. Image of a cut slice through the SaU 169 lunar meteorite showing its two main lithologies: impact melt breccia and regolith.

**Section 4**

SaU 169 was the 29th lunar meteorite found on Earth. Paper four is the first paper describing this meteorite. It discusses briefly the composition of the two main lithologies of the SaU 169 lunar meteorite (Figure 6), the impact melt breccia (87 vol%) and the adherent regolith breccia (13 vol%) with more emphasis on the lunar source, formation conditions, history on the moon, and Moon-Earth transfer history. The impact melt breccia is extremely enriched with KREEP components (potassium, rare earth elements, phosphorus), thorium 32.7 (ppm) and uranium 8.6 (ppm). This composition is characteristic for the lunar Mare Imbrium - Mare Procellarum regions.

The obtained age data showed a complex history, where crystallization of the impact melt occurred at 3909 ± 13 Ma, followed by exhumation of the impact melt breccia by a second impact at ~2800 Ma, which raised the sample to a regolith position at unconstrained depth. A third impact at ~200 Ma moved the material close to the lunar surface, where it mixed with solar-wind containing regolith. It was launched into space by a fourth impact at <0.34 Ma, and finally collided with the Earth sometime after 9.7 ± 1.3 kyr. Based on the high Th content (32.7 ppm) in the impact melt breccia SaU 169 must come from on of the Th hot spots on the Moon defined by Lunar Prospector γ–ray at the Aristarchus and Aristillus craters, the montes Carpathus-Fra Mauro region, and the Lalande crater region. Among these Th hot spots, only the area around Lalande and southeast of the crater Aristillus are compatible with the SaU 169 regolith Fe-Ti-Th concentrations. However, the age data of the SaU 169 render the Lalande crater area to be the most plausible source region for the SaU 169 since it contains a ~2800 Ma crater (Lalande, 2246 to 2803 Ma) and a ~200 Ma crater (e.g., Lalande A, 175 to 300 Ma).

**Section 5**

In paper five, the petrology, mineralogy and the shock metamorphism of the Martian meteorite SaU 094 is reported. The meteorite is a melanocratic olivine-porphyric rock of the shergottite group with affinities to lherzolitic shergottites (Figure 7). It is composed mainly of pyroxene (52 to 58.2 vol%), olivine (22.1 to 31 vol%), plagioclase (8.6 to 13 vol%), chromite and titanian chromite (0.9 to 1.0 vol%), traces of ilmenite (0.1 to 0.2 vol%), pyrrhotite, merrillite (<<0.1 vol%), and pockets consisting of green shock glass (4.8 to 6.7 vol%). The complete transformation of plagioclase to maskelynite, and the recrystallization of pyroxene, olivine and pyrrhotite indicate a strongly shocked meteorite with a shock grade of S6. SaU 094 is interpreted to be paired with SaU 005/008/051/060/090/120/125/130/131/150 (total mass ~11.38 kg) as all were found in the same area within a few kilometers distance and are similar in all aspects. These meteorites form the largest known Mars meteorite strewnfield. Its model composition is very similar to the Dar al Gani 476/489/670/735/876 shergottites from the Libyan Desert. Minor terrestrial weathering is evident as calcite veins and minor oxidation of sulfides. Possible source areas on Mars for the shergottites (having crystallization ages of a few 100 Ma) include the relatively young Tharsis volcanic region on Mars but also large areas

showing the presence of relatively young lava flows as evidenced by observations with Mars orbiters (Nyquist et al., 2001).

Figure 7. Image of the Martian meteorite SaU 094. Note the dark green, shocked olivine phenocrysts. The base of the section is ~4.5 cm.

**Appendices**

Appendix 1 is the list of meteorites collected and classified during this PhD work and published in the Meteoritical Bulletin (Russell et al., 2004; Russell et al., 2003).

Appendix 2 provides the complete data set of chemical analyses of ordinary chondrites used in Section 1.

Appendices 3 and 4 list the bulk chemical analyses for the reference soil samples and the soil under meteorite samples, respectively, studied in section 1.

Appendices 5 and 6 list the chemical analyses of leached reference soil samples and soil under meteorite samples, respectively, following aqua regia extraction. Those analyses are also in section 1.

**Reference**

BLAND P. (2001) Quantification of meteorite infall rates from accumulations in desert, and meteorite accumulation on Mars. In *Accretion of extraterrestrial matter throughout earths history* (eds. B. Peucker-Ehrenbrink and B. Schmitz), pp. 267-303. Kluwer Academic/Plenum Publishers, New York.

GLENNIE K. W., BOEUF M. G. A., HUGHES-CLARK M. W., MOODY-STUART M., PILAR W. F. H. and REINHARDT B. M. (1974) Geology of the Oman Mountains. *Verh. K. Ned. Geol. Mijnbouwkd. Genoot. Ged.* **31**, 423.

GROSSMAN J. N. (2000) The Meteoritical Bulletin, No. 84, 2000 August. *Meteoritics & Planetary Science* **35**, A199-A225.

GROSSMAN J. N. and ZIPFEL J. (2001) The Meteoritical Bulletin, No. 85, 2001 July. *Meteoritics & Planetary Science* **36**, A293-A322.

LE MÉTOUR J., MICHEL J. C., BÉCHENNEC F., PLATEL J. P. and ROGER J. (1995) *Geology and mineral wealth of the Sultanate of Oman*. Ministry of Petroleum and Minerals, Directorate General of Minerals, Sultanate of Oman, Muscat. pp. 1-285.

LE MÉTOUR J., PLATEL J. P., BÉCHENNEC F., BERTHIAUX A., CHEVREL S., DUBREUILH J., ROGER J. and WYNS R. (1993) Geological map of the Sultanate of Oman, 1:1'000'000, with explanatory notes. Sultanate of Oman, Ministry of Petroleum and Minerals, Directorate General of Minerals, Muscat.

MCSWEEN H. Y. J. (1999) *Meteorites and their parent planets*. Cambridge University Press, Cambridge, New York, Melbourne. pp. 310.

NORTON O. R. (2002) *The Cambridge encyclopedia of meteorites*. Cambridge University Press, the Edinbrugh Building, Cambridge CB2 2RU, UK, Cambridge. pp. 1-354.

NYQUIST L. E., BOGARD D. D., SHIH C.-Y., GRESHAKE A., STÖFFLER D. and EUGSTER O. (2001) Ages and geological histories of Martian Meteorites. In *Chronology and Evolution of Mars* (eds. R. Kallenbach, J. Geiss and W. K. Hartmann), pp. 105-164. ISSI Space Science Series, Kluwer, Dordrecht.

PAPIKE J. J. (1998) *Planetary Materials*. The Mineralogical Society of America, Washington. pp. 1-893.

PETERS T., BATTASHY M., BLÄSI H., HAUSER M., IMMENHAUSER A., MOSER L. and AL RAJHI A. (2001) Explanatory notes to the geological maps of Sur and Al Ashkharah, Sheets NF 40-8F and NF 40-12C, scale 1: 100'000. Ministry of Commerce and Industry, Directorate General of Minerals, Muscat.

PETERS T., IMMENHAUSER A., MERCOLLI I. and MEYER J. (1995) *Expanatory notes to geological map of Masirah Island North and Masirah South, Sheet K768-North and sheet K768-South, scale 1:50'000,*. Ministry of Petroleum and Minerals, Directorate General of Minerals, Muscat. pp. 1-81.

RUSSELL S. S., ZOLENSKY M. E., RIGHTER K., FOLCO L., JONES R., CONNOLLY H. C., GRADY M. M. and GROSSMAN J. N. (2005) The Meteoritical Bulletin, No. 89, 2005 September. *Meteoritics & Planetary Science* **40**, A201-A263.

RUSSELL S. S., FOLCO L., GRADY M. M., ZOLENSKY M. E., JONES R., RIGHTER K., ZIPFEL J. and GROSSMAN J. N. (2004) The Meteoritical Bulletin, No. 88, 2004 July. *Meteoritics & Planetary Science* **39**, A215-A272.

RUSSELL S. S., ZIPFEL J., FOLCO L., JONES R., GRADY M. M., ZOLENSKY M. E., MCCOY T. and GROSSMAN J. N. (2003) The Meteoritical Bulletin, No. 87, 2003 July. *Meteoritics & Planetary Science* **38**, A189-A248.

RUSSELL S. S., ZIPFEL J., GROSSMAN J. N. and GRADY M. M. (2002) The meteoritical Bulletin, No. 86, 2002 July. *Meteoritics & Planetary Science* **37**, A157-A184.

*Meteoritics & Planetary Science* 40, Nr 8, 1215–1239 (2005)
Abstract available online at http://meteoritics.org

# Weathering of meteorites from Oman: Correlation of chemical and mineralogical weathering proxies with $^{14}C$ terrestrial ages and the influence of soil chemistry

A. AL-KATHIRI[1, 2*], B. A. HOFMANN[3], A. J. T. JULL[4], and E. GNOS[1]

[1]Institut für Geologie, Universität Bern, Baltzerstrasse 1, CH-3012 Bern, Switzerland
[2]Directorate General of Commerce and Industry, Ministry of Commerce and Industry, Salalah, Oman
[3]Naturhistorisches Museum der Burgergemeinde Bern, Bernastrasse 15, CH-3005 Bern, Switzerland
[4]National Science Foundation Arizona Accelerator Mass Spectrometry Laboratory,
University of Arizona, 1118 East Fourth Street, Tucson, Arizona 85721, USA
*Corresponding author. E-mail: alikath@geo.unibe.ch

*(Received 05 January 2005; revision accepted 15 July 2005)*

**Abstract**–Fifty-four fragments of ordinary chondrites from 50 finds representing all searched areas in central Oman and all weathering stages were selected to compare the physical, chemical, and mineralogical effect of terrestrial weathering with $^{14}C$ terrestrial ages. $^{14}C$ ages range from 2.0 to >49 kyr with a median value of 17.9 kyr. The peak of the age range, which is between 10–20 kyr, falls in an arid climate period. A comparison of the chemical composition of Omani chondrites with literature data for unweathered H and L chondrites demonstrates a strong enrichment in Sr and Ba, and depletion in S during weathering. Water contents in H chondrites increase with terrestrial age, whereas L chondrites show a rapid initial increase followed by nearly constant water content. Correlating Sr, Ba, and $H_2O$ with age indicates two absorption trends: i) an initial alteration within the first 20 kyr dominated by $H_2O$ uptake, mainly reflecting Fe-Ni metal alteration, and ii) a second Ba- and Sr-dominated stage correlated with slower and less systematic weathering of troilite that starts after $H_2O$ reaches ~2 wt%. Sulfur released from troilite partly combines with Ba and Sr to form sulfate minerals. Other parameters correlated with $^{14}C$ age are degree of weathering, color of powdered meteorites, and the Ni/Fe ratio. Chemical analyses of 145 soils show a high degree of homogeneity over the entire interior Oman Desert, indicating large-scale mixing by wind. Soil samples collected from beneath meteorite finds typically are enriched in Ni and Co, confirming mobilization from the meteorites. High Cr and Ni concentrations in reference soil samples, which decrease from NE to SW, are due to detrital material from ultramafic rocks of the Oman Mountains.

## INTRODUCTION

Since 1999, Oman has become an important country for the recovery of hot desert meteorites (Grossman 2000; Grossman and Zipfel 2001; Russell et al. 2002, 2003, 2004). Before 1999, studies on Omani meteorites were limited to using six museum specimens (Franchi et al. 1995). A joint meteorite search program involving geologists from Bern, Switzerland (University of Bern and Natural History Museum Bern), and the Ministry of Commerce and Industry, Sultanate of Oman, was initiated in 2001. This search has resulted in the recovery of specimens from more than 263 individual falls during three field seasons in 2001–2003 (excluding thousands of samples from some large strewn fields, mainly Jiddat al Harasis [JaH] 073).

When meteorites reach the Earth's surface, they are exposed to a range of potential weathering agents such as water, oxygen-rich air, salts, wind, and temperature variations. Other factors, including the composition and porosity of meteorites and host soils/bedrocks, may also influence the mechanisms and rates of weathering. Weathering rates will further depend on the climate history since the fall occurred. As the degree of weathering of meteorites increases with their terrestrial age, old surfaces are likely to yield more highly-weathered meteorites than younger surfaces. Due to meteorite accumulation over long periods of time, hot or cold desert environments are most suitable for weathering studies (Bischoff and Geiger 1995; Bland et al. 1996; Stelzner et al. 1999; Welten 1999; Lee and Bland 2004).

In this paper, we investigate weathering-induced mineralogical and chemical changes of meteorites recovered from various areas in the central Oman Desert, compare weathering-related parameters (fragmentation, dispersion of fragments on the soil, alteration mineralogy, color of powdered meteorites, bulk chemistry) with $^{14}C$ terrestrial ages, and put these findings into the context of the geological and climatic history. The meteorites used for this study were described in the Meteoritical Bulletins 87–88 (Russell et al. 2003, 2004).

It is important to note that the regions as defined by the Meteoritical Society's Nomenclature Committee (Fig. 1) do not overlap fully with the geographical use of the names. Dhofar (Dho) and Jiddat al Harasis, for example, are geographical areas much larger than the area where meteorites are named Dho or JaH. Except in direct connection with meteorite names, our use of such names refers to the geographical usage.

## GEOLOGY OF THE INTERIOR OMAN DESERT

The central plains of the interior of Oman comprise more than 50% of the area of the country (Le Métour et al. 1995). These essentially flat areas lie at an altitude of between 50 and 250 m and are underlain by limestone, predominantly Miocene in age (minor Oligocene and Eocene). The horizontal bedding has remained largely undisturbed since marine deposition, with the exception of local salt tectonics. The area forms a vast peneplain partially covered by a layer of rocky debris. The Jiddat al Harasis is the largest of these limestone plains. It crops out extensively around Hayma and has almost no drainage network. These limestone plains are partially covered by aeolian sand dunes, which are still being shaped by the desert winds. These dune fields constitute the immense Rub al Khali Desert, and dunes accumulate locally to form ramlats (dune fields) in the north of Dhofar. A vast inland depression is located to the northeast of the central plains, the Umm as Samim sabkhah. Vast alluvial fans form a transitional belt to the Oman Mountains. Bedrock in the meteorite search area in the central Oman Desert consists mainly of the Hadhramaut Group (Bydoun 1966) and the Fars Group (Hughes-Clarke 1988). Both groups can be divided into marine and continental units (Chevrel et al. 1992). The Hadramaut marine deposits include highly recrystallized, nodular to thinly-bedded gray to brown limestone or dolostone (Platel et al. 1992) whereas the lacustrine deposits consist of micritic chalky limestone (Platel and Berthiaux 1992a, 1992b). The Fars marine deposits include green marl grading upwards into massive bioclastic and brecciated limestone (Platel and Berthiaux 1992b). The continental units includes gray to white micritic and brecciated lacustrine limestone, reddish conglomerate, and reddish siltstone and clay (Platel and Berthiaux 1992a). To the north, these rocks grade into a purplish red brecciated limestone (Chevrel et al. 1992). Quaternary deposits of the region are mainly wadi (a dry river occasionally flooded after heavy rain showers) sands and aeolian sand deposits consisting of high sand mounts, low active sand dunes, and aeolian sand veneers. Small domains of sub-recent to recent piedmont deposits and ancient to sub-recent travertine deposits crop out locally.

## CHARACTERIZATION OF METEORITE COLLECTION SURFACES AND CLIMATIC CONDITIONS

The Omani meteorite recovery areas are mainly restricted to the flat carbonate plains, where erosion and deposition since Tertiary deposition have been limited and meteorites have had a chance to accumulate over prolonged periods of time. The color/brightness contrast between the dark meteorites and the light carbonate surfaces facilitates identification of the meteorites.

Several areas of high meteorite find density occur in the Oman Desert. Find density is mainly a result of search intensity and suitability for search. The main collection areas are shown in Fig. 1. Collection surfaces typically consist of totally flat, loose limestone desert pavements, with silt/sand-sized fine material between limestone rocks. The average size of rock particles varies from a few mm to about 10 cm. Areas subject to slight erosion, with slightly irregular surface and larger limestone fragments (up to several cm), can be distinguished from obviously older peneplains, showing a reddish coloration of the surface and exhibiting smaller (typically 1 cm) limestone fragments. Shallow pits and rare sections exposed along wadis and road cuts show that soil formation can reach several meters deep at places, while in other areas limestone bedrock is exposed at the surface. Evidence for ponding of water after rare showers is common in shallow depressions (khabras) in the form of local sandy or clayey sediments displaying desiccation cracks. The climate in the searched area is dry and hot, with annual mean precipitation below 100 mm, in the Rub al Khali area below 50 mm (Sanlaville 1992). Yalooni station (18°56′N, 57°06′E) reports a mean annual rainfall 1981–1991 of 43.4 mm (annual variations 0–230 mm). Precipitation is mainly from cyclonic storms. However, the Indian Ocean is 35 to 230 km from collection areas and humid air is additionally brought into the desert by moist coastal air with common morning fog. Temperatures reach 50 °C in summer and can go below 0 °C occasionally during winter nights. We recorded January/February temperatures of 20–31 °C during the day and 4–12 °C during nights, and relative humidity of 30% to >90%. The dew point is frequently reached during winter in early morning hours, resulting in a wetting of rock, soil, and meteorite surfaces. Vegetation is sparse. Towards the coast, acacia trees are more common and rocks show a frequent cover by lichen, indicating higher availability of humidity.

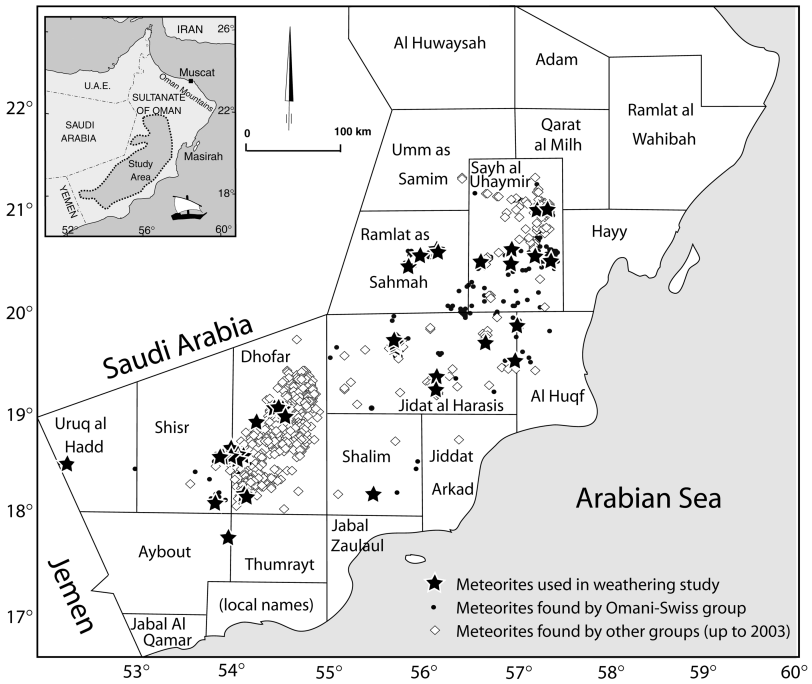


Fig. 1. Distribution of meteorite finds in Oman. Stars mark meteorites used in this study. Filled circles are meteorites collected during the Omani-Swiss meteorite search project until 2003. Diamonds represent published finds by other groups until 2003. Name boundaries are from the Meteoritical Society.

The present-day climate is representative of the last ~6 kyr, but older meteorites may have been subjected to several periods of wetter conditions (Sanlaville 1992; Burns et al. 2000; Fleitmann et al. 2003, 2004).

## SAMPLES AND METHODS

From the total of ~263 ordinary chondrite finds during our search program, 54 meteorite fragments from 50 individual finds representing as large a spread of weathering as possible were selected for chemical analysis and $^{14}C$ dating (Fig. 1). In the suite of dated samples, most chondrites with a low degree of weathering (W1) were intentionally included. Additionally, a sample of the Ghubara L5 chondrite was purchased and included in the set of samples, because this is one of the least weathered meteorites from Oman with a $^{14}C$ terrestrial age of 2–3 kyr (Ferko et al. 2002).

In addition to the meteorites, two types of soil samples were collected: i) 97 samples of soil under meteorites (SUM), and ii) 48 reference soil samples (RSS), typically taken from the top 5 cm of the soil at a distance of about 10 m from meteorite finds (including two calcrete samples from a depth of 20 cm). SUM samples were collected from beneath meteorites that were sufficiently large (>200 g) and firmly embedded in the soil. In strewn fields comprising several to hundreds of meteorite fragments, only a few representative soil samples were collected. RSS were collected from all major collection areas to represent all the different lithological formations. Soil samples typically consist of two major components: i) fine-grained silty material and ii) fragments of the bedrock up to several cm in size.

The mineralogy, including the weathering grades based on the Wlotzka (1993) scale, of all recovered meteorites and a few samples from each strewn field was studied in polished thin sections using transmitted and reflected light microscopy. For classification of meteorites, mineral chemistries of olivine and pyroxene were determined at the University of Bern, Bern, Switzerland, with a Cameca SX-50 microprobe equipped with wavelength dispersive spectrometers using natural and synthetic mineral standards, and beam conditions of 15 kV and 20 nA for silicates. The mineralogy of alteration phases was determined by reflected light microscopy using oil immersion, allowing the discrimination of magnetite, hematite, maghemite, and Fe-hydroxides. XRD was applied for the detection of specific minerals using powder sedimented on a silicon wafer and a Philips PW1800 diffractometer. Semi-quantitative mineral compositions for identification of alteration phases were obtained using energy dispersive X-ray spectrometry (EDS) on a SEM (CamScan CS4).

Cosmogenic $^{14}C$ was extracted from 200 to 850 mg (typically ~500 mg) meteorite samples using methods described previously (Jull et al. 1989, 1990, 1993, 1998) and measured by accelerator mass spectrometry (AMS) at the University of Arizona, Tucson, Arizona. For bulk chemistry, 47 fragments from 39 meteorites (Table 1) were ground in an agate mill and 5 g of each sample were submitted to Activation Laboratories (Ancaster, Ontario, Canada) for

Table 1. Weathering parameters compared with the $^{14}C$-terrestrial age for 39 ordinary chondrites.

| Meteorite | Type | Age (kyr) | Error (1σ) (kyr) | Alteration (W) | Fragmentation index (FI) | No. of fragments | Fragment dispersion (FD) (cm) | Meteorite powder color | Meteorite powder color (class) |
|---|---|---|---|---|---|---|---|---|---|
| Mean H chondrites | H | | | | | | | | |
| Aybut 001 | H6 | 5.1 | 1.3 | 1–2 | 1 | 1 | 0 | 5 YR 4/4 | 4 |
| UaH 002 | H3 | 9.4 | 1.3 | 1 | 1 | 1 | 0 | 5 YR 6/4 | 6 |
| SaU 228 | H6 | 9.7 | 1.3 | 2 | 1 | 1 | 0 | 5 YR 2/2 | 2 |
| Dho 1005 | H3/4 | 12.6 | 1.3 | 4 | 1 | 1 | 0 | 10 R 5/4 | 7 |
| Dho 020 | H4/5 | 12.7 | 1.3 | 4 | 1 | 1 | 0 | 10 R 5/4 | 7 |
| Shalim 003 | H5 | 13.0 | 1.3 | 3 | 0.51 | 50 | 250 | 10 YR 2/2 | 2 |
| Dho 814 | H5 | 14.1 | 1.3 | 2 | 1 | 1 | 0 | 5 YR 4/4 | 4 |
| Dho 1010 | H4 | 14.7 | 1.3 | 3 | 1 | 1 | 0 | 5 YR 3/2 | 3 |
| SaU 219 | H4 | 15.3 | 1.3 | 3 | 1 | 1 | 0 | 5 YR 2/2 | 2 |
| Dho 794 | H6 | 16.1 | 1.3 | 4 | 1 | 1 | 0 | 5 YR 2/2 | 2 |
| Dho 819 | H4 | 16.2 | 1.3 | 3 | 1 | 1 | 0 | 5 YR 2/2 | 2 |
| Dho 802 | H6 | 17.8 | 1.4 | 2 | 1 | 1 | 0 | 5 YR 6/4 | 6 |
| Dho 787 L* | H4 | 19.6 | 1.3 | 4 | 0.16 | 17 | 2000 | 5 YR 6/4 | 6 |
| Dho 835 | H5 | 26.8 | 1.4 | 4 | 1 | 1 | 0 | 10 R 5/4 | 7 |
| SaU 259 | H4 | 27.2 | 1.4 | 4 | 0.73 | 17 | 300 | 5 YR 6/4 | 6 |
| JaH 069 L* | H5 | 34 | 1.8 | 4 | 0.89 | 10 | 560 | 10 R 5/4 | 7 |
| Shişr 020 | H<4 | 36.5 | 2.6 | 3 | 0.98 | 4 | 720 | 10 R 5/4 | 7 |
| JaH 102 | H4 | 41.4 | 3.9 | 4 | 0.16 | 67 | 2000 | 5 YR 6/4 | 6 |
| Dho 807 | H5 | >47 | | 2 | 1 | 1 | 0 | 5 YR 3/2 | 3 |
| SaU 163 L* | H5 | >49 | | 3–4 | 0.55 | 36 | 300 | 5 YR 6/4 | 6 |
| Mean <15 kyr | | | | 2.6 | 0.85 | 8.2 | 250 | | 5 |
| Mean 15–30 kyr | | | | 3.5 | 0.85 | 6.3 | 357 | | 5 |
| Mean >30 kyr | | | | 3.1 | 0.67 | 27 | 755 | | 5.5 |
| Mean L chondrites | L | | | | | | | | |
| Ghubara | L5 | 2–3 | 1.3 | 0 | 1 | 1 | 0 | N3 | 1 |
| AH 011* | L6 | 3.0 | 1.3 | 1–2 | 0.79 | 101 | 156 | 5 YR 4/4 | 4 |
| SaU 001 | L4,5 | 5.5 | 1.3 | 1 | 1.00 | 1 | 130 | 5 YR 4/4 | 4 |
| Dho 1012 | L6 | 10.8 | 1.3 | 1 | 1 | 1 | 0 | 5 YR 3/2 | 3 |
| RaS 113 | L6 | 13.1 | 1.3 | 3 | 1 | 1 | 0 | 5 YR 3/2 | 3 |
| Shişr 025 | L6 | 13.2 | 1.3 | 2 | 0.97 | 8 | 0 | 5 YR 5/6 | 5 |
| RaS 111 | L6 | 15.8 | 1.3 | 2 | 0.88 | 2 | 4 | 5 YR 4/4 | 4 |
| JaH 073 (av 4)** | L6 | 19.7 | 1.3 | 2–4 | 0.92 | 2768 | 0 | | 4 |
| JaH 091 | L5 | 19.3 | 1.3 | 3 | 0.04 | 1000 | 5000 | 5 YR 3/2 | 3 |
| SaU 235 | L6 | 22.5 | 1.3 | 4 | 0.32 | 80 | 300 | 5 YR 6/4 | 6 |
| RaS 110 | L6 | 23.3 | 1.3 | 4 | 0.13 | 50 | 100 | 10 R 5/4 | 7 |
| Dho 805 | L6 | 30 | 1.6 | 3–4 | 1 | 1 | 0 | 10 R 5/4 | 7 |
| SaU 165 | L5 | 31.1 | 1.5 | 4 | 0.41 | 3 | 200 | 5 YR 6/4 | 6 |
| SaU 194 | L6 | 34.0 | 1.6 | 4 | 1 | 1 | 0 | 10 R 5/4 | 7 |
| Shişr 015 | L5 | 36.5 | 2.4 | 4 | 0.53 | 20 | 125 | 5 YR 6/4 | 6 |

Table 1. *Continued.* Weathering parameters compared with the $^{14}C$-terrestrial age for 39 ordinary chondrites.

| Meteorite | Type | Age (kyr) | Error (1σ) (kyr) | Alteration (W) | Fragmentation index (FI) | No. of fragments | Fragment dispersion (FD) (cm) | Meteorite powder color | Meteorite powder color (class) |
|---|---|---|---|---|---|---|---|---|---|
| RaS 112 | L6 | 38.2 | 2.4 | 4 | 0.86 | 4 | 200 | 10 R 5/4 | 7 |
| Dho 806 | L5 | 41.2 | 4.3 | 4 | 1 | 1 | 0 | 10 R 5/4 | 7 |
| Dho 005 L* | L6 | >47 | | 4 | 0.56 | >100 | 370 | 5 YR 6/4 | 6 |
| Dho 813 | L5 | >49 | | 3 | 1 | 1 | 0 | 5 YR 6/4 | 6 |
| Mean <15 kyr | | | | 1.5 | 0.96 | 18.8 | 47.7 | | 3 |
| Mean 15–30 kyr | | | | 3 | 0.55 | 650 | 901 | | 5 |
| Mean >30 kyr | | | | 4 | 0.77 | >5 | 128 | | 6 |

Table 1. *Continued.* Weathering parameters compared with the $^{14}C$-terrestrial age for 39 ordinary chondrites.

| Meteorite | Iron oxide (vol%) | Troilite oxide (vol%) | Max. oxide veins (μm) | Ba (ppm) | Sr (ppm) | Li (ppm) | S (wt%) | Fe (wt%) | Co (ppm) | Ni (ppm) | Zn (ppm) | As (ppm) | Ir (ppm) | $H_2O$ (wt%) |
|---|---|---|---|---|---|---|---|---|---|---|---|---|---|---|
| Mean H chondrites | | | | 3.5 | 9.5 | 1.7 | 2.2 | 27.6 | 834 | 16850 | 51 | 2 | 0.77 | |
| Aybut 001 | 25 | 5 | 8 | 4.7 | 20 | 1.3 | 1.1 | 29.6 | 808 | 14600 | 73 | 4.8 | 0.57 | 1.78 |
| UaH 002 | 15 | 0 | 15 | 8 | 61 | 1.3 | 1.5 | 28.7 | 846 | 15600 | 78 | 3.8 | 0.53 | 2.04 |
| SaU 228 | 50 | 5 | 15 | 6.2 | 13 | 2 | 1.2 | 25.3 | 800 | 15000 | 83 | 2* | 0.56 | 0.72 |
| Dho 1005 | 100 | 90 | 120 | 53 | 216 | 1.7 | 0.6 | 26.3 | 590 | 12000 | 89 | 2.1 | 0.57 | 2.44 |
| Dho 020 | 95 | 80 | 180 | 72 | 291 | 2.6 | 0.4 | 25.9 | 608 | 11900 | 73 | 1.8 | 0.56 | 2.6 |
| Shalim 003 | 95 | 20 | 300 | 5.1 | 19 | 1.1 | 1.6 | 24.1 | 780 | 14500 | 76 | 2.8 | 0.46 | 2.01 |
| Dho 814 | 40 | 2 | 10 | 11 | 80 | 1.5 | 1.5 | 29.1 | 849 | 16600 | 66 | 2.7 | 0.58 | 1.8 |
| Dho 1010 | 95 | 30 | 25 | 4 | 42 | 1.6 | 1.4 | 24.1 | 745 | 16000 | 66 | 2* | 0.59 | 2.12 |
| SaU 219 | 100 | 40 | 12 | 6.1 | 108 | 3.9 | 1.4 | 23.1 | 728 | 14800 | 84 | 1.3 | 0.54 | 2.12 |
| Dho 794 | 100 | 90 | 70 | 12 | 82 | 1.1 | 1.4 | 26.4 | 780 | 14000 | 81 | 3.7 | 0.54 | 2.08 |
| Dho 819 | 99 | 20 | 50 | 26 | 108 | 1.8 | 1.5 | 26.1 | 744 | 14300 | 87 | 1.8 | 0.51 | 2.66 |
| Dho 802 | 60 | 1 | 50 | 18 | 133 | 2.3 | 1.3 | 26.4 | 702 | 13900 | 76 | 2.2 | 0.56 | 2.41 |
| Dho 787 L* | 100 | 60 | 100 | 35 | 173 | 2 | 0.4 | 25.8 | 452 | 7520 | 71 | 2.8 | 0.41 | 2.22 |
| Dho 835 | 100 | 99 | 10 | 122 | 895 | 2.1 | 0.7 | 27 | 662 | 12300 | 59 | 3.4 | 0.53 | 2.35 |
| SaU 259 | 100 | 99 | 75 | 26 | 209 | 2.8 | 0.3 | 21.8 | 533 | 10800 | 62 | 1.3 | 0.53 | 2.78 |
| JaH 069 L* | 95 | 5 | 120 | 150 | 594 | 2.1 | 0.4 | 30.3 | 750 | 13200 | 75 | 4.6 | 0.63 | 2.62 |
| Shişr 020 | 99 | 40 | 30 | 265 | 938 | 2.2 | 0.5 | 29.6 | 733 | 13200 | 79 | 3.9 | 0.62 | 2.83 |
| JaH 102 | 99 | 95 | 150 | 95 | 399 | 2.1 | 0.6 | 24.8 | 740 | 14500 | 69 | 1.9 | 0.55 | 3.37 |
| Dho 807 | 60 | 5 | 100 | 5.8 | 28.45 | 1 | 0.8 | 30.3 | 883 | 17600 | 125 | 1.4 | 0.59 | 1.03 |
| SaU 163 L* | 98 | 10 | 400 | 101 | 228 | 4 | 0.6 | 28.5 | 745 | 14100 | 69 | 0.5 | 0.67 | 3.32 |
| Mean <15 kyr | 68 | 29 | 104 | 22 | 102 | 1.6 | 1.1 | 26.5 | 720 | 13747 | 75 | 3 | 0.54 | 1.97 |
| Mean 15–30 kyr | 94 | 52 | 61 | 49 | 288 | 2.2 | 0.9 | 25.9 | 669 | 12603 | 74 | 2.6 | 0.53 | 2.41 |
| Mean >30 kyr | 89 | 38 | 160 | 117 | 398 | 2.3 | 0.6 | 28.3 | 775 | 14850 | 85 | 1.9 | 0.61 | 2.64 |
| Mean L chondrites | | | | 3.5 | 11 | 1.8 | 2.2 | 21.8 | 550 | 11530 | 58 | 1.5 | 0.4 | |
| Ghubara | 1 | 0 | 20 | 4.5 | 11 | 1.2 | 0.6 | 25 | 599 | 12100 | 84 | 1.5* | 0.37 | 0.10 |
| AH 011* | 70 | 10 | 20 | 9.1 | 64 | 2.8 | 1.4 | 23 | 549 | 10205 | 79 | 2.5 | 0.37 | 2.15 |
| SaU 001 | 70 | 10 | 20 | 5.2 | 25 | 1.4 | 1.7 | 25.3 | 584 | 12100 | 85 | 1.5* | 0.45 | 1.45 |
| Dho 1012 | 3 | 1 | 20 | 4.6 | 34 | 1.6 | 0.5 | 22.6 | 775 | 15100 | 81 | 1.5 | 0.42 | 0.46 |

Table 1. *Continued.* Weathering parameters compared with the $^{14}C$-terrestrial age for 39 ordinary chondrites.

| Meteorite | Iron oxide (vol%) | Troilite oxide (vol%) | Max. oxide veins (μm) | Ba (ppm) | Sr (ppm) | Li (ppm) | S (wt%) | Fe (wt%) | Co (ppm) | Ni (ppm) | Zn (ppm) | As (ppm) | Ir (ppm) | $H_2O$ (wt%) |
|---|---|---|---|---|---|---|---|---|---|---|---|---|---|---|
| RaS 113 | 95 | 10 | 60 | 14 | 33 | 3.1 | 1.7 | 21.8 | 560 | 12700 | 69 | 1.5* | 0.35 | 1.37 |
| Shişr 025 | 90 | 30 | 20 | 115 | 51 | 1.4 | 1 | 21.9 | 528 | 10300 | 84 | 2.5 | 0.45 | 2.56 |
| RaS 111 | 30 | 5 | 30 | 3.7 | 17 | 1.4 | 1.2 | 20.5 | 548 | 12400 | 66 | 1.5* | 0.41 | 1.42 |
| JaH 073 (av 4)** | 93 | 40 | 49 | 49 | 120 | 3.1 | 1.4 | 22.1 | 450 | 9753 | 74 | 1.8 | 0.4 | 2.30 |
| JaH 091 | 95 | 40 | 15 | 3 | 13 | 1.1 | 0.8 | 20.4 | 550 | 11900 | 75 | 1.5* | 0.4 | 2.29 |
| SaU 235 | 100 | 95 | 70 | 4.3 | 34 | 1.9 | 0.4 | 17.6 | 409 | 7950 | 77 | 1.5* | 0.34 | 2.15 |
| RaS 110 | 100 | 80 | 40 | 13 | 130 | 2.8 | 0.5 | 21.5 | 465 | 9400 | 69 | 1.5* | 0.4 | 2.73 |
| Dho 805 | 95 | 30 | 20 | 16 | 87 | 2.2 | 0.6 | 24.5 | 541 | 9740 | 91 | 1.5 | 0.4 | 2.25 |
| SaU 165 | 100 | 95 | 50 | 45 | 209 | 1.2 | 0.2 | 26.6 | 571 | 10700 | 97 | 3.3 | 0.4 | 2.47 |
| SaU 194 | 100 | 95 | 40 | 73 | 181 | 14 | 0.8 | 24 | 644 | 13600 | 87 | 2.8 | 0.5 | 2.56 |
| Shişr 015 | 100 | 10 | 15 | 12 | 133 | 1.5 | 0.4 | 22.5 | 505 | 9760 | 217 | 1.3 | 0.46 | 2.51 |
| RaS 112 | 100 | 99 | 80 | 13 | 177 | 1.5 | 0.3 | 21 | 352 | 7020 | 62 | 1.5* | 0.43 | 2.17 |
| Dho 806 | 100 | 80 | 60 | 39 | 314 | 2.1 | 0.4 | 26.4 | 559 | 10800 | 120 | 3.9 | 0.48 | 2.17 |
| Dho 005 L* | 100 | 98 | 65 | 41 | 249 | 2.4 | 0.3 | 24.2 | 388 | 6917 | 95 | 2.5 | 0.4 | 2.03 |
| Dho 813 | 80 | 20 | 40 | 150 | 1140 | 2.40 | 0.8 | 23.8 | 601 | 10000 | 93 | 1.9 | 0.45 | 2.36 |
| Mean <15 kyr | 55 | 10 | 27 | 25 | 36 | 1.9 | 1.2 | 23.2 | 599 | 12084 | 80 | 1.8 | 0.40 | 1.35 |
| Mean 15–30 kyr | 86 | 48 | 37 | 15 | 67 | 2.1 | 0.8 | 21.1 | 494 | 10190 | 75 | 1.6 | 0.39 | 2.18 |
| Mean >30 kyr | 97 | 71 | 50 | 53 | 343 | 3.6 | 0.5 | 24.1 | 517 | 9828 | 110 | 2.5 | 0.45 | 2.32 |

2*, 1.5* = Mean H or L chondrite values are used instead of measurements below detection limit.
** = Fragmentation and dispersion of fragments based on 806 individuals.
AH 011* = Mean of the paired meteorites AH 010 and AH 011.
L* = Terrestrial age obtained after leaching the samples with ethanolamine thioglycollate.
(av 4) = Average chemical analysis of four samples from JaH 073.

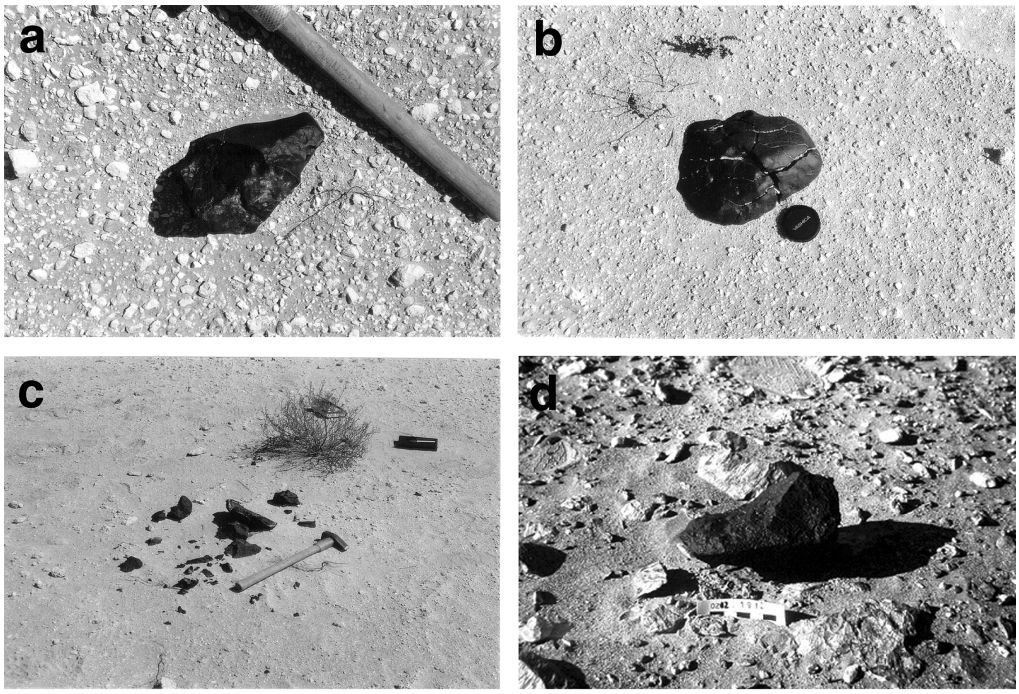


Fig. 2. Weathered meteorites recovered from the Oman Desert: a–c are from the JaH 073 strewn field and illustrate the effect of weathering on meteorites and its possible dependence on the surface type. a) Fresher (W2) meteorite with no weathering fractures on hard soil. b) Weathered (W3) meteorite with cross cutting fractures filled with calcite on softer soil. c) Fragmented, heavily weathered (W4) meteorite in sandy depression; a–c demonstrate the occurrence of different weathering grades within the same strewn field. d) The effect of aeolian abrasion on the meteorite Sayh al Uhaymir (SaU) 259, which is comparable to its effects on surrounding limestone rocks.

detailed analysis using a combination of INAA, ICP-MS, and ICP-OES.

The water content of meteorites was determined gravimetrically on powdered samples using the Penfield method at the Institute for Geological Science, University of Bern. Samples were dried at 105 °C prior to analysis.

Soil samples were sieved to obtain the <0.15 mm fraction, which was used for analyses. Thus, limestone fragments were excluded from the analyses. One hundred and forty-four soils, including two caliche samples, were analyzed without further treatment by ICP-OES following aqua regia extraction (Activation Laboratories). Thirty soil samples, including 1 sample at 20 cm below the surface, were ground in an agate mill and aliquots of 5 g were submitted for more detailed bulk analysis by a combination of INAA, ICP-MS, and ICP-OES.

Heavy minerals were separated from about 40 g of the <0.15 mm soil fraction from 8 RSS. The soils were treated with 5% HCl to remove carbonates and repeatedly washed in a beaker with demineralized water to remove clays. After drying, the heavy mineral fraction was separated using bromoform (density of 2.89 g/cm$^3$) and the heavy mineral content was determined gravimetrically. Polished thin sections were prepared from the low magnetic fraction of the heavy mineral concentrates and were analyzed on the electron microprobe.

## RESULTS

### Effects of Weathering Measured in the Field: Fragmentation, Fragment Dispersion, Aeolian Abrasion

We often found meteorites as single, more or less complete individuals. In many other cases, individuals were broken into a number of fragments, typically along cracks formed due to volume expansion during alteration and/or temperature fluctuations (Fig. 2). In extreme cases, fragments were distributed over an area of hundreds of square meters. Only in one case (JaH 091) does this fragmentation appear to be due to impact resulting in a breccia composed of meteorite and bedrock fragments. In all other cases we assume it to be due to physical and chemical weathering (temperature fluctuations and volume increase). In Table 1, we list the fragmentation index (FI) and the fragment dispersion factor (FD). The FI is defined as the mass of the largest fragment/total mass of all fragments as a measure of fragmentation of individuals. The FD is defined as the maximum distance between different fragments of a single fall. For the JaH 073 strewn field, the average FI was calculated from 806 individuals. The reasons for movement of meteorite fragments across the flat-lying soil are unclear. Possible factors are soil creep, water flow after rare heavy rain showers, wind and possibly movement by higher organisms

(birds, antelopes, camels, and man). The largely undisturbed JaH 073 strewn field demonstrates that these processes do not result in a systematic large-scale displacement of meteorites in >10,000 yr.

Rocks and meteorites lying on the surface of a flat desert plain are subject to mechanical erosion by aeolian abrasion, an effect also observed in other desert areas (Schlüter et al. 2002). Desert rocks are more eroded on the sides facing the direction of prevailing wind (Fig. 2d). Aeolian abrasion forms curved features and small slopes, with striations parallel to wind direction, on rock surfaces facing wind directions. Shaped curved surfaces with strong wind striation indicate the main aeolian abrasion direction. We found that rocks (including meteorites) occurring near sand dunes are more abraded. Measuring striations caused by aeolian abrasion shows two main wind directions, a stronger one from the southeast (130–140°) and a weaker one from the north (10°), mainly in the Jiddat al Harasis and Sayh al Uhaymir meteorite areas. Orientations of aeolian striations slowly shift to a dominant north direction (350–010°) towards southern (Shişr) areas, and abrasion intensity becomes weaker.

Aeolian abrasion features are relatively uncommon on the meteorites collected and are probably much less important than chemical weathering, only a few meteorites show aeolian abrasion surfaces similar to those of the surrounding limestones (Fig. 2d).

**Terrestrial Ages of Meteorites from Oman**

Out of 54 dated ordinary chondrites, 50 contain detectable amounts of $^{14}C$, indicating an age of <47,000 yr for the majority of finds (Tables 1 and 2). Only four samples did not contain any detectable $^{14}C$. Out of the dated samples, three were from the Dhofar 005 strewn field and three from the JaH 073 strewn field (Table 2). Ages obtained on JaH 073 range from 18.0 to 21.5 ± 1.3 kyr. For the purpose of this study, we use the mean value of 19.7 kyr for JaH 073. After assessment of pairings and including the Ghubara L5 chondrite (Franchi et al. 1995; Ferko et al. 2002), we obtained terrestrial ages from 50 chondrites. Previously dated finds include a CV3 (Sayh al Uhaymir [SaU] 202), 6.8 kyr, the lunar meteorite SaU 169, <9.7 kyr (Gnos et al. 2004); and the shergottite SaU 094, ~12.9 kyr (Gnos et al. 2000). The Ghubara L5 is the youngest meteorite so far reported from Oman. Its almost unaltered composition seems to indicate that maybe it is a recent fall. Its $^{14}C$ concentration of ~38 dpm/kg indicates a terrestrial age of 2–3 kyr (Ferko et al. 2002), whereas the average $^{14}C/^{10}Be$ ratio of ~2.24 (Ferko et al. 2002) is very close to the average production ratio of ~2.5, suggesting that Ghubara could be younger than 1000 yr. The lunar meteorite Dho 025, dated at 500–600 kyr (Nishiizumi and Caffee 2001), and the shergottite Dho 019, dated at 360 kyr (Nishiizumi et al. 2002), have the longest terrestrial ages for meteorites from Oman.

In order to address the possibility of a contamination of weathered meteorites with terrestrial $^{14}C$ we leached seven samples with ethanolamine thioglycollate (Table 2), a compound used to selectively dissolve iron oxides and hydroxides (Cornish and Doyle 1984). This approach was based on the assumption that organic contaminations would likely be associated with weathering products. All samples were further treated in the usual way (see Samples and Methods section), including phosphoric acid treatment, to remove carbonates. In three of the leached samples, $^{14}C$ concentrations were lower by 0.46 to 4.03 dpm/kg after leaching (in two cases reaching values below detection). In four cases, concentrations were increased by 0.89 to 3.87 dpm/kg. These variable data could be due to removal of contaminating $^{14}C$, data scatter, contamination during treatment, and/or heterogeneous distribution of $^{14}C$.

**Meteorite Powder Color and Weathering Grade**

Using the rock-color chart (Goddard et al. 1948), the color of meteorite powders prepared for geochemical analysis were compared with weathering grade (Wlotzka 1993) to test if there is any relationship between the intensity of weathering and the color of the powders. Metal and troilite in meteorites are altered to yellowish red iron hydroxides and iron oxides. With increasing weathering grade, the powder colors are increasingly dominated by the color of the weathering products. Powder colors were grouped to seven classes (Table 1). Fresh unweathered meteorites have a dark gray color (N3). With increasing amounts of weathered metal and troilite, the powder commonly grades to dusky brown, grayish brown, moderate brown, and finally light brown (5 YR 6/4) for strongly weathered meteorites (W3, W4). Some strongly weathered meteorites, e.g., Dho 794 (W4), are characterized by an unusually high abundance of magnetite causing unusually dark powders (Table 1), commonly grayish brown (5 YR 2/2).

**Mineralogy of Weathering Products**

All the meteorites collected, plus a few representative samples from each strewn field, were studied in polished thin sections using transmitted and reflected light microscopy. Microscopically, alteration in silicate minerals is restricted to staining with Fe-hydroxide particles. This is probably similar to the aggregates of goethite formed after smectite as a product of the initial rapid weathering as described by Bland et al. (1998c). In a meteorite powder (SaU 163), small amounts of smectitic clay minerals were detected by XRD after Fe-hydroxide dissolution using ethanolamine thioglycollate and enrichment of the fine-grained fraction of the powder by sedimentation of larger particles. Fe-Ni alloys and sulfide (troilite) are weakly to completely altered, corresponding to weathering grades W1–W4 (Wlotzka 1993). The alteration

Table 2. Terrestrial ages of various Omani meteorites: additional ordinary chondrites that have no chemical analysis, ordinary chondrites leached with ethanolamine thioglycollate, a carbonaceous chondrite, a lunar meteorite, and a Martian meteorite.

| Meteorite | Type | Bulk $^{14}C$ (dpm/kg) | Error (1σ) (dpm/kg) | Leached sample $^{14}C$ (dpm/kg) | Age (kyr) | Error (1σ) (kyr) | Leached sample age (kyr) |
|---|---|---|---|---|---|---|---|
| H chondrites | | | | | | | |
| SaU 209 | H5 S1 W2 | 26.12 | 0.13 | | 4.8 | 1.30 | |
| Dho 816 | H5 S2 W2 | 2.95 | 0.18 | | 6.6 | 1.30 | |
| Dho 799 | H4 S2 W3 | 13.35 | 0.28 | | 10.3 | 1.3 | |
| JaH 120 | H5 S1 W2 | 11.52 | 0.14 | | 11.5 | 1.3 | |
| Dho 787 | H4 S1/2 W4 | 4.34 | 0.13 | | 19.6 | 1.3 | |
| Shişr 032 | H5 S2 W1 | 10.27 | 0.13 | | 12.5 | 1.3 | |
| Ras 114 | H5 S1/2 W3 | 3.81 | 0.16 | | 20.7 | 1.3 | |
| SaU 250 | H4–6 S2 W3 | 3.66 | 0.13 | | 21.0 | 1.3 | |
| Dho 835 | H5 S1/2 W4 | 1.82 | 0.13 | 3.72 ± 0.14 | 26.8 | 1.4 | 20.9 ± 1.3 |
| Shişr 020 | H4–6 S1 W3 | 0.56 | 0.15 | 2.70 ± 0.21 | 36.5 | 2.6 | 23.5 ± 1.4 |
| Dho 999 | H5 S1 W4 | 1.07 | 0.23 | | 31.2 | 2.2 | |
| JaH 069 | L5 S1/2 W4 | 1.62 | 0.25 | 0.83 ± 0.23 | 28.5 | 1.8 | 34 ± 2.6 |
| Shişr 017 | H4 S5 W4 | 0.66 | 0.14 | | 35.1 | 2.2 | |
| SaU 163 | H5 S1/2 W3–4 | 3.56 | 0.15 | −0.47 ± 0.20 | 21.2 | 1.3 | >50 |
| L chondrites | | | | | | | |
| UaH 001 | LL5 S2 W2 | 12.73 | 0.16 | | 12.1 | 1.3 | |
| JaH 078 | L6 S4 W2 | 5.36 | 0.10 | | 18.7 | 1.3 | |
| Jah 073 | L6 S4 W3 | 5.76 | 0.12 | | 18 | 1.3 | |
| Jah 073 | L6 S4 W2 | 4.75 | 0.09 | | 19.6 | 1.3 | |
| Jah 073 | L6 S4 W4 | 3.79 | 0.11 | | 21.5 | 1.3 | |
| Dho 005 | L6 S4 W4 | 0.75 | 0.14 | | 34.6 | 2 | |
| Dho 005 | L6 S5(4) W4 | 0.56 | 0.10 | 4.43 ± 0.20 | 37.4 | 2.0 | 20.2 ± 1.4 |
| Dho 005 | L6 S4/5 W4 | 0.37 | 0.13 | −0.09 ± 0.28 | 40.6 | 3.1 | >47 ± 26.6 |
| Dho 813 | L5 S4 W3 | −0.14 | 0.14 | 0.75 ± 0.12 | >49 | | 34.9 ± 1.9 |
| Various meteorites | | | | | | | |
| SaU 202 | CV3 2/3.3 | 26.05 | 0.28 | | 6.8 | 1.3 | |
| SaU 169[a] | Lunar | 20.23 | 0.26 | | 9.7 | 1.3 | |
| SaU 094 | Martian | 12.77 | 0.26 | | 12.9 | 1.3 | |

[a] $^{10}Be$ = 8.05 ± 0.30 dpg/kg.

products occur as replacements of pre-existing minerals and as matrix staining and veins cross-cutting the meteorites. Typically, it is observed that weathering in Fe-Ni proceeds faster than in troilite, in some cases the metal alloy is completely weathered, while troilite shows only minor weathering. Similarly, Lee and Bland (2004) observed almost completely altered Fe-Ni metal besides considerable volumes of troilite, which remained unaltered in hot desert meteorites. We classified several alteration features to provide a refined alteration scheme for ordinary chondrites and to compare these weathering parameters with $^{14}C$ ages (Table 1).

Fe-Ni metal shows an initial development of oxide/hydroxide coatings leading to total replacement of metal grains in advanced stages of alteration. Boundaries between fresh Fe-Ni and alteration phases are always sharp. Taenite shows a somewhat higher degree of resistance than kamacite and can sometimes be observed as relicts. The alteration mineralogy is dominated by maghemite and Fe hydroxides, but magnetite and hematite are commonly observed as well (Fig. 3a). In a few meteorites, magnetite and hematite are the dominant minerals replacing Fe-Ni, most prominent in Dho 794, an H6 chondrite. Mössbauer spectra and XRD patterns of dated ordinary chondrites from the Daraj locality of the Libyan Sahara, the Nullarbor region of Australia, and Roosevelt County, New Mexico, USA, suggest a suite of ferric iron weathering products that include goethite, magnetite, maghemite, ferrihydrite, lepidocrocite, and akaganéite (Bland et al. 1996).

In contrast to Fe-Ni, troilite undergoes gradational changes during alteration with diffuse boundaries between fresh and altered phases, commencing with a decreased reflectivity associated with a development of microfractures on {0001}. An undetermined sulfidic alteration phase is being developed at this stage. Strongly anisotropic marcasite is found in some samples, and a thin film of pyrite precipitated at the contact between troilite and Fe oxides and hydroxides. If oxidation of all sulfides is completed, hydroxides are the major product of troilite weathering with only minor maghemite and hematite present, magnetite was not observed.

Calcite is commonly found as fine-grained, filling in

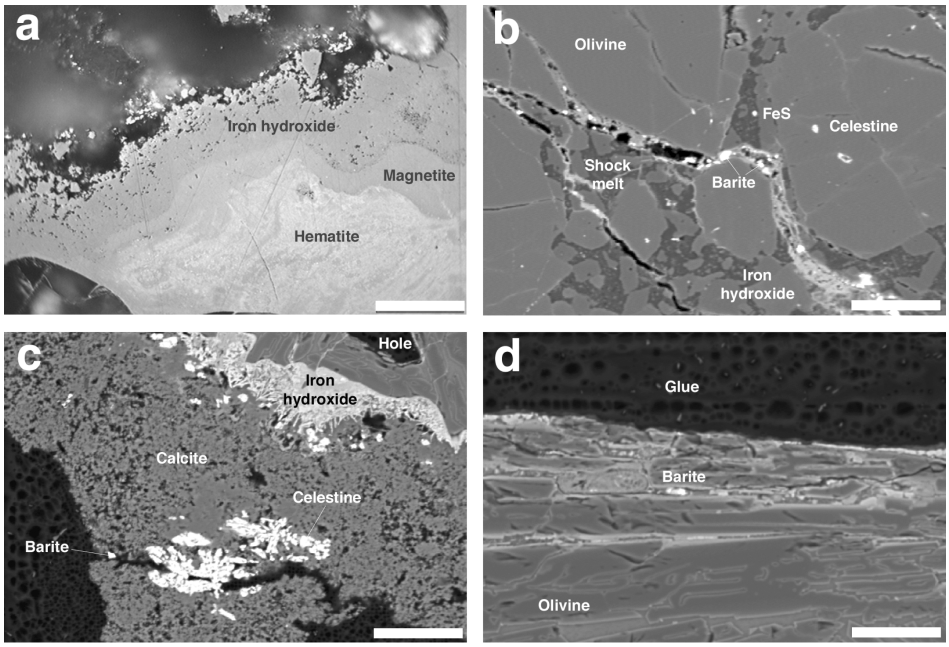


Fig. 3. Alteration mineralogy: a) reflected light micrograph illustrating different layers of weathering products of metal and troilite in Al Huqf (AH) 010. Scale bar is 20 µm. b) Network of fissures in Dho 813 filled with iron hydroxides, barite and celestine. Scale bar is 40 µm. c) Large crack in Dho 835 filled with Sr-bearing calcite (<1 wt% SrO), in which idiomorphic crystals of celestine and isolated barite occur. Iron hydroxide rims the fusion crust visible on the top right of image. Scale bar is 25 µm. d) Partially crystallized fusion crust in Dho 835 showing weathering on its outer side (top). The lighter-colored material on top is glassy material altering to hydroxides. These areas are also chlorine-enriched. Scale bar is 50 µm. Figs. 3b, 3c, and 3d are BSE images.

fractures associated with metal alteration products, and also occurs as a surface coating on those parts of meteorites originally buried in the soil. Calcite also occurs in minor amounts occluding intergranular pores in weathered meteorites. Calcite is precipitated as crystals with a maximum size of 20–30 µm sized crystals from water during occasional wetting of the meteorites (rainwater, temporary ponds, and dew) and may enclose sand grains or silt from the surrounding soil. Microcrystalline quartz of clearly secondary origin is occasionally observed in small pores in the matrix, typically within secondary Fe hydroxides.

In three ordinary chondrites with high Ba and Sr concentrations (Dho 813, Dho 835, and Shişr 020; Table 1), tiny barite and celestine crystals (Figs. 3b, 3c, and 3d) with a maximum grain size of 10 µm were detected. The crystals occur mainly in fractures and in voids filled with iron oxides/hydroxides, calcite, or anhydrite. In Fig. 3c, two clusters of celestine grains occur associated with Sr-bearing calcite (<1 wt% SrO), in sample Dho 835 barite crystals occur aligned in a chlorine-enriched alteration product replacing fusion crust glass (Fig. 3d). As well as barite and celestine, Ba-rich celestine grains were also observed.

A pale green mineral, which is confined to the lower part of meteorite surfaces (in direct contact with soil) and within fractures of weathered ordinary chondrites, is frequently observed. This material usually occurs as a thin layer without visible crystals and occasionally can be observed on soil particles in direct contact with meteorites.

For identification of the green material, three samples were analyzed (two from JaH 073 and one from JaH 070) using X-ray diffraction (XRD) on a Si single crystal plate. To obtain compositional information, some analyses of the green material from a third sample from the meteorite JaH 073 were performed by EDS. Since the samples originate from the lower part of the meteorite fixed in the soil, they are contaminated with soil minerals such as quartz, calcite, and sometimes dolomite. Results from chemical analysis of the green material match characteristics of the serpentine group minerals nepouite and pecoraite ($Ni_3Si_2O_5(OH)_4$), the Ni-analogs of lizardite (nepouite) and clinochrysotile (pecoraite). Pecoraite is a known weathering product of iron meteorites in desert environments (Faust et al. 1969; Lee and Bland 2004). XRD patterns show three relatively broad reflections at 7.5, 3.8, and 2.5 Å, indicating poorly crystallized material. The EDS analyses correspond to a Ni/Si atomic ratio of 3.6:2. We tentatively identify this mineral as Ni-serpentine. The Ni/Co ratio ranges between 14 and 44 with an average of 29 (chondritic ratio is 20) for 5 analyses, indicating a preferential enrichment of Ni in serpentine minerals during weathering.

**Chemistry of Meteorite Alteration**

The geochemical analysis of the ordinary chondrite finds investigated and their comparison to mean unweathered H and L chondrite compositions (Mason 1971; Kallemeyn et al. 1989; Hofmann et al. 2000; Friedrich et al. 2003) demonstrate

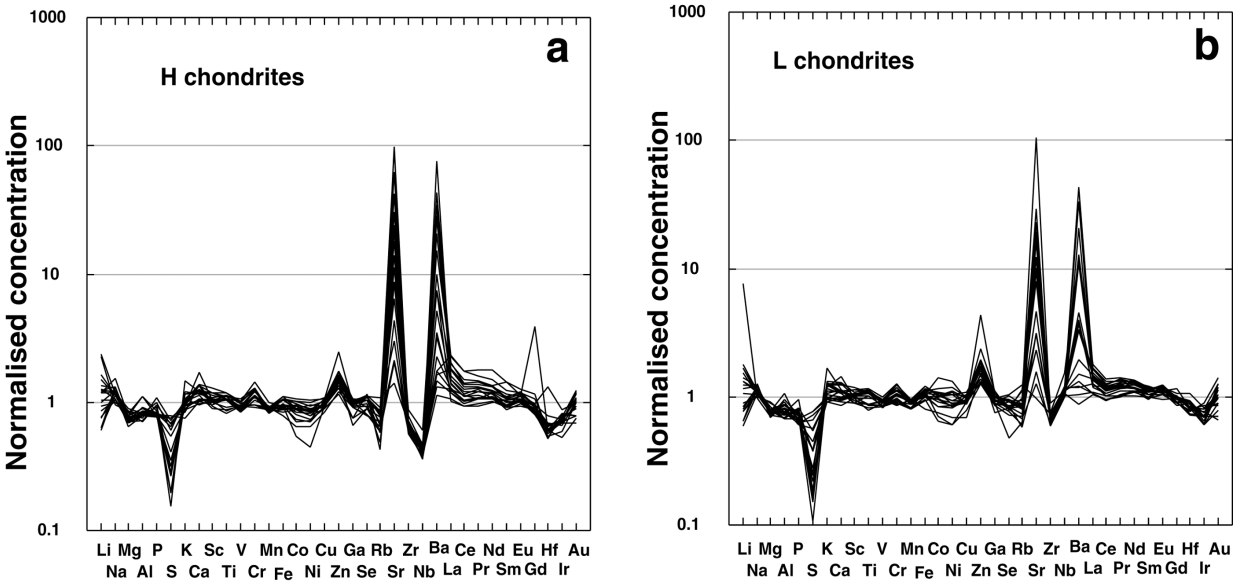


Fig. 4. Logarithmic plots of the bulk chemical composition of weathered H chondrites (a) and (b) L chondrite finds normalized to the mean bulk chemical composition of unweathered H and L chondrites (Mason 1967). Sr and Ba are strongly enriched relative to the mean chondritic abundance; smaller enrichments are observed for Li and Zn. Note the weak enrichment of light rare earth elements (LREE) and the depletion of S relative to the mean chondritic abundance.

that Ba and Sr concentrations in meteorites from Oman are sensitive weathering proxies that can best be correlated with the weathering grade. The less altered meteorites have relatively low concentrations of Ba and Sr (4 and 10.2 ppm, respectively), whereas heavily weathered, older meteorites contain up to 265 ppm Ba (76× chondritic) and 1140 ppm Sr (106× chondritic, Fig. 4). The L chondrites are less enriched in Ba (maximum 42× chondritic). Less altered meteorites contain up to 1.67 wt% S, while the S content decreases to 0.33 wt% in strongly altered meteorites (Table 1). Also, small enrichments of Zn and possibly Li are observed (<10× chondritic) and slight enrichments of light REE are indicated by the data (Figs. 4 and 5). Some strongly weathered meteorites are depleted in Ni (down to 0.45× chondritic). A comparison of the mean chemical composition of three terrestrial age groups (<15 kyr, 15–30 kyr, and >30 kyr) of the analyzed chondrites (Fig. 5 and Table 3) illustrates the above mentioned chemical observations as a function of terrestrial age. Loss of Mg is indicated by a lowering of the Mg/Mn ratio by 8% (L) to 10% (H) for the age group >30 kyr, as observed by Bland et al. (1998c).

The water content bound in secondary minerals of the investigated meteorites ranges from 0.72–3.37 wt% in H chondrites and from 0.1 wt% to 2.73 wt% in L chondrites (Table 1). The lowest water content in the H group was recorded for SaU 228 (W2), which yielded a terrestrial age of 9.7 ± 1.3 kyr and the highest water content was determined in JaH 102 (W4) dated at 41.4 ± 3.9 kyr. The almost unaltered Ghubara L5 chondrite (weak alteration is observed in near surface metal) has the lowest water content in the L group, the highest content was measured in the strongly altered RaS 110 (W4) dated at 23.3 ± 1.3 kyr. The water content in both H and L chondrites shows a frequency maximum at 2–2.5 wt%. It was observed that some heavily weathered younger meteorites (e.g., Uruq al Hadd [UaH] 002: 9.7 kyr; Dho 1005: 12.6 kyr; Al Huqf [AH] 011: 3.0 kyr) have water contents comparable to older falls (Table 1). The average water content for H chondrite age groups (<15 kyr, 15–30 kyr, and >30 kyr) is 1.97 wt%, 2.40 wt%, and 3.04 wt%. The average water content for L chondrites (<15 kyr, 15–30 kyr, and >30 kyr) is 1.35 wt%, 2.18 wt%, and 2.32 wt%.

A plot of water content versus terrestrial age of meteorites (Fig. 6) shows a rapid initial increase from 0–15 kyr followed by slower increase of water content for H chondrites. L chondrites also show a rapid initial increase in water content from 0–20 kyr, but older samples show no further increase with increasing age. Three H5 and three L6 chondrites from Açfer region, Algeria (Stelzner et al. 1999) show a similar curve of increasing water content with increasing age and weathering grade.

### Correlation of Weathering Parameters with $^{14}C$ Age

In Table 1, physical, mineralogical, and chemical properties that may vary with terrestrial age are presented for 39 samples/falls for which both $^{14}C$ terrestrial ages and chemical analysis are available. By comparing mean values for the age groups 0–15, 15–30, and >30 kyr, the following age-dependences can be recognized: i) strongly age-dependent: Sr, Ba, S, and $H_2O$ contents, meteorite powder

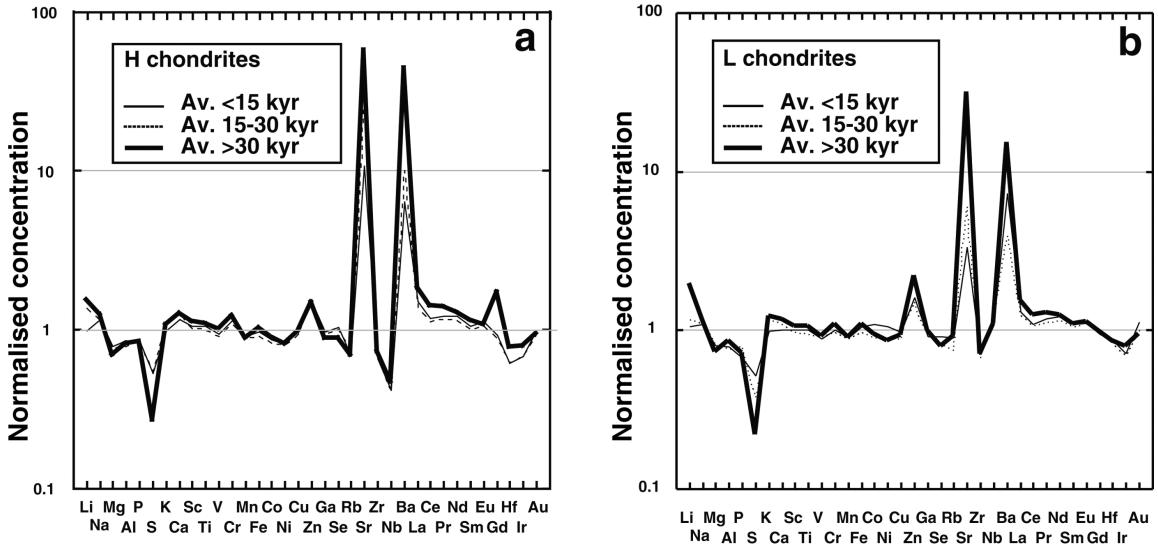


Fig. 5. Logarithmic plots of the bulk chemical composition of weathered H and L chondrites normalized to the mean chemical composition of unweathered H (a) and L chondrites (b) (Mason 1967). Data from the weathered finds are grouped into three categories <15 kyr, 15–30 kyr, and >30 kyr. Sr and Ba contents increase and S decreases with increasing terrestrial age. Small enrichments are observed for Li and Zn.

color, and width of oxide veins; ii) medium age-dependent: weathering grade, metal oxidation, troilite oxidation, fragmentation index, dispersion index, and Li; iii) weakly age-dependent: Ni, Zn, and As; iv) no clear age dependence: Fe and Co. A matrix of the correlation coefficients between the different weathering proxies and $^{14}C$ terrestrial ages (Table 4) at 95% confidence level supports the observations listed in Table 1. Significant positive correlations agree with properties increasing with terrestrial age. On the other hand, significant negative correlations are shown by properties declining with terrestrial age. The best correlations between different weathering proxies are observed for alteration-metal oxidation, Ba-Sr, and metal oxidation-troilite oxidation. It must be noted that there likely are relationships between terrestrial age and some of the weathering proxies that have correlation coefficients below statistical significance, e.g., oxide vein thickness. Age groups 0–15, 15–30, and >30 kyr (Table 1) show a steady increase of vein thickness with age but low correlation coefficients are due to a few strongly deviating measurements. The statistically significant decrease of Ni/Fe (Table 4) with age is supported by the observed mobility of Ni from some meteorites into the underlying soil (see below).

**Soil Chemistry: Aqua Regia Extraction-OES**

Analyses of 46 RSS (<0.15 mm) by aqua regia extraction-OES (Table 5) show that the surface soils are compositionally homogeneous over wide areas of the Oman interior desert, even though the areas are underlain by different marine and lacustrine stratigraphic units (Fig. 7a). This indicates strong aeolian mixing of surface soils over the entire desert. Compared with RSS (averaging 40 ppm Ni and 4.8 ppm Co), SUM shows significant enrichments in Ni (average 77 ppm) and Co (5.3 ppm), excluding one extreme sample containing 6752 ppm Ni and 216 ppm Co.

Compared with the average upper crustal value of 20 ppm Ni and 10 ppm Co (Taylor and McLennan 1985), SUM are enriched in Ni, whereas Co is enriched only in a few samples where the Ni content exceeds 240 ppm (Fig. 8b). In the most extreme case, SUM show a Ni value which is 337 times the average crustal content and a Co value of 21.5 times crustal (Fig. 8b). RSS show a weak enrichment of Ni (up to 47 ppm), but no clear enrichment of Co is observed (Figs. 7a and 8a). Also, S and Ca in SUM and RSS are enriched relative to average crustal values. While the sulfur enrichment can be explained by the presence of gypsum in the desert soil and Ca is derived from limestone, the reason for the Ni enrichment is not obvious. Two calcretes sampled at 20 cm below the surface show high Sr concentrations of 1370 and 2900 ppm (average 2133 ppm Table 5), indicating a significant mobility of Sr during recent soil formation processes.

Differences in composition between RSS and SUM samples are evidently a result of the mobilization of Ni and Co from the overlaying meteorite to the underling soil during chemical weathering. Ni tends to leach from limonite as a result of weathering of Fe-Ni metal in ordinary chondrites (Norton 2002). In cases where the SUM Ni and Co concentrations were higher than in the reference sample (RSS), the Ni/Co ratio of the contamination $(Ni/Co)_{met}$ was calculated as follows: $(Ni/Co)_{met}$ = Ni (SUM) – Ni (RSS) / Co (SUM) – Co (RSS). The $(Ni/Co)_{met}$ ratios range from 24.5 to 75 (mean 40), clearly higher than the chondritic value of 20, indicating preferential loss of Ni over Co.

Table 3. Averaged geochemical analyses of H and L chondrite age groups.

| Elements | Unit | Method | Av. chondrites | <15 kyr | <15 kyr | 15–30 kyr | 15–30 kyr | >30 kyr | >30 kyr |
|---|---|---|---|---|---|---|---|---|---|
| H chondrites | | | | Av. (n = 8) ± 1σ | Av./av. chondritic | Av. (n = 7) ± 1σ | Av./av. chondritic | Av. (n = 5) ± 1σ | Av./av. chondritic |
| Li | ppm | 2 | 1.7 | 1.62 ± 0.47 | 0.95 | 2.28 ± 0.87 | 1.34 | 2.28 ± 1.09 | 1.34 |
| Na | % | 1 | 0.57 | 0.64 ± 0.05 | 1.12 | 0.68 ± 0.12 | 1.19 | 0.70 ± 0.04 | 1.23 |
| Mg | % | 3 | 14.2 | 11.11 ± 0.80 | 0.78 | 10.9 ± 0.1 | 0.77 | 10.1 ± 1.0 | 0.71 |
| Al | % | 3 | 1.01 | 0.85 ± 0.12 | 0.84 | 0.81 ± 0.05 | 0.80 | 0.88 ± 0.15 | 0.87 |
| P | % | 3 | 0.097 | 0.08 ± 0.01 | 0.85 | 0.08 ± 0.01 | 0.85 | 0.08 ± 0.01 | 0.85 |
| S | % | 3 | 2 | 1.15 ± 0.44 | 0.57 | 1.00 ± 0.51 | 0.50 | 0.59 ± 0.15 | 0.30 |
| K | % | 3 | 0.08 | 0.08 ± 0.01 | 0.97 | 0.09 ± 0.02 | 1.06 | 0.09 ± 0.01 | 1.03 |
| Ca | % | 3 | 1.2 | 1.36 ± 0.19 | 1.13 | 1.52 ± 0.27 | 1.27 | 1.47 ± 0.13 | 1.22 |
| Sc | ppm | 1 | 8 | 8.20 ± 0.63 | 1.03 | 8.44 ± 0.97 | 1.06 | 8.88 ± 0.60 | 1.11 |
| Ti | % | 3 | 0.06 | 0.06 ± 0.01 | 1.02 | 0.06 ± 0.01 | 1.03 | 0.07 ± 0.01 | 1.09 |
| V | ppm | 2 | 61 | 56.4 ± 4.1 | 0.92 | 56.3 ± 3.1 | 0.92 | 59.6 ± 3.8 | 0.98 |
| Cr | ppm | 1 | 3400 | 3740 ± 401 | 1.10 | 3873 ± 622 | 1.14 | 4146 ± 283 | 1.22 |
| Mn | ppm | 3 | 2260 | 2008 ± 54 | 0.89 | 2015 ± 132 | 0.89 | 2001 ± 89 | 0.89 |
| Fe | % | 1 | 27.6 | 26.6 ± 2.2 | 0.97 | 25.2 ± 2.0 | 0.91 | 28.7 ± 2.3 | 1.04 |
| Co | ppm | 1 | 834 | 753 ± 101 | 0.90 | 657 ± 121 | 0.79 | 770 ± 63 | 0.92 |
| Ni | ppm | 1 | 16850 | 14525 ± 1738 | 0.86 | 12517 ± 2597 | 0.74 | 14520 ± 1813 | 0.86 |
| Cu | ppm | 2 | 90 | 88.8 ± 5.7 | 0.99 | 83.7 ± 4.6 | 0.93 | 88.8 ± 7.1 | 0.99 |
| Zn | ppm | 3 | 51 | 75.5 ± 8.1 | 1.51 | 74.4 ± 11.0 | 1.49 | 83.7 ± 23.7 | 1.67 |
| Ga | ppm | 2 | 5.2 | 5.07 ± 0.53 | 0.98 | 4.93 ± 0.47 | 0.95 | 4.67 ± 0.75 | 0.90 |
| Se | ppm | 2 | 7 | 7.24 ± 0.79 | 1.03 | 7.06 ± 0.80 | 1.01 | 6.54 ± 0.91 | 0.93 |
| Rb | ppm | 2 | 3 | 2.03 ± 0.62 | 0.68 | 2.26 ± 0.36 | 0.75 | 2.21 ± 0.46 | 0.74 |
| Sr | ppm | 2 | 9.5 | 93 ± 104 | 9.79 | 244 ± 290 | 25.7 | 438 ± 349 | 46.1 |
| Zr | ppm | 2 | 9.5 | 6.23 ± 0.65 | 0.66 | 6.31 ± 0.37 | 0.66 | 6.60 ± 1.02 | 0.69 |
| Nb | ppm | 2 | 1.1 | 0.45 ± 0.05 | 0.41 | 0.46 ± 0.03 | 0.42 | 0.51 ± 0.09 | 0.46 |
| Ba | ppm | 3 | 3.5 | 20.5 ± 26.5 | 5.87 | 35.1 ± 39.5 | 10.0 | 123 ± 95 | 35.2 |
| La | ppm | 2 | 0.3 | 0.46 ± 0.14 | 1.52 | 0.41 ± 0.08 | 1.38 | 0.55 ± 0.10 | 1.82 |
| Ce | ppm | 2 | 0.84 | 1.00 ± 0.23 | 1.19 | 0.95 ± 0.13 | 1.13 | 1.18 ± 0.20 | 1.41 |
| Pr | ppm | 2 | 0.12 | 0.15 ± 0.03 | 1.22 | 0.14 ± 0.02 | 1.16 | 0.17 ± 0.02 | 1.39 |
| Nd | ppm | 2 | 0.58 | 0.71 ± 0.15 | 1.22 | 0.66 ± 0.06 | 1.15 | 0.75 ± 0.10 | 1.29 |
| Sm | ppm | 2 | 0.21 | 0.22 ± 0.04 | 1.06 | 0.21 ± 0.02 | 0.99 | 0.24 ± 0.04 | 1.14 |
| Eu | ppm | 2 | 0.07 | 0.08 ± 0.01 | 1.11 | 0.07 ± 0.01 | 1.07 | 0.08 ± 0.01 | 1.08 |
| Gd | ppm | 2 | 0.32 | 0.29 ± 0.04 | 0.92 | 0.29 ± 0.02 | 0.89 | 0.49 ± 0.42 | 1.55 |
| Hf | ppm | 2 | 0.25 | 0.15 ± 0.02 | 0.62 | 0.15 ± 0.01 | 0.62 | 0.18 ± 0.08 | 0.73 |
| Ir | ppb | 1 | 770 | 553 ± 41.3 | 0.70 | 517 ± 50 | 0.65 | 612 ± 45 | 0.77 |
| Au | ppb | 1 | 230 | 235 ± 23.1 | 1.02 | 211 ± 43 | 0.92 | 229 ± 48 | 0.99 |
| L chondrites | | | | n* = 6 | | n* = 10 | | n* = 10 | |
| Li | ppm | 2 | 1.8 | 1.91 ± 0.80 | 1.06 | 2.09 ± 0.81 | 1.16 | 3.54 ± 4.6 | 1.97 |
| Na | % | 1 | 0.65 | 0.72 ± 0.05 | 1.1 | 0.71 ± 0.04 | 1.1 | 0.74 ± 0.06 | 1.14 |
| Mg | % | 3 | 15.2 | 12.1 ± 0.9 | 0.8 | 12.1 ± 0.9 | 0.8 | 11.1 ± 0.5 | 0.73 |
| Al | % | 3 | 1.1 | 0.87 ± 0.10 | 0.79 | 0.84 ± 0.06 | 0.76 | 0.95 ± 0.14 | 0.86 |
| P | % | 3 | 0.11 | 0.07 ± 0.01 | 0.67 | 0.09 ± 0.01 | 0.79 | 0.08 ± 0.01 | 0.72 |

Table 3. *Continued.* Averaged geochemical analyses of H and L chondrite age groups.

| Elements | Unit | Method | Av. chondrites | <15 kyr | <15 kyr | 15–30 kyr | 15–30 kyr | >30 kyr | >30 kyr |
|---|---|---|---|---|---|---|---|---|---|
| S | % | 3 | 2.17 | 1.13 ± 0.53 | 0.52 | 0.81 ± 0.40 | 0.38 | 0.47 ± 0.25 | 0.22 |
| K | % | 3 | 0.09 | 0.09 ± 0.01 | 0.99 | 0.10 ± 0.02 | 1.17 | 0.11 ± 0.01 | 1.23 |
| Ca | % | 3 | 1.28 | 1.29 ± 0.09 | 1.01 | 1.40 ± 0.26 | 1.09 | 1.48 ± 0.13 | 1.16 |
| Sc | ppm | 1 | 8.9 | 8.97 ± 0.40 | 1.01 | 8.72 ± 0.80 | 0.98 | 9.36 ± 0.86 | 1.05 |
| Ti | % | 3 | 0.07 | 0.07 ± 0.01 | 1.01 | 0.06 ± 0.01 | 0.94 | 0.07 ± 0.01 | 1.06 |
| V | ppm | 2 | 65 | 57.8 ± 2.3 | 0.89 | 59.2 ± 2.9 | 0.91 | 59.9 ± 3.5 | 0.92 |
| Cr | ppm | 1 | 3800 | 3838 ± 402 | 1.01 | 3675 ± 483 | 0.97 | 4193 ± 436 | 1.1 |
| Mn | ppm | 3 | 2460 | 2212 ± 105 | 0.9 | 2173 ± 148 | 0.88 | 2203 ± 144 | 0.9 |
| Fe | % | 1 | 21.8 | 23.2 ± 1.5 | 1.06 | 21.1 ±2.3 | 0.97 | 24.1 ± 2.0 | 1.1 |
| Co | ppm | 1 | 550 | 599 ± 90 | 1.09 | 495 ± 60 | 0.9 | 517 ± 109 | 0.94 |
| Ni | ppm | 1 | 11530 | 12084 ± 1799 | 1.05 | 10215 ± 1657 | 0.89 | 9828 ± 2321 | 0.85 |
| Cu | ppm | 2 | 86 | 83.9 ± 5.74 | 0.98 | 77 ± 10 | 0.89 | 80.1 ± 6.9 | 0.93 |
| Zn | ppm | 3 | 50 | 80.3 ± 6.2 | 1.61 | 75.2 ± 8.8 | 1.5 | 110 ± 50 | 2.2 |
| Ga | ppm | 2 | 5.2 | 4.75 ± 0.49 | 0.91 | 4.86 ± 0.34 | 0.93 | 5.13 ± 0.51 | 0.99 |
| Se | ppm | 2 | 8.9 | 8.21 ± 0.83 | 0.92 | 7.32 ± 1.59 | 0.82 | 7.05 ± 0.38 | 0.79 |
| Rb | ppm | 2 | 2.8 | 2.51 ± 0.50 | 0.9 | 2.1 ± 0.4 | 0.75 | 2.54 ± 0.54 | 0.91 |
| Sr | ppm | 2 | 10.8 | 36.2 ± 18.8 | 3.35 | 64.9 ± 50 | 6.01 | 343 ± 356 | 31.8 |
| Zr | ppm | 2 | 8.9 | 6.25 ± 0.25 | 0.7 | 5.99 ± 0.52 | 0.67 | 6.23 ± 0.84 | 0.7 |
| Nb | ppm | 2 | 0.4 | 0.45 ± 0.02 | 1.13 | 0.47 ± 0.07 | 1.18 | 0.44 ± 0.03 | 1.1 |
| Ba | ppm | 3 | 3.5 | 25.4 ± 44.3 | 7.26 | 13.7 ± 15.2 | 3.92 | 53.2 ± 47.5 | 15.2 |
| La | ppm | 2 | 0.3 | 0.39 ± 0.05 | 1.3 | 0.38 ± 0.06 | 1.25 | 0.46 ± 0.06 | 1.53 |
| Ce | ppm | 2 | 0.84 | 0.92 ± 0.08 | 1.09 | 0.91 ± 0.10 | 1.08 | 1.04 ± 0.1 | 1.24 |
| Pr | ppm | 2 | 0.12 | 0.14 ± 0.01 | 1.18 | 0.14 ± 0.02 | 1.13 | 0.15 ± 0.01 | 1.28 |
| Nd | ppm | 2 | 0.58 | 0.71 ± 0.05 | 1.23 | 0.67 ± 0.06 | 1.15 | 0.72 ± 0.05 | 1.25 |
| Sm | ppm | 2 | 0.21 | 0.23 ± 0.01 | 1.1 | 0.22 ± 0.02 | 1.05 | 0.23 ± 0.02 | 1.1 |
| Eu | ppm | 2 | 0.07 | 0.08 ± 0.01 | 1.11 | 0.08 ± 0.01 | 1.12 | 0.08 ± 0.01 | 1.13 |
| Gd | ppm | 2 | 0.32 | 0.3 ± 0.01 | 0.94 | 0.31 ± 0.03 | 0.98 | 0.31 ± 0.02 | 0.97 |
| Hf | ppm | 2 | 0.18 | 0.16 ± 0.01 | 0.87 | 0.15 ± 0.02 | 0.83 | 0.16 ± 0.02 | 0.86 |
| Ir | ppb | 1 | 565 | 400 ± 46 | 0.71 | 391 ± 26 | 0.69 | 446 ± 38 | 0.79 |
| Au | ppb | 1 | 160 | 178 ± 23 | 1.12 | 159 ± 20 | 1 | 153 ± 41 | 0.95 |

1 = INAA.
2 = ICP-MS.
3 = ICP-OES.
Average H, L chondrite values from Mason (1971).
Average for Zn and Ir from mean of Friedrich (2003) and Kallemeyn (1989).
n* = Number of analyzed meteorites, including paired samples from strewn field.
Av. = Average.

### Soil Chemistry: Total Analysis

Not surprisingly, total soil analyses (<0.15 mm) generally show higher concentrations for most elements than the aqua regia leach (Table 6). This is most evident for Cr where the leach average is 33 ppm and the total average 1427 ppm, compared with 35 ppm in mean upper continental crust (Taylor and McLennan 1985). Most elements are present at least partly in a form inaccessible to the aqua regia attack employed. Total analyses also demonstrate the homogeneity of the chemical composition of soils over the different meteorite collection surfaces in the Oman deserts independent of the underlying geological formations.

Comparing the total analysis results with the average chemical composition of the upper continental Earth crust (Taylor and McLennan 1985) shows that the RSS and SUM samples are strongly enriched in Cr (up to 80×), moderately enriched (7× to 15×) in Se, Ni, and Ca and slightly enriched in Hf, S, Ti, Mg, and Sr (Fig. 7b). Depletions relative to average upper crust are mainly observed for Ta, P, Rb, Ga, Na, Cs, K, Fe, Sc, and Al, probably due to the carbonate-rich lithology. As in leach analyses, total analyses show that soil underneath meteorites is enriched in Ni. We found chromite to be the main carrier of anomalous Cr in the soils. To test for a possible meteoritic origin, as observed in Ordovician limestones in southern Sweden (Schmitz et al. 2001, 2003), 43 chromite grains from 8 samples were analyzed with the electron microprobe (Table 7). By comparison with chondritic chromites of Schmitz et al. (2003), our ZnO, $TiO_2$, and $Cr_2O_3$ values are lower, and the $Al_2O_3$ and MgO values are higher than in ordinary chondrites demonstrating that the chromites are non-meteoritic in origin.

## DISCUSSION

### Terrestrial Ages of Omani Meteorites

The distribution of terrestrial ages of the ordinary chondrites studied (Fig. 9) shows the largest peak in the 10–15 kyr range. Only 16% of meteorites have terrestrial ages <10 kyr and 28% have ages >30 kyr, a distribution that is significantly different from other sites investigated (Sahara, Australia, western United States; Table 8) where 44–85% of samples are <10 kyr and only 0–18.5% are >30 kyr (Jull et al. 1990; Jull 1993; Bland et al. 1998c; Bland and Bevan 2000; Welten et al. 2004). The distribution of ages from Oman is more comparable with age distributions of ordinary chondrites from Roosevelt County, New Mexico, USA (Bland et al. 1998c), and the Allan Hills icefield, Victoria Land, Antarctica (Jull et al. 1998) (Table 8). Our age distribution data are very similar to those obtained on other samples from Oman and Saudi Arabia (Jull 2001).

In order to check how representative our suite of samples selected for terrestrial age dating is, we compared the weathering degrees of this suite with the weathering degree of all our finds and all published finds from Oman (Table 9). Because we intentionally included samples of low degree of weathering, these are overrepresented. The high average age of dated meteorites is consistent with the presence of a high percentage of strongly weathered (W3–4) finds.

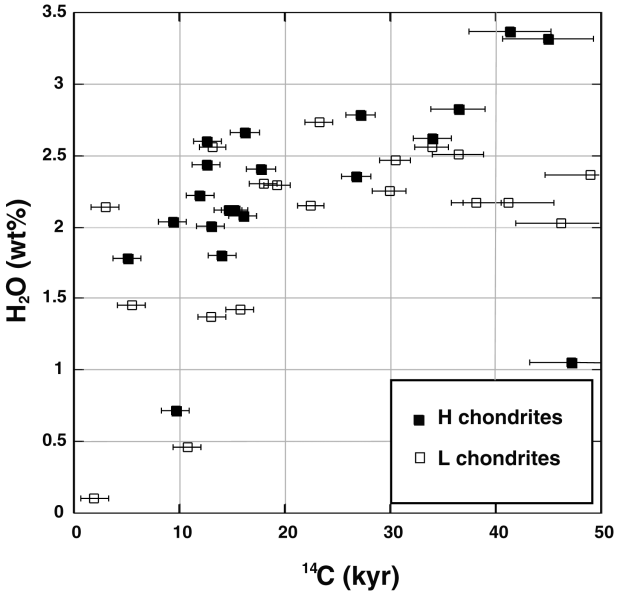


Fig. 6. Plot of water content of Omani H and L chondrites against their terrestrial age. H chondrites show an initially rapid increase of water content with age, up to ~10 kyr, followed by a period of slower increase with age. L chondrites also show an initially rapid increase in water content up to a saturation at ~20 kyr followed by a constant level with increasing terrestrial age.

The weathering rate at different sites appears to depend on local conditions, as was also observed in other hot desert regions (Bland et al. 1996, 1998c; Jull et al. 1998; Bland and Bevan 2000; Jull 2001). There may be several reasons for the relatively high average terrestrial age of Omani meteorites. Besides the unlikely possibility of sampling bias towards high terrestrial ages, it appears that the meteorite accumulation surfaces in Oman are very stable, which is supported by the find of lunar meteorite Dho 025 with a terrestrial age of 500–600 kyr (Nishiizumi and Caffee 2001). The presence of such stable and old surfaces leads to the accumulation of a high percentage of older meteorites relative to younger ones. In general, the $^{14}C$ terrestrial ages correlate well with the visual weathering grade and most weathering parameters (Table 1). Only a few samples differ from the general trend. Possible problems include the presence of unrecognized strewn fields (resulting in occurrence of fragments with variable and in part significant shielding to cosmic rays) and the possible contamination with terrestrial $^{14}C$ (that may be enclosed in inert alteration products such as quartz and magnetite). Such contamination might be an explanation for the relatively common occurrence of ages in

Table 4. Correlation matrix of weathering proxies and $^{14}C$ terrestrial ages at 95% confidence level.

| | Age (kyr) | Weathering grade | FI | FD | Powder color | Iron oxidation (vol%) | Troilite oxidation (vol%) | Oxide veins (cm) | Ba (ppm) | Sr (ppm) | S (wt%) | Ni/Co | Ni/Fe |
|---|---|---|---|---|---|---|---|---|---|---|---|---|---|
| Age | | | | | | | | | | | | | |
| Weathering grade | 0.64[a] | | | | | | | | | | | | |
| FI | –0.23 | –0.40[a] | | | | | | | | | | | |
| FD | 0.09 | 0.16 | –0.66[a] | | | | | | | | | | |
| Powder color | 0.61[a] | 0.57[a] | –0.15 | –0.02 | | | | | | | | | |
| Iron oxidation | 0.52[a] | 0.86[a] | –0.34[a] | 0.20 | 0.39[a] | | | | | | | | |
| Troilite oxidation | 0.42[a] | 0.75[a] | –0.33[a] | 0.11 | 0.48[a] | 0.62[a] | | | | | | | |
| Oxide veins | 0.27 | 0.34[a] | –0.27 | 0.05 | 0.14 | 0.31 | 0.10 | | | | | | |
| Ba | 0.52[a] | 0.27 | 0.12 | 0.04 | 0.49[a] | 0.32 | 0.14 | 0.18 | | | | | |
| Sr | 0.60[a] | 0.34[a] | 0.11 | 0.00 | 0.50 | 0.29 | 0.22 | 0.05 | 0.85[a] | | | | |
| S | –0.57[a] | –0.53[a] | 0.38[a] | –0.19 | –0.65[a] | –0.27 | –0.54[a] | –0.14 | –0.33[a] | –0.34[a] | | | |
| Ni/Co | –0.26 | –0.16 | 0.04 | 0.06 | –0.26 | –0.04 | –0.03 | –0.14 | –0.36[a] | –0.45[a] | 0.30 | | |
| Ni/Fe | –0.41[a] | –0.39[a] | 0.20 | 0.01 | –0.61[a] | –0.36[a] | –0.40[a] | –0.04 | –0.26 | –0.32[a] | 0.57[a] | 0.50[a] | |
| $H_2O$ | 0.57[a] | 0.68[a] | –0.34[a] | 0.20 | 0.61[a] | 0.73[a] | 0.44[a] | 0.39[a] | 0.49[a] | 0.39[a] | –0.26 | –0.17 | –0.28 |

[a]Significant values based on 95% confidence limits.
FI = Fragmentaion index.
FD = Fragment dispersion.

Table 5. Averaged leachate analyses for different soil types, Omani interior deserts.

| Element | Units | MUC | RSS | RSS | SUM | SUM | Calcrete* | Calcrete |
|---|---|---|---|---|---|---|---|---|
| | | | Av. (n = 46) ± 1 | Av./MUC | Av. (n = 97) ± 1 | Av./MUC | Av. (n = 2) ± 1 | Av./MUC |
| Na | % | 2.89 | 0.11 ± 0.19 | 0.04 | 0.05 ± 0.05 | 0.02 | 0.15 ± 0.17 | 0.05 |
| Mg | % | 1.33 | 1.33.1 ± 0.3 | 1 | 1.21 ± 0.25 | 0.91 | 1.48 ± 1.16 | 1.11 |
| Al | % | 8.04 | 0.49 ± 0.07 | 0.06 | 0.45 ± 0.08 | 0.06 | 0.48 ± 0.08 | 0.06 |
| P | % | 0.105 | 0.02 ± 0.01 | 0.15 | 0.01 ± 0.01 | 0.13 | 0.01 ± 0.01 | 0.07 |
| S | % | 0.026 | 0.05 ± 0.03 | 1.76 | 0.04 ± 0.06 | 1.67 | 0.45 ± 0.43 | 17.4 |
| K | % | 2.8 | 0.08 ± 0.01 | 0.03 | 0.07 ± 0.01 | 0.02 | 0.09 ± 0.02 | 0.03 |
| Ca | % | 3 | 17.9 ± 2.05 | 5.97 | 16.6 ± 1.61 | 5.53 | 20.7 ± 4.8 | 6.91 |
| Sc | ppm | 11 | 2.55 ± 0.30 | 0.23 | 2.29 ± 0.39 | 0.21 | 1.93 ± 0.24 | 0.18 |
| Ti | % | 0.3 | 0.06 ± 0.01 | 0.2 | 0.05 ± 0.01 | 1.77 | 0.04 ± 0.01 | 0.15 |
| V | ppm | 60 | 33.3 ± 4.7 | 0.56 | 28.4 ± 5.1 | 0.47 | 30.8 ± 1.0 | 0.51 |
| Cr | ppm | 35 | 35.4 ± 6.0 | 1.01 | 30.3 ± 5.6 | 0.86 | 40.6 ± 5.2 | 1.16 |
| Mn | ppm | 600 | 222 ± 37 | 0.37 | 192 ± 32 | 0.32 | 142 ± 5 | 0.24 |
| Fe | % | 3.5 | 0.92 ± 0.12 | 0.26 | 0.80 ± 0.16 | 0.23 | 0.71 ± 0.08 | 0.2 |
| Co | ppm | 10 | 4.81 ± 1.22 | 0.48 | 5.3 ± 1.9 (7.5 ± 21.5 ) | 0.75 | 3.79 ± 0.07 | 0.38 |
| Ni | ppm | 20 | 39.9 ± 19.6 | 1.99 | 76.9 ± 68.5 (146 ± 686) | 7.28 | 27.5 ± 2.0 | 1.37 |
| Zn | ppm | 71 | 7.09 ± 5.16 | 0.1 | 5.63 ± 3.65 | 0.08 | 1.43 ± 1.3 | 0.02 |
| Sr | ppm | 350 | 260 ± 66 | 0.74 | 216 ± 63 | 0.62 | 2133 ± 1075 | 6.09 |
| Zr | ppm | 190 | 23.6 ± 5.7 | 0.12 | 23.3 ± 4.9 | 0.12 | 19.5 ± 2.54 | 0.1 |
| Ba | ppm | 550 | 89.1 ± 44.6 | 0.16 | 75.1 ± 27.3 | 0.14 | 172 ± 167 | 0.31 |
| La | ppm | 30 | 8.8 ± 1.5 | 0.29 | 7.77 ± 1.41 | 0.26 | 5.86 ± 0.42 | 0.2 |
| Pb | ppm | 20 | 7.6 ± 1.6 | 0.38 | 7.09 ± 3.55 | 0.35 | 8.25 ± 1.82 | 0.41 |

Ni and Co values in parentheses are the average values, including the anomalous sample.
MUC = Mean Earth upper continental crust values, from Taylor and McLennan (1985).
n = Number of analysis.
Av. = Average.
RSS = Reference soil samples.
SUM = Soil under meteorite.
* = Calcrete samples from 20 cm below the surface.

the 35–45 kyr range, many, but not all, of which may actually be >50 kyr. Leaching experiments demonstrated that in some cases $^{14}C$ can be removed from the Fe-alteration phases, indicating that several dpm/kg of $^{14}C$ may be due to terrestrial contamination. Modern terrestrial carbon has a $^{14}C$ activity of 13,560 dpm/kg, 270 times more than the saturation activity in ordinary chondrites. Therefore, a contamination with only 100 ppm of modern terrestrial carbon adds 1.36 dpm/kg of $^{14}C$ and in this case would reduce the apparent terrestrial age from >45 to 30 kyr. In meteorites with younger terrestrial ages this effect is obviously less severe because alteration products are less abundant and low degrees of contamination have less effect on the terrestrial age (100 ppm of modern terrestrial carbon results in an age reduction from 15.0 to 13.8 kyr). In a recent study by Welten et al. (2004) on meteorites from the Dar al Gani region, Libya, a $^{14}C$ terrestrial age of 34.4 ± 0.9 kyr on an H4 ordinary chondrite (DaG 343) was obtained. However, both the weathering-normalized $^{36}Cl$ and the $^{41}Ca$ concentration point to a terrestrial age of ~150 kyr (with large uncertainty). This discrepancy may be due to $^{14}C$ contamination.

We believe that $^{14}C$ terrestrial ages are good approximations for residence times on Earth, but for meteorites >30 kyr they must be regarded as minimum ages because of the aforementioned possibilities of contamination. Four meteorites (8%) have no detectable $^{14}C$ (two of them after Fe-hydroxide leaching) giving ages of >45 kyr. Compared to other hot deserts, no meteorites with $^{14}C$ terrestrial age of >42 kyr are reported from the Sahara Desert, but two are reported from the western United States and two from Roosevelt County, USA (Bland et al. 1998b, 1998c; Jull et al. 1990, 1993; Welten et al. 2004). Climatic variations may also be an important factor affecting the terrestrial age distribution of meteorites. The frequency maximum of ages at 10–15 kyr corresponds to a period of dry climate similar to present-day conditions (Sanlaville 1992), which was followed by an enhanced period of monsoon activity at 9.6 kyr (Fleitmann et al. 2003). It appears possible that initial weathering under dry conditions seals pores with Fe hydroxides, slowing down further weathering and increasing the rate of survival of meteorites from certain time periods (Bland et al. 1996, 1998a). Hence, in order to understand the deficit of younger meteorites, we would have to assume that there was selective removal of younger meteorites. There is no evidence to support this observation from the available data.

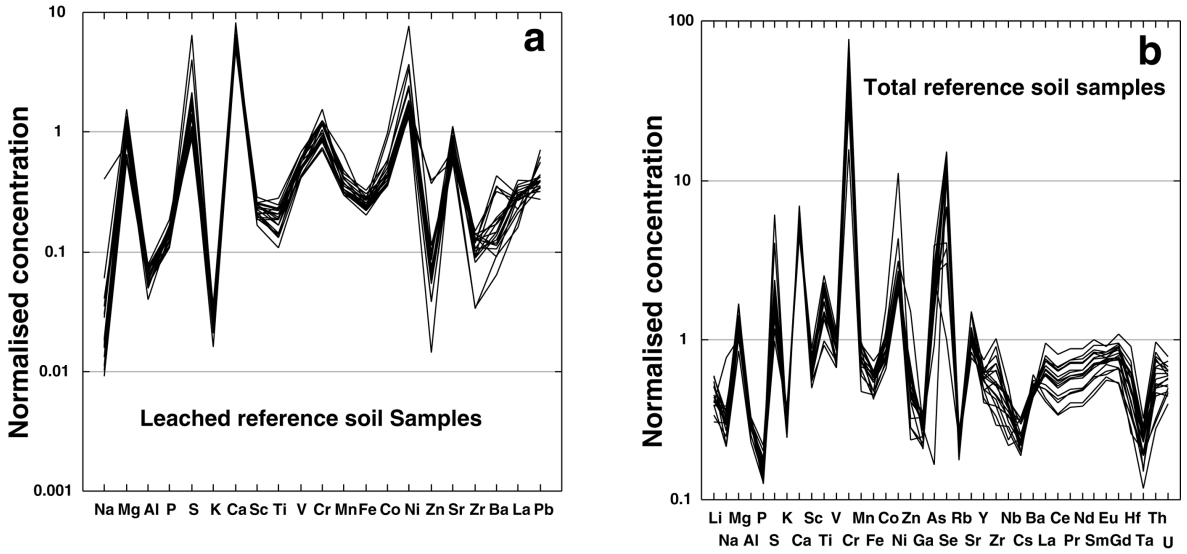


Fig. 7. a) Logarithmic plot of reference soil leachate samples normalized to mean upper continental crust values (Taylor and McLennan 1985). The reference soil samples are mainly enriched in Ca, S, and Ni, depleted in Na, K, Zn, Al, Zr, and Ba. b) Logarithmic plot of total reference soil samples normalized to mean upper continental crust values. The reference soil samples are strongly enriched in Cr, Sc, Ni, Ca, S, Ti, Mg, Sr, and depleted in Ta, P, Rb, Ga, Na, Cs, K, Fe, Sc, and Al.

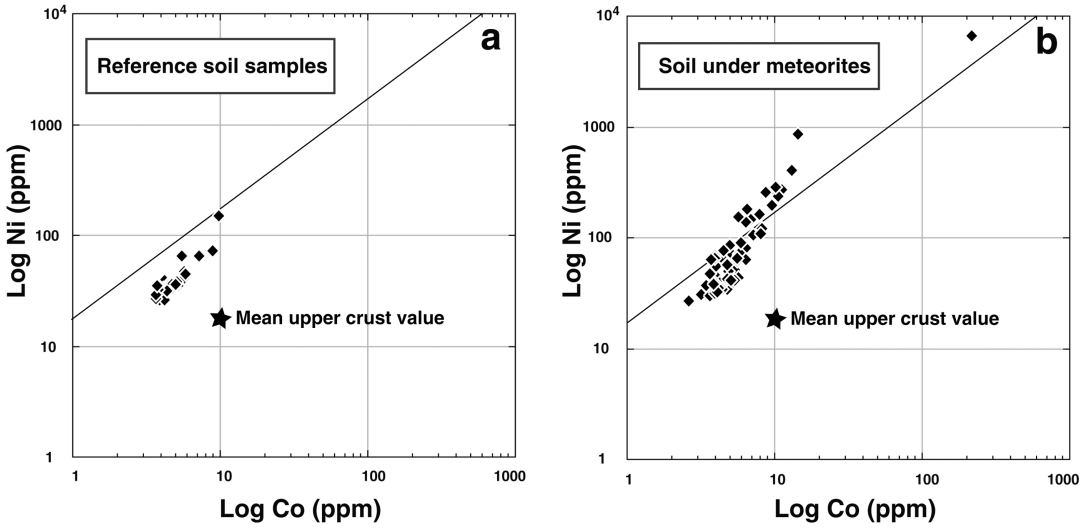


Fig. 8. Logarithmic plot of Ni versus Co content (leachates) in reference soil samples (a) and soil under meteorite samples (b) showing local strong mobilization of these elements from the meteorite to the underlying soil as a result of the weathering process. The reference line represents the chondritic Ni/Co ratio.

**Weathering of Meteorites: General**

It is likely that meteorites weather more intensely in wet and humid areas, and that the older meteorites are stronger weathered. Temperature fluctuations from summer to winter and between day and night could affect the weathering intensities. The alteration of meteorites starts as soon as they arrive on the Earth's surface due to chemical (water, air, salts), physical (temperature fluctuations, wind) and possibly biological (microbial activity) influences. The presence of water and oxygen will oxidize the metal, troilite, and hydrate the ferromagnesian minerals, leading to a volume increase of the meteorite. The complete transformation of 10 vol% iron metal (molar volume 7.12 $cm^3$), in an H chondrite to goethite (molar volume 20.76 $cm^3$) results in a volume increase of 19% (10% for L chondrites). Taking into account the complete transformation of 5.5 wt% troilite in H chondrites (6.0 in L chondrites), the total volume increase in H chondrites will be 19.8% (10.2% for L chondrites). The volume increase will be partially buffered by intergranular

Table 6. Averaged total analyses of soil under meteorite and reference soil samples, Omani interior deserts.

| Element | Unit | Method | MUC | RSS | RSS | SUM | SUM |
|---|---|---|---|---|---|---|---|
| | | | | Av. (n = 18) | Av./MUC | Av. (n = 12) | Av./MUC |
| Li | ppm | 2 | 20 | 8.9 ± 1.7 | 0.45 | 8.05 ± 0.91 | 0.4 |
| Na | % | 1 | 2.89 | 0.97 ± 0.35 | 0.34 | 0.96 ± 0.15 | 0.33 |
| Mg | % | 3 | 1.33 | 1.64 ± 0.29 | 1.24 | 1.4 ± 0.26 | 1.06 |
| Al | % | 3 | 8.04 | 2.39 ± 0.21 | 0.3 | 2.45 ± 0.30 | 0.3 |
| P | % | 3 | 0.11 | 0.02 ± 0.01 | 0.16 | 0.02 ± 0.01 | 0.14 |
| S | % | 3 | 0.026 | 0.05 ± 0.03 | 2.04 | 0.08 ± 0.14 | 3.04 |
| K | % | 3 | 2.8 | 0.92 ± 0.1 | 0.33 | 1.03 ± 0.16 | 0.37 |
| Ca | % | 3 | 3 | 15.9 ± 1.9 | 5.3 | 14.8 ± 2.6 | 4.94 |
| Sc | ppm | 1 | 11 | 7.68 ± 1.09 | 0.7 | 6.79 ± 1.28 | 0.62 |
| Ti | % | 3 | 0.3 | 0.53 ± 0.13 | 1.77 | 0.47 ± 0.14 | 1.55 |
| V | ppm | 2 | 60 | 53.1 ± 8.48 | 0.89 | 43.6 ± 11.5 | 0.73 |
| Cr | ppm | 1 | 35 | 1600 ± 571 | 45.7 | 1253 ± 676 | 36 |
| Mn | ppm | 3 | 600 | 471 ± 80 | 0.78 | 405 ± 98 | 0.67 |
| Fe | % | 1 | 3.5 | 1.98 ± 0.30 | 0.57 | 1.69 ± 0.38 | 0.48 |
| Co | ppm | 2 | 10 | 9.17 ± 2.11 | 0.92 | 9.64 ± 3.40 | 0.96 |
| Ni | ppm | 2 | 20 | 61.6 ± 41.2 | 3.08 | 126 ± 123 | 6.32 |
| Zn | ppm | 3 | 71 | 36.2 ± 19.6 | 0.51 | 33.4 ± 15.2 | 0.47 |
| Ga | ppm | 2 | 17 | 4.92 ± 0.78 | 0.29 | 4.79 ± 0.97 | 0.28 |
| As | ppm | 1 | 1.5 | 3.39 ± 1.35 | 2.26 | 2.95 ± 0.75 | 1.97 |
| Se | ppm | 2 | 0.05 | 0.49 ± 0.23 | 9.88 | 0.46 ± 0.23 | 9.21 |
| Rb | ppm | 2 | 112 | 25.1 ± 2.35 | 0.22 | 26.5 ± 2.5 | 0.24 |
| Sr | ppm | 2 | 350 | 381 ± 76.5 | 1.09 | 351 ± 111 | 1 |
| Y | ppm | 2 | 22 | 12.9 ± 1.9 | 0.57 | 11.1 ± 2.2 | 0.51 |
| Zr | ppm | 2 | 190 | 109 ± 38.3 | 0.57 | 98.3 ± 34.2 | 0.52 |
| Nb | ppm | 2 | 25 | 9.04 ± 1.94 | 0.36 | 8.13 ± 2.16 | 0.33 |
| Cs | ppm | 2 | 3.7 | 0.91 ± 0.17 | 0.25 | 0.84 ± 0.11 | 0.23 |
| Ba | ppm | 3 | 550 | 271 ± 26.2 | 0.49 | 311 ± 58.8 | 0.57 |
| La | ppm | 2 | 30 | 19.2 ± 4.23 | 0.64 | 16.4 ± 4.7 | 0.55 |
| Ce | ppm | 2 | 64 | 34.8 ± 8.0 | 0.54 | 29.3 ± 8.6 | 0.46 |
| Pr | ppm | 2 | 7.1 | 4.31 ± 0.95 | 0.61 | 3.68 ± 1.02 | 0.52 |
| Nd | ppm | 2 | 26 | 16.1 ± 3.5 | 0.62 | 13.6 ± 3.7 | 0.52 |
| Sm | ppm | 2 | 4.5 | 3.26 ± 0.67 | 0.72 | 2.77 ± 0.71 | 0.62 |
| Eu | ppm | 2 | 0.88 | 0.66 ± 0.09 | 0.75 | 0.6 ± 0.1 | 0.68 |
| Gd | ppm | 2 | 3.8 | 3.03 ± 0.56 | 0.8 | 2.65 ± 0.65 | 0.7 |
| Hf | ppm | 2 | 5.8 | 2.94 ± 0.98 | 0.51 | 2.63 ± 0.89 | 0.45 |
| Ta | ppm | 2 | 2.2 | 0.50 ± 0.12 | 0.23 | 0.46 ± 0.15 | 0.21 |
| Th | ppm | 2 | 10.7 | 6.25 ± 2.05 | 0.58 | 4.83 ± 1.9 | 0.45 |
| U | ppm | 2 | 2.8 | 1.62 ± 0.29 | 0.58 | 1.39 ± 0.36 | 0.5 |

1 = INAA.
2 = ICP-MS.
3 = ICP-OES.
MUC = Mean Earth upper continental crust values, from Taylor and McLennan (1985).
n = Number of analysis.
Av. = Average.
RSS = Reference soil samples.
SUM = Soil under meteorite.

porosity, demonstrated by Lee and Bland (2004). Based on a typical chondrite porosity of 10 vol% (Consolmagno et al. 1988), L chondrites with low porosity and most H chondrites will experience a significant bulk volume increase.

The volume increase results in the development of cracks and an appearance similar to bread crust (Fig. 2b). Widening of cracks may occur by daily temperature fluctuations combined with a mechanical infiltration of sand grains into cracks and eventually leads to the fragmentation of the meteorite (Fig. 2c). Recent work showed that thermal effects such as diurnal heating and cooling are very important in fracturing rocks in semi-arid landscapes (McFadden et al. 2005). Cracks are filled with iron oxides or hydroxides and calcite.

Omani meteorites are generally characterized by weathering grades ranging from W1 to W4 (Wlotzka 1993).

Table 7. Omani soil chromites compared with fossil meteorite chromites.

| Chromite source | RSS | Ophiolite | Extraterrestrial |
|---|---|---|---|
| Location | Oman | Oman | South Sweden |
| No. of grains | 43 | | 323 |
| $SiO_2$ | 0.13 | 0 | n.a. |
| $Cr_2O_3$ | 44.01 | 49 | 57.4 |
| $Al_2O_3$ | 23.47 | 19.9 | 5.8 |
| MgO | 12.19 | 15 | 2.5 |
| $TiO_2$ | 0.17 | 0.4 | 2.9 |
| $V_2O_5$ | n.a. | n.a. | 0.9 |
| $Fe_2O_3$ | 1.55 | n.a. | n.a. |
| FeO | 16.44 | 14.7 | 27.7 |
| MnO | 0 | 0.43 | 0.81 |
| NiO | 0.1 | n.a. | n.a. |
| ZnO | 0.16 | n.a. | 0.82 |
| CaO | 0.07 | 0.02 | n.a. |
| Total | 98.29 | 99.45 | 98.9 |

RSS = Reference soil samples.
n.a. = Not analyzed.
Extraterrestrial chromite grains from Schmitz et al. (2003).
Ophiolitic chromites from Arai et al. (2004).

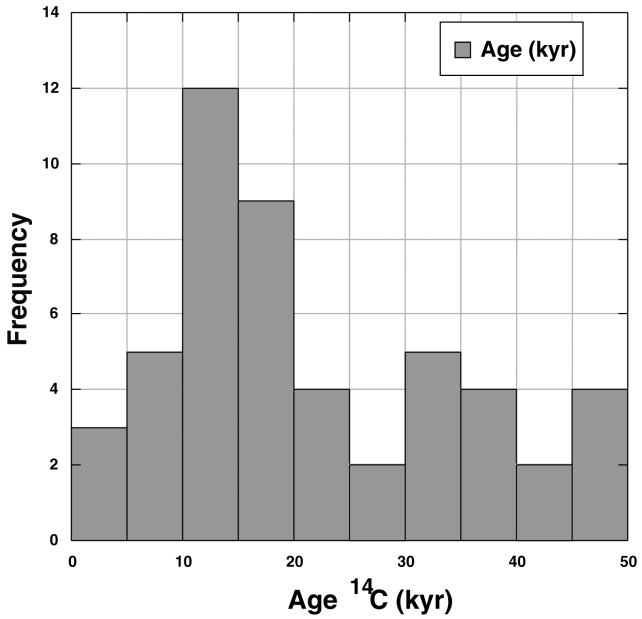


Fig. 9. Terrestrial age frequency histogram of 50 ordinary chondrites from Oman showing a peak at 10–15 kyr. The range 0–10 kyr old meteorites account for 16%, whereas 28% meteorites are older than 30 kyr. Four meteorites without detectable $^{14}$C are shown in the 45–50 kyr bar.

Interestingly, only a few W5 and no W6 meteorites were identified in Oman either by us or other classification teams (Grossman 2000; Grossman and Zipfel 2001; Russell et al. 2002, 2003, 2004), which suggests a relatively high stability of olivine and pyroxene under desert conditions. Because of the lack of weathering grades >4 even in the few samples with terrestrial ages >50 kyr, the fate of highly weathered meteorites remains unclear. Fluctuations in past climatic conditions such as the peak of Indian Ocean monsoon precipitation at about 9.6 kyr (Fleitmann et al. 2003) may explain the strong weathering (W4) of some (probably paired) Dhofar meteorites (Dho 020, 787, and 1005; Table 1) that have fallen shortly before this wet period as their terrestrial ages range from 12–12.7 kyr. Similarly, it seems possible that the abundance peak of meteorites preserved at 10–15 kyr coincides with the strongly arid period between 10 and 20 kyr (e.g., Sanlaville 1992). Factors like the details of soil-meteorite relationships (local topography, depth of burial), the climatic conditions, aeolian abrasion, age of the meteorites, the composition and porosity of the meteorites are factors likely to influence weathering. It seems that under the present climatic conditions physicochemical disintegration is one of the most important weathering factors.

**Weathering of Meteorites: Geochemistry**

The most consistent and systematic effects of meteorite weathering seen in the geochemical data are an increase of Sr, Ba, $H_2O$, and depletion of S concentrations with increasing terrestrial age (Figs. 6 and 10). The clear increase of Ba and Sr concentrations with terrestrial age (Fig. 10) can be used as a proxy for terrestrial age. Dho 807 deviates from the above observed trends, as all weathering parameters point to a younger age in contrast to the obtained >47 kyr (by repeat dating using different aliquots). Enrichment and depletion effects are observed for some other elements (Li, Zn, possibly LREE) but to a much smaller degree (Fig. 4 and Fig. 5). Our observations of the enrichment of Ba, Sr, and $H_2O$ with increasing terrestrial age of ordinary chondrites from Oman are similar to results obtained on chondrites from Açfer region, Algeria (Stelzner et al. 1999).

During weathering stages W1–W4 most of the water incorporated by meteorites is bound to iron hydroxides formed by metal oxidation. Total oxidation of 10 vol% metal in H chondrites (5 vol% in L chondrites) and of troilite (4.0 vol% in H, 4.4 vol% in L chondrites, calculated from mean S in unweathered chondrites (Mason 1967), to goethite would yield a water content of 3.64 wt% for H chondrites and 2.39 wt% for L chondrites. The maximum observed values of 3.37 wt% for H chondrites and 2.73 wt% for L chondrites are partially above calculated levels. The excess water could be within clays and phyllosilicates. A strongly weathered meteorite (W5) from the Açfer region, Algeria (Stelzner et al. 1999) has the highest water content reported for a weathered ordinary chondrite (9 wt%). This meteorite shows significant replacement of olivine and pyroxene by the phyllosilicates serpentine and/or smectite. A plot of Ba and Sr concentrations against water content (Fig. 11) shows only minor Ba and Sr enrichment up to 2 wt% water, followed by a stronger absorption trend for samples with >2 wt% water. This

Table 8. Statistics of Omani terrestrial ages compared with data from other hot deserts and Allan Hills, Antarctica (all ordinary chondrites).

| Location | Reference | n | Median | Mean | St. dev. | Range | % 0–10 kyr | % >30 kyr |
|---|---|---|---|---|---|---|---|---|
| HaH, Libya | Jull et al. 1990 | 13 | 5.4 | 8.3 | 8.7 | 3.5 to 35 | 84.6 | 7.7 |
| Nullarbor, Australia | Bland et al. 1998, 2000 | 36 | 6.4 | 12.2 | 11.7 | 0.7 to 33.4 | 58.3 | 11.1 |
| Açfer, Algeria | Bland et al. 1998 | 51 | 10.3 | 11.6 | 8.6 | 0.67 to 42.4 | 49 | 3.9 |
| Western USA | Jull et al. 1993 | 27 | 11.6 | 15.8 | 13.8 | 0 to >47.5 | 44.4 | 18.5 |
| Dar al Gani, Libya | Welten et al. 2004 | 17 | 14.8 | 14.4 | 9.7 | 2.5 to >31 | 41.2 | 5.9 |
| Oman | This study | 50 | 17.9 | 21.5 | 13 | 2 to >49 | 16 | 28 |
| Allan Hills, Antarctica | Jull et al. 1998 | 72 | 26.2 | 23.9 | 13.5 | 0.3 to 48 | 22.2 | 43.1 |
| Roosevelt County, USA | Bland et al. 1998 | 18 | 26.3 | 27.2 | 11.1 | 7.0 to >46.0 | 11.1 | 38.9 |

Table 9. A comparison of weathering grades of Omani ordinary chondrites.

| | Omani OC[a] | This study OC[b] | Dated samples |
|---|---|---|---|
| n | 1264 | 263 | 50 |
| | % | % | % |
| W0 | 0.4 | 0 | 2 |
| W1 | 4.5 | 2.7 | 8 |
| W2 | 15.9 | 15.6 | 26 |
| W3 | 46.5 | 40.3 | 24 |
| W4 | 32.7 | 41.4 | 40 |

[a]From The Meteoritical Bulletin, No. 84–88.
[b]Omani-Swiss meteorite search campaigns 2001–2003.

indicates that initially weathering is restricted to Fe-Ni metal, while troilite remains fresh to only partially weathered. Only during advanced weathering is troilite oxidized (metal is completely to strongly weathered) (Table 1 and Fig. 12) resulting in a release of sulfur which reacts with Ba and Sr derived from the soil porewater to form barite and celestine of low solubility (Figs. 3b, 3c, and 3d). This is supported by the occurrence of barite, celestine, and anhydrite crystals in fractures and holes filled by iron oxides/hydroxides and calcite. Also barite is reported from a number of weathered meteorites from Sahara (Bischoff and Geiger 1995).

### Correlation of Weathering Parameters with $^{14}C$ Age

Norton (2000) compared weathering grades with the terrestrial ages of meteorites collected from Roosevelt County, New Mexico (Wlotzka et al. 1995), and came up with the following relationship: W2: 0.5–15 kyr; W3: 15–30 kyr; W4: 20–35 kyr; W5 and W6 30 to >45 kyr. In comparison, the meteorites from our Omani collection show a similar increase in the degree of weathering with age, but with some significant differences. We found that meteorites with weathering grades W3 and W4 have terrestrial ages of >30 kyr (Table 1). In contrast, some young meteorites (12–16 kyr) also show weathering grades of W4. One possible explanation for this behavior could be the temporary burial of the meteorite in the subsoil, where higher humidity and higher salt contents may result in a more intense alteration of metal and troilite relative to meteorites remaining on the surface. Another influence is the morphology of the surface; meteorites lying in small depressions where water ponds during heavy showers and salts accumulate after evaporation show more rapid rates of weathering. This may cause meteorites from the same fall to have variable weathering grades, as observed in the SaU 001 and JaH 073 strewn fields. Similar observations are reported from the Dar al Gani meteorite field, Libyan Sahara (Schlüter et al. 2002).

Weathering of ordinary chondrites in Oman follows two steps: a rapid initial oxidation followed by a steady rate of weathering, since most metal in the meteorites is completely altered at ~20 kyr (Fig. 13). Mössbauer determination of oxidation of H, L (LL) ordinary chondrites (Bland et al. 1996), from the Daraj locality of the Libyan Sahara; the Nullarbor region of Australia, and Roosevelt County, New Mexico, USA, show a similar rapid initial oxidation followed by a more gradual weathering. These authors proposed that a new meteorite fall arriving on Earth weathers rapidly owing to its high initial porosity. Newly formed weathering products from the oxidation of Fe-Ni metal, troilite, and ferromagnesian silicates block the pores, thus reducing the ability of water to penetrate the sample and consequently make further degradation slower. For the initial step, our results agree with this explanation, but for the second step our observations in Oman show that metal is completely altered in most meteorites with a terrestrial age ≥20 kyr. However, slow weathering will continue as a result of the alteration of troilite and ferromagnesian silicates (not observed in this study) and due to physical weathering under the influence of climate.

### Soil Geochemistry and Heavy Minerals

Our data demonstrate that the chemistry of soils is very homogeneous throughout the meteorite collection areas in central Oman so that the influence of soil chemistry on meteorite weathering can be taken as constant for all meteorites recovered.

The high Cr and Ni concentrations observed in reference soils from various regions of the Oman Desert, relative to the upper continental crust, are due to the presence of detritus from the Semail ophiolite located to the northeast of the searched regions. The high Cr (Table 7) concentrations are

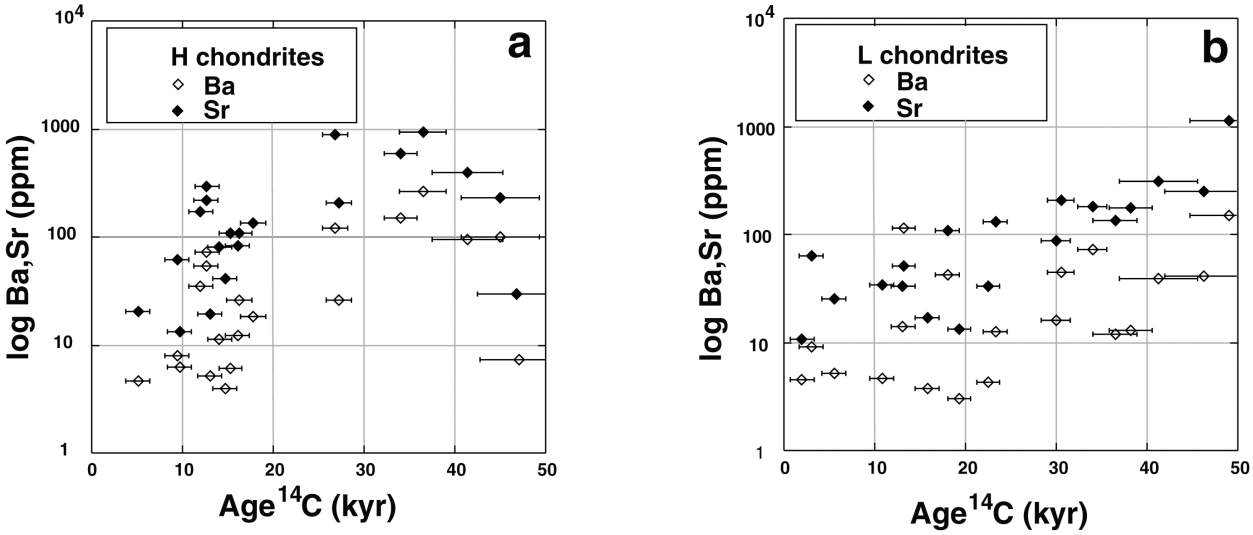


Fig. 10. a) Logarithmic plot of Ba and Sr concentrations in H (a) and L chondrites (b) versus terrestrial age indicating an increase in Ba and Sr content with increasing terrestrial age. Note that the H chondrites show a steeper slope than the L chondrites.

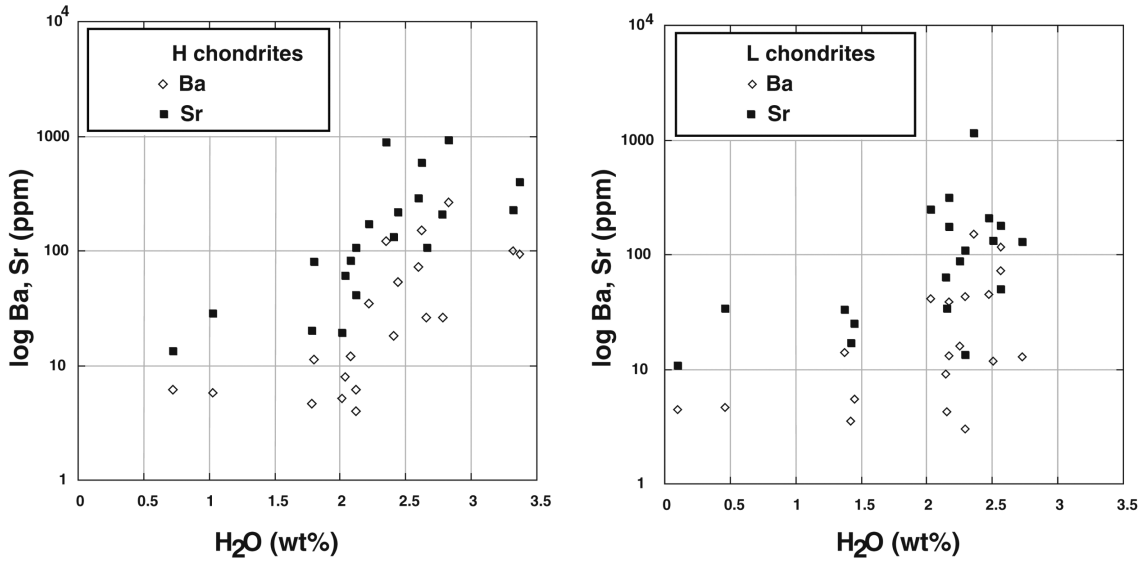


Fig. 11. Logarithmic plots of Ba and Sr versus water content in H (a) and L chondrites (b). Both H and L chondrites show an initial weak absorption of Ba and Sr followed by a steeper absorption trend beginning at ~2 wt% water. This indicates that sulfide alteration is the driving force for Ba and Sr uptake.

correlated with the presence of ophiolitic mantle chromite (Arai et al. 2004). A further argument for a detrital origin is the gradual decrease of Cr and Ni concentrations in soil with increasing distance to the alluvial fans rich in ophiolitic rocks derived from the Oman Mountains.

## CONCLUSIONS

The effects of weathering on ordinary chondrites collected in the central deserts of Oman are comparable with results obtained on meteorites from other hot desert environments (Jull et al. 1993; Bland et al. 1996; Stelzner et al. 1999). Initial fast oxidation of iron metal is followed by more gradual oxidation of troilite. No weathering grades exceeding W4 were observed, indicating a considerable stability of pyroxene and olivine in this desert environment. We believe that fragmentation is a result of the combined effects of volume increase, diurnal thermal cycling, and infiltration of soil material into cracks due to wind and water. Geochemically, the major influences of weathering are an accumulation of Sr, Ba, and $H_2O$, and a loss of S. Soils under meteorites are contaminated with Ni and Co, Ni/Co ratios higher than chondritic values indicate a higher mobility of Ni.

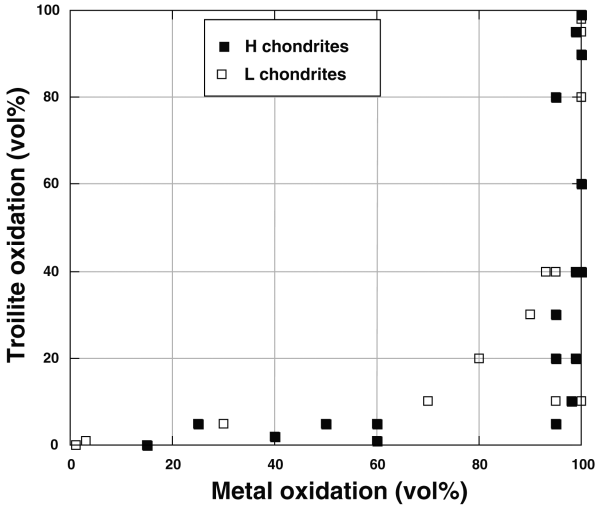


Fig. 12. Metal oxidation against troilite oxidation estimated using reflected light microscopy. The plot demonstrates that the oxidation of troilite is slower than that of metal, and troilite oxidation only goes to completeness after total oxidation of metal.

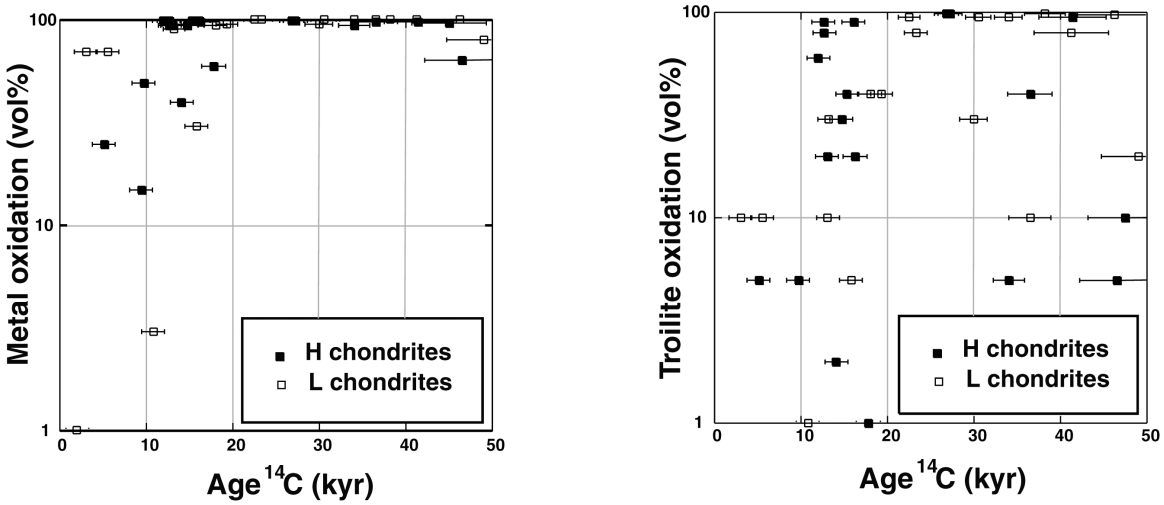


Fig. 13. a) Percentage (vol%) of metal oxidation in H and L chondrites versus terrestrial age showing complete iron metal oxidation within 20 kyr. b) percentage (vol%) of troilite oxidation in H and L chondrites versus terrestrial age. The trend is similar to the metal oxidation but the degree of oxidation is more variable and oxidation remains incomplete in many samples up to 50 kyr.

The changes observed in mineralogy and chemistry as a function of terrestrial age are consistent with a weathering process controlled by a combination of rapid iron metal oxidation and slow troilite oxidation. Fast iron metal oxidation is correlated with rapid rates of water absorption. The slower oxidation of troilite releases sulfate, allowing the steady precipitation of Ba and Sr sulfates over time. Thus, relative to water absorption, Ba and Sr uptake is initially slow. The initially rapid cementation of pores with iron hydroxides, followed by a more gradual weathering process, results in a general decrease of weathering rates over time. However, the rate of purely physical weathering will remain constant.

As soils from the interior Oman Desert are very homogeneous in bulk chemistry, the influence of soil geochemistry on meteorite weathering can therefore be assumed to be nearly constant over the whole study area. The local surface topography (hard/soft soil, depressions, and small hills) has an influence on the weathering of meteorites. This is evidenced by different degrees of weathering observed in individuals from a single meteorite fall. High Cr and Ni concentrations in soils are derived from the Semail ophiolite in the Oman Mountains.

*Acknowledgments*–Dr. Hilal Al Azri, Ministry of Commerce and Industry, Muscat, and Akram Al Muraza, Khalid Musallam Al Rawas, and Sami Al Zubaidi, Ministry of Commerce and Industry, Salalah, are thanked for their support during the project. Ruth Mäder, Manuel Eggimann, and Jeff

Johnson are thanked for analytical support. K. Welten, P. Bland, and M. Lee are acknowledged for their revision and important comments. This study was supported by the Swiss National Science Foundation (grant 2100-064929), the United States National Science Foundation (grant EAR01-15488) and the National Aeronautics and Space Administration (grant NAG5-11979).

*Editorial Handling*—Dr. Ian Franchi

## REFERENCES

Arai S., Uesugi J., and Ahmed A. H. 2004. Upper crustal podiform chromitite from the northern Oman ophiolite as the stratigraphically shallowest chromite in ophiolite and its implication for Cr concentration. *Contributions to Mineralogy and Petrology* 147:145–154.

Bischoff A. and Geiger T. 1995. Meteorites from the Sahara: Find locations, shock classification, degree of weathering, and pairing. *Meteoritics* 30:113–122.

Bland P. A., Berry F. J., Smith T. B., Skinener S. J., and Pillinger C. T. 1996. The flux of meteorites to the Earth and weathering in hot desert ordinary chondrite finds. *Geochimica et Cosmochimica Acta* 60:2053–2059.

Bland P. A., Berry F. J., and Pillinger C. T. 1998a. Rapid weathering in Holbrook: An iron-57 Mössbauer spectroscopy study. *Meteoritics & Planetary Science* 33:127–129.

Bland P. A., Coway A., Smith T. B., Berry F. J., Swabey S. E. J., and Pillinger C. T. 1998b. Calculating flux from meteorite decay rates: A discussion of problems encountered in deciphering a $10^5$–$10^6$ year integrated meteorite flux at Allan Hills and a new approach to pairing. In *Meteorites: Flux with time and impact effects,* edited by Grady M. M., Hutchinson R., McCall G. J. H., and Rothery D. A. London: The Geological Society. pp. 43–58.

Bland P. A., Sexton A. S., Jull A. J. T., Bevan A. W. R., Berry F. J., Thornley D. M., Astin T. R., Britt D. T., and Pillinger C. T. 1998c. Climate and rock weathering: A study of terrestrial age dated ordinary chondritic meteorites from hot desert regions. *Geochimica et Cosmochimica Acta* 62:3169–3184.

Bland P. A. and Bevan A. W. R. 2000. Ancient meteorite finds and the Earth's surface environment. *Quaternary Research* 53:131–142.

Burns S. J., Fleitmann D., Matter A., Neff U., and Mangini A. 2001. Speleothem evidence from Oman for continental pluvial events during interglacial periods. *Geology* 29:623–626.

Bydoun Z. R. 1966. Geology of the Arabian peninsula, eastern Aden protectorate, and part of Dhofar. USGS Professional Paper #560. pp. 1–49.

Chevrel S., Berthiaux A., Platel J. P., and Roger J. 1992. Explanatory notes to geological map of Shişr. Sheet NF 39-08, scale 1: 250,000. Muscat, Oman: Ministry of Petroleum and Minerals.

Consolmagno G. J., Britt D. T. and Stoll C. P. 1988. The porosities of ordinary chondrites: Models and interpretation. *Meteoritics & Planetary Science* 33:1221–1229.

Cornish L. and Doyle A. 1984. Use of ethanolmine thioglycollate in the conservation of pyritized fossils. *Palaeontology* 27:421–424.

Faust G. T., Fahey J. J., Mason B., and Dwornik E. J. 1969. Pecoraite, $Ni_6Si_4O_{10}(OH)_8$, nickel analog of clinochrysotile, formed in the Wolf Creek meteorite. *Science* 165:59–60.

Ferko T. E., Wang M.-S., Hillegonds D. J., Lipschutz M. E., Hutchison R., Franke L., Scherer P., Schultz L., Benoit P. H., Sears D. W. G., Singhvi A. K., and Bhandari N. 2002. The irradiation history of the Ghubara (L5) regolith breccia. *Meteoritics & Planetary Science* 37:311–327.

Fleitmann D., Burns S. J., Mudelsee M., Neff U., Kramers J., Mangini A., and Matter A. 2003. Holocene forcing of the Indian monsoon recorded in a stalagmite from southern Oman. *Science* 300:1737–1739.

Fleitmann D., Burns S. J., Neff U., Mudelsee M., Mangini A., and Matter A. 2004. Palaeoclimatic interpretations of high-resolution oxygen isotope derived from annually laminated speleothems from southern Oman. *Quaternary Science Reviews* 23:935–945.

Franchi I. A., Delisle G., Jull A. J. T., Hutchison R., and Pillinger C. T. 1995. An evaluation of the meteorite potential of the Jiddat al Harasis and the Rub al Khali regions of southern Arabia. LPI Technical Report #95-02. pp. 29–30.

Friedrich J. M., Wang M.-S., and Lipschutz M. E. 2003. Chemical studies of L chondrites. V: Compositional patterns for 49 trace elements in 14 L4–6 and 7 LL4–6 falls. *Geochimica et Cosmochimica Acta* 67:2467–2479.

Gnos E., Hofmann B., Franchi I. A., Al-Kathiri A., Hauser M., and Moser L. 2000. Sayh al Uhaymir 094: A new martian meteorite from the Oman Desert. *Meteoritics & Planetary Science* 37:835–854.

Gnos E., Hofmann B., Al-Kathiri A., Lorenzetti S., Eugster O., Whitehouse M. J., Villa I. M., Jull A. J. T., Eikenberg J., Spettel B., Krähenbühl U., Franchi I. A., and Greenwood R. C. 2004. Pinpointing the source of a lunar meteorite: Implications for the evolution of the moon. *Science* 305:657–659.

Goddard E. N., Trask P. D., De Ford R. K., Rove O. N., Singewald J. T., Jr., and Overbeck R. M. 1948. Rock-color chart. Boulder, Colorado: Geological Society of America. 11 p.

Grossman J. N. 2000. The Meteoritical Bulletin, No. 84. *Meteoritics & Planetary Science* 35:A199–A225.

Grossman J. N. and Zipfel J. 2001. The Meteoritical Bulletin, No. 85. *Meteoritics & Planetary Science* 36:A293–A322.

Hofmann B. A., Nyström J. O., and Krähenbühl U. 2000. The Ordovician chondrite from Brunflo, central Sweden III. Geochemistry of terrestrial alteration. *Lithos* 50:305–324.

Hughes-Clarke M. W. 1988. Stratigraphy and rock unit nomenclature in the oil-producing area of interior Oman. *Journal of Petroleum Geology* 11:5–60.

Jull A. J. T., Donahue D. J., and Linick T. W. 1989. Carbon-14 activities in recently fallen meteorites and Antarctic meteorites. *Geochimica et Cosmochimica Acta* 53:2095–2100.

Jull A. J. T., Wlotzka F., Palme H., and Donahue D. J. 1990. Distribution of terrestrial age and petrologic type of meteorites from western Libya. *Geochimica et Cosmochimica Acta* 54: 2895–2898.

Jull A. J. T., Donahue D. J., Cielaszyk E., and Wlotzka F. 1993. Carbon-14 terrestrial ages and weathering of 27 meteorites from the southern High Plains and adjacent areas (USA). *Meteoritics* 28:188–195.

Jull A. J. T., Cloudt S., and Cielaszyk E. 1998. $^{14}C$ terrestrial ages of meteorites from Victoria Land, Antarctica, and the infall rates of meteorites. In *Meteorites: Flux with time and impact effects,* edited by Grady M. M., Hutchison R., McCall G. J. H., and Rothery D. A. London: The Geological Society. pp. 75–91.

Jull A. J. T. 2001. Terrestrial ages of meteorites. In *Accretion of extraterrestrial matter throughout Earth's history,* edited by Schmitz B. and Peuker-Ehrenbrin B. New York: Kluwer Academic/Plenum Publishers. pp. 241–266.

Kallemeyn G. W., Rubin A. E., Wang D., and Wasson J. T. 1989. Ordinary chondrites: Bulk compositions, classification, lithophile-element fractionations, and composition-petrographic type relationships. *Geochimica et Cosmochimica Acta* 53:2747–2767.

Le Métour J., Michel J. C., Béchennec F., Platel J. P., and Roger J. 1995. *Geology and mineral wealth of the Sultanate of Oman*. Muscat, Oman: Ministry of Petroleum and Minerals. pp. 1–285.

Lee M. R. and Bland P. A. 2004. Mechanisms of weathering of meteorites recovered from hot and cold deserts and the formation of phyllosilicates. *Geochimica et Cosmochimica Acta* 68:893–916.

Mason B. 1967. Extraterrestrial mineralogy. *American Mineralogist* 52:307–325.

Mason B. 1971. *Handbook of elemental abundance in meteorites.* New York: Gordon and Breach. 555 p.

McFadden L. D., Eppes M. C., Gillespie A. R., and Hallet B. 2005. Physical weathering in arid landscapes due to diurnal variation in the direction of solar heating. *Geological Society of America Bulletin* 117:161–173.

Nishiizumi K. and Caffee M. W. 2001. Exposure histories of lunar meteorites Dhofar 025, 026, and Northwest Africa 482 (abstract). *Meteoritics & Planetary Science* 36:148–149.

Nishiizumi K., Okazaki R., Park J., Nagao K., Masarik J., and Finkel R. C. 2002. Exposure and terrestrial history of Dhofar 019 Martian meteorite (abstract #1366). 33rd Lunar and Planetary Science Conference. CD-ROM.

Norton O. R. 2002. *The Cambridge encyclopedia of meteorites.* Cambridge: Cambridge University Press. 354 p.

Platel J. P. and Berthiaux A. 1992a. Explanatory notes to geological map of Al ‘Ayn (Muqshin). Sheet NF 40-01, scale 1:250,000. Muscat, Oman: Ministry of Petroleum and Minerals.

Platel J. P. and Berthiaux A. 1992b. Explanatory notes to geological map of Hayma. Sheet NF 40-02, scale: 1:250,000. Muscat, Oman: Ministry of Petroleum and Minerals.

Platel J. P., Berthiaux A., Roger J. and Chevrel S. 1992. Explanatory notes to geological map of Shalim. Sheet NF 40-06. Muscat, Oman: Ministry of Petroleum and Minerals.

Russell S. S., Zipfel J., Grossman J. N., and Grady M. M. 2002. The Meteoritical Bulletin, No. 86. *Meteoritics & Planetary Science* 37:A157–A184.

Russell S. S., Zipfel J., Folco L., Jones R., Grady M. M., Zolensky M. E., McCoy T., and Grossman J. N. 2003. The Meteoritical Bulletin, No. 87. *Meteoritics & Planetary Science* 38:A189–A248.

Russell S. S., Folco L., Grady M. M., Zolensky M. E., Jones R., Righter K., Zipfel J., and Grossman J. N. 2004. The Meteoritical Bulletin, No. 88. *Meteoritics & Planetary Science* 39:A215–A272.

Sanlaville P. 1992. Changements climatiques dans la Péninsule Arabique durant le Pléistocène supérieur et l’Holocène. *Paléorient* 181:5–26.

Schlüter J., Schultz L., Thiedig B., Al-Mahdi B. O., and Abu Aghreb A. E. 2002. The Dar al Gani meteorite field (Libyan Sahara): geological setting, pairing of meteorites, and recovery density. *Meteoritics & Planetary Science* 37:1079–1093.

Schmitz B., Tassinari M. and Peuker-Ehrenbrink B. 2001. A rain of ordinary chondritic meteorites in the Early Ordovician. *Earth and Planetary Science Letters* 194:1–15.

Schmitz B., Häggström T., and Tassinari M. 2003. Sediment-dispersed extraterrestrial chromite traces a major asteroid disruption event. *Science* 300:961–964.

Stelzner T., Heide K., Bischoff A., Weber D., Scherer P., Schultz L., Happel M., Schrön W., Neupert U., Michel R., Clayton R. N., Mayeda T. K., Bonani G., Haidas I., Ivy-Ochs S., and Suter M. 1999. An interdisciplinary study of weathering effects in ordinary chondrites from the Açfer region, Algeria. *Meteoritics & Planetary Science* 34:787–794.

Taylor S. R. and McLennan S. M. 1985. *The continental crust: Its composition and evolution.* Oxford: Blackwell Scientific Publications. 328 p.

Welten K. C. 1999. Concentrations of siderophile elements in nonmagnetic fractions of Antarctic H and L chondrites: A quantitative approach on weathering effects. *Meteoritics & Planetary Science* 34:259–270.

Welten K. C., Nishiizumi K., Finkel R. C., Hillegonds D. J., Jull A. J. T., Franke L., and Schultz L. 2004. Exposure history and terrestrial ages of ordinary chondrites from the Dar al Gani region, Libya. *Meteoritics & Planetary Science* 39:481–498.

Wlotzka F. 1993. A Weathering scale for the ordinary chondrites (abstract). *Meteoritics* 28:460.

Wlotzka F., Jull A. J. T., and Donahue D. J. 1995. Carbon-14 terrestrial ages of meteorites from Açfer, Algeria. LPI Technical Report #95-02. pp. 72–73.


Image of the Shisr 043 iron meteorite in place of find. The number on the label is the field number.

# Shisr 043 (IIIAB medium octahedrite): The first iron meteorite from the Oman desert

A. Al-Kathiri[1, 2]*, B. A. Hofmann[3], E. Gnos[1], O. Eugster[4], K. C. Welten[5] and U. Krähenbühl[6]

[1]Institut für Geologie, Universität Bern, Baltzerstrasse 1, CH-3012 Bern, Switzerland
[2]Directorate General of Commerce and Industry, Ministry of Commerce and Industry, Salalah, Sultanate of Oman
[3]Naturhistorisches Museum der Burgergemeinde Bern, Bernastrasse 15, CH-3005 Bern, Switzerland.
[4]Physikalisches Institut, Abteilung für Weltraumforschung und Planetologie, Universität Bern, Sidlerstrasse 5, CH-3012 Bern, Switzerland
[5]Space Science Laboratory, 7 Gauss Way, University of California, Berkeley, CA 94720-7450, USA
[6]Departement für Chemie und Biochemie, Universität Bern, Freiestrasse 3, CH-3012 Bern, Switzerland
*Corresponding author. E-mail: alikath@geo.unibe.ch

**Abstract**— The iron meteorite Shisr 043 is a single mass of 8267g found in the south Oman desert 42 km NE of the Shisr village. It is the first iron identified among the >1400 individual meteorites reported from Oman. The meteorite is a slightly elongated mass showing only minor rusting, partially smooth, partially rough surface with octahedral cleavage, and partially preserved metallic fusion crust typically 0.75 mm thick.

The undeformed Widmanstätten pattern with a mean kamacite bandwidth of 1.0 ± 0.1 mm (n = 97) indicates structural classification as a medium octahedrite. From the bulk composition, Ni = 8.06 wt%, Ga = 18.8 ppm, Ge = 37.25 ppm, and Ir = 3.92 ppm, the meteorite is classified as IIIAB, the most common group of iron meteorites. The cosmic-ray exposure (CRE) age based on $^{3}$He, $^{21}$Ne, $^{38}$Ar concentrations and $^{10}$Be-$^{21}$Ne, $^{26}$Al-$^{21}$Ne and $^{36}$Cl-$^{36}$Ar ratios is 290 ± 20 Ma. This age falls within the range observed for type IIIAB iron meteorites, but does not coincide with the main cluster. The cosmogenic noble gas and radionuclide data indicate that Shisr 043 had a relatively small pre-atmospheric mass. The low degree of weathering is consistent with a young terrestrial age of <10,000 years based on the saturated $^{41}$Ca concentration. Shisr 043 is not paired with any of the other eight known iron meteorites from the Arabian Peninsula.

## INTRODUCTION

Iron meteorites comprise about 5% of falls (Grady 2000; McSween 1999; Norton 2002) but are underrepresented in hot and cold desert finds: irons represent 1.3% of Antarctic finds (Bevan et al. 1998) and 0.4% in the Dar al Gani area, Libya (Schlüter et al. 2002). Despite of the large number of meteorite finds in Oman since 1999 and the relatively high fraction of rare types such as lunar and martian achondrites (Grossman 2000; Grossman and Zipfel 2001; Russell et al., 2002, 2003, 2004, 2005), Shisr 043 is the only iron meteorite among >1400 finds reported from Oman during 2000-2005 (or 0.07%). Shisr 043 was recovered during a joint Omani-Swiss meteorite search program initiated in 2001 which involves geologists from Bern, Switzerland (University of Bern and Natural History Museum Bern), and the Ministry of Commerce and Industry, Sultanate of Oman. During this search program, samples from more than 260 individual meteorite falls were

recovered (Al-Kathiri et al. 2005). A closer characterization of Shisr 043 was initiated because of the under-representation of irons in Oman while several irons are known from Saudi Arabia; therefore, testing for possible pairing appeared important.

## SAMPLES AND METHODS

After recovery the iron mass was cleaned with pressurized air and two parallel cuts were made after fixation of rust with cyanomethacrylate. The end piece (90x50x10 mm, 326.1 g) was etched while sub-samples from the slice (95x50x6 mm, 172.0 g) were used for subsequent analyses. Weathering-related materials were collected immediately adherent to the meteorite (coarse oxide flakes, fine oxide flakes, magnetic and nonmagnetic soil fraction). In addition, two types of bulk soil samples were collected: I) a sample of soil under the meteorite (SUM), II) a reference soil sample (RSS), taken from the top 5 cm at a distance of about 10 m from the meteorite. Soil samples were sieved to obtain the fractions <0.15 mm which was analyzed.

Chemical analyses of fresh metal were performed at several laboratories using the following methods: Inductively Coupled Plasma Emission Spectroscopy (ICP-OES) was performed at the Department for Chemistry and Biochemistry, University of Bern; Instrumental Neutron Activation Analysis (INAA) and Inductively Coupled Plasma Mass Spectrometry (ICP-MS) were performed commercially at Activation Laboratories Ltd., Ancaster, Ontario, Canada; X-ray fluorescence (XRF) analyses were obtained nondestructively on polished sections at the Institute of Geology, University of Fribourg, Switzerland, using a Philips PW 2400 spectrometer and the semi-quantitative program Uniquant 5.

A freshly cut and polished surface of the meteorite was etched with nitric acid (3% in ethanol) to develop the Widmanstätten pattern (Fig. 1a). The average kamacite bandwidth was measured using the software "NIH image" on digital images obtained from the etched section.

Noble gas analyses of a sample of 52.45 mg were performed at the Physics Institute of the University of Bern. The sample was heated in vacuum at 90°C for several days in the storage arm of the extraction system to reduce adsorbed atmospheric gases. The noble gases were extracted by RF-heating in a single step at 1700°C in a Mo crucible. Completeness of the gas release was checked by adding a final step at 1740°C. The mass spectrometric analyses and background corrections were performed according to the description by Eugster et al. (1993) using our system B. The following blanks were subtracted (units of $10^{-8}$cm$^3$STP/g): $^3$He <0.00004, $^4$He = 0.02, $^{20}$Ne = 0.0008, $^{40}$Ar = 0.4. The errors given correspond to a 95% confidence level.

A sample of ~98 mg was ultrasonically agitated in 0.2 N HCl to dissolve possible troilite inclusions. The purified metal sample of 97.7 mg was dissolved in 1.5 N $HNO_3$, along with a carrier solution containing Be, Al, Cl, Ca and Mn. After taking an aliquot for chemical analysis by atomic absorption spectrometry, Cl was isolated as AgCl. Be, Al and Ca were separated by anion exchange chromatography, acetylacetone solvent extraction, and cation exchange chromatography techniques described in Lavielle et al. (1999). The separated fractions of Be, Al, Cl and Ca were further purified and converted to BeO, $Al_2O_3$, AgCl and $CaF_2$ for AMS measurements. The ratios of $^{10}$Be/Be, $^{26}$Al/Al and $^{41}$Ca/Ca were determined using the Lawrence Livermore National Laboratory AMS facility (Roberts et al. 1997). After making corrections for background and chemical blanks, the measured ratios were normalized to AMS standards (Nishiizumi

2004; Nishiizumi et al. 1984, 2000; Sharma et al. 1990).

The microhardness of the meteorite was measured on polished sections using a reflected light microscope (Leitz Durimet 2) equipped with a Vickers hardness probe and a 100g weight. Six profiles were measured perpendicular to the different natural surface types (Fig. 1b). In order to check the quality of our hardness measurements hardness profiles were measured on a polished standard metal with a known hardness of HV 585 (100g wt.) and on two meteorites with homogeneous hardness, the IA Odessa and IIB São Julião de Moreira (Buchwald 1975).

Sieved soil samples were analyzed without further treatment by ICP-OES following aqua regia extraction (Activation Laboratories Ltd., Ancaster, Ontario, Canada). For bulk chemistry, weathered oxide crust adherent to the meteorite, magnetic and nonmagnetic soil fraction, SUM and RSS samples were ground in an agate mill and five grams of each sample were submitted for analysis by ICP-MS to Activation Laboratories Ltd., Ancaster, Ontario, Canada.

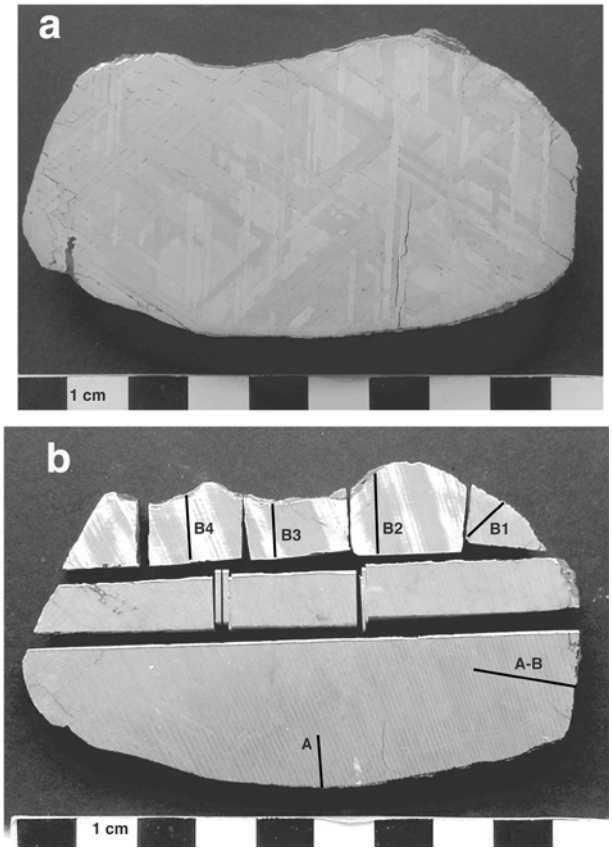


Fig. 1. Cut slabs: a) Etched end-piece displaying typical Widmanstätten pattern. Fracturing parallel to kamacite bands is common. Partially corroded troilite inclusion at lower left. Note the heat-affected zone at the lower edge of the sample. b) Section indicating the position of microhardness profiles shown in figure 4. All samples for analyses were obtained from the central part of the narrow bar. Striation is a cutting artifact.

## RESULTS

### Field Observations and Macroscopic Description of the Surface

Shisr 043 was found on January 21, 2003 in the south Oman desert (18° 35.546'N, 53° 48.748'E), 42 km NE of Shisr village. The meteorite was found on sub-recent alluvial fan material of Quaternary, 1.6 Ma to present age (Chevrel et al. 1992). The sediments largely consist of fine-grained silty to sandy material with some unsorted, but well-rounded clasts of hard bioclastic limestone derived from the Dammam Formation of Eocene age (Chevrel et al. 1992). Few quartz geodes are locally found likely to be derived from the Late Paleocene-Eocene Umm er Radhuma Formation, which is mainly composed of carbonates.

About two thirds of the meteorite were buried in the soil when it was found (Fig. 2c). The exposed part appears smooth and shiny with a dark brown color. The buried part is covered by reddish brown, flaky rust, and locally by a calcite crust, especially in the upper 3 cm below the surface.

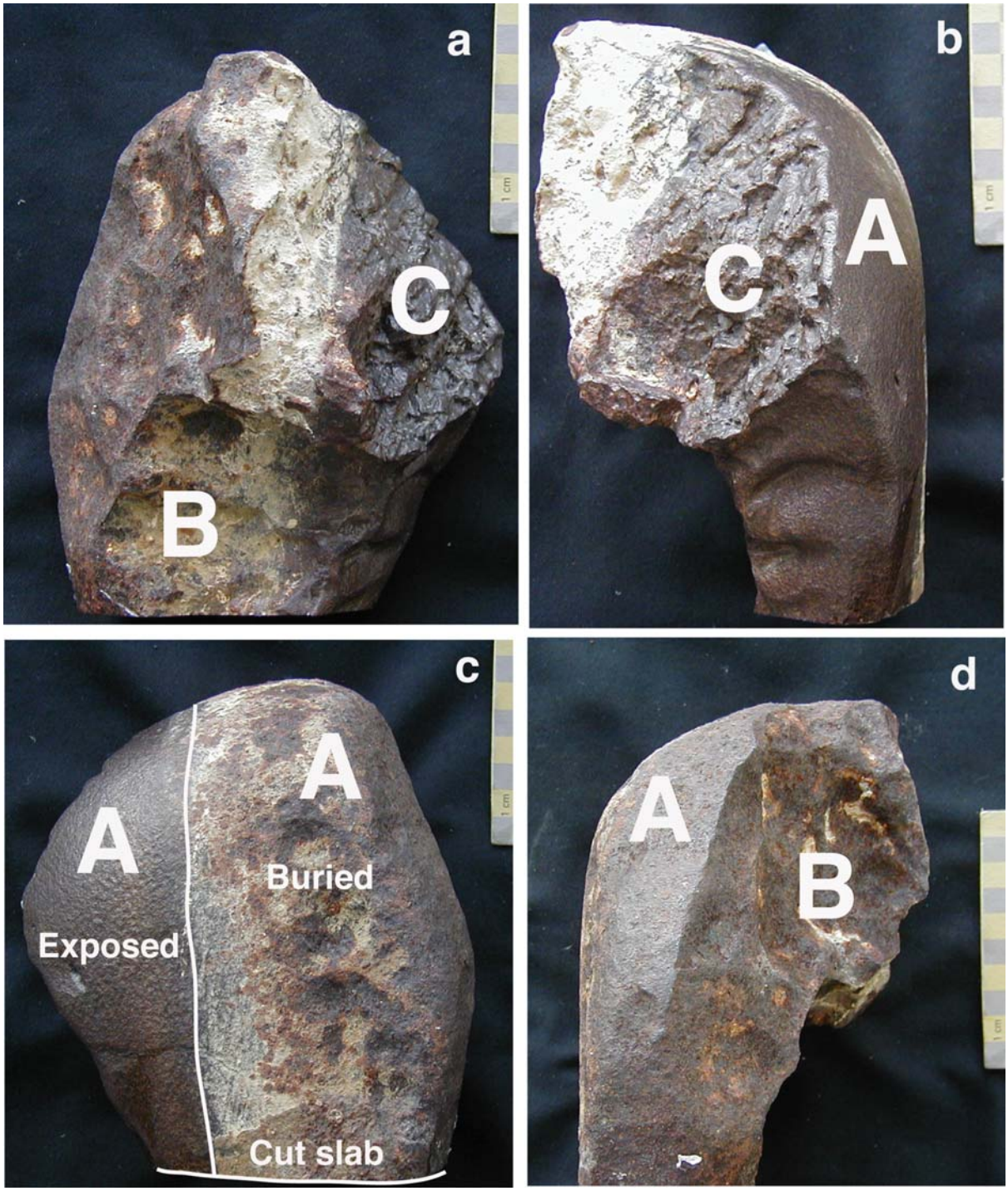


Fig. 2. Different views of Shisr 043 illustrating the differences in surface types (A-C). Note that about two thirds of the meteorite were buried in the soil as visible in A and C. The line at the bottom of 2C indicates the location of the etched slab and also used for hardness measurements.

Shisr 043 is of irregular shape with maximum dimensions of 19x14.5x5-10 cm. The single mass had a total weight of 8267g prior to cutting. An additional 140 g of magnetic oxide was recovered from the immediate surroundings. Three meteorite surface types can be distinguished (Fig. 2): Surface type A dominates the meteorite on several sides. This surface type is smooth and gently curved covering approximately 60% of the meteorite. Only in one area regmaglypts are visible. The rest of the

meteorite has two surfaces with different orientations and characteristics. B is concave, has abundant shallow pits 2 to 5 cm in diameter, and is at least partly covered by metallic fusion crust, specially accumulated at boundaries between surface A and B. Surface C is characterized by octahedral cleavage planes up to 5 cm in size, with octahedral plane orientations corresponding to those of the Widmanstätten pattern in the etched section. The formation of surface types A and B could be due to different orientations in flight, or surface B could be formed due to breakup of surface A shortly after entering the earth's atmosphere. Surface type C clearly results from a late breakup event after which not much ablation did occur.

**Structure, Mineralogy, and Micro Hardness**

The Widmanstätten pattern is clearly developed after etching (Fig. 1a). The average kamacite bandwidth obtained on undeformed kamacite bands is 1.0 ± 0.1 mm (n = 97, not corrected for orientation). The taenite lamellae typically are 10 to 50 μm thick. Only one troilite aggregate of 1 by 4 mm was observed on approximately 88 $cm^2$ of cut surface. There is evidence of fracturing, mainly along the octahedral planes of the Widmanstätten pattern, as seen in figure 1a. Neumann bands are abundant.

The meteorite is partially covered by fusion crust reaching a maximum thickness of 1.7 mm (typically up to 0.75 mm) on surface B (Fig. 3). The fusion crust consists of multiple layers of Fe-Ni metal with abundant microspherules of magnetite/wüstite reaching a maximum of 10 μm in diameter. At many places the outermost 0.4 mm of the fusion crust is weathered to iron hydroxides and iron oxides. However, its inner limit is defined by a sharp boundary to the heat-affected zone $\alpha_2$.


Fig. 3. Image taken under a stereo microscope under oblique illumination showing the different heat-affect zones formed during the meteorites atmospheric trajectory. The exterior part of the fusion crust is altered to iron oxides and hydroxides as result of terrestrial weathering.

Beneath the metallic fusion crust, the heat-affected zone $\alpha_2$ is optically observed in the etched section using medium magnification and oblique illumination (Fig. 3). It is seen as a fine-grained dim rim following the contours of the meteorite and ranges in width from 0.25 mm to 0.4 mm. This zone is known to be caused by a rapid diffusionless transformation of kamacite to unequilibrated serrated iron–$\alpha_2$ under temperature briefly exceeding 750 ºC

(Buchwald 1975). Below a depth of 0.75 mm to 4 mm occurs a heat-affect zone not seen optically but recovered by hardness measurements. This zone shows systematic hardness increase with depth resembling the recovery zone as described by Buchwald (1975).

Initial hardness measurements demonstrated that Shisr 043 is strongly shock hardened, thus providing a possibility to investigate the depth of heat penetration during atmospheric entry by measuring hardness profiles. Six hardness profiles were subsequently measured (Fig. 1b), one on surface A (profile A), four on surface B (profiles B1 to B4) and one on the area between surface A and B (profile A-B).

Hardness measurements on three fusion crust profiles show an increase of hardness with depth. The average Vickers hardness (HV) at different depths is 361 at 0.02 mm, 378 at 0.05 mm, and 441 ± 35 at 0.1 mm.

Hardness values from the concave surface B1-B4 profiles (Figs. 4a-d), measured from the surface or from below the fusion crust (profile B1 does not contain fusion crust) to a depth of several mm show: 1) a first zone of decreased hardness (resembling the heat-affect $\alpha_2$) to a depth of about 0.5 mm reaching a minimum hardness of HV 213 ± 47; 2) a second zone (recovery zone) of systematic hardness increase reaching its minimum depth of about 2 mm (HV 405 ± 47) in profile B3 (Fig. 4c) and a maximum depth of approx. 4 mm (HV 413 ± 47) in profile B2 (Fig. 4b). This zone reaches a depth of about 2.6 mm (Fig. 4a) in profile B1 (HV 280 ± 47) and a depth of 3.5 mm (Fig. 4d) in profile B4 (HV 405 ± 47). 3) A third zone in which the hardness remains more or less constant with increasing depth. This zone does not show heat-affect formed during atmospheric passage. It is thought to resemble the unaltered interior of Shisr 043 with hardness values prior to atmospheric entry.

Hardness measurements obtained on surface A, profile A, lack the first zone as described above. Instead, the profile begins with the recovery zone but at a higher hardness with a minimum value HV 283 ± 47 (Fig. 4e). The zone extends to a depth of slightly less than 4 mm from which a sharp drop of hardness occurs before reaching the zone not affected by heat.

The hardness measured on profile A-B shows a distinctive behavior, different from other profiles (Fig. 4f). In the zone of 0-0.8 mm depth the hardness varies from HV 270 to 376. In general this profile exhibits a wavy hardness profile from about 1mm deep down to about 12 mm, followed by a jump of hardness down to 20 mm reaching a hardness of HV 387 ± 47.

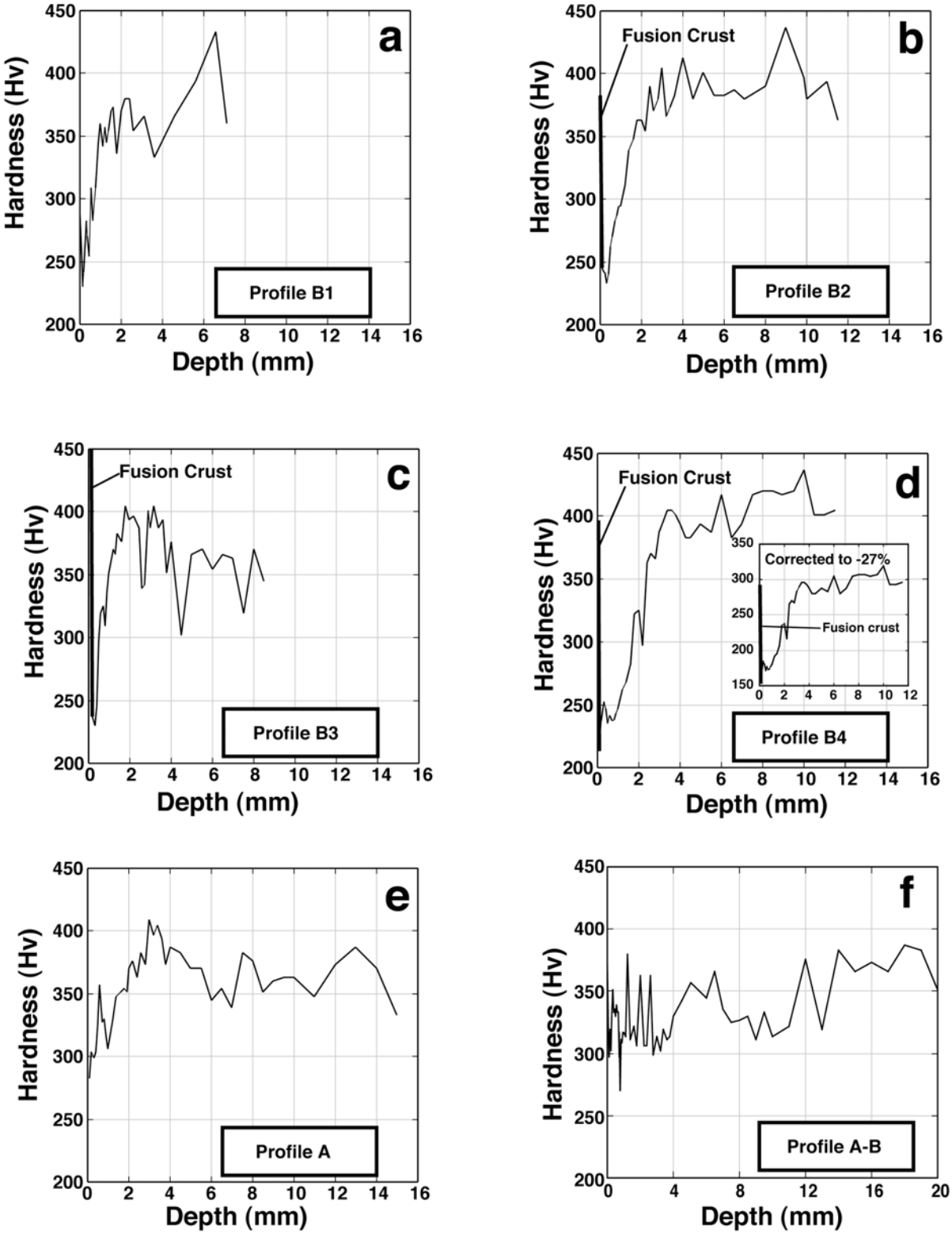


Fig. 4. Six hardness profiles (a-f) measured on three different meteorite surfaces. The location of the profiles is indicated in figure 1b. In 4d a correction of -27% is applied on the raw hardness data, showing the hardness values shifted into the range of shock-hardned octahedrite kamacite (Buchwald 1975).

The average Vickers hardness in the heat-unaffected interior of the meteorite is 372 ± 29 (n=95) for kamacite and 477 ± 69 (n=29) for taenite. The average estimated hardness error is HV ± 47 for all six profiles without the fusion crust. The average estimated hardness error for the metallic fusion crust is HV ± 35.

Taking hardness averages for distinctive zones (0-0.5 mm, >0.5-1.0 mm, >1.0-2.0 mm, >2.0-4.0 mm, etc. shows that the heat-affected zone probably extends to a depth of 7.1 mm (end of profile) in profile B1 and to a depth of 11.5 mm (end of the profile) in profiles B2 and B4 (Fig. 5).

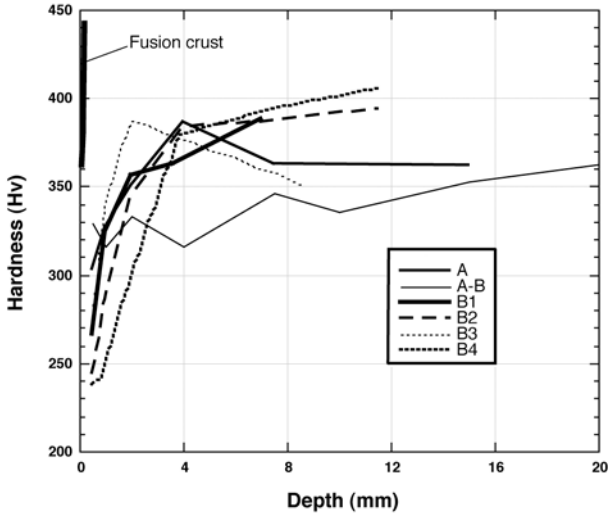


Fig. 5. Hardness averages for specific depth zones (0-0.5 mm, >0.5-1.0 mm, >1.0-2.0 mm, >2.0-4.0 mm, etc.) of the individual profiles, showing that the heat-affected zone probably extends to a depth of 7.1 mm in profile B1 (end of profile) and to a depth of 11.5 mm in profiles B2 and B4 (end of the profile). However, the heat-affected zone ends at 4 mm in profiles A, A-B and B3.

Twelve hardness measurements obtained on a standard with known hardness, HV 585 at load of 100 g, gave a range between HV 592-689 and an average of HV 630 ± 28, that is 7% higher than the standard. 13 hardness measurements made on the IA Odessa iron meteorite show a range of HV 228-279 and an average of HV 260 ± 16, which is 29% higher than its typical value of HV 185 (Buchwald 1975). And 13 hardness measurements obtained on the IIB São Julião iron meteorite show a range of HV 230-264 and an average of HV 247 ± 9, which is 24% higher than its typical value of HV 188 (Buchwald 1975).

Alteration products are found as thin crust of iron oxides and hydroxides (including magnetite, maghemite, and goethite) covering some part of the surface of the meteorite, and as fillings in impact-generated cracks penetrating to a depth of about 2 cm into the meteorite. By comparing the thickness of corrosion crust in sections from below the soil surface with sections from air exposed parts of the meteorite it is clear that corrosion is stronger in the buried parts, with a thickness of corrosion crust of 200-400 μm, as compared with 50-80 μm in the air exposed part. The fusion crust also is better preserved in the exposed part. Taenite lamellae are significantly more resistant to weathering than kamacite.

**Chemistry of Fresh Metal**

Chemical analyses of metal unaffected by weathering performed by several methods are summarized in Table 1. The average chemical composition of the fresh metal of Shisr 043 is very similar to the mean for IIIAB irons (Mittlefehldt et al. 1998) (Fig. 6 and Table 1). The Ir content obtained by ICP-MS (1.8 ppm) and the Ga content obtained by INAA (14.4 ppm) were not used for calculating the mean composition for Shisr 043

because this Ga content is lower than the typical values from the IIIAB group (Mittlefehldt et al. 1998) and this Ir content is rather low for the Au content measured by both methods (Wasson et al. 1998). The Ni content of the Shisr 043 is in the range of the IIIAB, IIE, IIIE, and IVA groups. Analysis using the ICP-MS method show Cu, Ga and Au contents very close to the Nyaung and Willison IIIAB meteorites (Wasson et al. 1998). A comparison of the chemical composition of Shisr 043 with other iron meteorites from the Arabian Peninsula shows that its chemical composition is very close to al-Ghanim (IIIAB) for most elements, and to Wabar (IIIAB) for Ga and Ge. But Wabar has a slightly lower concentration of Ni and a higher concentration of Ir (Grady 2000).

Table 1. Chemical analyses of Shisr 043 compared to the mean of IIIAB irons.

| Method | | ICP-OES | AAS | ICP-MS | INAA | XRF | MEAN | Mean IIIAB# | Mean IIIAB* |
|---|---|---|---|---|---|---|---|---|---|
| Fe | wt% | 91.60 | 90.5 | | | 90.9 | 91.00 | | |
| Co | wt% | 0.50 | 0.53 | 0.52 | 0.45 | 0.49 | 0.50 | 0.49 | 0.50 |
| Ni | wt% | 8.08 | 8.1 | 8.08 | 8.10 | 7.97 | 8.07 | 8.6 | 8.49 |
| P | wt% | 0.14 | | | | 0.12 | 0.13 | 0.19 | 0.56 |
| Cr | ppm | | | | 78 | | 78 | | 40 |
| Cu | ppm | | | 174 | 125 | 134 | 144 | | 160 |
| Ga | ppm | | | 18.80 | 14.4** | | 18.80 | 18.80 | 19.70 |
| Ge | ppm | | | 36.20 | 38.3 | | 37.25 | 37.30 | 38.90 |
| As | ppm | | | 8.50 | 3.3 | | 5.90 | | 10.5 |
| Sb | ppm | | | 0.06 | 0.06 | | 0.06 | | 0.265 |
| W | ppm | | | 1.40 | 1.34 | | 1.37 | | 1 |
| Re | ppm | | | 0.40 | 0.32 | | 0.36 | | |
| Ir | ppm | | | 1.8** | 3.92 | | 3.92 | .014-20.7 | 4.1 |
| Pt | ppm | | | 14.30 | 6 | | 10.15 | | |
| Au | ppm | | | 0.60 | 0.58 | | 0.59 | | 1.2 |
| Total | wt% | | | | | | 99.73 | | |

ICP-OES = inductively coupled plasma optical emission spectrometry.
AAS = Atomic absorption spectrometry.
ICP-MS = inductively coupled plasma mass spectrometry.
INAA = instrumental neutron activation analysis.
XRF = X-ray fluorescence analysis.
# From Mittlefehlt et al. (1998).
*From Mason (1971).
** Values not used for calculation of average, see text.

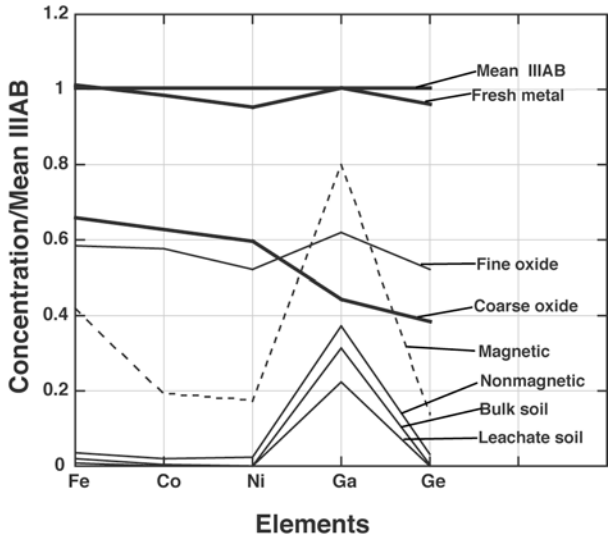


Fig. 6. Fe, Co, Ni, Ga and Ge contents normalized to the mean composition of IIIAB irons (Mittlefehldt et al. 1998) and (Mason 1971). Shisr 043 metal is very similar to mean IIIAB iron meteorites. Both coarse and fine oxide flakes show dilution of meteoritic components. The magnetic and nonmagnetic fraction from adherent soil, and the soil under meteorite show a systematic decrease in the major elements commonly related to iron meteorites. Ga in fine oxides indicates contamination from soil.

**Chemistry of Weathering Products and Soil**

The part of the meteorite originally buried in the soil is partially covered by reddish brown, strongly magnetic flakes of iron (hydr)oxides resulting from weathering of the iron meteorite. Five types of materials reflecting different interactions between meteorite and soil were analyzed and compared with unaltered meteorite and reference soil (Table 2). Two types of weathered flakes were distinguished: coarse (3-20 mm) flakes directly attached to the meteorite (col. 1, Table 2) and fine flakes (0.5-2 mm) found next to the coarse flakes and on the soil below the meteorite (col. 2, Table 2). Coarse flakes were hand-picked, fine flakes were separated as highly magnetic separate from the 0.15-2 mm soil fraction. Soil (<0.15 mm) adhering to meteoritic material was separated into a magnetic (col. 3, Table 2) and a nonmagnetic fraction (col. 4, Table 2). A sample of soil from beneath the meteorite (SUM, col. 5, 6 Table 2) representing material in less direct contact with the meteorite than adhering soil and a reference soil sample (RSS, col. 7, 8, Table 2) were also analyzed by bulk- and aqua regia leach methods (fraction <0.15 mm in both cases).

Chemical analyses of major oxides show that meteoritic elements in the coarse flakes are diluted due to the addition of O and H. Concentrations of meteoritic elements (Fe, Ni, Co, P, Cu, Ge, Ir) decrease in the order coarse oxide, fine oxide, adhering soil (magnetic and nonmagnetic), SUM, and RSS. In the same sequence, typical soil elements (CaO, $Al_2O_3$) and most trace elements are increasing due to increasing soil components. The adhering soil (magnetic and nonmagnetic) is enriched in elements typically concentrated in heavy minerals such as V, Cr, Zn and Zr, possibly due to a wind-induced heavy mineral enrichment. Still, Ni and Co occurs in meteoritic proportions in the magnetic fraction. In the nonmagnetic fraction, Ni/Co is increased relative to the magnetic fraction indicating a preferential transfer of relatively mobile Ni from the oxide fraction to nonmagnetic soil particles. Sr/Ca ratios are much higher in the meteorite oxide than in the soil, proving a preferential enrichment of Sr during weathering as is commonly observed in chondrites (Al-Kathiri et al. 2005). Barium, on the other hand, is not strongly enriched as in chondrites but bound to soil material. Other elements enriched in the oxides are Mo (based on bulk concentrations) and U (based on Th/U ratios of 3.4-4.4 in soils and 1.7-1.9 in fine oxides).

Comparing the chemical composition of the coarse and fine oxide flakes with the mean composition of medium octahedrites (Om) and/or IIIAB (Mason 1971) shows that the oxide flakes are clearly depleted in the major elements commonly related to iron meteorites such as Fe, Co, Ni, Ga, and Ge (Fig. 6 and Table 2), with a possible loss of Fe, Ni, Co relative to Ga and Ge in the fine fraction. However, the magnetic fraction of the adherent soil is enriched in Ga relative to the oxide flakes (Fig. 6).

In both leached soil analyses and total soil analyses (Table 2) the concentrations of Ni and Co, and the ratios of Ni/Fe and Ni/Co are higher in the SUM sample than in the RSS, indicating a transfer of Ni and Co from the meteorite to the soil. The total bulk soil analysis shows a high Cr concentration in both the SUM (865 ppm) and the RSS (1550 ppm) compared to the mean upper crustal value of 35 ppm (Taylor and McLennan 1985), a feature commonly observed in Oman desert soils (Al-Kathiri et al. 2005).

Table 2. Analyses of Shisr 043 weathering products and soil.

| | Units | Oxide flakes | | Adhering soil | | SUM | | RSS | |
|---|---|---|---|---|---|---|---|---|---|
| | | Coarse | Fine | Magnetic | Nonmagnetic | Bulk | Leachate | Bulk | Leachate |
| | | 1 | 2 | 3 | 4 | 5 | 6 | 7 | 8 |
| $SiO_2$ | wt% | 1.28 | 3.19 | 15.74 | 47.64 | | | | |
| $Al_2O_3$ | wt% | 0.16 | 0.43 | 3.95 | 6.13 | 4.48 | 0.91 | 4.47 | 0.82 |
| $Fe_2O_3$ | wt% | 84.94 | 75.82 | 54.42 | 4.74 | 2.40 | 1.19 | 2.96 | 1.14 |
| MnO | wt% | <0.01 | 0.01 | 0.27 | 0.08 | 0.06 | 0.03 | 0.07 | 0.02 |
| MgO | wt% | 0.16 | 0.35 | 3.45 | 2.79 | 2.62 | 1.49 | 2.40 | 1.29 |
| CaO | wt% | 0.84 | 1.81 | 4.16 | 17.43 | 19.62 | 21.65 | 19.97 | 20.44 |
| $Na_2O$ | wt% | 0.24 | 0.25 | 0.84 | 1.50 | 1.31 | 0.06 | 1.13 | 0.04 |
| $K_2O$ | wt% | 0.11 | <0.01 | 0.41 | 1.18 | 1.31 | 0.09 | 1.27 | 0.08 |
| $TiO_2$ | wt% | 0.02 | 0.16 | 6.20 | 1.30 | 0.67 | 0.09 | 1.06 | 0.10 |
| $P_2O_5$ | wt% | 0.22 | 0.17 | 0.07 | 0.06 | 0.03 | 0.03 | 0.03 | 0.02 |
| LOI | wt% | 8.44 | 10.91 | 7.52 | 15.88 | | | | |
| TOTAL | wt% | 96.41 | 93.10 | 97.02 | 98.74 | | | | |
| | | | | | | | | | |
| Sc | ppm | 2 | 2 | 16 | 10 | 7 | 2.3 | 8 | 2.2 |
| V | ppm | <5 | 35 | 824 | 80 | 51 | 24 | 65 | 25 |
| Cr | ppm | 75 | 243 | 7310 | 1490 | 865 | 26 | 1550 | 26 |
| Fe | % | 59.4 | 53.0 | 38.1 | 3.3 | 1.68 | 0.83 | 2.07 | 0.80 |
| Co | ppm | 3119 | 2892 | 957 | 103 | 12.1 | 8 | 9.5 | 4 |
| Ni | ppm | 50150 | 44400 | 14500 | 2025 | 125 | 110 | 50.2 | 29 |
| Cu | ppm | 59 | 69 | 44 | 20 | 8.4 | 9 | 8.1 | 10 |
| Zn | ppm | <30 | <30 | 314 | 42 | 24 | 26 | 31 | 28 |
| Ga | ppm | 8 | 12 | 15 | 7 | 5.9 | 4 | 5.8 | 4 |
| Ge | ppm | 15 | 20 | 5.3 | 1.2 | 0.2 | | 0.3 | |
| Rb | ppm | <2 | 2 | 11 | 30 | 25.8 | | 24.3 | |
| Sr | ppm | 191 | 580 | 301 | 376 | 296 | 241 | 272 | 202 |
| Y | ppm | <1 | 1.3 | 10.3 | 18.6 | 11.0 | 5 | 13.6 | 5 |
| Zr | ppm | 16 | 33 | 209 | 730 | 124 | 7 | 172 | 7 |
| Nb | ppm | <1 | <1 | 27 | 15 | 8.2 | | 9.7 | |
| Mo | ppm | 24 | 19 | 20 | 17 | 2 | <0.5 | 1 | <0.5 |
| Ba | ppm | 7 | 34 | 111 | 240 | 252 | 48 | 241 | 35 |
| La | ppm | 0.1 | 1.3 | 9.3 | 17.2 | 15.6 | 6 | 22.0 | 5 |
| Ce | ppm | 0.3 | 2.3 | 21.1 | 32.2 | 29.8 | | 43.7 | |
| Pr | ppm | <0.05 | 0.2 | 1.7 | 3.2 | 3.8 | | 5.3 | |
| Nd | ppm | 0.1 | 1.0 | 8.0 | 13.7 | 14.7 | | 20.9 | |
| Sm | ppm | <0.1 | 0.2 | 1.9 | 3.2 | 2.9 | | 4.2 | |
| Eu | ppm | <0.05 | <0.1 | 0.5 | 0.7 | 0.66 | | 0.81 | |
| Gd | ppm | <0.1 | 0.2 | 1.8 | 3.0 | 2.7 | | 3.7 | |
| Tb | ppm | <0.1 | <0.1 | 0.3 | 0.5 | 0.4 | | 0.5 | |
| Dy | ppm | <0.1 | 0.2 | 1.8 | 3.1 | 2.3 | | 3.1 | |
| Ho | ppm | <0.1 | <0.1 | 0.4 | 0.6 | 0.5 | | 0.7 | |
| Er | ppm | <0.1 | 0.1 | 1.2 | 2.2 | 1.5 | | 1.8 | |
| Tm | ppm | <0.1 | <0.1 | 0.2 | 0.4 | 0.2 | | 0.3 | |
| Yb | ppm | <0.1 | 0.1 | 1.2 | 2.2 | 1.4 | | 1.9 | |
| Lu | ppm | -0.0 | -0.0 | 0.2 | 0.4 | 0.2 | | 0.3 | |
| Hf | ppm | 0.3 | 0.7 | 5.0 | 17.2 | 3.0 | | 4.3 | |
| Ta | ppm | <0.1 | <0.1 | 2.2 | 1.1 | 0.5 | | 0.3 | |
| Th | ppm | <0.1 | 0.6 | 2.9 | 6.4 | 5.0 | | 8.4 | |
| U | ppm | <0.1 | 0.3 | 1.5 | 2.0 | 1.5 | | 1.9 | |
| | | | | | | | | | |
| Ni/Fe | | 0.084 | 0.084 | 0.038 | 0.061 | 0.007 | 0.013 | 0.002 | 0.004 |
| Ni/Co | | 16.08 | 15.35 | 15.15 | 19.66 | 10.36 | 13.38 | 5.30 | 8.05 |
| Sr/Ca | | 0.032 | 0.045 | 0.010 | 0.003 | 0.002 | 0.002 | 0.002 | 0.001 |
| Th/U | | | 1.71 | 1.94 | 3.20 | 3.44 | | 4.40 | |

Be <1, W<1, In<0.2, Ag<0.5, Tl<0.1 [ppm]
Analytical method: ICP-MS except for Fe ( ICP-OES)
LOI = loss of ignition
1) strongly magnetic oxide flakes, several mm to 2 cm in size
2) strongly magnetic fine oxide flakes, fraction 0.5-2 mm
3) soil material originally adhering to coarse oxide flakes, sieved to <0.15mm, magnetic fraction
4) soil material originally adhering to coarse oxide flakes, sieved to <0.15mm, nonmagnetic fraction
5) soil collected under the meteorite, bulk analysis
6) soil collected under the meteorite, aqua regia leach analysis of fraction <0.15 mm
7) reference soil collected 10m from meteorite, fraction <0.15 mm, bulk analysis
8) reference soil collected 10m from meteorite, fraction <0.15 mm, aqua regia leach analysis

**Cosmogenic Noble Gases**

For the partitioning of the noble gases into the cosmogenic (c), trapped (tr), and radiogenic (r) components certain assumptions have to be made: solar noble gases have never been observed in iron meteorites. Thus, we assume that no trapped solar He, Ne, and Ar are present in our sample. This assumption is supported by the observed $^{36}Ar/^{38}Ar$ ratio of 0.652 ± 0.007 that is close to the purely cosmogenic value of ~0.65 for small iron meteorites (Lavielle et al. 1999).

Radiogenic $^{4}He$ is also assumed to be negligibly small relative to cosmogenic $^{4}He$: we observe a $^{4}He/^{3}He$ ratio of 3.11±0.04, a ratio that is usually observed for the cosmogenic component of surface samples of iron meteorites (Fechtig et al. 1960; Signer and Nier 1960; Voshage 1982; Voshage and Feldmann 1979; Voshage et al. 1983). Furthermore, as $(^{40}Ar/^{38}Ar)_c = 0.2$ (Eugster et al., 1993) $^{40}Ar$ is essentially of radiogenic origin from $^{40}K$ decay. Data for noble gases are given in Tables 3 and 4.

Table 3. Noble gas isotope data for a 52.45 mg split of Shisr 043 (concentrations in $10^{-8}$ cm$^3$ STP/g).

| $^{4}He$ | $^{20}Ne$ | $^{40}Ar$ | $^{4}He/^{3}He$ | $^{20}Ne/^{22}Ne$ | $^{22}Ne/^{21}Ne$ | $^{36}Ar/^{38}Ar$ | $^{40}Ar/^{36}Ar$ |
|---|---|---|---|---|---|---|---|
| 1260 | 5.66 | 35.1 | 3.11 | 0.929 | 1.106 | 0.652 | 2.08 |
| ± 40 | ± 0.2 | ± 1.8 | ± 0.04 | ± 0.02 | ± 0.02 | ± 0.007 | ± 0.09 |

Most isotopic ratios of the cosmic-ray produced noble gases depend on the meteoroid size and the shielding depth of the investigated sample within the meteoroid. For observed trends and the information on this subject see the references given above. Depth-sensitive cosmogenic noble gas ratios include $^{4}He/^{3}He$, $^{4}He/^{21}Ne$, and $^{4}He/^{38}Ar$, whereas the $^{3}He/^{38}Ar$ is relatively constant at 16-17. In lightly shielded iron meteorite samples the $^{4}He/^{3}He$ ratio is about 3, and the $^{4}He/^{21}Ne$ and $^{4}He/^{38}Ar$ ratios are in the range of 190-250 and 50-60, respectively. The cosmogenic noble gas ratios obtained from Shisr 043 (Table 4) are in the range of the values given above.

Table 4. Cosmogenic noble gases (concentrations in $10^{-8}$ cm$^3$ STP/g, age in Ma).

| $^{3}He$ | $^{21}Ne$ | $^{38}Ar$ | $^{4}He/^{3}He$ | $^{4}He/^{21}Ne$ | $^{4}He/^{38}Ar$ | $^{22}Ne/^{21}Ne$ | CRE age |
|---|---|---|---|---|---|---|---|
| 406 | 5.50 | 25.8 | 3.11 | 229 | 50 | 1.09 | 298 |
| ± 14 | ± 0.25 | ± 0.9 | ± 0.05 | ± 9 | ±3.0 | ± 0.02 | ± 12 |

Assumptions: $^{3}He_{tr} = 0$, $^{4}He_{tr} = 0$, $(^{20}Ne/^{22}Ne)_c = 0.8$, $(^{20}Ne/^{22}Ne)_{tr} = 9.8$, $(^{21}Ne/^{22}Ne)_{tr} = 0.029$, $(^{36}Ar/^{38}Ar)_c = 0.64$, $(^{36}Ar/^{38}Ar)_{tr} = 5.32$.

The production rates of cosmogenic noble gases and radionuclides in iron meteorites are strongly dependent on shielding conditions. The $^{4}He/^{21}Ne$ ratio of 229 ± 9 in Shisr 043 is similar to $^{4}He/^{21}Ne$ ratios of 227-237 found in four small iron meteorites (Brownfield, Carlton, Morradal, Norfolk) studied by Lavielle et al. (1999). We used the published noble gas data and the $^{10}Be$-$^{21}Ne$ and $^{36}Cl$-$^{36}Ar$ ages of these four meteorites to determine the average production rates of $^{3}He$, $^{21}Ne$ and $^{38}Ar$ in small irons. We thus derived a $^{3}He$ production rate ($P_3$) of 132 ± 10, a $^{21}Ne$ production rate ($P_{21}$) of 1.96 ± 0.08, and a $^{38}Ar$ production rate ($P_{38}$) of 8.15 ± 0.44, all in units of $10^{-10}$ cm$^3$ STP/g per Ma. The resulting CRE ages, $T_i$, are obtained from $T_i = N_i/P_i$, where *i* is the mass and N the concentration of the cosmogenic nuclide. From the measured $^{3}He$, $^{21}Ne$ and $^{38}Ar$ concentrations, we thus calculate ages of 309 ± 26 Ma, 281 ± 17 Ma and 316 ± 20 Ma, respectively, yielding a (weighted) average age of 298 ± 12 Ma.

### Cosmogenic Radionuclides

We also used the measured concentrations of $^{10}$Be, $^{26}$Al and $^{36}$Cl (Table 5) as internal shielding parameters for calculating the production rates of $^{21}$Ne and $^{36}$Ar. Based on the $^{10}$Be-$^{21}$Ne, $^{26}$Al-$^{21}$Ne and $^{36}$Cl-$^{36}$Ar methods (Lavielle et al. 1999) we find CRE ages of 275 ± 14 Ma ($^{10}$Be-$^{21}$Ne), 271 ± 15 Ma ($^{26}$Al-$^{21}$Ne) and 299 ± 15 Ma ($^{36}$Cl-$^{36}$Ar) for Shisr 043. These three ages yield an average CRE age of 282 ± 12 Ma, consistent with the age calculated above. Finally, the high $^{41}$Ca concentration of 28 ± 2 dpm/kg is indistinguishable from the saturation value of 24 ± 2 dpm/kg (Fink et al. 1991), indicating a very short terrestrial age.

Table 5. Concentrations of cosmogenic radionuclides (in dpm/kg) in Shisr 043.

| Mass (mg) | $^{10}$Be | $^{26}$Al | $^{36}$Cl | $^{41}$Ca |
|---|---|---|---|---|
| 97.8 | 5.62 ± 0.11 | 3.94 ± 0.12 | 24 ± 1 | 28 ± 2 |

## DISCUSSION

### The Shisr 043 Iron Meteorite Find

It is unclear why the fraction of iron meteorites among all finds in Oman is as low as 0.07%. With more than 1400 meteorites reported from Oman and irons constituting 5% of observed meteorite falls (Grady 2000; McSween 1999; Norton 2002), about 60 iron meteorites should have been found in Oman. There are two possible explanations for this anomaly: 1) due to the easy recognition of the iron meteorites they may have been collected by ancient inhabitants or people passing through the Oman desert across the old trade routes; 2) due to the high density of the iron meteorites (~8 gcm$^{-3}$), they are more likely to slowly sink into the sandy soil and finally be completely covered. The first possibility is not supported by finds of tools made of meteoritic iron in Oman or nearby countries like it is the case for ancient Egypt (Bevan and Laeter 2002). The second possibility is supported by the fact that many meteorites found during our search program were almost submerged in the soil. Also, heavy steel drill-bits from oil exploration (within less than 50 years) were found buried by 50-80% in the soil. The second possibility may also explain the relatively high abundance of lunar and martian meteorites in Oman, as they are less dense compared to chondrites and iron meteorites so their tendency to sink in the soil is less pronounced. Shisr 043 was found on a sub-recent alluvial fan. Possibly it was partly re-exposed to the surface as a result of reworking of the alluvial fan during rare flood periods.

### Structure, Mineralogy and Micro Hardness

The average kamacite bandwidth of 1.0 ± 0.1 mm leads to a structural classification as medium octahedrite (Om). Medium octahedrites are represented in the groups IIIAB and IAB but not in the chemically similar groups IIE (Ogg) and IIIE (Og). The structure of Shisr 043 is fully consistent with a IIIAB classification. The generally high hardness indicates that the meteorite has been strongly shocked during its pre-atmospheric history, probably as part of its parent body history. The high shock record is supported by the fine-grained heat-affected zone $\alpha_2$ (Buchwald 1975) and the observation of Neumann lines on a well-etched slab (Norton 2002). The strongly shocked nature also is characteristic for the IIIAB group (Buchwald 1975). The metallic fusion crust, and the heat-affected zone of Shisr 043 have deviating hardness values. The hardness measured on the steel standard, the IA Odessa, and the IIB iron São Julião de Moreira is higher than their typical hardness values as reported by Buchwald (1975). Even the measured minimum values are higher than their typical hardness values indicating an instrumental error tending towards high

hardness. The smaller error for the standard steel (7%) but larger error for the iron meteorites (24-29%, average 27%) is probably caused by their larger compositional and/or structural variation. By applying a correction of -27% on the hardness obtained from profile B4 made on surface B the hardness values are shifted in the range of kamacite (Fig. 4d) from typical octahedrite (Buchwald 1975).

Hardness profiles on surfaces A, B, and at the intersection between the two surfaces show different behaviors for each surface indicating different heat-effects during the meteorite's atmospheric travel. In general, measurable heating effects corresponding to a heating exceeding 750 °C (Buchwald 1975) reach to a depth of 1.2 mm and heating to 300-750 °C reach to a depth of 4 mm, corresponding to the hardness-affected recovered zone of (Buchwald 1975).

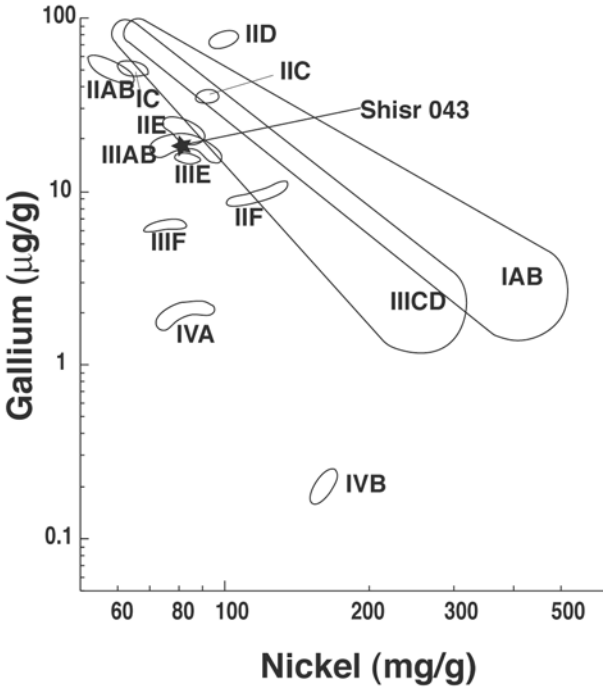


Fig. 7. A plot of Ni versus Ga clearly positions the meteorite in the field of IIIAB group.

**Comparison with Other Iron Meteorites From the Arabian Peninsula**

Besides Shisr 043, eight iron meteorites are known from the Arabian Peninsula (Table 6), all from Saudi Arabia (Holm 1962). Although these finds were made 141 to >900 km from Shisr 043, we will consider them for possible pairing (Table 6) as there is evidence for human transport of Wabar masses (Grady 2000). The al-Ghanim (IIIAB) iron meteorite is closest to Shisr 043 in terms of distance, structural classification and, except for small variations, in chemical composition.

**Chemistry of Fresh Metal**

The fresh metal chemical composition is in the range of the IIIAB group (Mason 1971). Its Cu, Ga and Au contents are very close to those of the meteorites Nyaung and Willison IIIAB and its average composition is close to the al-Ghanim medium octahedrite (Wasson et al. 1998). The Ni content is in the range of IIIAB, IIE, IIIE, IAB, and IVA groups. The IIE and IIIE are the nearest chemical groups to the IIIAB group, but in this case they can be excluded due to their high Cu content, lower Ga content in IIIE group, and slightly higher Ga content in IIE group (Mittlefehldt et al. 1998). In a Ga versus Ni plot Shisr 043 falls in the field of IIIAB group (Fig. 7). Groups IAB and IVA are clearly excluded due to their different contents of Ga (Fig. 7) and P.

However, al-Ghanim is strongly oxidized whereas Shisr 043 shows only minor oxidation on the surface of the part submerged in soil and in thin fractures <2 cm deep, thus they likely have very different terrestrial ages. Wabar is similar in its chemical (IIIAB) and structural classification (Om), but differs by its lower Ni content (7.62 wt%) and higher Ir content (6 ppm). Also, Wabar is medium shocked as revealed by micro hardness (Buchwald 1975), in contrast to the strongly shocked Shisr 043. The small preatmospheric mass indicated by cosmogenic noble gas ratios and radionuclide concentrations also is an argument against pairing of Shisr 043 with the large Wabar meteorite. Naif is reported to be a transported piece of Wabar, whereas South Dhana and ar-Rakhbah are strongly oxidized. Alkhamasin is excluded because of its different structural (Ogg) and chemical classification (IIAB). No data are available for the small and distant Rub' al-Khali 003 iron.

Table 6. Comparison of Shisr 043 to other iron meteorites reported from the Arabian Peninsula.

| Meteorite | Units | Shisr 043 | al-Ghanim | ar-Rakhbah | Naifa | Wabar | Rub' al-Khali 003 | South Dahna | Kumdah | Alkhamasin |
|---|---|---|---|---|---|---|---|---|---|---|
| | | | | | (Wabar) | | | | | |
| Distance to Shisr 043 [km] | | 0 | 141 | 262 | 311 | 476 | ~500 | 725 | 937 | 963 |
| Year of find | | 2002 | 1960 | 1955 | 1932 | 1885 | 1957 | 1957 | 1973 | 1973 |
| Mass [kg] | | 8.27 | 0.5 | 0.46 | 0.008 | 2533 | 0.018 | 275 | ? | 1200 |
| Structure | | Om | Om | | Om | Om | no data | octahedrite | | Ogg |
| Degree of oxidation | | minor | strong | complete | minor | minor | ? | strong | complete | minor |
| Chemical group | | IIIAB | IIIAB | | IIIAB | IIIAB | | | | IIAB |
| Kamacite band width [mm] | | 1.0 | | 0.95 | 1.0 | | | | | |
| Fe | wt% | 91.00 | | | | | | | | |
| Ni | wt% | 8.07 | 7.91 | | | 7.62 | | | | |
| P | wt% | 0.13 | | | | 0.11 | | | | |
| Co | wt% | 0.50 | 0.51 | | | 0.55 | | | | |
| Cr | ppm | 78 | 108 | | | | | | | |
| Cu | ppm | 144 | 170 | | | | | | | |
| Ga | ppm | 18.80 | 20.3 | | | 21.30 | | | | |
| Ge | ppm | 37.25 | 41.4 | | | 38.40 | | | | |
| As | ppm | 5.90 | 5.25 | | | | | | | |
| Sb | ppm | 0.06 | 0.04 | | | | | | | |
| W | ppm | 1.37 | 1.02 | | | | | | | |
| Re | ppm | 0.36 | 0.2 | | | | | | | |
| Ir | ppm | 3.92 | 2.34 | | | 6.00 | | | | |
| Pt | ppm | 10.15 | 11.5 | | | | | | | |
| Au | ppm | 0.59 | 0.73 | | | | | | | |

Arabian Peninsula iron meteorites are from Holm (1962) and Grady (2000)

## Chemistry of Altered Metal and Soil

The iron oxide flakes are weathered parts from the iron meteorite as is confirmed by their high contents of P, Ni, Co, Ge, Ir. The flakes are restricted to the part of the meteorite buried in the soil. The surface of the buried part is more strongly weathered because it is more subjected to moisture captured by the soil from night dew, slower water evaporation after rare rain showers, and salts concentrated in the soil. Besides mechanical soil admixtures, meteoritic iron oxide can be shown to have accumulated Sr, Mo and U from the soil. Sr accumulation is also common in chondrites. Due to the low concentration of sulfur in Shisr 043 (as troilite), Sr capturing due to release of sulfate resulting from sulfide oxidation and precipitation of $SrSO_4$ appears unlikely here. The higher Co and Ni content in the SUM sample compared to the RSS clearly indicate contamination from the meteorite to the

underlying soil as observed under many chondrites (Al-Kathiri et al. 2005).

### Preatmospheric Size, CRE-and Terrestrial Ages

Considering the uncertainties in the measured $^{41}$Ca concentration as well as in the saturation value, we can only constrain the terrestrial age to less than 10 kyr. Based on the radionuclide concentrations alone we cannot exclude the possibility that Shisr 043 is a recent fall, although an age of at least several decades seems likely considering the significant amount of weathering products found on the buried part of the meteorite.

The average CRE age calculated from cosmogenic $^{3}$He, $^{21}$Ne, and $^{38}$Ar and the corresponding production rates given above is 298 ± 12 Ma. This age is consistent with the average CRE age of 282 ± 12 Ma based on the $^{10}$Be-$^{21}$Ne, $^{26}$Al-$^{21}$Ne and $^{36}$Cl-$^{36}$Ar methods. We therefore adopted a mean value of 290 ± 20 Ma (2σ) as the preferred CRE age. This age falls within the range of ages found for IIIAB irons, but does not coincide with the cluster around 650 Ma observed in the $^{40}$K-$^{41}$K exposure age distribution (Wieler 2002) or with the corresponding cluster around ~450 Ma in the $^{36}$Cl-$^{36}$Ar distribution (Lavielle et al. 1999).

The cosmogenic noble gases (Table 4) indicate that the sample that we analyzed orginates from the surface layer of the meteoroid or that the preatmospheric size of the meteoriod was relatively small. The high $^{10}$Be and $^{26}$Al concentrations indicate that Shisr 043 had a pre-atmospheric radius between 10 and 25 cm. If we consider that this meteorite had a small pre-atmospheric mass, this will make it unlikely to be paired with any of the iron meteorite finds from the Arabian Peninsula.

## CONCLUSIONS

Shisr 043 is a single, 8267 g mass of a type IIIAB iron meteorite showing preserved metallic fusion crust and heat affected zones. The kamacite bandwidth, the chemical composition, and the Vickers hardness (HV) all are consistent with a strongly shocked IIIAB medium octahedrite classification for Shisr 043. The accumulation of fusion crust on the concaved surface B, the variable thicknesses of the heat-affect zone at surface A and surface B, and the variable hardness profiles from different surface types indicate that each surface has been subjected to different heating conditions during atmospheric trajectory. Cosmogenic isotope ratios indicate that Shisr 043 had a small pre-atmospheric mass, its CRE age of 290 ± 20 Ma is characteristic for the IIIAB group iron age range, and the $^{41}$Ca saturation points to a sub-recent fall. Shisr 043 is the only iron meteorite so far reported from Oman, while many more should be expected among >1400 Oman meteorite finds, based on a 5% proportion among observed falls. This anomaly may be due to collecting or preferential sinking of heavy irons into the soil. Shisr 043 seems not to be paired with any of the other iron meteorite finds from the Arabian Peninsula.

*Acknowledgments*– Dr. Hilal Al Azri, Ministry of Commerce and Industry, Muscat, and Akram Al Muraza, Khalid Musallam Al Rawas, and Sami Al Zubaidi, Ministry of Commerce and Industry, Salalah, are thanked for their support during the project. Manuel Eggimann performed the XRF measurements and Peter Marmet helped with cutting and etching of the meteorite. This study was supported by the Swiss National Science Foundation (grants 2100-064929 and 200020-107681).

## REFERENCES


AL-KATHIRI A., HOFMANN B. A., JULL A. J. T. and GNOS E. 2005. Weathering of meteorites from Oman: Correlation of chemical and mineralogical weathering proxies with $^{14}C$ terrestrial ages and the influence of soil chemistry. *Meteoritics & Planetary Science* 40:1215-1239.

ALBRECHT A., SCHNABEL C., VOGT S., XUE S., HERZOG G. F., BEGEMANN F., WEBER H. W., MIDDLETON R., FINK D. and KLEIN J. 2000. Light noble gases and cosmogenic radionuclides in Estherville, Budulan and other mesosiderites: Implications for exposure histories and production rates. *Meteoritics & Planetary Science* 35:975-986.

AYLMER D., BONANNO V., HERZOG G. F., WEBER H., KLEIN J. and MIDDLETON R. 1988. $^{26}Al$ and $^{10}Be$ production rates in iron meteorites. *Earth and Planetary Science Letters* 88:107-118.

BEVAN A. and LAETER D. 2002. *Meteorites: A journey through space and time*. Washington: D. C: Smithsonian Institution Press: in association with the University of New South Wales Press. pp. 1-214.

BEVAN A. W. R., BLAND P. A. and JULL A. J. T. 1998. Meteorite flux in the Nullarbor Region, Australia. In *Meteorites: Flux with time and impact effects,* edited by Grady M. M., Hutchinson R., McCall G. J. H., and Rothery D. A. London: The Geological Society. pp. 59-73.

BUCHWALD V. F. 1975. *Handbook of iron meteorites. Their history, distribution, composition, and structure*. Los Angeles: University of California Press. pp. 1-1418.

CHEVREL S., BERTHIAUX A., PLATEL J. P. and ROGER J. 1992. *Explanatory notes to Geological map of Shisr, sheet NF 39-08, scale 1:250'000.* Muscat: Sultanate of Oman, Ministry of Petroleum and Minerals.

EUGSTER O., MICHEL T., NIEDERMANN S., WANG D. and YI W. 1993. The record of cosmogenic, radiogenic, fissiogenic, and trapped noble gases in recently recovered Chinese and other chondrites. *Geochimica et Cosmochimica Acta* 57:1115-1142.

FECHTIG H., GENTNER W. and KRISTEN G. 1960. Räumliche Verteilung der Edelgasisotope im Eisenmeteoriten Treysa. *Geochimica et Cosmochimica Acta* 18:72-80.

FINK D., KLEIN J., MIDDLETON R., VOGT S. AND HERZOG G. F. 1991. $^{41}Ca$ in iron falls, Grant and Estherville: Production rates and related exposure age calculations. *Earth and Planetary Science Letters* 107:115-128.

Grady M. M. 2000. *Catalogue of Meteorites*. London: Cambridge University Press. pp. 1-689.

GROSSMAN J. N. 2000. The Meteoritical Bulletin, No. 84, 2000 August. *Meteoritics & Planetary Science* 35:A199-A225.

GROSSMAN J. N. and ZIPFEL J. 2001. The Meteoritical Bulletin, No. 85, 2001 July. *Meteoritics & Planetary Science* 36:A293-A322.

HOLM D. A. 1962. New meteorite localities in the Rub' Al Khali, Saudi Arabia. *American Journal of Science* 260:303-309.

LAVIELLE B., MARTI K. and CAFFEE M. 1999. The $^{36}Cl$-$^{36}Ar$- $^{40}K$- $^{41}K$ records and cosmic ray production rates in iron meteorites. *Earth and Planetary Science Letters* 170:93-104.

MASON B. 1971. *Handbook of elemental abundance in meteorites*. New York: Gordon & Breach pp. 1-555.

MCSWEEN H. Y. J. 1999. *Meteorites and their parent planets*. Cambridge, New York, Melbourne: Cambridge University Press. pp. 1-310.

MITTLEFEHLDT D. W., MCCOY J. T., GOODRICH C. A. and KRACHER A. 1998. Non-chondritic meteorites from asteroidal bodies. In *Planetary Materials*, edited by J. J. Papike). Washington: The Mineralogical Society of America. pp. 1-195.

NISHIIZUMI K. 2004. Preparation of $^{26}Al$ AMS standards. *Nuclear Instruments and Methods in Physics Research*. B223-224:388-392.

NISHIIZUMI K., CAFFEE M. W. and DEPAOLO D. J. 2000. Preparation of $^{41}Ca$ AMS standards. *Nuclear Instruments and Methods in Physics Research*. B172:399-403.

NISHIIZUMI K., ELMORE D., MA X. Z. and ARNOLD J. R. 1984. $^{10}Be$ and $^{26}Al$ depth profiles in an Apollo 15 drill core. *Earth and Planetary Science Letters* 70:157-163.

NORTON O. R. 2002. *The Cambridge encyclopedia of meteorites*. Cambridge: Cambridge University Press, the Edinbrugh Building, Cambridge CB2 2RU, UK. pp. 1-354.

ROBERTS M. L., BENCH G. S., BROWN T. A., CAFFEE M. W., FINKEL R. C., FREEMAN S. P. H. T., HAINSWORTH L. J., KASHGARIAN, MCANINCH J. E., PROCTOR I. D., SOUTHON J. R. and VOGEL J. S. 1997. The LLNL AMS facility. *Nuclear Instruments and Methods in Physics Research* B123:57-61.

RUSSELL S. S., ZOLENSKY M. E., RIGHTER K., FOLCO L., JONES R., CONNOLLY H. C., GRADY M. M. and GROSSMAN J. N. 2005. The Meteoritical Bulletin, No. 89, 2005 September. *Meteoritics & Planetary Science* 40:A201-A263.

RUSSELL S. S., FOLCO L., GRADY M. M., ZOLENSKY M. E., JONES R., RIGHTER K., ZIPFEL J. and GROSSMAN J. N. 2004. The Meteoritical Bulletin, No. 88, 2004 July. *Meteoritics & Planetary Science* 39:A215-A272.

RUSSELL S. S., ZIPFEL J., FOLCO L., JONES R., GRADY M. M., ZOLENSKY M. E., MCCOY T. and GROSSMAN J. N. 2003. The Meteoritical Bulletin, No. 87, 2003 July. *Meteoritics & Planetary Science* 38:A189-A248.

RUSSELL S. S., ZIPFEL J., GROSSMAN J. N. and GRADY M. M. 2002. The meteoritical Bulletin, No. 86, 2002 July. *Meteoritics & Planetary Science* 37:A157-A184.

SCHLÜTER J., SCHULTZ L., THIEDIG B., AL-MAHDI B. O. and ABU AGHREB A. E. 2002. The Dar al Gani meteorite field (Libyan Sahara): geological setting, pairing of meteorites, and recovery density. *Meteoritics & Planetary Science* 37:1079-1093.

SHARMA P., KUBIK P. W., FEHN U., GOVE G. E., NISHIIZUMI K. and ELMORE D. 1990. Development of $^{36}$Cl standards for AMS. *Nuclear Instruments and Methods* B52:410-415.

SIGNER P. and NIER A. O. 1960. The distribution of cosmic-ray-produced rare gases in iron meteorites. *Journal of Geophysical Research* 65:2947-2964.

TAYLOR S. R. and MCLENNAN S. M. 1985. *The continental Crust: its composition and evolution.* Oxford: Blackwell Scientific publications. pp. 1-312.

VOSHAGE H., FELDMANN H. and BRAUN O. 1983. Investigations of cosmic-ray-produced nuclides in iron meteorites: More data on the nuclides of potassium and noble gases, on exposure ages and meteoroid sizes. *Zeitschrift Für Naturforschung* 38a:273-280.

VOSHAGE H. 1982. Investigations of cosmic-ray-produced nuclides in iron meteorites: Identification of noble gas abundance anomalies. *Earth and Planetary Science Letters* 61:32-40.

VOSHAGE H. and FELDMANN H. 1979. Investigations of cosmic-ray-produced nuclides in iron meteorites: Exposure ages, meteoroid sizes and sample depths determined by spectrometric analyses of potassium and rare gases. *Earth and Planetary Science Letters* 45:293-308.

WASSON J. T., CHOI B.-G., JERDE E. A. and ULFF-MØLLER F. 1998. Chemical classification of iron meteorites: New members of the magmatic groups. *Geochimica et Cosmochimica Acta* 62:715-724.

WIELER R. 2002. Cosmic-ray-produced noble gases in meteorites. *Reviews of Mineralogy and Geochemistry* 47:125-170.

# The regolith portion of the lunar meteorite Sayh al Uhaymir 169

A. Al-Kathiri[1, 2]*, E. Gnos[1] and B. A. Hofmann[3]

[1]Institut für Geologie, Universität Bern, Baltzerstrasse 1, CH-3012 Bern, Switzerland
[2]Directorate General of Commerce and Industry, Ministry of Commerce and Industry, Salalah, Sultanate of Oman
[3]Naturhistorisches Museum der Burgergemeinde Bern, Bernastrasse 15, CH-3005 Bern, Switzerland.

*Corresponding author. E-mail: alikath@geo.unibe.ch

**ABSTRACT**—Sayh al Uhaymir 169 is a composite lunar meteorite from Oman that consists of 13 vol% polymict regolith, adhering to 87 vol% impact-melt breccia. The regolith shows two formation stages and contains the following clasts: Ti-poor to Ti-rich basalts, gabbros to granulites, and regolith breccias. The younger regolith additionally contains a highland gabbronorite clast with anorthite ($An_{96-97}$), forsteritic ($Fo_{85}$) and fayalitic ($Fo_{12}$) mineral clasts, and impact melt shards. The average regolith bulk chemical composition and REE content lie between the soil and regolith breccias of Apollo 12 and 14, with more affinity to Apollo 14. The largest clast is a grey KREEP breccia identical in its chemical composition and total REE content to the ITE- rich high-K KREEP rocks of the Apollo 14 landing site, pointing to a similar source. The regolith shows characteristic lunar ratios of Fe/Mn (74-80) and K/U (535-1682). The Sc content, the Sm versus $Al_2O_3$ and the La/Yb values show that the SaU 169 average regolith is very similar to the Apollo 14 regolith breccias but different to regoliths from other Apollo landing sites and lunar far side highland regolith. All data point to a regolith origin at the lunar front side with strong influence from Procellarum terrane KREEP rocks.

## INTRODUCTION

SaU 169 is a complete, light gray-greenish stone (70 x 43 x 40 mm) with a mass of 206.45 g found in the Sultanate of Oman in January 2002 (Russell et al. 2003; Gnos et al. 2004). The rock consists of two contrasting lithologies (Fig. 1a). Approximately 87 vol% (estimates based on 8 parallel tomographic sections) consists of a holocrystalline, fine-grained poikilitic polymict KREEP-rich impact melt breccia, the other 13 vol% are shock-lithified regolith.

Although the impact melt breccia is characterized by extremely high Th, U, K, REE, P (KREEP) contents (Gnos et al. 2004; Gnos et al. in preparation), the regolith part of SaU 169 also shows unusually high contents of KREEP-elements. The regolith yielded important complementary data to constrain the complex lunar history of SaU 169 especially on the absolute and relative timing of impact events (Gnos et al. 2004). This work will concentrate on studying the regolith chemistry, its rock clasts and the resulting constrains for its origin on the lunar surface.

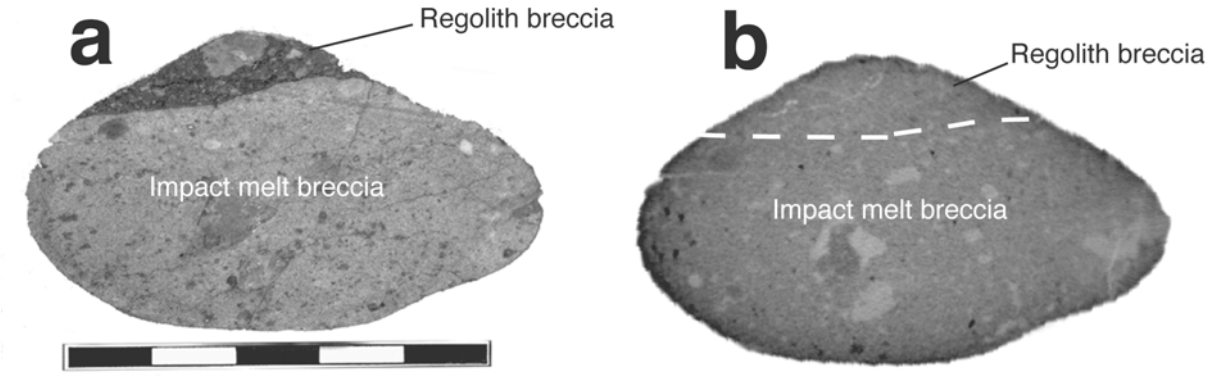


Fig. 1. Cut slice (a) and X-ray tomogram (b, at a few mm distance to cut) showing the interior of SaU 169. The tomography was taken prior to cutting allowing to select the most promising location in advance. Denser material (e.g., large olivine or orthopyroxene clasts) appear dark, the less dense plagioclase fragments are light gray in color. Note the subtle difference in gray shading and texture of the regolith part in the tomography.

A regolith layer completely covers the underlying lunar bedrock, except perhaps on some very steep slopes (e.g., Papike et al. 1991). The formation of the regolith is known to be due to the breakup of the lunar bedrock as a result of bombardment of the Moon's surface with meteorites of variable sizes, ranging from <1mm to tens of kilometers. All lunar samples returned by the Apollo and the Luna missions were from the regolith part, rendering the regolith the main source of rock information for the Moon. All direct measurements of physical and chemical properties of lunar material have been made on rocks and soils collected from the regolith (Papike et al. 1991). Beside that, all remote sensing data come from the very top of the lunar regolith, maximum to 20 cm deep. As the moon is an atmosphere-free body, it is continuously bombarded by small meteoroids, solar wind- and cosmic-ray particles from beyond the solar system. The continuous bombardment with meteoroids causes mixing of regolith material. In this process material from the very surface of the Moon, affected by solar and/or cosmic-ray particles, may become overturned and/or covered. Beside the data obtained from the Apollo and Luna missions and the lunar orbiters (e.g. Clementine (1994), Lunar Prospector (1998-1999) and SMART-1 (2004-present)) lunar meteorites are very important samples providing additional material from random locations on the lunar surface far from the Apollo and the Luna landing sites (Korotev 2005).

Based on the high Th content (32.7 ppm) in the SaU 169 impact melt breccia part, the impact melt part must come from one of the Th hot spots defined by Lunar Prospector γ–ray Th-maps (Lawrence et al. 1999) at the Aristarchus and Aristillus craters, the Montes Carpathus-Fra Mauro region, and the Lalande crater region. Among these Th hot spots, only the area around Lalande and southeast of the crater Aristillus is compatible with our regolith Fe-Ti-Th-K concentrations {Haskin, 2000 #244;Gillis, 2004 #243} derived from remote sensing element distribution maps. However, the age data of the SaU 169 render the Lalande crater area the most plausible source region for the SaU 169 since it contains craters with ages in good agreement with those obtained from SaU 169; a ~2800 Ma crater (Lalande), a ~200 Ma crater (e.g., Lalande A) and a young crater in the order of a few kilometers which is possibly responsible for the ejection of the meteorite to the Earth (Gnos et al. 2004). It will be shown in this stuffy that the chemistry of the average regolith, the volcanic clast types, the KREEP clast and the $TiO_2$ content in the basalt clasts all

point to source rock in the vicinity of the Apollo 12 and 14 landing sites.

## METHODS

Before cutting the meteorite, X-ray tomography was applied at the Federal Material testing Laboratory (EMPA, Dübendorf, Switzerland) to non-destructively obtain information about its interior (Fig. 1b). The industrial computer tomography (CT) scanner applied was a Scientific Measurement Systems (SMS, Austin, Texas) instrument operated at 400 kV, 2.25 mA, using linear array detectors, and a detector aperture of 0.25 x 0.5 mm. Tomographs obtained had a resolution of 0.15 mm (pixel size).

One doubly-polished thin section with 1.2 $cm^2$ of regolith was studied by transmitted and reflected light microscopy. Mineral compositions were determined on a Cameca SX-50 microprobe at the Institute of Geological Sciences, University of Bern, using natural and synthetic mineral standards, wavelength dispersive spectrometers, beam conditions of 15 kV and 20 nA and variable beam diameter for silicates, oxides, sulfides and glass. Back-scattered electron images (BSE) and mineral maps were obtained on a Jeol JXA-8200 microprobe at the Institute of Geological Sciences, University of Bern, using beam conditions of 15 kV and 20 nA.

Chemical analysis on homogenized aliquots using ICP-MS and ICP-OES methods were obtained at the Department for Chemistry and Biochemistry, University of Bern, and the Activation Laboratories Ltd., Ancaster, Ontario, Canada. INAA data were obtained at the Max-Planck-Institute for chemistry Mainz, Germany, and the Activation Laboratories Ltd., Ancaster, Ontario, Canada. Combined chemical analysis using ICP-MS, ICP-OES and INAA were obtained on an aliquot of 117 mg from the KREEP clast and an aliquot of 185 mg from the average regolith. Mineral modes were determined by point counting on BSE images.

## RESULTS

### Regoliths and Shock History

In the regolith part of the rock two different regoliths related to three shock events can be distinguished (Fig. 2). As expected in a regolith, the shock stage of individual clasts varies strongly ranging from impact melts to basically unshocked clasts. In the regolith part of SaU 169, two regolith stages labeled II and III (III is younger than II) can be distinguished. The stage II regolith, including the light-colored KREEP breccia clast (Figs. 1 and 2), is characterized by a dark matrix (smaller grain-size). At the contacts to stage II regolith and the impact melt breccia, stage III regolith is bordered by a zone of shock melt-flow bands of impact melt glass containing 100-600 $\mu$m-sized vesicles (Fig. 3). Stage III impact melt glass also transects the older regolith material (Fig. 2).

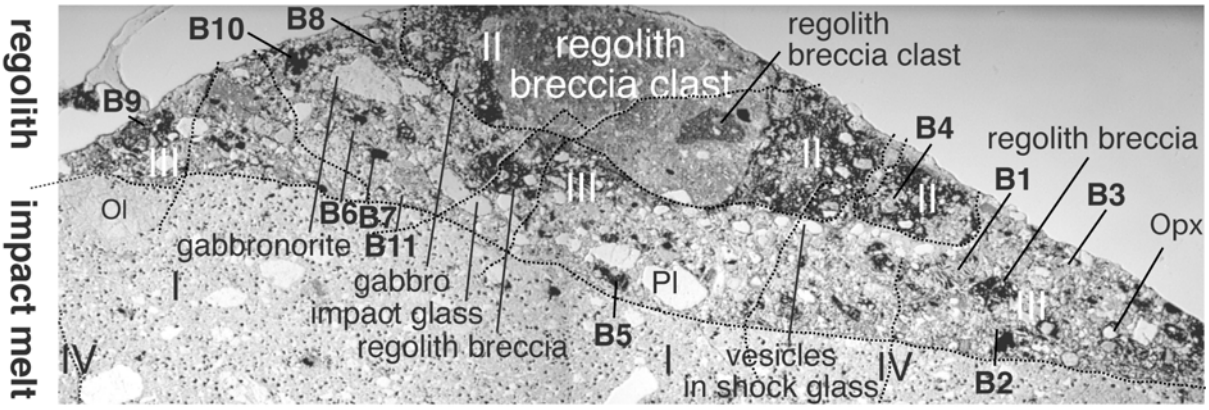


Fig. 2. Thin section overview photograph of the regolith part of the SaU 169 showing the regolith and adjacent impact melt breccia. Marked with I to IV are clearly distinguishable stages of breccia and shock vein formation. B1-B11 mark the analyzed volcanic clasts. Abbreviations: Ol = olivine; Pl = plagioclase; Opx = orthopyroxene.

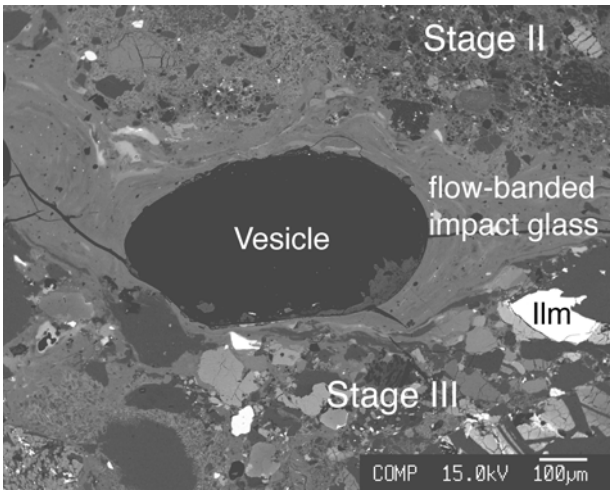


Fig. 3. Vesicle-rich flow-banded shock melt bordering the stage-III regolith at the contact to stage-II regolith.

**Regolith Clasts**

Both regolith stages comprise crystalline and glassy volcanic rocks, magmatic lithic fragments, breccia fragments, fragments of mafic gabbroic rock clasts or granulites, and crystal fragments. The basaltic rock fragments reach a maximum size of approx. 2.0 mm x 0.9 mm (Fig. 2). The largest clast has a size of approximately 7.5 mm x 4 mm. It is a grey KREEP regolith breccia clast situated in the central part of regolith lithology II and contains itself fragments of regolith breccias (Figs. 1, 2). A set of parallel, glassy shock veins (stage IV in Fig. 2) crosscut the two regoliths and the impact melt breccia. All mineral and rock fragments are embedded in a fine-grained crystalline groundmass. Yellow and orange glass fragments and glass beads occur only in regolith stage III.

**Mineralogy of Rock Clasts**

The basalt clasts are composed of 10-500 $\mu$m-sized minerals, chiefly plagioclase laths, prismatic pyroxenes, olivine and ilmenite. Fe-Mg silicates in the basalts generally display strong compositional zoning, and several clasts restricted to the younger regolith contain clinopyroxene with pyroxferroite rims. The classification of pyroxenes in the basalt clast is based on the nomenclature described by Morimoto et al. (1988). The mineral chemistry and the modal composition of 11 individual basalt clasts

were determined (Figs. 2 and 4) and the results are compiled in Table 1. By using mineral modes and mineral chemistry a bulk compositional range for each basaltic clast was estimated (Table 1). Based on the lunar basalt classification suggested by Neal and Taylor (1992) and Le Bas (2001) the full range from Ti-rich ($TiO_2$ >6 wt%) to Ti-poor ($TiO_2$ <1.5 wt%) basalts including aluminous ($Al_2O_3$ >11 wt%) members as well as picrobasalts (Le Bas 2001) are present. In general, all analyzed basalts are low-K (K <2000 ppm) basalts (Neal and Taylor 1992).

Table 1. Mineral and modal composition of analyzed basalts, gabbros and breccia clasts in SaU 169 regoliths (stages II-III).

| Clast ( lithology; stage) | Lithology | Mineralogy | Pyx [vol%] | ol [vol%] | opaques [vol%] | plg [vol%] | glass [vol%] | est. FeO [wt%] | est. MgO [wt%] | est. $Al_2O_3$ [wt%] | est. $TiO_2$ [wt%] | est. $K_2O$ [wt%] |
|---|---|---|---|---|---|---|---|---|---|---|---|---|
| Volcanic | | | | | | | | | | | | |
| Basalt 1 (III) | augite-pigeonite basalt (aluminous medium-Ti) | zoned Px($En_{43-59}Wo_{9-23}$) Prx ($En_2Wo_{13}$) Pl ($An_{90}Or_{0-1}$) Ilm ($Ilm_{91}$) Spl($Chr_{19}Usp_{60}$) | 39 | - | 3 | 58 | - | 8.6-22.9† | 0.5-6.7† | 17.1-19.0† | 2.6-3.0† | 0.02-0.03† |
| Basalt 2 (III) | pigeonite-augite basalt (Ti-poor) | Px ($En_{20-52}Wo_{7-27}$) Prx ($En_1Wo_{14-17}$) Pl ($An_{86-87}Or_{0-1}$) Spl ($Chr_{6-10}Usp_{87-82}$) | 67 | - | 2 | 31 | - | 17.9-33.6† | 0.3-12.9 | 8.4-9.8 | 1.3-1.4 | 0.07-0.08 |
| Basalt 3 (III) | pigeonite basalt (aluminous Ti-poor) | Px ($En_{46}Wo_{18}$) Pl ($An_{90}Or_{0-1}$) Chr ($Chr_{42-45}Usp_{10}$) | 47 | - | 6 | 48 | - | 12.0 | 8.9 | 15.4 | 1.0 | 0.03 |
| Basalt 4 (III) | augite-pigeonite basalt (Ti-poor) | Px ($En_{26-40}Wo_{18-31}$) Prx ($En_{13-19}Wo_{18-19}$) Pl ($An_{75-85}Or_{1-2}$) Ilm ($Ilm_{98}$) Spl ($Chr_8Usp_{79}$) | 68 | - | 1 | 31 | - | 14.7-28.3 | 3.2-9.2 | 8.2-9.6 | 1.3-1.7 | 0.06 |
| Basalt 5 (III) | olivine basalt picrobasalt (Ti-rich) | Pl ($An_{65-95}Or_{1-3}$) Ol ($Fo_{47-62}$) Ilm ($Ilm_{84-85}$) | - | 63 | 11 | 26 | - | 22.4-28.0† | 20.4-21.1 | 6.2-7.5 | 7.2-8.7 | 0.01-0.02 |
| Basalt 6 (III) | augite basalt (aluminous Ti-rich) | Px ($En_{22-32}Wo_{23-28}$) Pl ($An_{75-82}Or_{1-2}$) Ol ($Fo_{61-62}$) Ilm ($Ilm_{97}$) | 41 | - | 14 | 45 | - | 10.6 | 4.8 | 18.6 | 6.4 | 0.07 |
| Basalt 7 (III) | Olivine-pigeonite basalt (aluminous medium-Ti) | Px ($En_{65-68}Wo_7$) Pl ($An_{78-87}Or_1$) Ol ($Fo_{63-64}$) Ilm ($Ilm_{96}$) | 47 | 7 | 6 | 40 | - | 13.9 | 14.7 | 11.5 | 5.0 | 0.04 |
| Basalt 8 (III) | olivine basalt, probably picrobasalt (very fine grained) | Ol ($Fo_{48-55}$) Chr ($Chr_{38}Usp_{26}$) | - | 69 | 7 | - | 24 | - | - | - | - | - |
| Basalt 9 (III) | Augite-pigeonite basalt (aluminous Ti-poor) | Px ($En_{38-49}Wo_{9-22}$) Prx ($En_{2-7}Wo_{9-15}$) Pl ($An_{85-91}Or_{0-1}$) Ol ($Fo_{60}$) Ilm ($Ilm_{96}$) | 58 | 1 | 3 | 39 | - | 14.1-30.1 | 1.2-8.5 | 11.9-13.9 | 1.1-1.5 | 0.02 |
| Basalt 10 (III) | picrobasalt (aluminous medium-Ti) | Px ($En_{04-14}Wo_{25-34}$) Pl ($An_{73-83}Or_{1-2}$) Ilm ($Ilm_{98}$) | 48 | - | 3 | 49 | | 19.8 | 2.4 | 13.9 | 2.9 | 0.15 |
| Basalt 11 (III) | picrobasalt (ferrous) | | 6 | 67 | 1 | - | 26 ($SiO_2$) | 45 | 5.5 | 0.3 | 0.9 | 0.03 |
| Non-volcanic | | | | | | | | | | | | |
| Gabbro (III) | Gabbronorite | Px ($En_{41-48}Wo_{5-24}$) Pl ($An_{96-97}Or_0$) Ol ($Fo_{61}$) | | | | | | | | | | |
| Breccia (II) | KREEP breccia clast | Trd, Pl ($An_{78-97}Or_{0-1}$) | | | | | | | | | | |

Px = pyroxene; Prx = pyroxferroite; Ol = olivine; Pl = plagioclase; Ilm = ilmenite; Chr = chromite; Spl = spinel; Trd = Tridymite.
(II) and (III) refer to regolith stages shown in Figure 2.

Two Ti-rich basalts were found (basalt 5 and basalt 6; Fig. 4). Basalt 5 is an olivine picrobasalt composed of 63 vol% olivine ($Fo_{47-62}$), 26% plagioclase ($An_{65-95}$ $Or_{1-3}$), and 11% ilmenite ($Ilm_{84-85}$). Basalt 6 is an aluminous Ti-rich augite basalt composed of 41 vol% pyroxene

($En_{22-32}Wo_{23-28}$), 45 % plagioclase ($An_{75-82}Or_{1-2}$) and 14 % ilmenite ($Ilm_{87}$).

Basalt 8 is very fine-grained olivine picrobasalt consisting of 69 vol% olivine ($Fo_{48-55}$), 7 % opaque minerals (chromite ($Chr_{38}$ $Usp_{26}$), ilmenite and 24 % glass (Fig. 4). Basalt 11 is a very small volcanic clast (~140 x 160 μm) found in the regolith stage III within the flow- banded shock melt (Fig. 4). It is composed of 67 vol% fayalite ($Fo_{18}$), 6% ferroaugite ($En_{21}Wo_{42}$), 26% interstitial silica and 1 % ilmenite (Table 1 and Table 2). A bulk rock composition calculated from the mineral chemistry shows that it is a Fe-rich, alkali-poor picrobasalt.

Table 2. Microprobe analysis (wt%) of basalt 11 volcanic clast

| | Fayalite | Fayalite | Ferroaugite | Ferrougite | Silica | Silica |
|---|---|---|---|---|---|---|
| $SiO_2$ | 31.53 | 31.75 | 50.35 | 50.57 | 96.17 | 97.69 |
| $TiO_2$ | 0.08 | 0.05 | 0.28 | 0.33 | 0.08 | 0.05 |
| $Cr_2O_3$ | 0.06 | b.d. | b.d. | b.d. | b.d. | b.d. |
| $Al_2O_3$ | 0.02 | 0.04 | 0.43 | 0.50 | 0.25 | 0.97 |
| FeO | 59.30 | 59.23 | 21.98 | 20.38 | 2.50 | 1.09 |
| MnO | 0.88 | 0.85 | 0.37 | 0.34 | 0.04 | b.d. |
| NiO | b.d. | 0.03 | b.d. | b.d. | 0.03 | b.d. |
| MgO | 7.13 | 7.07 | 6.98 | 7.23 | 0.16 | b.d. |
| CaO | 0.11 | 0.14 | 19.07 | 20.48 | 0.10 | 0.21 |
| $Na_2O$ | b.d. | b.d. | 0.08 | 0.08 | b.d. | 0.06 |
| $K_2O$ | b.d. | b.d. | b.d. | b.d. | b.d. | 0.10 |
| Total | 99.11 | 99.16 | 99.54 | 99.91 | 99.33 | 100.17 |
| Normalized to | 4 O | 4 O | 6 O | 6 O | 4 O | 4 O |
| Si | 1.014 | 1.019 | 1.999 | 1.990 | 1.968 | 1.969 |
| Ti | 0.002 | 0.001 | 0.008 | 0.010 | 0.001 | 0.001 |
| Cr | 0.002 | 0.000 | 0.000 | 0.000 | 0.000 | 0.000 |
| Al | 0.001 | 0.002 | 0.020 | 0.023 | 0.006 | 0.023 |
| Fe | 1.595 | 1.590 | 0.730 | 0.671 | 0.043 | 0.018 |
| Mn | 0.024 | 0.023 | 0.013 | 0.011 | 0.001 | 0.000 |
| Ni | 0.000 | 0.001 | 0.000 | 0.000 | 0.000 | 0.000 |
| Mg | 0.342 | 0.338 | 0.413 | 0.424 | 0.005 | 0.000 |
| Ca | 0.004 | 0.005 | 0.811 | 0.864 | 0.002 | 0.004 |
| Na | 0.000 | 0.000 | 0.006 | 0.006 | 0.000 | 0.002 |
| K | 0.000 | 0.000 | 0.000 | 0.000 | 0.000 | 0.003 |
| Mg% | 17.6 | 17.5 | 21.1 | 21.7 | - | - |
| Fe% | 82.4 | 82.5 | 41.5 | 44.1 | - | - |
| Ca% | - | - | 37.4 | 34.2 | - | - |

b.d. = Below detection

Three aluminous medium-Ti basalts (basalts 1, 7 and 10; Fig. 4) are present. Basalt 1 is a pigeonite-augite basalt containing 39 vol% prismatic pyroxenes ($En_{43-59}Wo_{9-23}$), 58% plagioclase ($An_{90}Or_{0-1}$) and 3% opaque minerals (ilmenite ($Ilm_{91}$) and ulvöspinel ($Chr_{19}Usp_{60}$). It contains zoned prismatic pigeonite crystals with pyroxferroite ($En_2Wo_{13}$) rims. Basalt 7 is an olivine-pigeonite basalt composed mainly of 47 vol% pigeonite ($En_{65-68}Wo_{07}$), 7 % olivine ($Fo_{63-64}$), 40 % plagioclase ($An_{78-87}Or_1$) and 6 % ilmenite ($Ilm_{96}$). Basalt 10 is an augite basalt composed of 48 vol% low-Mg augite ($En_{4-14}Wo_{25-34}$), 49 % plagioclase ($An_{73-83}Or_{1-2}$), and 3% ilmenite ($Ilm_{98}$).

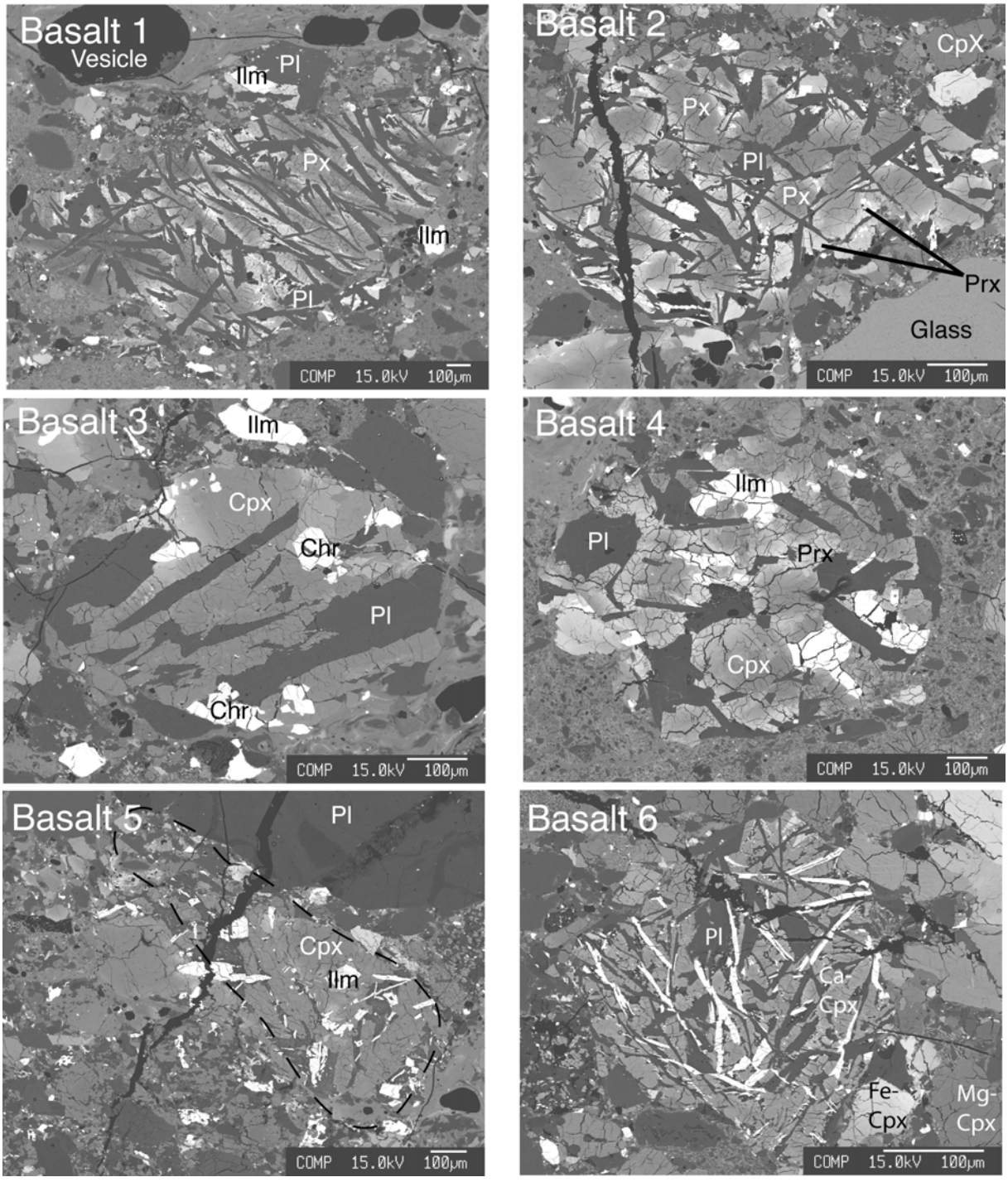
Basalt 1
Vesicle
Ilm
Pl
Px
Ilm
PL
COMP 15.0kV 100µm
Basalt 2
CpX
Px
Pl
Px
Prx
Glass
COMP 15.0kV 100µm
Basalt 3
Ilm
Cpx
Chr
Pl
Chr
COMP 15.0kV 100µm
Basalt 4
Ilm
Pl
Prx
Cpx
COMP 15.0kV 100µm
Basalt 5
Pl
Cpx
Ilm
COMP 15.0kV 100µm
Basalt 6
Pl
Ca-
Cpx
Fe-
Cpx
Mg-
Cpx
COMP 15.0kV 100µm

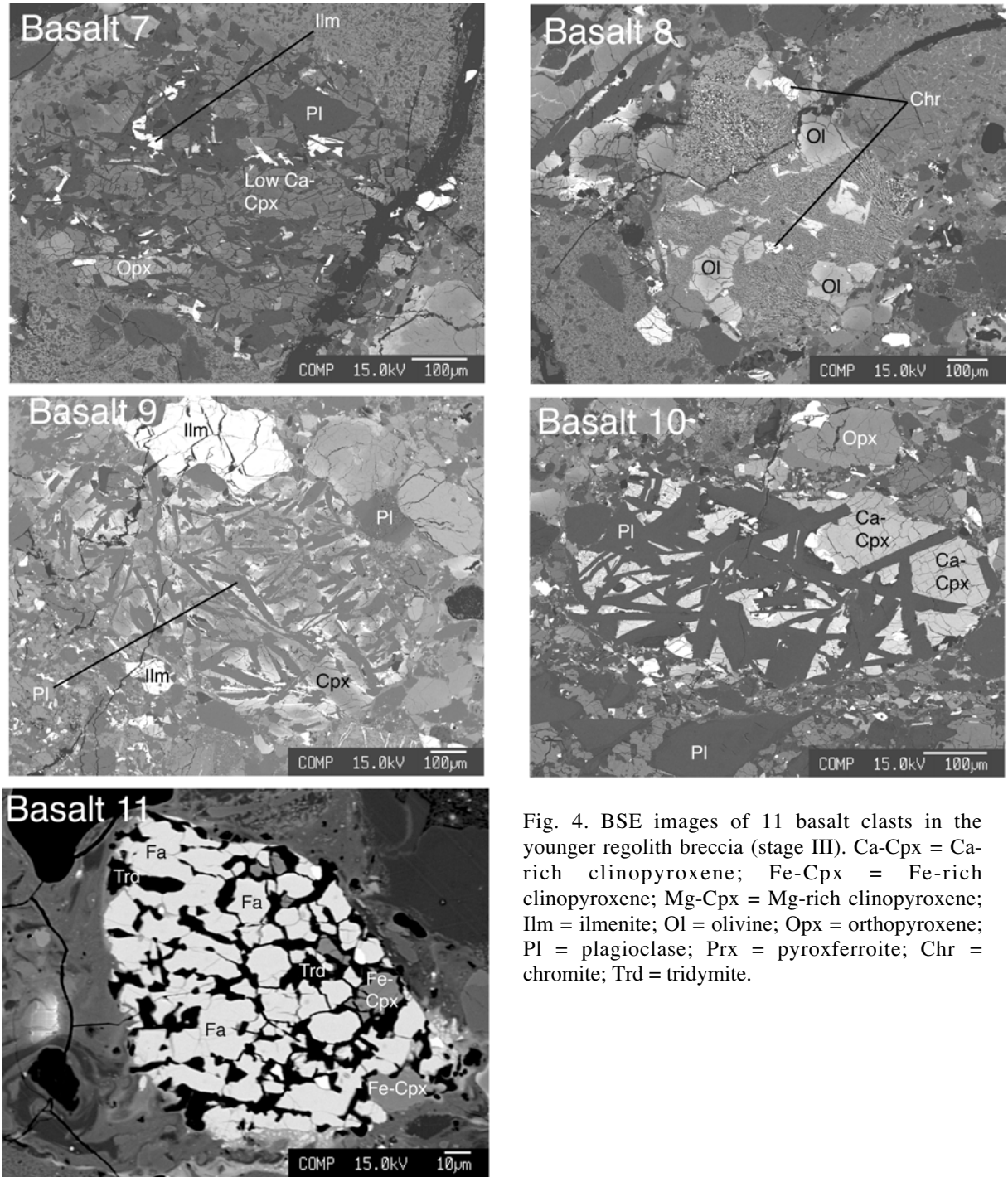


Fig. 4. BSE images of 11 basalt clasts in the younger regolith breccia (stage III). Ca-Cpx = Ca-rich clinopyroxene; Fe-Cpx = Fe-rich clinopyroxene; Mg-Cpx = Mg-rich clinopyroxene; Ilm = ilmenite; Ol = olivine; Opx = orthopyroxene; Pl = plagioclase; Prx = pyroxferroite; Chr = chromite; Trd = tridymite.

Ti-poor basalts are more abundant, four basalts were found (three of them are aluminous) based on the model composition (Table 1) they are: pigeonite basalt (basalt 3), pigeonite-augite basalt (basalt 2) and augite-pigeonite basalts (basalts 4 and 9). They are composed of 0-68 vol% prismatic pyroxene ($En_{20-68}Wo_{7-31}$), 0-69 % olivine ($Fo_{63-64}$), 24-48 % plagioclase ($An_{75-91}Or_{0-2}$) and 1-7 % opaque minerals (ilmenite ($Ilm_{96-98}$), chromite ($Chr_{42-45}Usp_{10}$) and ulvöspinel ($Chr_{6-8}Usp_{60-87}$)). Some zoned pigeonite crystals have a rim of pyroxferroite ($En_{1-7}Wo_{9-17}$). Basalts 3, and 9 (Fig. 4) are aluminous basalts with estimated $Al_2O_3$ contents of 15.4 wt% and 13.9 wt% respectively.

Two gabbronorite clasts are shown in figure 5. The larger clast (2 mm x 1.2 mm; Fig. 5a) consists of zoned pyroxene ($En_{41-48}$ $Wo_{5-24}$), plagioclase ($An_{96-97}$ $Or_0$) and olivine ($Fo_{61}$).

The most prominent of the regolith breccia clasts is the 7.5 mm large KREEP clast (Figs. 1, 2) mainly consisting of a very fine-grained grey matrix enclosing larger mineral clasts of Ca-rich plagioclase ($An_{78-97}$), olivine (typically <500 $\mu$m) and few laths or angular grains of silica. The clast further contains abundant ilmenite and hypidiomorphic zircons up to 50 $\mu$m in size. The breccia clast also contains at least one regolith breccia fragment (Fig. 2). Silica minerals and zircon occur also in other regolith breccia clasts (Fig. 6).

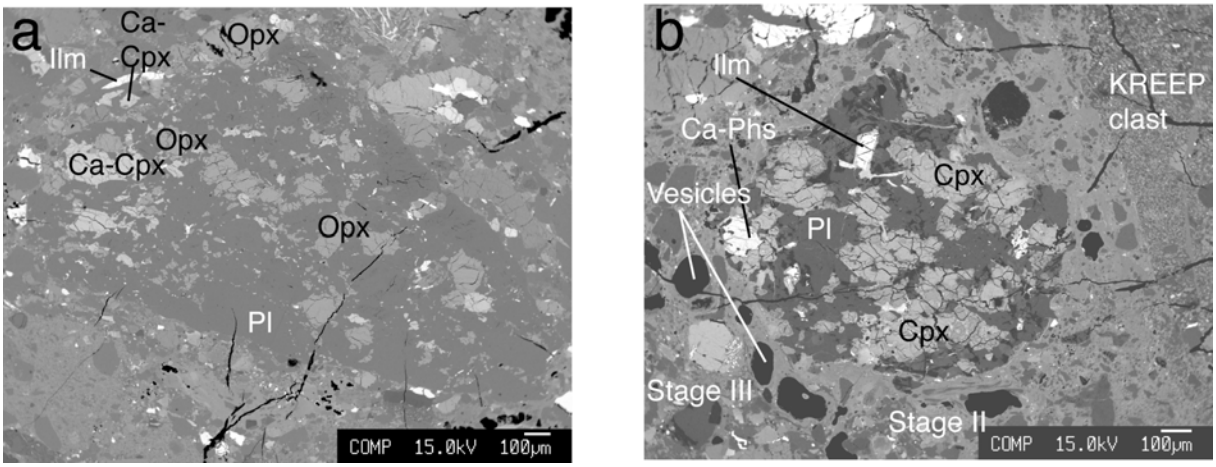


Fig. 5. The two largest gabbroic rock fragments. (a) Gabbronorite, and (b) gabbro consisting mainly of plagioclase (Pl), orthopyroxene (Opx), clinopyroxene (Cpx), Ca-rich clinopyroxene (Ca-Cpx), ilmenite (Ilm), and Ca-phosphate (Ca-Phs).

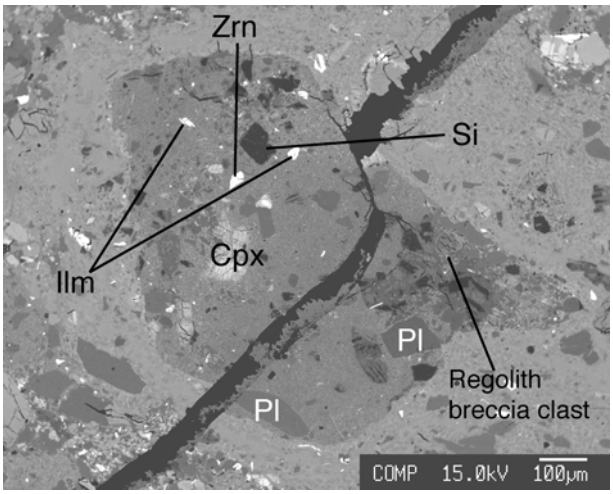


Fig. 6. Regolith breccia clast cut by crack filled with terrestrial calcite. The breccia consists mainly of a very fine groundmass containing plagioclase (Pl), clinopyroxene (Cpx) and ilmenite (Ilm) fragments. An idiomorphic $SiO_2$-grain (Si) and a zircon clast (Zrn) are also visible.

## Mineral Clasts

Mineral clasts in the regoliths are commonly ≤1mm in size, only few plagioclase clasts are >1 mm with a largest grain of 2 mm size (Fig. 2). Pyroxene and olivine clasts are <600 $\mu$m and ilmenites are 100-400 $\mu$m. Unzoned mineral clasts in the regolith breccia cover a wider compositional range than rock fragments. The plagioclase clast chemistry ranges from $An_{74}$ to $An_{94}$ and $Or_0$ to $Or_2$. No anorthite content higher than $An_{94}$ was observed in feldspar clasts in the matrix.

Most olivine clasts in the regolith are Mg-rich ($Fo_{66-73}$) with one unzoned olivine clast in the stage III regolith breccia showing a composition of $Fo_{84}$. On the other hand a >200 μm-sized, unzoned olivine grain of fayalitic composition ($Fo_{12}$) is also present in the stage III regolith breccia (Fig. 7). Pyroxene clasts include both Mg- and Fe-rich members and Ca-rich to Ca-poor clinopyroxenes. Pyroxenes displaying exsolution texture (Fig. 8) are rare. Ilmenite clasts show a wider compositional range of $Ilm_{85-96}$ than ilmenites in basalt clasts. Troilite is observed as small fragments in the regolith ground mass and as very tiny inclusions in the largest glass fragment (Fig. 9a).

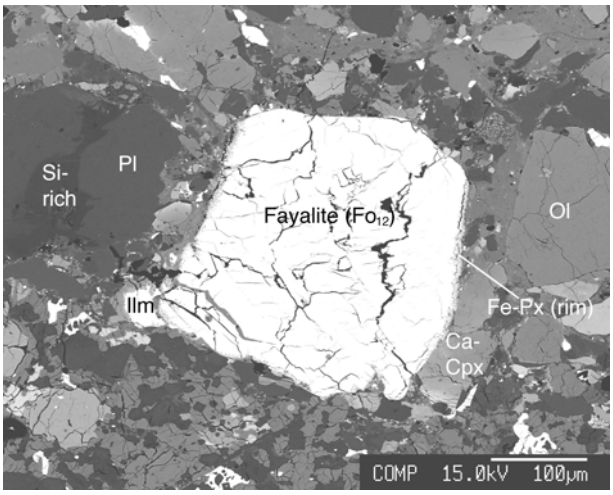


Fig. 7. Large compositionally homogenous fayalite clast ($Fo_{12}$). Note the thin Fe-rich pyroxene rim on the fayalite. Ol = Mg-Fe olivine; Ca-px = Ca-rich clinopyroxene; Ilm = ilmenite; Pl = plagioclase; Si-rich = $SiO_2$ –rich melt.

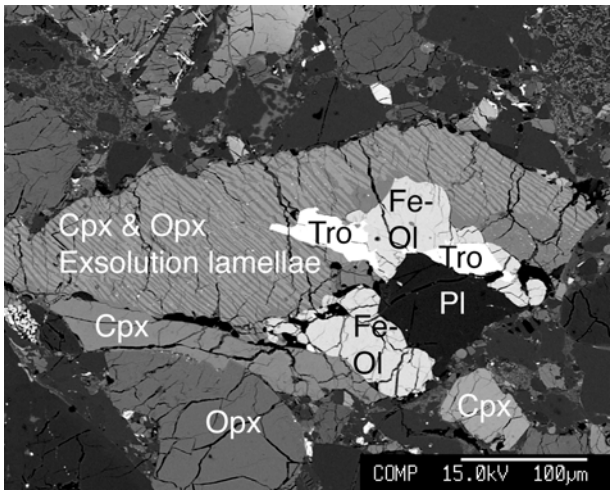


Fig. 8. Rock clast consisting mainly of Ca-pyroxene showing exsolution lamellae of Mg-pyroxene (dark). It is associated with plagioclase (Pl), Mg-orthpyroxene (Opx), Fe-rich olivine (Ol), and troilite (Tro).

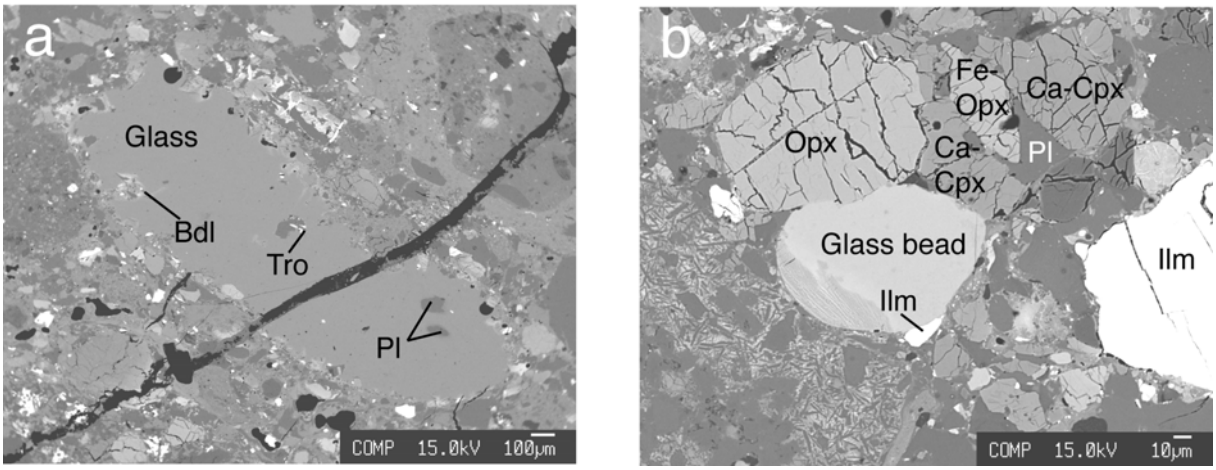


Fig. 9. Impact glass fragments. (a) 2 mm-sized glass shard containing small inclusions of plagioclase (Pl), troilite (Tro) and baddeleyite (Bdl; $ZrO_2$). (b) Small glass bead surrounded by pyroxene, plagioclase, and ilmenite. Note the quenched crystallites in the glass bead at the contact to a fine-crystalline impact melt pocket.

## Glass

Only in the stage III regolith breccia contains unaltered yellow and orange glass shards and beads. Glass beads range from <1mm to a maximum size of 2 mm (Fig. 9). They are commonly elongated in shape with irregular boundaries. The largest glass fragment contains small inclusions of plagioclase, troilite and baddeleyite (Fig. 9a). The major elements composition of glass clasts is identical to the average regolith except for one bead having higher $Al_2O_3$, CaO and lower FeO content, probably due to contamination of plagioclase schlieren (Table 3). The glass beads have Mg/Al ratios of ~0.5 (Table 3), which is different from Mg/Al ratios of 1.7 to 3 found in lunar volcanic glass (Deleno 1986).

Table 3. Microprobe analysis (wt%) of glass fragments, glass beads and banded shock melt.

| | Glass fragment | Plagioclase inclusion | Glass fragment | Glass bead | Glass bead | Glass bead | Grey band | Grey band | Av. grey bands (n=10) | Light band | Light band | Dark band | Dark band |
|---|---|---|---|---|---|---|---|---|---|---|---|---|---|
| $SO_3$ | n.a. | n.a. | n.a. | n.a. | n.a. | n.a. | 0.21 | 0.22 | 0.17(7) | 0.01 | 0.01 | 0.09 | 0.04 |
| $P_2O_5$ | n.a. | n.a. | n.a. | n.a. | n.a. | n.a. | 0.38 | 0.37 | 0.31(7) | 0.00 | 0.02 | 0.21 | 0.07 |
| $SiO_2$ | 46.97 | 47.82 | 47.09 | 46.86 | 46.8 | 47.02 | 45.63 | 45.83 | 46.13(71) | 47.59 | 47.23 | 45.49 | 46.23 |
| $TiO_2$ | 2.25 | 0.03 | 2.36 | 2.3 | 2.25 | 2.23 | 2.19 | 2.15 | 2.11(13) | 1.05 | 1.12 | 1.34 | 0.45 |
| $Cr_2O_3$ | 0.24 | b.d. | 0.21 | 0.3 | 0.33 | 0.31 | 0.17 | 0.20 | 0.18(6) | 0.12 | 0.18 | 0.06 | 0.06 |
| $Al_2O_3$ | 17.39 | 30.82 | 17.49 | 17.51 | 17.53 | 17.45 | 20.95 | 20.32 | 21.18(91) | 1.23 | 1.88 | 23.39 | 30.12 |
| FeO | 11.62 | 2.56 | 11.29 | 11.28 | 11.25 | 11.21 | 9.81 | 9.54 | 8.78(91) | 27.80 | 31.35 | 8.16 | 2.96 |
| MnO | 0.18 | 0.02 | 0.14 | 0.17 | 0.16 | 0.18 | 0.14 | 0.16 | 0.14(2) | 0.46 | 0.57 | 0.15 | 0.06 |
| NiO | b.d. | b.d. | 0.03 | 0.04 | 0.02 | 0.04 | 0.00 | 0.05 | 0.01(2) | 0.02 | b.d. | b.d. | b.d. |
| MgO | 8.00 | 1.41 | 7.67 | 7.79 | 7.78 | 7.82 | 5.80 | 6.15 | 5.68(48) | 6.46 | 5.71 | 5.23 | 1.89 |
| CaO | 11.62 | 15.41 | 11.38 | 11.61 | 11.38 | 11.38 | 12.64 | 12.92 | 12.94(42) | 13.30 | 10.68 | 13.51 | 16.80 |
| $Na_2O$ | 0.57 | 1.53 | 0.62 | 0.62 | 0.61 | 0.58 | 0.87 | 0.84 | 0.89(7) | 0.22 | 0.11 | 0.90 | 1.00 |
| $K_2O$ | 0.37 | 0.07 | 0.37 | 0.37 | 0.39 | 0.36 | 0.48 | 0.45 | 0.44(10) | 0.01 | 0.04 | 0.33 | 0.16 |
| Total | 99.21 | 99.67 | 98.65 | 98.85 | 98.50 | 98.58 | 99.27 | 99.19 | 98.96(21) | 98.25 | 98.91 | 98.87 | 99.85 |
| Mg/Al | 0.52 | - | 0.50 | 0.51 | 0.51 | 0.51 | 0.32 | 0.34 | 0.31 | 6.00 | 3.45 | 0.25 | 0.07 |

Av. = Average
n.a. = Not analyzed
b.d. = Below detection

The flow-banded shock melt glass associated with the younger regolith (stage III) is composed of bands showing different grey shadings on BSE images (Fig. 3). Dark bands, grey areas and light bands can be distinguished. Microprobe analysis of these different bands showed that the dark flow bands are enriched in $Al_2O_3$, the grey areas have lower $Al_2O_3$ content and the light bands are similarly low in $Al_2O_3$ but enriched in FeO (Table 3). The grey areas have Mg/Al ratios of about ~0.3, but the dark and light band have strongly variable Mg/Al ratios ranging from 0.07 to 6.00 (Table 3).

## Regolith Bulk Chemistry

Typical lunar Fe/Mn elemental ratios (moon 60-80; Papike 1998; Papike et al. 2003) were obtained for the regolith (80) and the KREEP clast (74). K/U values for the average regolith (1682) and the KREEP clast (1253) are also typically lunar (moon 1700; Papike 1998; Papike et al. 2003). An α-autoradiograph of SaU 169 (Gnos et al. in preparation) demonstrated that Th and U contents in SaU 169 are significantly lower in the regolith part than in the impact melt breccia lithology.

A comparison of the CI chondrite-normalized REE contents (Fig. 10a) (Evensen et al. 1978) of soils and regolith breccias from Apollo 11-17 landing sites (Haskin and Warren 1991) and the Apollo 14 KREEP breccias (Warren and Wasson 1979) shows that the SaU 169 bulk regolith REE pattern is lower than soil and regolith breccias from Apollo 14 landing site (both minimum and maximum), but higher than the maximum values of Apollo 11, 12 15, 16 and 17 soils (Fig. 10a). The REE-content of the SaU 169 average regolith lies between the Apollo 14 and Apollo 12 soils and regolith breccias (Fig. 10a). A plot of the SaU 169 average

regolith chemical composition and the averages Apollo 12 and 14 soils and regolith breccias also showed that the SaU 169 regolith is intermediate between Apollo 12 and 14 regoliths (Fig. 10b). The KREEP clast REE content is very similar to the KREEP component based on the average composition of Apollo 14 breccias (Fig. 10a).

By normalizing the REE contents of SaU 169 lithologies, the Apollo 14 ultra-KREEPy impact melt rocks (UK IMR; Jolliff 1998), the average of the Apollo 16 ultra-KREEPy impact melt rocks (UK Ima and UK Imb; Jolliff 1998) and the average model KREEP composition (Korotev 2000) to the Apollo 14 high-K KREEP rocks (Fig. 11; Table 4; Jolliff 1998; Warren 1989), a similar degree of enrichment of all REE's is observed in all three analyzed SaU 169 lithologies. Most notably, the composition of the KREEP clast is very similar to the composition of the Apollo 14 high-K KREEP used for normalization. The impact melt breccia (Gnos et al. 2004), the KREEP clast, the average model KREEP composition (Korotev, 2000) and the bulk regolith show similar REE trends (Fig. 11). Among the lithologies with flat REE spectra in figure 11, the SaU 169 impact melt breccia (Gnos et al. in preparation) has the highest elemental concentrations, whereas the average model KREEP composition (Korotev 2000) lies between the SaU 169 bulk regolith and the SaU 169 KREEP clast (Fig. 11). On other hand, the ultra-KREEPy Apollo 14 and 16 impact melt rocks (Jolliff 1998) have the highest REE concentration but display significant fractionations compared with SaU 169 lithologies and the average model KREEP composition (Fig. 11).

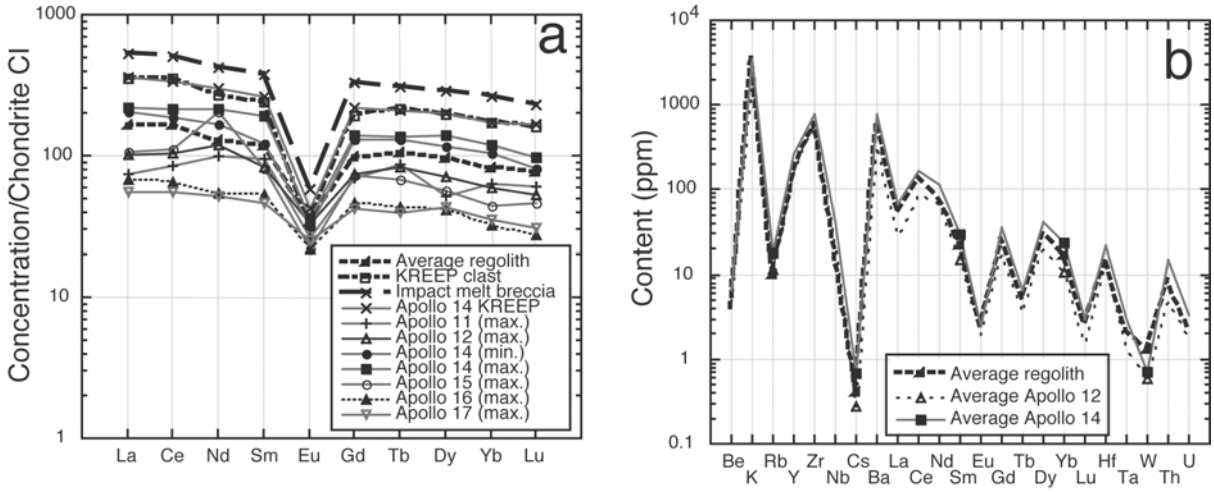


Fig. 10. a) REE contents of the average SaU 169 regolith normalized to CI chondritic composition (Evensen et al. 1978), and compared with soil and regolith breccias from Apollo 11-17 landing sites (Haskin and Warren, 1991). The SaU 169 regolith REE contents fall between the Apollo 14 and 12 values, but above the maximum contents of Apollo 11, 12 15, 16 and 17. REE values of the SaU 169 KREEP clast found in the regolith (Table 4) and the SaU 169 impact melt breccia (Gnos et al. 2004; in preparation) are also shown. b) Chemical composition of the average regolith and the Apollo 12 and 14 soil and regolith breccia (Haskin and Warren 1991). Values for Cs are in ppb instead of ppm as listed in the lunar source book (see Papike (1998) for comparison).

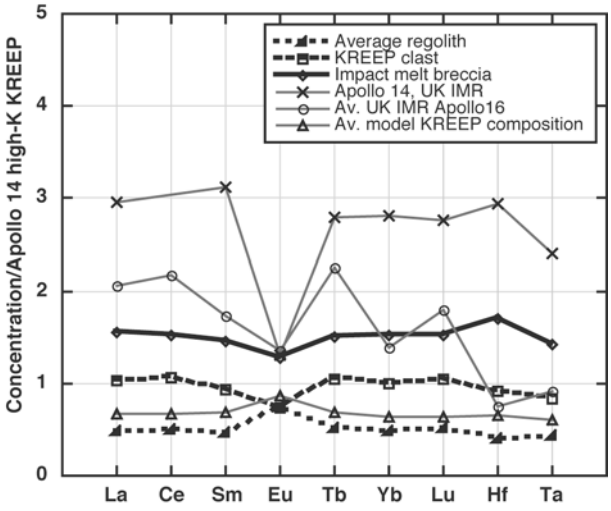


Fig. 11. SaU 169 lithologies (impact melt breccia, regolith, and, KREEP clast) normalized to the Apollo 14 high-K KREEP values (Table 4; Jolliff 1998; Warren 1989). Note that the KREEP clast and the regolith are similar to Apollo 14 high-K KREEP rocks and the average model KREEP compositions. UK IMR = ultra-KREEP impact melt rocks; IMB N = impact melt breccia (Korotev 2000). Average model KREEP composition from Korotev (2000).

The bulk regolith breccia and the KREEP clast are not depleted in alkalis based on K/U of 1680 and K/U of 1253, respectively (Fig. 10b). In contrast, the SaU 169 impact melt breccia is depleted in alkalis (K/U 535) relative to other KREEP elements (Gnos et al. 2004).

The SaU 169 Sc concentrations of 28 ppm in the regolith breccia and of 18 ppm in the KREEP clast are higher than those of the Apollo 16 regolith breccias, which are <12 ppm (Cahill et al. 2004; Korotev 1997). A plot of Sm versus $Al_2O_3$ (Fig. 12) shows that the regolith breccia plots in the field of the Apollo 14 regolith breccias (Cahill et al. 2004; Warren and Wasson, 1980). The KREEP clast plots at slightly higher concentrations. This distinguishes them from the Apollo 16 regolith breccias and the far side highlands regolith (Cahill et al. 2004). The SaU 169 regolith La/Yb values are ~3.1. This is similar to the high-K KREEP (Jolliff, 1998; Warren 1989) values form the Apollo 14 landing site (Table 4).

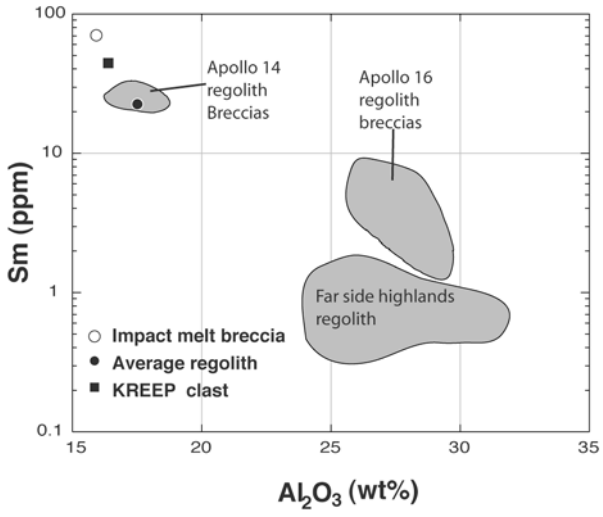


Fig. 12. Sm versus $Al_2O_3$ diagram, showing that the SaU 169 lithologies, and more pronounced the SaU 169 regolith part are related to the Apollo 14 KREEP suite and regolith breccias, but very different from Apollo 16 landing site and the lunar far side highland regolith.

Table 4. Chemical analysis of SaU 169 bulk regolith, KREEP clast compared to Apollo 14 and 16 KREEP rocks, and SaU 169 impact melt breccia.

| | SaU 169 Bulk regolith | SaU 169 KREEP clast | SaU 169 impact melt breccia | Apollo 14 | Average model | Apollo 14 | Apollo 14 | Apollo 16 | Apollo 16 |
|---|---|---|---|---|---|---|---|---|---|
| | Breccia | Breccia | IMB | IMB | KREEP composition | High-K KREEP | Ultra-KREEP | Ultra-KREEP | Ultra-KREEP |
| | wt% | wt% | wt% | wt% | wt% | wt% | wt% | wt% | wt% |
| $SiO_2$ | 46.9 ‡ | 46.86 | 45.15 | 48.3 | 49.5 | 50.3 | 50 | n.a. | n.a. |
| $Al_2O_3$ | 17.54 | 16.34 | 15.88 | 16.76 | 15.77 | 15.1 | 11.6 | 15.7 | 19.5 |
| $FeO_{tot}$ | 11.09 | 8.8 | 16.67 | 10.32 | 10.76 | 10.3 | 9.34 | 10.1 | 5.06 |
| MgO | 7.94 | 6.92 | 11.09 | 10.22 | 9.16 | 8.29 | 5.64 | 3.6 | 6.35 |
| CaO | 11.72 | 10.6 | 10.16 | 10.13 | 10.21 | 9.79 | 12.5 | 11.5 | 17.5 |
| $Na_2O$ | 0.78 | 1.18 | 0.98 | 0.81 | 0.88 | 0.94 | 0.8 | 0.49 | 0.47 |
| $K_2O$ | 0.46 | 0.88 | 0.54 | 0.68 | 0.57 | 0.96 | 3.98 | 2.1 | 0.52 |
| $TiO_2$ | 2.49 | 1.47 | 2.21 | 1.68 | 2.21 | 2 | 4.2 | 1.12 | 2.56 |
| $Cr_2O_3$ | 0.19 | 0.12 | 0.14 | n.a. | n.a. | 0.18 | 0.17 | 0.09 | 0.12 |
| | ppm | ppm | ppm | ppm | ppm | ppm | ppm | ppm | ppm |
| Sc | 28 | 18 | 25 | 21.1 | 25.1 | 23 | 41.4 | 17.1 | 12.8 |
| Cr | 1310 | 811 | 992 | 1245 | 1760 | 1200 | 1140 | 5900 | 845 |
| Co | 19 | 12 | 31 | 33 | 16 | 25 | 42 | 28 | 12 |
| Rb | 10 | 20 | 13.7 | 16.2 | 18 | 22 | 81 | 42 | 21 |
| Sr | 214 | 230 | 359 | 156 | 208 | 200 | 220 | 290 | 140 |
| Zr | 596 | 1397 | 2835 | 1200 | 1010 | 1400 | 4760 | 480 | 1270 |
| Cs | 0.4 | 0.9 | 0.8 | 0.77 | 0.76 | 1 | 3 | 2.1 | 0.8 |
| Ba | 593 | 1351 | 1520 | 905 | 748 | 1300 | 3250 | 2500 | 825 |
| La | 52 | 113 | 170 | 88.8 | 73 | 110 | 325 | 282 | 170 |
| Ce | 139 | 297 | 427 | 216 | 190 | 280 | n.a. | 733 | 482 |
| Nd | 76.9 | 162 | 257 | n.a. | 118 | 178 | n.a. | 460 | 332 |
| Sm | 21.9 | 44.9 | 70.15 | 37 | 33 | 48 | 150 | 127 | 40 |
| Eu | 2.43 | 2.45 | 4.2 | 2.73 | 2.86 | 3.3 | 4.34 | 5.36 | 3.61 |
| Tb | 5.08 | 10.5 | 15.1 | 7.7 | 6.8 | 10 | 27.9 | 27.4 | 17.8 |
| Yb | 16.9 | 36 | 54.7 | 26.7 | 23 | 36 | 101 | 77 | 23.2 |
| Lu | 2.53 | 5.24 | 7.64 | 3.76 | 3.2 | 5 | 13.8 | 10.9 | 7 |
| Hf | 14.8 | 34.7 | 64.3 | 29.7 | 25 | 38 | 112 | 16.8 | 40 |
| Ta | 2.14 | 4.16 | 7.1 | 3.62 | 3 | 5 | 12 | 2.7 | 6.4 |
| Th | 8.44 | 21.7 | 32.7 | 16.1 | 12 | 22 | 51 | 36 | 21 |
| U | 2.27 | 5.83 | 8.6 | 4.5 | 3.3 | 6.1 | 14.4 | 5.7 | 7.4 |
| La/Yb | 3.1 | 3.1 | 3.1 | 3.3 | 3.2 | 3.1 | 3.2 | 3.7 | 7.3 |

SaU 169 bulk regolith, KREEP clast and Impact melt breccia are from Gnos et al. (2004).
IMB = Impact melt breccia.
Average model KREEP composition form Korotev (2000).
Apollo 14 High-K KREEP from Warren (1989) and Jolliff (1998).
Apollo 14 and 16 ultra-KREEP impact melt rocks from Jolliff (1998).
‡ Microprobe value on regolith shock glass.
n.a. = Not analyzed.

## DISCUSSION

### Shock History

As expected in a lunar regolith the shock stage of individual clasts varies strongly and the shock indicators range from shock melt fragments to basically unshocked clasts. Estimation of the shock grade that led to the shock-lithification of the regoliths is difficult because shock grade indicators like the formation of shock melts are influenced by the rock porosity (Kieffer 1976; Osinski 2005). Thus, much lower shock pressures may lead to melting in regoliths than in solid rocks on which the classification of Stöffler et al. (1991) is based on. By combining the petrologic with radiometric and noble gas data (Gnos et al. 2004; Lorenzetti et al. 2005) it is most likely that the older regolith of SaU 169 became shock lithified ~200 Ma ago during an impact, and attached to a fragment of the 3909 ± 13 Ma old Imbrium impact melt breccia (Gnos et al. 2004). At this stage the regolith was at a depth of a few meters. This impact brought the impact melt breccia and attached older regolith into the younger regolith position. It is believed that this was close to the surface, because the younger regolith shows a solar-wind noble gas component (Gnos et al. 2004; Lorenzetti et al. 2005). Moreover, the lithologic content of this younger regolith is different, containing impact melt glass shards and beads, pyroxferroite-bearing basalts, picrobasalts, and a Fe-rich picrobasalt clast. A vesicle-rich flow-banded impact melt glass separates it from the older regolith. The younger regolith probably became shock-lithified during the last recorded impact on the Moon ≈ 340000 years ago which launched SaU 169 into a solar system orbit (Gnos et al. 2004; Lorenzetti et al. 2005). As stage IV shock veins (Fig. 2) crosscut all lithologies including the vesicle-rich flow-banded melt bordering the younger regolith (stage III), this event possibly corresponds to the impact that launched the rock to the Earth.

### Regolith Components and Mineralogy

The wide range of Ti-poor to Ti-rich basalts and their variable mineral compositions (especially in the younger regolith) point to basalts derived from different sources. Most plagioclase clasts and plagioclase in rock fragments have compositions ranging from $An_{74}$ to $An_{94}$ and $Or_0$ to $Or_2$. Anorthite contents exceeding $An_{94}$ are extremely rare. They were only observed in one gabbronorite clast ($An_{96-97}$) in the younger regolith (Fig. 5a), and in the KREEP clast ($An_{97}$) in the older regolith (Fig. 2). This points to a limited contribution of anorthositic highland rocks. The very low Fe contents in plagioclase indicate that all analyzed larger mineral clasts have a plutonic origin (Papike et al. 1991). The presence of Mg-rich olivine ($Fo_{84}$) and Fe-rich olivines ($Fo_{12}$) is also remarkable. Forsterite-rich (dunite) clasts in regolith breccia are so far only reported from Apollo 17 landing site, and likely are derived from Serenitatis (Ryder et al. 1997). The presence of dunite (>90 vol% forsterite) xenoliths in lunar meteorite Dho 310 (Demidova et al. 2003), however, suggests that such material may be more widespread. Even more exceptional is the large fayalite clast (Fig. 7), apparently derived from a strongly evolved magmatic rock. Fayalite with similar composition was reported from Dho 287A (mare basalt portion) in the late-stage mesostasis part ($Fo_{0-15}$; Anand et al. 2003) and recently in the polymict regolith breccia NWA 3136 (Kuehner et al. 2005). The fayalite-rich picrobasalt clast (Fig. 4; Table 2) could represent a volcanic equivalent of such highly evolved magmas.

Based on criteria described by Deleno (1986) to distinguish volcanic glass from impact-melt glass, all analyzed glass fragments in the younger SaU 169 regolith are impact-melt glasses. The impact glass

corroborate the noble gas data (Gnos et al. 2004; Lorenzetti et al. 2005) which showed that the younger regolith represents the top few-tens of centimeters of a lunar soil at the impact site from which the meteorite was launched into space.

**Rock Chemistry**

The SaU 169 regolith displays typical lunar Fe/Mn and K/U values.
The REE concentrations, normalized to the CI chondritic composition (Evensen et al. 1978), and the bulk chemical composition of the average regolith, fall between the compositional fields of Apollo 14 and Apollo 12 soils and regolith breccias (Fig. 10a and b). Also the KREEP clast REE content is very similar to the Apollo 14 KREEP breccias (Warren and Wasson 1979). In addition, the Apollo 12 soil has 1.7 ppm U and 6.4 ppm Th and the Apollo 14 soil has 1.5 ppm U and 6.7 ppm Th (McKay et al. 1991). These values are higher than those from other Apollo and Luna missions, but close to SaU 169 average regolith containing 2.27 ppm U and 8.44 ppm Th (Table 4). This indicates source proximity of the SaU 169 regolith to both Apollo 12 and 14 landing sites, like the Lalande crater region proposed by Gnos et al. (2004) on the basis of age results and Th-Fe-Ti-K concentrations {Lawrence, 1999 #242;Haskin, 2000 #244;Gillis, 2004 #243}.

Normalizing the SaU 169 lithologies as shown in figure 11 to the Apollo 14 high-K KREEP shows that the composition of the SaU 169 KREEP clast is very similar to the composition of the Apollo 14 high-K KREEP lithology, indicating that it probably derived from the same region. This is also reflected in the total REE content of 879 ppm of the SaU 169 KREEP clast, close to the 890 ppm measured in Apollo 14 high-K KREEP (Warren 1989). Normalized REE data clearly show that the SaU 169 KREEP clast and the SaU 169 bulk regolith are different from the ultra-KREEPy impact-melt rocks from Apollo 14 and 16 (Jolliff 1998). In comparison with data compiled by Korotev (1997) and Cahill et al. (2004), the Sc content and the Sm-$Al_2O_3$ concentrations (Fig. 12) show that the SaU 169 average regolith is most similar to the Apollo 14 KREEP suite and regolith breccias, but different from other Apollo landing sites, and the lunar far side highland regolith. A lunar source region in vicinity of the Apollo 14 and 12 landing sites is likely because the chemical composition of the SaU 169 regolith lies between the soil and regolith breccia from the Apollo 14 and 12 sites and shows strong chemical and compositional similarities with Apollo 14 high-K KREEP. Most basalt clasts have $TiO_2$ contents in the range of Ti-poor basalts (four) and medium-Ti basalts (three) indicating strong contribution of mare basalts similar to those observed at Apollo 12, Luna 24 and Apollo 14 sites (Le Bas, 2001; Papike et al. 1991). This again supports proximity of the SaU 169 regolith source to Apollo 12 and 14 landing sites. Only two Ti-rich basalts were detected indicating small contribution of mare basalts from other sources.

The variable BSE tones of the flow-banded shock melt are indicative of assimilated clast compositions. Light colored bands most likely resulted from melting mineral or rock clasts with high FeO contents, and the dark bands result from melting of $Al_2O_3$-rich clasts like plagioclase (Table 3). Grey portions are interpreted as a homogenized mixture of molten clasts from the regolith stage III. Its composition hence is interpreted to represent the average bulk composition of the younger regolith and appears to be similar KREEP-enriched as the bulk regolith composition listed in Table 4.

Ferroaugite-fayalite-quartz-bearing volcanic rocks are known in terrestrial peralkaline and tholeiitic suites (e.g., Scaillet and MacDonald 2001). In a compilation on silicate liquid immiscibility Roedder (1979) described the close association of Fe-rich basaltic with

potassic granitic melt in lunar samples. In our volcanic clast (Fig. 4), closely associated ilmenite-fayalite seems to coexist with ferroaugite. The interstitial phase is silica glass. Although alkali feldspar is also a characteristic late-crystallizing phases in association with this assemblage, it was not observed. This, however, may only be due to the very small size of the volcanic rock. The Fe-rich rock clast probably derived from the volcanic or subvolcanic part of a highly evolved magma containing fayalite-rich olivine such as that found in regolith stage III (Fig. 7).

**Comparison With KREEPy Lunar Meteorites**

Among all lunar meteorites reported, only Calcalong Creek (Hill and Boynton 2003) and Dho 287A (Anand et al. 2003) are KREEPy. Although Dho 287A is reported as a KREEPy lunar meteorite, no clear KREEP clasts are present but the high abundance of KREEPy mesostasis may be an evidence for KREEP assimilation (Anand et al. 2003). Dho 287A has 0.53 wt% $Na_2O$, 0.19 wt% $K_2O$, 0.21 wt% $P_2O_5$, 0.9 ppm Th and total REE of 76 ppm (La, Ce, Nd, Sm, Eu, Tb, Yb and Lu) (Anand et al. 2003). This is much lower than in the SaU 169 regolith breccia and impact melt breccia lithologies. After SaU 169, the Calcalong Creek polymict breccia is known to have the second highest average Th content. However, with 0.49 wt% $Na_2O$, 0.24 wt% $K_2O$, 4.3 ppm Th, 1.18 ppm U and total REE of 155 ppm (La, Ce, Nd, Sm, Eu, Gd, Tb, Dy, Ho, Tm, Yb and Lu) (Hill and Boynton, 2003) concentrations are also well below those of SaU 169. On the other hand, one KREEP clast (clast F) described from the Calcalong Creek (Hill and Boynton, 2003) contains 0.91 wt% $Na_2O$, 0.87 wt% $K_2O$, 12.14 ppm Th, 3.34 ppm U and total REE of 444 ppm (La, Ce, Nd, Sm, Eu, Gd, Tb, Dy, Ho, Tm, Yb and Lu) (Hill and Boynton, 2003). These values are in the range of SaU 169 lithologies, lower than in the KREEP clast but slightly above the average regolith composition.

SaU 169 is clearly different from other lunar meteorites found in the south of Oman, (Dho 025, 262, 081) which sample highland compositions and probably are derived from lunar far side (Cahill et al. 2004; Cohen et al. 2004). Although olivine with nearly pure fayalitic composition was found in the SaU 169 regolith, NWA 3136 (Korotev and Irving 2005), and Dho 287A (Anand et al. 2003) source-crater pairing is unlikely. This shows that fayalites are probably spread over large areas on the lunar surface. In a recent compilation Korotev (2005) also proposed that the impact melt breccia of the SaU 169 represent a separate group of lunar meteorites that is different from other known lunar meteorites due to its very high Th and incompatible elements.

**Regolith Origin on the Moon**

Based on a combination of age and chemical data obtained on SaU 169, the history of the rock was constrained to the area surrounding the Imbrium basin (Gnos et al. 2004). If these data are combined with the noble gas data of Lorenzetti et al. (2005), and the data presented in this study, the original dataset can be refined.

The noble gas data indicate that the shock-compaction of the older regolith occurred at a depth of a few meters in ground at ~200 Ma (Gnos et al. 2004). Thus the older regolith probably represents a sample of a relatively deep-seated regolith from the Lalande crater area. The younger regolith (stage III in figure 2), compositionally distinct from the older regolith, contains a solar wind noble gas component (Gnos et al. 2004; Lorenzetti et al. 2005) which means that components of this regolith were exposed at the very surface of the Moon.

A source area for the SaU 169 in the region of the Apollo 14 and 12 landing sites is very likely because: 1) the regolith bulk chemistry and its REE content fall

between those of the soil and regolith breccia of the Apollo 12 and 14 (Haskin and Warren 1991); 2) The bulk chemistry and the REE content of the KREEP clast is very similar to that of the Apollo 14 ITE-rich high-K KREEP (Jolliff 1998; Warren 1989); 3) The Sm versus $Al_2O_3$ (Fig. 12) data show that the regolith breccia plot in the field of the Apollo 14 regolith breccias (Cahill et al. 2004; Warren and Wasson 1980); 4) Most basalts clast have $TiO_2$ contents in the range of Ti-poor basalts (four) and medium Ti basalts (three) indicating strong contribution of mare basalts similar to those from the Apollo 12, Luna 24 and Apollo 14 (Le Bas 2001; Papike et al. 1991); 5) The Fe-Ti-Th-K ratios derived from remote sensing data {Lawrence, 1999 #242;Haskin, 2000 #244;Gillis, 2004 #243} are consistent with the regolith bulk chemistry for this area; 6) The Th and U concentrations in returned Apollo 12 and 14 soils are close to those of the SaU 169 average regolith. 7) KREEP-basalts, common at the Apollo 15 landing located on the eastern rim of the Imbrium basin (but not at the Apollo 12 and 14 sites) are not observed in the SaU 169 regolith. 8) Fe-rich basaltic rocks like our basalt 11 (Fig. 4) were common in the Apollo 12 collection (e.g., Roedder, 1979).

These chemical data and the proximity of the proposed Lalande crater area to the Apollo 12 and 14 landing sites (Fig. 13) are consistent with the work by Gnos et al. (2004) proposing that the Lalande impact crater is the most plausible site where the SaU 169 impact melt breccia was excavated and brought to a regolith position ~ 2800 Ma ago.

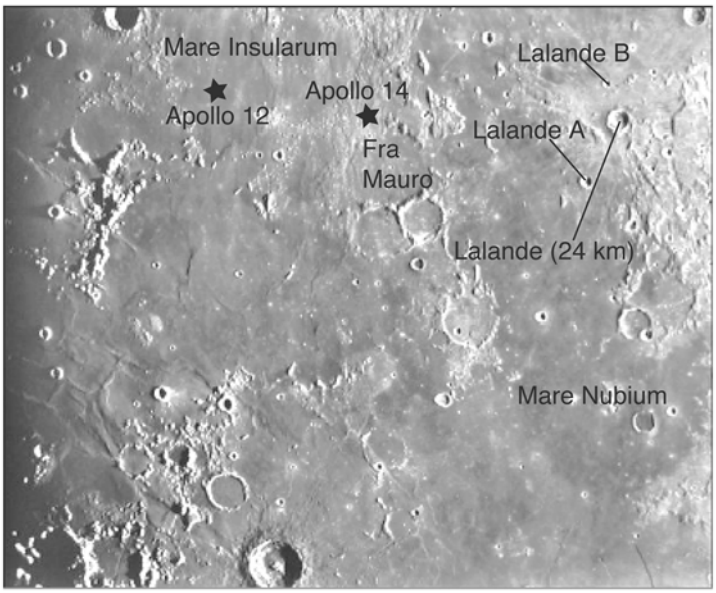


Fig. 13. Photograph of the Apollo 14 and 12 landing region (www.lunarrepublic.com/atlas /index.shtml) showing the Mare Insularum and the Mare Imbrium suspected to be the possible lunar source region for the SaU 169 meteorite. Because the Lalande impact is located to the east of the lower corner of the Mare Insularum, this supports the work by (Gnos et al. 2004) proposing that the SaU 169 impact melt breccia (oldest part of SaU 169) was excavated to a regolith position (regolith stage-II, in Fig. 2) by the Lalande impact at ~ 2800 Ma.

## CONCLUSIONS

SaU 169 is a unique lunar meteorite sampling mainly Procellarum Terrane-derived material. Its regolith comprises rock and mineral fragments embedded in a fine ground mass. Only one highland anorthosite rock fragment was found. The SaU 169 regolith and the KREEP breccia clast have chemical compositions typical to lunar KREEP rocks and are comparable with soils and regolith breccias sampled at the Apollo 14 and Apollo 12 landing sites. The Sc content, the Sm-$Al_2O_3$ relations (Fig. 11) and the La/Yb value (Table 4) are also similar to the Apollo 14 KREEP suite and regolith breccia. The ferroaugite-fayalite-silica picrobasalt clast and the large magmatic fayalite clast probably represent highly evolved magmas as studied in Apollo 12 material (Roedder 1979). The chemical composition of the SaU 169 regolith is clearly different from that of

other lunar meteorites except one KREEP clast (clast F) described from the Calcalong Creek lunar meteorite (Hill and Boynton 2003).

*Acknowledgments*– Dr. Hilal Al Azri, Ministry of Commerce and Industry, Muscat, and Akram Al Muraza, Khalid Musallam Al Rawas, and Sami Al Zubaidi, Ministry of Commerce and Industry, Salalah, are thanked for their support during the project. This study was supported by the Swiss National Science Foundation grants 2100-064929, 200020-107681 and microprobe credits 21-26579.89 and 200021-103479/1.

## REFERENCES

Anand, M., Taylor L. A., Misra K. C., Demidova S. and Nazarov M. A. 2003. KREEPy lunar meteorite Dhofar 287A: A new lunar mare basalt. *Meteoritics & Planetary Science* 38: 485-499.

Cahill J. T., Floss C., Anand M., Taylor L. A., Nazarov M. A. and Cohen B. A. 2004. Petrogenesis of lunar highlands meteorite: Dhofar 081, Dar al Gani 262, and Dar al Gani 400. *Meteoritics & Planetary Science* 39: 503-529.

Cohen B. A., James O. B., Taylor L. A., Nazarov M. A. and Barsukova L. D. 2004. Lunar highland meteorite Dhofar 026 and Apollo sample15418: Two strongly shocked, partialy melted, granulitic breccias. *Meteoritics & Planetary Science* 39: 1419-1447.

Deleno J. W. 1986. Pristine lunar glasses: Criteria, data and implications. *Proceedings, Lunar and Planetary Science conference* 16: D201-D213.

Demidova S., Nazarov M. A., Kurat G., Brandstätter F. and Ntaflos T. 2003. Lunar meteorite Dhofar 310: A polymict breccia with deep-seated lunar crustal material. *Meteoritics & Planetary Science* 38: (A30).

Evensen N. H., Hamilton P. J. and O N., R. K. 1978. Rare-earth abundance in chondritic mereorites. *Geochimica et cosmochimica Acta* 42: 1199-1212.

Gillis J. J., Jolliff B. L. and Korotev R. L. .2004. Lunar surface geochemistry: Global concentrations of Th, K, and FeO as derived from lunar prospector and Clementine data. *Geochimica et cosmochimica Acta* 68: 3791-3805.

Gnos E., Hofmann B., Al-Kathiri A., Lorenzetti S., Eugster O., Whitehouse M. J., Villa I. M., Jull A. J. T., Eikenberg J., Spettel B., Krähenbühl U., Franchi I. A. and Greenwood R. C. 2004. Pinpointing the source of a lunar meteorite: Implications for the evolution of the moon. *Science* 305: 657-659.

Haskin L. A. and Warren P. 1991. Lunar chemistry. In *Lunar source book; A user's guide to the moon.* Cambridge: Cambridge University Press. pp. 357-474

Haskin L. A., Gillis J. J., Korotev R. L. and Jolliff B. L. 2000. The material of the lunar Procellarum KREEP terrain: A synthesis of data from geomorphological mapping, remote sensing, and sample analysis. *Journal of Geophysical Research* 105: 20403-20415.

Hill D. H. and Boynton W. V. 2003. Chemistry of the Calcalong Creek lunar meteorite and its relationship to lunar terrenes. *Meteoritics & Planetary Science* 38: 595-626.

Jolliff B. L. 1998. Large-scale separation of K-frac and KREEP-frac in the source regions of Apollo impact-melt breccias, and a revised estimate of the KREEP composition. *International Geology Review* 40: 916-935.

Kieffer, S. W. 1976. Shock processes in porous quartzite: Transmission electron microscope observations and theory. Contributions to Mineralogy and Petrology, 59, 41-93.

Korotev R. 1997. Some things we can infer about the Moon from the composition of the Apollo 16 regolith. *Meteoritics & Planetary Science* 32: 447-478.

Korotev R. 2000. The great lunar hot spot and the composition and origin of the Apollo mafic ("LKFM") impact-melt breccia. *Journal of Geophysical Research* 105: 4317-4345.

Korotev R. L. 2005. Lunar geochemistry as told by lunar meteorites. *Chemie der Erde* 65: 297-346.

Korotev R. L. and Irving M. A. 2005. Compositions of three lunar meteorites: Meteorite Hills 01210, Northwest Africa 001, and Northeast Africa 3136. *Lunar & Planetary Science* XXXVI: 1220.pdf.

Kuehner S. M., Irving M. A., Rumbl D. I., Hupé A. C. and Hupé G. M. 2005. Mineralogy and Petrology of lunar meteorite NWA 3136: A glass-welded mare regolith of mixed heritage. *Lunar & Planetary Science* XXXVI: 1228.pdf.

Lawrence D. J., Feldman W. C., Barraclough B. L., Binder A. B., Elphic R. C., Maurice S., Miller M. C. and Prettyman T. H. 1999. Hihg resolution measurements of absolute thorium abundances on the lunar surface. *Geophysical Research Letters* 26: 2681-2684.

Le Bas M. J. 2001. Report of the working party on the classification of the lunar igneous rocks. *Meteoritics & Planetary Science* 36: 1183-1188.

Lorenzetti S., Busemann H. and Eugster O. 2005. Regolith history of lunar meteorites. *Meteoritics & Planetary Science* 40: 315-327.

McKay D. S., Heiken G., Basu A., Blanford G., Simon S., Reedy R., French B. M. and Papike J. J. 1991. The Lunar regolith. In *Lunar source book; A user's guide to the moon.* Cambridge: Cambridge University Press. pp. 285-356

Morimoto N., Cairmann, Fabries J., Ferguson A. K., Ginzburg I. V., Ross M., Seifert F. A., Zussman J., Aoki K. and Gottardi G. 1988. Nomenclature of Pyroxenes. *Schweizerische Mineralogische und Petrographische Mitteilungen* 68: 95-111.

Neal C. R. and Taylor L. A. 1992. Petrogenesis of mare basalts: A record of lunar volcanism. *Geochimica et Cosmochimica Acta* 56: 2177-2211.

Osinski, G. R. 2005. Shock-metamorphosed and shock-melted $CaCO_3$-bearing sandstones from the Houghton impact structure, Canada: Melting of calcite at ~10-20 GPa. Lunar and Planetary Science, XXXVI: 2038.pdf.

Papike J. J., Taylor L. A. and Simon S. B. 1991. Lunar minerals. *In The evolution of the igneous rocks,* edited by H. S. *Yoder*. Princeton: Princeton University Press. pp. 15-58

PAPIKE J. J. 1998. *Planetary Materials*. Washington DC: The Mineralogical Society of America. pp. 1-893.

Papike J. J. 1998. Comparative planetary mineralogy: Chemistry of melt-derived pyroxene, feldspar, and olivine. *In Planetary materials,* edited by J. J. Papike. Washington, D.C: Mineralogical Society of America. pp. 7-01-7-11

Papike J. J., Karner J. M. and Shearer C. K. 2003. Determination of planetary basalt parentage: A simple technique using the electron microprobe. *American Mineralogist* 88: 496-472.

Roedder E. 1979. Silicate liquid immiscibility in magmas. *In Lunar source book; A user's guide to the moon*. Cambridge: Cambridge University Press. pp. 121-181

Scaillet B. and MacDonald R. 2001. Phase relations of peralkaline silicic magmas and petrogenetic implications. *Journal Petrology* 42: 825-845.

Warren P. H. and Wasson J. T. 1979. The origin of KREEP. *Reviews of Geophysics and Space Physics* 17: 73-88.

Warren P. H. and Wasson J. T. 1980. Further foraging for pristine nonmare rocks: Correlations between geochemistry and longitude. *Proceedings, $11_{th}$ Lunar and Planetary Science Conference*: 431-470.

Warren P. H. 1989. Major-element diversity, trace-element uniformity (almost). In *Workshop on Moon transition: Apollo 14, KREEP, and evolved lunar rocks*, edited by J. G. Taylor, and P. H. Warren. Houston: Lunar and planetary institute, LPI Technical Report. pp. 149-153

# Pinpointing the Source of a Lunar Meteorite: Implications for the Evolution of the Moon

Edwin Gnos,[1]* Beda A. Hofmann,[2] Ali Al-Kathiri,[1] Silvio Lorenzetti,[3] Otto Eugster,[3] Martin J. Whitehouse,[4] Igor M. Villa,[1] A. J. Timothy Jull,[5] Jost Eikenberg,[6] Bernhard Spettel,[7] Urs Krähenbühl,[8] Ian A. Franchi,[9] Richard C. Greenwood[9]

The lunar meteorite Sayh al Uhaymir 169 consists of an impact melt breccia extremely enriched with potassium, rare earth elements, and phosphorus [thorium, 32.7 parts per million (ppm); uranium, 8.6 ppm; potassium oxide, 0.54 weight percent], and adherent regolith. The isotope systematics of the meteorite record four lunar impact events at 3909 ± 13 million years ago (Ma), ~2800 Ma, ~200 Ma, and <0.34 Ma, and collision with Earth sometime after 9.7 ± 1.3 thousand years ago. With these data, we can link the impact-melt breccia to Imbrium and pinpoint the source region of the meteorite to the Lalande impact crater.

The elevated Th content of the lunar Procellarum terrane was recognized during the Apollo gamma-ray remote mapping program (*1*). The terrane, which includes Mare Imbrium and Mare Procellarum, is characterized by K-REE-P (or KREEP) [potassium (K), rare earth elements (REE), and phosphorus (P)] rock, which is enriched in incompatible elements (*2*–*5*). Such material was returned by all Apollo missions (*6*). KREEP-rich material is confined to areas surrounding the Imbrium basin and the Montes Carpatus–Lalande belt (*7*), where the impact deposits provide a datable marker of lunar stratigraphy (*6*, *8*). The age of the Imbrium basin has been inferred from isotope-system shock-resetting data and is debated to be either 3770 or 3850 million years old (*9*, *10*).

Sayh al Uhaymir (SaU) 169 is a 206.45-g rock found in the Sultanate of Oman (*11*). The rock consists of two lithologies (Fig. 1). About 87% by volume (estimates based on tomographic sections) (fig. S1) consists of a holocrystalline, fine-grained polymict impact-melt breccia (stage I in Fig. 1) containing 25 to 40 vol % of shocked rock and mineral clasts. The rock clasts are coarse-grained norites, gabbronorites, and mafic granulites. Crystal clasts comprise plagioclase ($An_{57-94}$), orthopyroxene ($En_{44-78}Wo_{1-7}$), olivine ($Fo_{58-67}$), and minor ilmenite, clinopyroxene, spinel, tridymite, or kamacite (table S1). The mineral chemistry of clasts suggests the presence of norites to olivine norites and subordinate, more evolved magmatites (granodiorites to granites) and a few granulites at the impact area. No highland anorthosites ($An_{>97}$) were identified.

The fine-crystalline impact melt (generally <200-μm grain diameter) consists of short-prismatic, low-Ca pyroxene ($En_{61-64}Wo_{3-4}$), mildly shocked plagioclase ($An_{75-81}$), and potassium feldspar, ilmenite, whitlockite, olivine ($Fo_{58-59}$), zircon, troilite, kamacite, and tridymite (see also table S1). The impact melt ilmenites contain unusually high $Nb_2O_5$ (~0.5 wt %), which distinguishes them from known lunar ilmenites (*6*). The impact melt is partially rimmed by shock-lithified regolith (13 vol%). We distinguish two stages of regolith formation (II and III in Fig. 1) from compositional differences. Regolith II and III comprise clasts of crystalline and glassy volcanic rocks, magmatic rocks, breccias, mafic granulites, and crystal fragments. Only stage III regolith is bordered by flow-banded glass and contains yellow and orange glass fragments (including glass beads), olivine basalts, pyroxferroite-bearing basalts, and an anorthosite clast. The basaltic clasts encompass the full range of compositions from Ti-rich to Ti-poor basalts, including aluminous members and picrobasalts (table S2). Glassy shock veins (stage IV in Fig. 1)

[1]Institut für Geologie, Universität Bern, Baltzerstrasse 1, CH-3012 Bern, Switzerland. [2]Naturhistorisches Museum der Burgergemeinde Bern, Bernastrasse 15, CH-3005 Bern, Switzerland. [3]Physikalisches Institut, Abteilung für Weltraumforschung und Planetologie, Universität Bern, Sidlerstrasse 5, CH-3012 Bern, Switzerland. [4]Laboratory for Isotope Geology, Swedish Museum of Natural History, Box 50007, SE-104 05, Stockholm, Sweden. [5]National Science Foundation–Arizona Accelerator Mass Spectrometry Laboratory, University of Arizona, 1118 East Fourth Street, Tucson, AZ 85721, USA. [6]Paul Scherrer Institut, 5232 Villigen, Switzerland. [7]Max-Planck-Institut für Chemie, Abteilung Kosmochemie, 55020 Mainz, Germany. [8]Departement für Chemie und Biochemie, Universität Bern, Freiestrasse 3, CH-3012 Bern, Switzerland. [9]Planetary and Space Sciences Research Institute, Open University, Milton Keynes MK7 6AA, UK.

*To whom correspondence should be addressed: gnos@geo.unibe.ch

crosscut impact melt and regolith and record the latest impact event.

The chemical composition of the meteorite has been characterized by using complementary methods. Nondestructive γ-ray spectroscopy of the uncut rock yielded a typically lunar K/U ratio of 554. The mean of three oxygen isotope measurements of the impact melt ($\delta^{17}O$ = 3.37‰, $\delta^{18}O$ = 6.48‰, and $\Delta^{17}O = 0.001 \pm 0.032$‰) plots on the Earth-Moon fractionation line (*12*). Chemical analyses were obtained from the impact melt, the regolith, and a large breccia clast (Table 1 and Fig. 1). Th, U, and K concentrations are similar for powder aliquots of the impact melt and for the bulk rock. A lunar origin for the meteorite is indicated by lunar element ratios (*6*) such as Fe/Mn (moon, 60 to 80; impact melt, 79; regolith, 78; regolith clast, 74) and K/U ratios (moon, 320 to 3800; impact melt, 535; regolith, 1682; clast, 1253).

The SaU 169 impact-melt breccia is chemically similar to Apollo KREEP impact-melt breccias (*4*), with slightly lower Al and Si, and higher Na, Ti, and P. However, with 32.7 ppm Th, 8.6 ppm U, and 1332 ppm $REE_{tot}$, the impact melt is more enriched in KREEP elements than is any other known lunar rock (*6*). Mean concentrations in Apollo 14 to 17 Th-rich impact-melt breccias range from 8.2 to 16.7 ppm (*13*). Relative to Apollo KREEP-rich impact melts, it is enriched in incompatible trace elements by a factor of 2 to 4 (Fig. 2). The alkali elements K, Rb, and Cs occur at levels typical for Apollo impact melts but are depleted relative to other incompatible trace elements: K/Th, Rb/Th, and Cs/Th are only 0.35 ± 0.02 of the Apollo impact-melt breccia values (Fig. 2), which indicates a decoupling of the alkalis during incompatible trace-element fractionation. A low Rb/Sr of 0.04 shows that it is not related to highly evolved KREEP differentiates (Rb/Sr, 0.10 to 0.56) (*13*). The siderophile elements Ni, Co, Ir, and Au are present at levels similar to Apollo impact melts and require ~0.5% of a meteoritic component.

The average regolith (Fig. 1 and Table 1) has a composition similar to Apollo 12, 14,

**Table 1.** Whole-rock chemistry.

| Oxides or elements | Impact-melt breccia 827 mg* | Average regolith 185 mg† | KREEP clast 117 mg† |
|---|---|---|---|
| | | *wt %* | |
| $SiO_2$ | 45.15 | 46.9‡ | – |
| $Al_2O_3$ | 15.88 | 17.54 | 16.34 |
| $FeO_{tot}$ | 10.67 | 11.09 | 8.80 |
| MnO | 0.14 | 0.14 | 0.12 |
| MgO | 11.09 | 7.94 | 6.92 |
| CaO | 10.16 | 11.72 | 10.60 |
| $Na_2O$ | 0.98 | 0.78 | 1.18 |
| $K_2O$ | 0.54 | 0.46 | 0.88 |
| $TiO_2$ | 2.21 | 2.49 | 1.47 |
| $ZrO_2$ | 0.38 | 0.08 | 0.19 |
| BaO | 0.17 | 0.07 | 0.15 |
| $Cr_2O_3$ | 0.14 | 0.19 | 0.12 |
| $P_2O_5$ | 1.14 | 0.42 | 0.76 |
| S | 0.33 | | |
| Total | 98.98 | 99.82 | |
| | | *ppm* | |
| Sc | 25 | 28 | 18 |
| V | 36 | 61 | 36 |
| Cr | 992 | 1310 | 811 |
| Co | 31 | 19 | 12 |
| Ni | 204 | 82 | 58 |
| Cu | 9 | <20 | <20 |
| Zn | 31 | <60 | <60 |
| Rb | 13.7 | 10.0 | 20.0 |
| Sr | 359 | 214 | 230 |
| Y | 532 | 162.5 | 338 |
| Zr | 2835 | 596 | 1397 |
| Nb | 124 | 18 | 112 |
| Cs | 0.8 | 0.4 | 0.9 |
| Ba | 1520 | 593 | 1351 |
| La | 170 | 52 | 113 |
| Ce | 427 | 139 | 297 |
| Pr | 57.45 | 17.1 | 35.6 |
| Nd | 256.5 | 76.9 | 162 |
| Sm | 70.15 | 21.9 | 44.9 |
| Eu | 4.20 | 2.43 | 2.45 |
| Gd | 86.4 | 25.3 | 50.4 |
| Tb | 15.1 | 5.08 | 10.5 |
| Dy | 94.15 | 30.7 | 63.9 |
| Ho | 21.3 | 6.36 | 13 |
| Er | 58.05 | 18.6 | 39.3 |
| Tm | 9.13 | 2.72 | 5.96 |
| Yb | 54.65 | 16.9 | 36 |
| Lu | 7.64 | 2.53 | 5.24 |
| Hf | 64.3 | 14.8 | 34.7 |
| Ta | 7.1 | 2.14 | 4.16 |
| W | 3.45 | 1.3 | 2.5 |
| Ir ppb | 4.2 | | |
| Au ppb | 6 | | |
| Pb | 13.8 | <10 | <10 |
| Th | 32.7 | 8.44 | 21.70 |
| U | 8.6 | 2.27 | 5.83 |
| Sum REE (ppm) | 1332 | 418 | 879 |
| Fe/Mn (wt) | 76.5 | 79.5 | 73.6 |
| Mg/(Fe+Mg) (mol) | 0.65 | 0.56 | 0.58 |
| K/U (wt) | 521 | 1682 | 1253 |
| Th/U (wt) | 3.80 | 3.72 | 3.72 |

*Combined inductively coupled plasma mass spectrometry and optical emission spectrometry, and instrumental neutron activation analysis. †Inductively coupled plasma mass spectrometry and optical emission spectrometry. ‡Microprobe value on regolith shock glass.

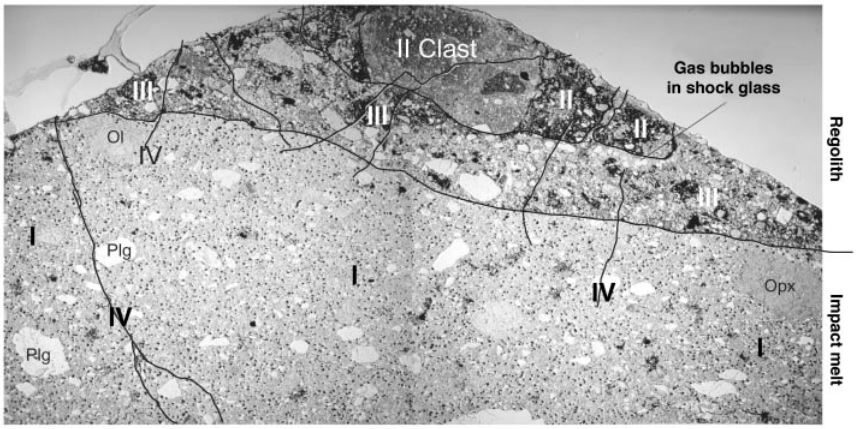


**Fig. 1.** Thin-section photograph showing the different lithologies and their age relationship: I, impact-melt breccia. II and III, two types of regolith (III intrudes II). IV designates shock veins as youngest formation. Ol, olivine; Plg, plagioclase; Opx, orthopyroxene. Image width is 35 mm.

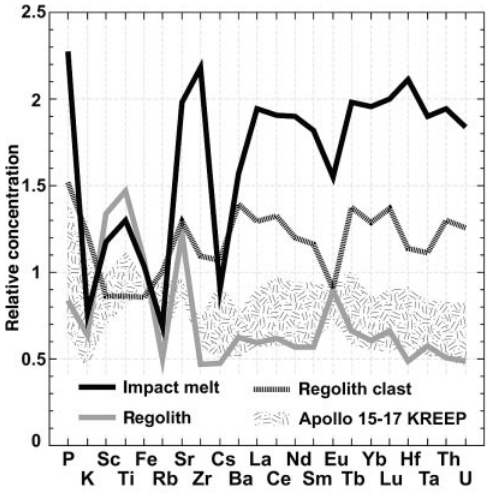


**Fig. 2.** Element abundances of impact-melt breccia, regolith II and III combined, and a polymict breccia clast in regolith II normalized to average Apollo 14 high-Th impact-melt breccias (*13*). Data for Apollo 15 to 17 impact melts are shown for comparison. Compared with Apollo data, P, Zr, REE, Th, and U contents are significantly higher, but K, Cs, and Rb, as well as Al and Si (typically fractionated in potassium feldspar), are lower.

and 15 regoliths. In contrast to the impact melt, the regolith is not depleted in Na and K (Fig. 2), as shown by the higher K/U of 1682. The regolith clast is an evolved KREEP rock (Fig. 2) with 21.7 ppm Th, but it is unrelated to the impact melt, on the basis of its K/U ratio of 1253. The exceptionally high Th, U, and K contents restrict the provenance of SaU 169 to the Imbrium area (*13*).

We determined the ages of the four impact events using isotopic data. $^{207}$Pb-$^{206}$Pb isotope ratios (table S3) were obtained in thin section by ion-microprobe analysis on 12 poikilitic impact-melt zircons and yielded a crystallization age of 3909 ± 13 Ma [2σ; mean square weighted deviation (MSWD), 0.33] (Fig. 3). $^{39}$Ar-$^{40}$Ar data (table S4) were obtained on a feldspar concentrate from the impact melt. The irregular age spectrum in combination with the Ca/K concentrations indicate a resetting of the Ca-rich feldspars at ~2800 Ma and a younger disturbance at <500 Ma affecting the potassium feldspars (fig. S2).

The duration of cosmic-ray exposure (CRE) of the impact-melt breccia and the younger regolith (stage III in Fig. 1) was obtained from light noble gas isotopic characteristics (table S5). All three samples analyzed show He loss; hence, the $^{3}$He CRE age is not significant. The production rates for $^{21}$Ne and $^{38}$Ar depend on the chemical composition and on shielding depth during exposure to cosmic rays. The $(^{22}Ne/^{21}Ne)_c$ value of 1.197 for the impact melt and 1.200 for the regolith indicate irradiation at a shielding depth of a few tens of centimeters. Using the method for calculating production rates proposed by (*14*) at the lunar surface and (*15*) during transfer in space, and assuming a typical shielding of 40 g/cm$^2$, we obtained lunar surface CRE ages from $^{21}$Ne and $^{38}$Ar of 200 ± 40 Ma and 182 ± 36 Ma for the impact melt, and 150 ± 30 Ma and 192 ± 38 Ma for the regolith. The $^{38}$Ar CRE age extracted from the $^{39}$Ar-$^{40}$Ar data is also 192 ± 20 Ma (table S4 and fig. S2).

By adopting a saturation activity for $^{10}$Be of 25 dpm/kg as given by (*16*), we found the upper time limit for a small rock exposure during Moon-Earth transfer, estimated from $^{10}$Be (table S6), to be 0.34 Ma. Thus, the exposure in free space is negligibly short compared with the total CRE. We conclude that the CRE ages are lunar regolith residence times. Like most lunar meteorites (*17*), SaU 169 thus seems to have resided in the upper meter of the regolith before launch into space, as supported by our CRE ages and by the solar wind component found in the stage III regolith (table S5). The terrestrial age obtained by $^{14}$C and $^{10}$Be methods is ≤9700 ± 1300 years (table S6).

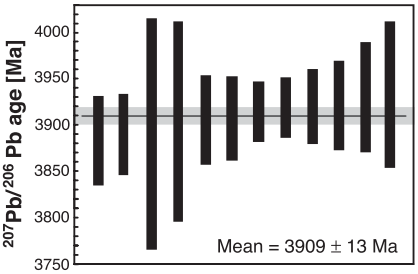


**Fig. 3.** $^{207}$Pb/$^{206}$Pb ages of 12 zircons from the impact melt. Data are corrected for common Pb (*24*) and yield a weighted average age of 3909 ± 13 Ma (2σ; MSWD = 0.33).

The combined age data indicate a complex lunar history. Crystallization of the impact melt occurred at 3909 ± 13 Ma, followed by exhumation by a second impact at ~2800 Ma, which raised the sample to a regolith position at unconstrained depth. A third impact at ~200 Ma moved the material closer to the lunar surface, where it mixed with solar-wind–containing regolith. It was launched into space by a fourth impact at <0.34 Ma.

The 3909 ± 13 Ma $^{207}$Pb-$^{206}$Pb zircon age on the impact melt is an accurate estimate for the Imbrium impact event. The small difference from the 3770 ± 20 or 3850 ± 20 Ma range obtained by whole-rock $^{39}$Ar-$^{40}$Ar system (*9*, *10*, *18*) confirms that the argon system yields reliable age estimates. The age difference may reflect the imprecisely known $^{40}$K decay constant. A recalculation of the argon ages with the decay value proposed by (*19*) results in a ~1% age increase.

We were able to constrain the SaU 169 provenance even more tightly by using Lunar Orbiter images in combination with Clementine-derived Fe-Ti maps, Lunar Prospector Th maps, Clementine color-ratio images (750/950 nm), lunar crater ages (*20*, *21*) (table S7), and data from the Apollo and Luna missions. The source location is based on the following assumptions: (i) The high Th (32.7 ppm) impact melt is derived from one of the highest Th areas defined by Lunar Prospector γ-ray mapping; (ii) The regolith Fe-Ti-Th concentrations are representative of the regolith of the ejection area; (iii) The age disturbances at ~2800 and 200 Ma were caused by impacts that were able to disturb the Ar system; (iv) The ejection crater from which the rock was launched to Earth is on the order of a few kilometers (*17*).

The Lunar Prospector γ-ray mapping demonstrated that the surface occurrence of KREEP is confined to the near-side Procellarum terrane (*2*–*5*, *22*, *23*). Because the bulk Th content of the impact melt (Table 1) is higher than any pixel of the Lunar Prospector measurements (maximum, 9.36 to 10.40 ppm) (*7*), we assume that SaU 169 must come from one of the Th hot spots (fig. S3), which are located at the Aristarchus and Aristillus craters, the Montes Carpathus–Fra Mauro region, and the Lalande crater region (*7*). Among these Th hot spots, only the area around Lalande and southeast of the crater Aristillus are compatible with our regolith Fe-Ti-Th concentrations (table S7). In both areas, a young (bright-halo), small crater as a possible launch-to-Earth crater is evident. However, the age data for SaU 169 render the Lalande crater area (9°W 5°S) the most plausible because it contains a ~2800 Ma crater (Lalande, 2246 to 2803 Ma) and a ~200 Ma crater (e.g., Lalande A, 175 to 300 Ma) (table S7). Based on the comprehensive data set presented, we conclude that an origin from the Lalande crater area is most likely.

SaU 169 is the only large high-KREEP sample for which simultaneous determinations of precise age and chemistry are available. The Imbrium impact age dates a strong decline of large impacts in the inner solar system corresponding to the beginning of life-supporting conditions on Earth.

**References and Notes**

1. A. E. Metzger, J. I. Trombka, L. E. Peterson, R. C. Reedy, J. R. Arnold, *Science* **179**, 800 (1973).
2. L. A. Haskin, J. L. Gillis, R. L. Korotev, B. L. Jolliff, *J. Geophys. Res.* **105**, 20403 (2000).
3. B. L. Jolliff, J. J. Gillis, L. A. Haskin, R. L. Korotev, M. A. Wieczorek, *J. Geophys. Res.* **105**, 4197 (2000).
4. R. L. Korotev, *J. Geophys. Res.* **105**, 4317 (2000).
5. M. A. Wieczorek, R. J. Phillips, *J. Geophys. Res.* **105**, 20417 (2000).
6. G. H. Heiken, D. T. Vaniman, B. M. French, *Lunar Source Book: A User's Guide to the Moon* (Cambridge University Press, Cambridge, 1991).
7. D. J. Lawrence *et al.*, *Geophys. Res. Lett.* **26**, 2681 (1999).
8. D. E. Wilhelms, *U.S. Geol. Survey Prof. Pap.* **1348**, 1 (1987).
9. B. A. Cohen, T. D. Swindle, D. A. Kring, *Science* **290**, 1754 (2000).
10. D. Stöffler, G. Ryder, *Space Sci. Rev.* **96**, 9 (2001).
11. S. Russell *et al.*, *Meteorit. Planet. Sci.* **38**, A189 (2003).
12. U. Wiechert *et al.*, *Science* **294**, 345 (2001).
13. B. L. Jolliff, *Int. Geol. Rev.* **40**, 916 (1998).
14. C. Hohenberg, K. Marti, F. Podosek, R. Reedy, J. Shirck, *Proc. Lun. Planet. Sci. Conf. 9th*, 2311 (1978).
15. O. Eugster, T. Michel, *Geochim. Cosmochim. Acta* **59**, 177 (1995).
16. C. Tuniz *et al.*, *Geophys. Res. Lett.* **10**, 804 (1983).
17. P. H. Warren, *Icarus* **111**, 338 (1994).
18. G. B. Dalrymple, G. Ryder, *J. Geophys. Res.* **101**, 26069 (1996).
19. K. Min, R. Mundil, P. R. Renne, K. R. Ludwig, *Geochim. Cosmochim. Acta* **64**, 73 (2000).
20. R. B. Baldwin, *Icarus* **71**, 19 (1987).
21. R. B. Baldwin, *Icarus* **61**, 63 (1985).
22. R. C. Elphic *et al.*, *J. Geophys. Res.* **107**, **E4**, 8-1 (2002).
23. W. C. Feldman, O. Gasnault, S. Maurice, D. J. Lawrence, R. C. Elphic, *J. Geophys. Res.* **107, E3**, 5-1 (2002).
24. Materials and methods are available as supporting material on *Science* Online.
25. Funded by Swiss National Foundation grants 21-64929.01, 20-61933.00, and credit 21-26579.89. Thanks to H. Al-Azri and K. Musallam for support; to L. R. Gaddis, USGS, for Lunar Orbiter images; and to J. Kramers, J. Ridley, L. Diamond, D. Fleitmann, T. Armbruster, and B. Hacker for reviews.

**Supporting Online Material**

www.sciencemag.org/cgi/content/full/305/5684/657/DC1
Materials and Methods
SOM Text
Figs. S1 to S3
Tables S1 to S7
References

21 April 2004; accepted 4 June 2004

Image of the SaU 094 Martian meteorite on Omani soil.

*Meteoritics & Planetary Science* 37, xxx–xxx (2002)
Available online at http://www.uark.edu/meteor

# Sayh al Uhaymir 094—A new martian meteorite from the Oman desert

E. GNOS[1*], B. HOFMANN[2], I. A. FRANCHI[3], A. AL-KATHIRI[4], M. HAUSER[1] AND L. MOSER[1]

[1]Institute for Geological Sciences, Baltzerstrasse 1, 3012 Berne, Switzerland
[2]Natural History Museum Bern, Bernastrasse 15, 3005 Berne, Switzerland
[3]Planetary Sciences Research institute, Open University, Milton Keynes MK7 6AA, United Kingdom
[4]Directorate General of Minerals, Ministry of Commerce and Industry, Salalah, Sultanate of Oman
*Correspondence author's e-mail address: gnos@geo.unibe.ch

*(Received 2001 November 7; accepted in revised form 2002 March 12)*

**Abstract**–Sayh al Uhaymir (SaU) 094 is a 223.3 g, partially crusted, strongly to very strongly shocked melanocratic olivine-porphyric rock of the shergottite group showing a microgabbroic texture. The rock consists of pyroxene (52.0–58.2 vol%)—dominantly prismatic pigeonite ($En_{60–68}Fs_{20–27}Wo_{7–9}$) associated with minor augite ($En_{46–49}Fs_{15–16}Wo_{28–31}$)—brown (shock-oxidized) olivine ($Fo_{65–69}$; 22.1–31%), completely isotropic interstitial plagioclase glass (maskelynite; $An_{50–64}Or_{0.3–0.9}$; 8.6–13.0%), chromite and titanian magnesian chromite (0.9–1.0%), traces of ilmenite ($Ilm_{80–86}$), pyrrhotite ($Fe_{92–100}$; 0.1–0.2%), merrillite (<<0.1%), and pockets (4.8–6.7%) consisting of green basaltic to basaltic andesitic shock glass that is partially devitrified into a brown to black product along boundaries with the primary minerals. The average maximum dimensions of minerals are: olivine (1.5 mm), pyroxene (0.3 mm) and maskelynite (0.3 mm). Primary melt inclusions in olivine and chromite are common and account for 0.1–0.6% of the rock. X-ray tomography revealed that the specimen contains ~0.4 vol% of shock-melt associated vesicles, up to 3 mm in size, which show a preferred orientation. Fluidization of the maskelynite, melting and recrystallization of pyroxene, olivine and pyrrhotite indicate shock stage S6. Minor terrestrial weathering resulted in calcite-veining and minor oxidation of sulfides. The meteorite is interpreted as paired with SaU 005/008/051. The modal composition is similar to Dar al Gani 476/489/670/735/876, with the exception that neither mesostasis nor titanomagnetite nor apatite are present and that all phases show little zonation. The restricted mineral composition, predominance of chromite among the oxides, and abundance of olivine indicate affinities to the lherzolitic shergottites.

## INTRODUCTION

Twenty-four unpaired meteorites presently known are attributed to Mars. The most compelling evidence that links them to Mars are relative abundances and isotopic compositions of trapped gases in shergottite shock glasses that are in agreement with direct martian atmosphere compositions measured by the 1976 Viking lander missions (*e.g.*, Bogard and Johnson, 1983). Most martian meteorites are differentiated rocks characterized by young crystallization ages, characteristic C, N, O and noble gas isotopic compositions (*e.g.*, Clayton and Mayeda, 1996; Dreibus and Wänke, 1987; Wänke, 1991), and distinct major and trace element concentrations (*e.g.*, Steele and Smith, 1982; McSween and Jarosewich, 1983; Lodders, 1998). To this suite belong basaltic, gabbroic and lherzolithic rocks (shergottites), clinopyroxenites-wehrlites (nakhlites), a dunite (Chassigny) and an orthopyroxenite. Since the report of putative biological signatures in the martian meteorite Allan Hills (ALH) 84001 (McKay *et al.*, 1996), and in context with intense exploration of Mars by space missions, publications on Mars meteorites have exploded. At the same time, the number of known independent Mars meteorites has increased from 12 to presently 24 (total weight of ~83 kg) since the recent compilations on martian meteorites by McSween and Treiman (1998) and Papike (1998). The new martian meteorite described here was found in the Sayh al Uhaymir region in interior Oman in February 2001 by two of us (M. H. and L. M.) in a joint meteorite search campaign with the Ministry of Commerce and Industry, Sultanate of Oman and was named Sayh al Uhaymir (SaU) 094 (Grossman and Zipfel, 2001). The rock was sampled on flat-bedded Miocene fresh-water limestone deposits of the Fars group (Le Métour *et al.*, 1985). The meteorite is very likely paired with SaU 005, 008 and 051 (Grossmann, 2000; Grossman and Zipfel, 2001) because all were found within a few kilometers distance and are macroscopically similar.

The aim of this paper is to report on the petrography, mineralogy and shock metamorphism of SaU 094. Chemical



Prelude preprint MS#4704

investigations and age dating (terrestrial age, exposure age, formation/ejection ages) are under way.

## ANALYTICAL METHODS

Before cutting we applied x-ray tomography to the meteorite at the Federal Material Testing Laboratory (EMPA, Dübendorf) to non-destructively obtain information about its interior. The industrial computed tomography (CT) scanner applied was made by Scientific Measurement Systems (SMS, Austin, Texas). It was operated at 400 kV, 2.25 mA using linear array detectors, detector aperture 0.25 × 0.5 mm. Tomographs obtained had a resolution of 0.1 mm (pixel size).

Doubly polished thin sections were studied by transmitted and reflected light microscopy, carbon coated and then used for microprobe and cathode luminescence (25 kV, 80 nA) investigations. Because maskelynite and shock glass are isotropic and show little chemical variation we used standard oils and the immersion method for determination of refractive indices on small fragments of maskelynite and shock glass.

Mineral compositions were obtained on a Cameca SX-50 microprobe at Bern University using natural and synthetic mineral standards, wavelength dispersive spectrometers, and beam conditions of 15 kV and 20 nA for silicates, oxides, sulfides and glass. Sulfide standards were used for analyzing the sulfides. Counting times were 20 s on peak and background for major elements, and up to 60 s for trace elements. For all glasses the spot size was ~15 $\mu$m. The possibility of element diffusion during glass analysis was excluded by analyzing the same spot several times in sequence and using different measurement times, which resulted in no variation. For phosphate analysis we used rare earth element (REE) phosphate or REE glass standards, peak and background settings as described by Scherrer *et al.* (2000), a 10 $\mu$m spot and 25 kV, 20 nA beam conditions with 100 s REE counting times. Data were reduced using the PAP procedure.

Small vesicles and alteration products therein were examined using scanning electron microscopy of selected vesicle-rich rock chips. Samples were gold-coated.

Oxygen isotopic composition was determined by laser fluorination of powdered aliquots following the procedure described in Miller *et al.* (1999).

## PETROGRAPHY AND MINERALOGY

Sayh al Uhaymir 094 is 4 × 7 × 5 cm in size, weighs 223.3 g and has a relatively angular shape. Two of the rock's four main faces are coated by very thin black fusion crust (rock color chart RCC 5YR 2/1), the other two are broken surfaces of brownish tint (10YR 4/1). Millimeter-sized dark olivine megacrysts are macroscopically visible on its surface and in cut sections (Fig. 1). On a cut surface, the olivine megacrysts appear brownish gray to black (RCC 5YR 3/1) and are set in an olive-gray (5Y 4/1) groundmass consisting of maskelynite and clinopyroxene (Fig. 1a,b,c). On the surface of the meteorite a few fractures, up to 4 cm in length, are apparent.

X-ray tomographs allowed us to distinguish areas rich in olivine (dark speckles), areas consisting of maskelynite and clinopyroxene (lighter gray speckles), and unexpectedly large, millimeter-sized vesicles present throughout the rock (Fig. 2). Most of these vesicles, which characteristically form the central part of larger shock melt pockets, seem unrelated to fractures.

The primary identification of the rock (Grossman and Zipfel, 2001) was made on five polished thin sections of <1 mm sized fragments from the surface of the meteorite. After cutting of the rock three additional thin sections were prepared perpendicular to one of the faces of the meteorite showing a fusion crust (Fig. 1b,c).

In thin section SaU 094 shows an olivine-porphyric texture without obvious foliation or lineation (Figs. 1 and 3a). Yellowish to dark brown (commonly patchy) hypidiomorphic olivine crystals or clusters of crystals (average maximum dimension 1.5 mm) are embedded in a fine-grained groundmass consisting of prismatic light cream-colored clinopyroxene crystals (mostly pigeonite) and interstitial feldspathic glass (maskelynite) (average maximum dimension 0.3 mm; Fig. 3a). Point counting of two thin sections yielded 22.1–31.0 vol% olivine, 52.0–58.2% pyroxene (pigeonite and augite were not distinguishable) and 8.6–13.0% maskelynite (Table 1). Accessory minerals are chromite (0.9–1.0%), pyrrhotite ± pentlandite (0.1–0.2%) and traces of merrillite. Melt inclusions in olivine (Fig. 3b), chromite and pyroxene account for 0.1–0.6%, and shock melts (Fig. 3c) for 4.8–6.7% of the rock. 4.0–4.1% of this shock melt is finely recrystallized and dark brown to black; the remaining 0.7–2.7% consists of fresh green glass (Table 1). Maskelynite displays a dark bluish-green cathode luminescence without obvious zonation. The fusion crust, though externally visible over significant portions of the meteorite's surface, was only occasionally encountered in thin section. In contrast to shock glass, the fusion crust is a brown, bubble-rich glass (Fig. 3d).

The mineral modes are comparable with the rough estimates given for SaU 005/008 (Zipfel, 2000; Table 1). The mineral modes, especially the high amount of olivine, are similar to Dar al Gani (DaG) 476/489/670/735 (Folco *et al.*, 2000; Mikouchi *et al.*, 2001; Zipfel *et al.*, 2000; Wadhwa *et al.*, 2001) with the exceptions that phosphates are very rare and no mesostasis containing Fe-rich olivine was found (Table 1). The high abundance of olivine and the slightly zoned mineralogy indicate affinities to lherzolitic shergottites (*e.g.*, Gleason *et al.*, 1997; Harvey *et al.*, 1993; Treiman, 1990). Without considering the shock melt, thin section SaU 094C contains >90 vol% mafic minerals (Table 1). SaU 094 thus takes an intermediate position between mafic and ultramafic shergottites, and according to its mineral mode and grain size has to be classified as melanocratic olivine microgabbro with transitions to olivine clinopyroxenite (Streckeisen, 1976). Grain size and texture are similar to terrestrial doleritic dikes/sills or microgabbroic intrusions.

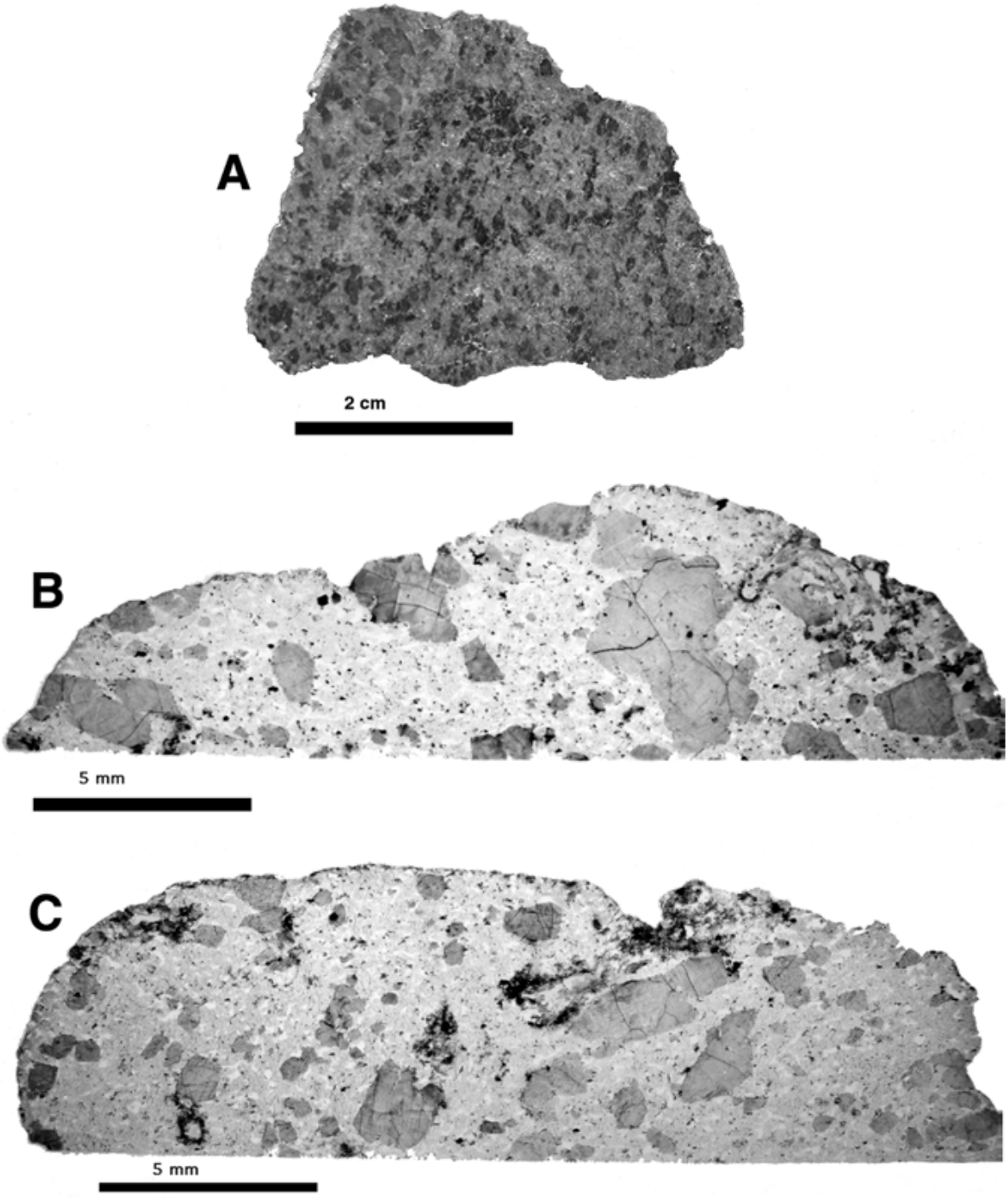


FIG. 1. (a) Slice of SaU 094. Dark patches are olivine crystals and local impact melt; the lighter areas consist of clinopyroxene and maskelynite. Images (b) and (c) are two thin sections cut perpendicular to the surface and used for point-counting and microprobe analyses. Larger crystals are olivine. Dark areas are finely-crystallized zones rimming green shock glass.

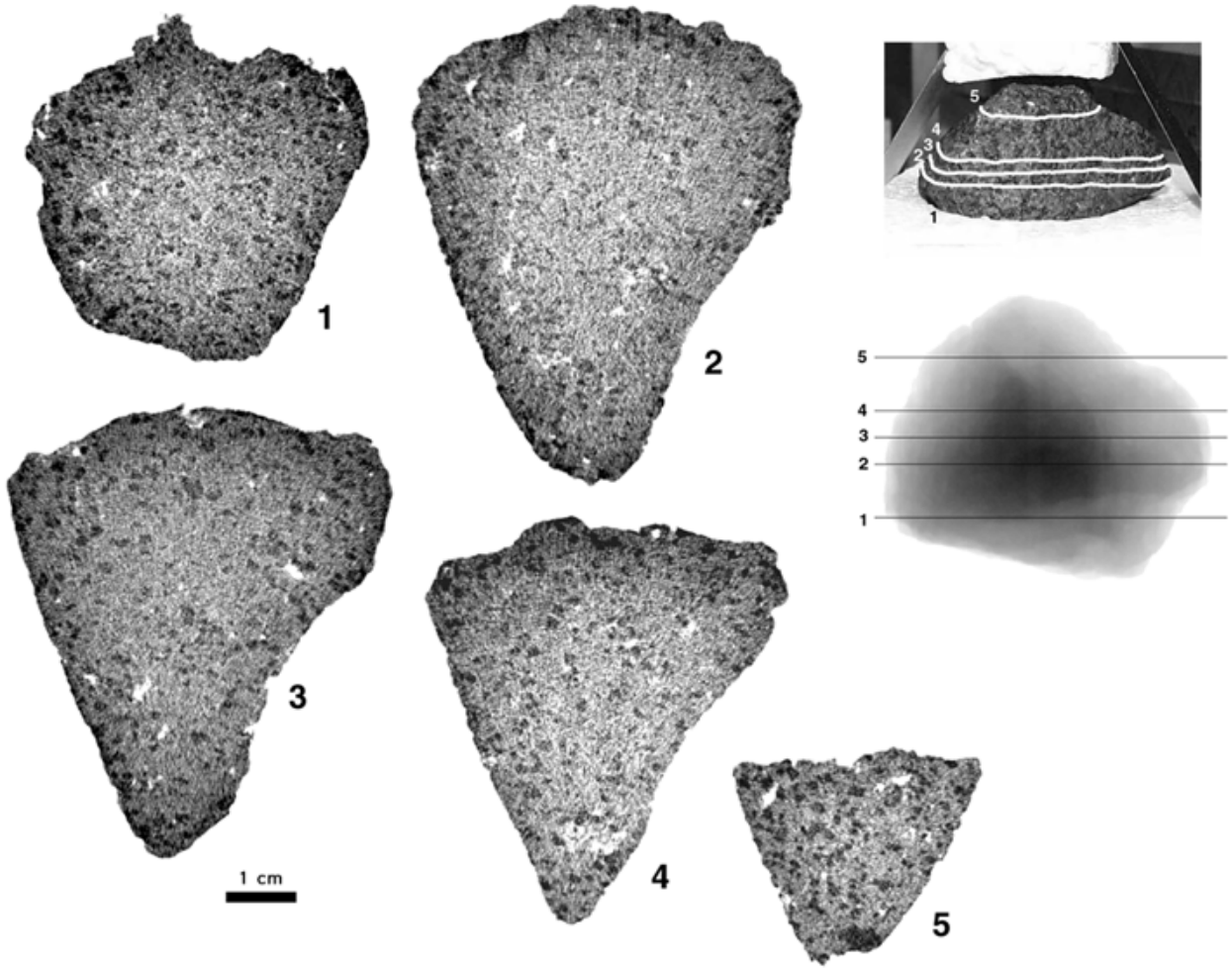


FIG. 2. X-ray tomograms of SaU 094 made at the Federal Institution for Material Research, Dübendorf, before cutting the rock. The top right image shows the stone in analysis position with the traces of the five parallel tomographs. The image below shows the same sections on a transmission x-ray image taken at a right angle relative to the tomographs. Numbers refer to the tomographic sections. Original pixel size of the x-ray images is 0.1 mm. Dark areas are olivines, gray areas correspond to the groundmass (including shock melts) and the white areas are vesicles in melt pockets.

FIG. 3. (*right*) Photomicrographs of SaU 094. (a) Microgabbroic texture consisting of millimeter-sized olivine crystals set in a groundmass of prismatic pigeonite and maskelynite. Transmitted light, section D, width of image 3.8 mm. (b) Olivine crystal containing abundant small melt inclusions (darker patches) characteristically surrounded by radial cracks. Section C, width of image 1.4 mm. (c) Pocket of green impact glass with orbicular and elongated vesicles and flow structures in unhomogenized melt. Along the pocket boundary the melt is crystallized into feathery crystals of both clinopyroxene and olivine. Crossed polarizers, section D, width of image 0.5 mm. (d) Thick rim of bubble-rich glassy fusion crust. Note the sharp boundary of the darker fusion crust (top) to the lighter impact glass that contains feather-like crystals. Section D, width of image 0.5 mm. (e) Zoned chromite grain with speckled Cr-rich core and ulvöspinel-enriched rim (see Fig. 6i). Dark area in center is a magmatic melt inclusion. Reflected light, oil immersion, section D, base of image 0.16 mm. (f) Pyrrhotite showing coarse granular pentlandite (lighter area) and small pentlandite exsolutions lamellae. Associated platy oxide grains on top are ilmenite, on the left chromite. Reflected light, oil immersion, section C, width of image 0.09 mm. (g) Bright orange secondary Mg-Fe-Si silicate (Alt) found in association with melted areas. Its mineralogic composition is unknown. Plain polarized light, section D, width of image 0.5 mm. (h) Scanning electron image of vesicle in impact melt glass containing gypsum crystals, probably derived from alteration of sulfide during martian or terrestrial alteration. Width of image 145 $\mu$m.

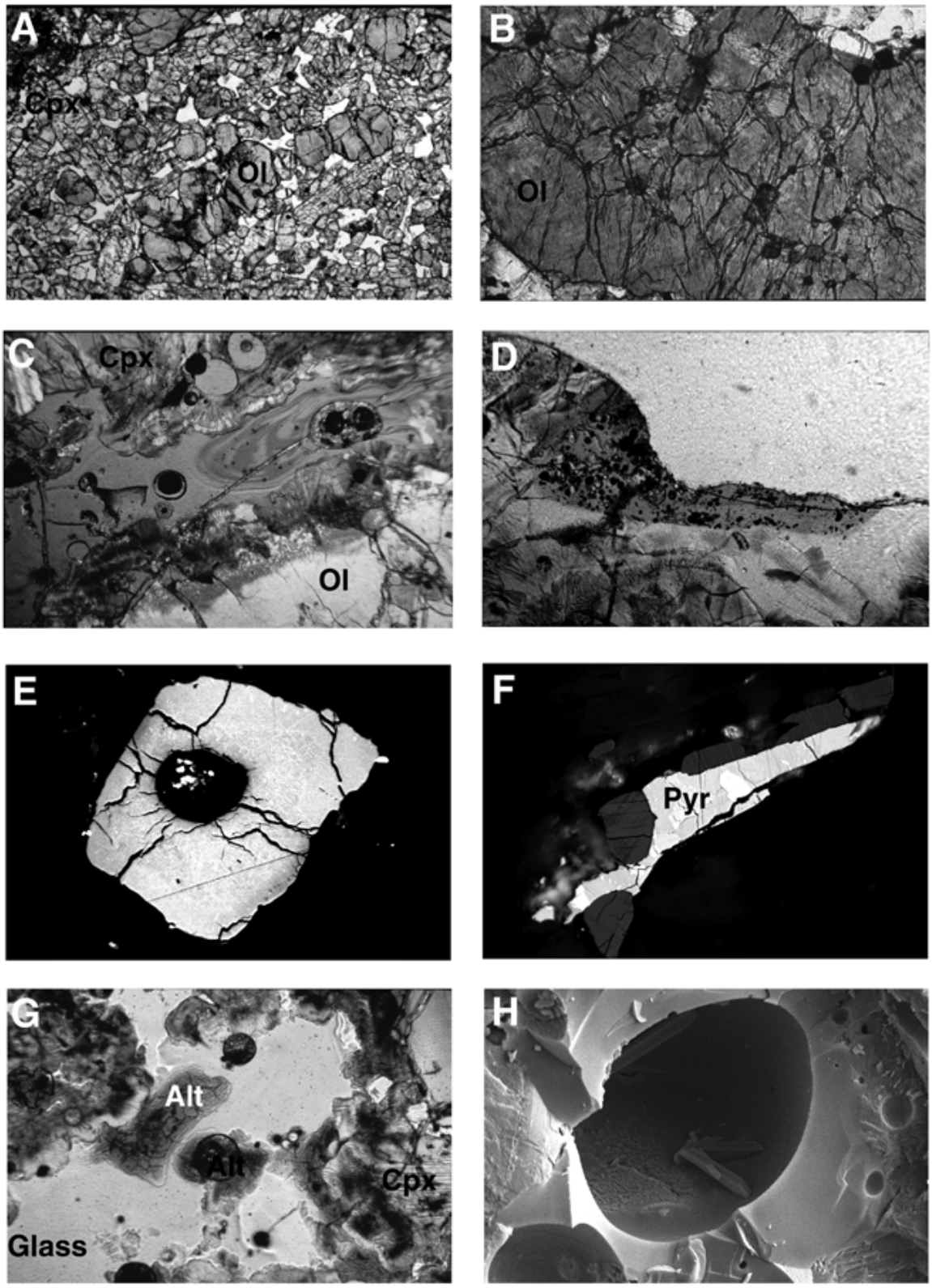
A
Cpx
Ol
B
Ol
C
Cpx
Ol
D
E
F
Pyr
G
Alt
Alt
Cpx
Glass
H

TABLE 1. Modal composition of SaU 094 compared with other martian meteorites.

| Meteorite | SaU 094 ($n$ = 1300) (section C) | SaU 094 ($n$ = 1300) (section D) | SaU 005 and 008* | DaG 476 and 489† | EETA79001A‡ | LEW 88516§ |
|---|---|---|---|---|---|---|
| Lithology | Olivine clinopyroxenite# | Gabbro | Basalt@ | Basalt@ | Basalt@ | Lherzolite@ |
| **Pyroxene (total)** | **52.0** | **58.2** | **~48** | **55.3–64.6** | **69–73** | **>20–44.5** |
| Pigeonite | | | | 44.1–53-? | 55–63 | |
| Augite | | | | 2.9–12.7 | 3.2–8.5 | |
| Orthopyroxene | | | | 1.5–4.0 | 3.4–7.2 | |
| **Olivine (total)** | **31.0** | **22.1** | **~25** | **10.4–24** | **7–10** | **39.2–57** |
| dark | 3.7 | 1.6 | | | | |
| light | 27.3 | 20.5 | | | | |
| **Maskelynite** | **8.6** | **13.7** | **~15** | **12–17** | **16–18** | **<10–16** |
| **Opaques** | **1.1** | **1.1** | | **0.9–3.9** | **2.2–4.0** | **<5** |
| Chromite | 0.9 | 1.0 | | 0–0.6 | | 0.8–3 |
| Ilmenite | tr | tr | | | | |
| Pyrrhotite | 0.2 | 0.1 | | 0–0.6 | | <1 |
| Merrillite | **tr** | **tr** | | **tr–1.5** | **tr–0.4** | **0.9–1** |
| **Mesostasis** | | | | **–** | **tr–0.3** | |
| **Impact glass** | **6.7** | **4.8** | **~9** | **4–7.2** | **–** | **–** |
| Unaltered glass | 2.7 | 0.7 | | | | |
| Recryst glass | 4.0 | 4.1 | | | | |
| **Primary inclusions** | **0.6** | **0.1** | | | | |
| **Alteration minerals** | **tr** | **tr** | **–** | **1–3.1** | **–** | **–** |
| **"Shock cavities"** | **(0.4$)** | **(0.4$)** | | | | |

*Zipfel (2000).
†Zipfel *et al.* (2000); Folco *et al.* (2000); Wadhwa *et al.* (2001); Mikouchi *et al.* (2001).
‡McSween and Jarosewich (1983).
§Gleason *et al.* (1997); Treiman *et al.* (1994); Lodders (1998).
#Two out of 1300 points are red alterations in glass; if impact melt is not included and opaques substracted the rock contains 8.9 vol% maskelynite.
$Shock cavities point-counted on x-ray tomography images (Fig. 2); not present in the two point-counted thin sections.
@As described by authors.
Abbreviations: tr = trace.

Chromite grains are isometric, opaque to brownish translucent and show an average maximum diameter of 0.10 mm. In reflected light (oil immersion) they commonly show a slightly browner Ti-rich rim (Fig. 3e). Intergrowths with ilmenite are common. 5–10 $\mu$m sized, isometric chromite inclusions are characteristic in the cores of some olivines. Chromite grains rarely show inclusions of sulfides. Ilmenite typically occurs as laths showing lamellar twinning (Fig. 3f) and is often associated with chromite and sulfides.

Merrillite occurs in trace amounts and was only found using the cathode luminescence technique, where it shows a yellow color. The grains are isolated and occur associated with maskelynite and along olivine rims.

Sulfide grains (average maximum dimension 0.07 mm) are commonly elongated and consist of polycrystalline pyrrhotite carrying two types of pentlandite inclusions: type 1 are hypidiomorphic crystals up to 10 $\mu$m in size (Fig. 3f); type 2 are tiny (>1 to 2 $\mu$m) oriented exsolutions (Fig. 3f; see also Fig. 9). Image analysis of nine high-magnification photomicrographs indicates the presence of 8.5 ± 2.5 vol% pentlandite in the sulfides. In areas where the rock was shock-melted, pyrrhotite forms granular globules (8.4% of sulfide grains) also containing pyrrhotite (incomplete shock-melt?). Pyrrhotite may fill small cracks (3.2% of sulfide grains) in the silicates, and also occurs in melt inclusions in olivine (1.2% of sulfide grains). Investigation of pyrrhotite using a magnetic colloid (Bitter method; Soffel, 1991) showed that pyrrhotite is dominantly non-magnetic. Magnetic areas of very small size were only observed in close association with nearby weathering products, indicating a possible oxidation-related origin of the small amounts of magnetic pyrrhotite present.

Oval-shaped multiphase melt inclusion are common in olivine characteristically surrounded by radial cracks in the host mineral (Fig. 3b). The size of the inclusions is below 0.1 mm. Qualitative data show that the melt inclusions contain Ca-rich clinopyroxene, spinel, pyrrhotite, and a glassy silicate matrix.

Although the inclusions appear similar to those described by Goodrich and Zipfel (2001) from SaU 005, the microprobe beam could not be sufficiently focused to obtain proper single phase analyses.

In thin section, millimeter to centimeter-sized pockets of a green shock glass are observed. The green glass characteristically contains gas bubbles or vesicles that may reach several millimeters (Figs. 2 and 3c). At the contact to the surrounding silicates a dark brown to black zone occurs characterized by crystallization of acicular and commonly skeletal olivine or clinopyroxene crystals (Fig. 3c,d). Sulfide droplets and rounded (partially melted) chromite grains are common. Around melt pockets olivine and pyroxene show textures suggesting that parts of the grains were melted and subsequently recrystallized into a fine-grained zone largely with conservation of the original grain shape. The refractive index of four green glass fragments is 1.634–1.638, with some variation within one grain. Considering that some melt pockets in olivine- or pigeonite-dominated areas have a very different composition (Table 2), the obtained values probably do not represent the full range of shock glass refractive indices. In the section investigated the shock glass shows no luminescence but in the recrystallized fine-grained parts a weak orange to reddish luminescence of unknown origin is locally observed.

The rock contains ~0.4% of millimeter-sized vesicles forming the central part of millimeter to centimeter-sized shock melt pockets. The five x-ray tomographs taken parallel to each other (Fig. 2) revealed that these vesicles, and conceivably also the melt pockets, have an elongated shape and show a preferred orientation (Fig. 4). The smallest vesicles (<<1 mm) are spherical in shape (Fig. 3c).

The calculated density is 3.309 g $cm^{-3}$ with vesicles excluded and 3.296 g $cm^{-3}$ with 0.4 vol% vesicles included. The measured density of a 16 g piece is 3.226 g $cm^{-3}$. The measured value is probably slightly lower due to microporosity.

Products of terrestrial weathering are present throughout the meteorite in minor amounts. Calcite veinlets are especially common in a 3–10 mm thick zone at the surface of the meteorite (see vein crossing the vesicle in Fig. 3c). Some calcite veins clearly crosscut the locally preserved fusion crust. Patches of Fe hydroxide, most likely of terrestrial weathering origin, occur throughout the meteorite as fillings of tiny cracks and as small pockets of finely layered oxidation products of an unidentified phase or mix phases (Fig. 3g). Pyrrhotite usually shows no sign of oxidation; however, rare grains even in the meteorite's interior are strongly oxidized with partial alteration to marcasite and Fe-hydroxides. In vesicles Fe-hydroxides, fine-grained (<1 $\mu$m) calcite and fine-grained to coarse idiomorphic gypsum (Fig. 3f) were identified as common alteration products.

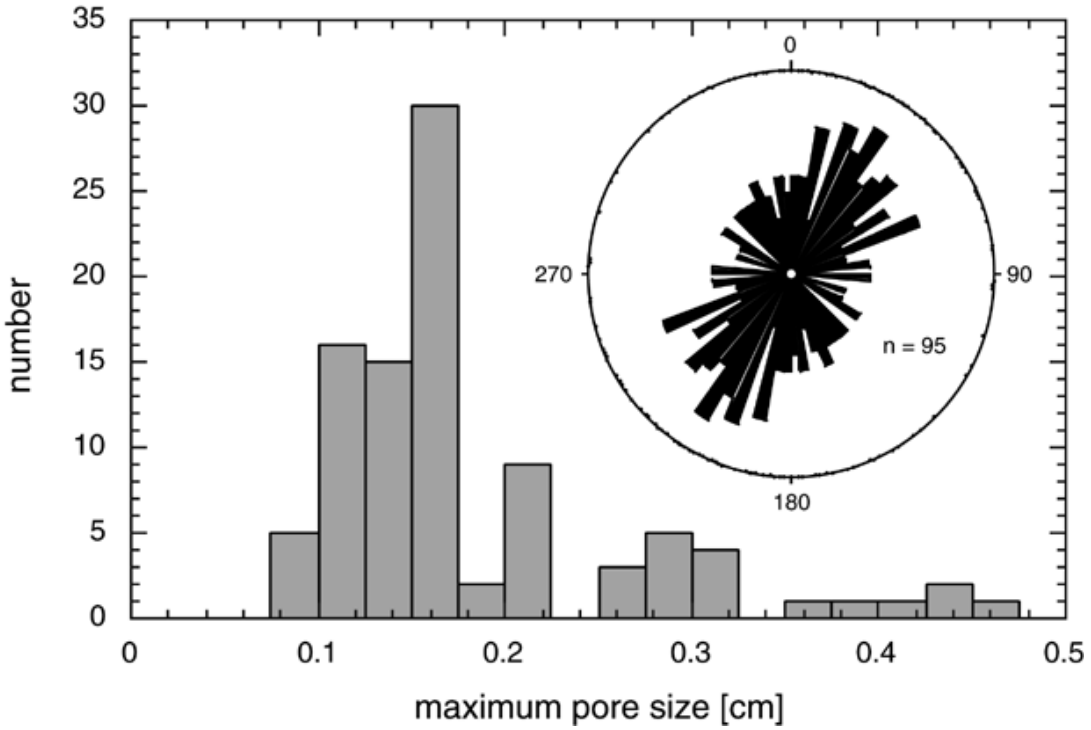


FIG. 4. Histogram of vesicle size (maximum length) and vesicle orientation obtained from the five parallel x-ray tomographs (Fig. 2). Note the clear preferred orientation of the vesicles in SaU 094 shown in the rose diagram.

TABLE 2. Shock melt and fusion crust glasses in SaU 094.

| Sample | Shock glass | | | | | Fusion crust | | Mafic shergottites | | Ultramafic shergottites | | | |
|---|---|---|---|---|---|---|---|---|---|---|---|---|---|
| | SaU 094D Pocket 1 | SaU 094D Pocket 2 | SaU 094D Pocket 3 | Range | Range (except pocket D3) | SaU 094C #4* | Range | SaU $094_{calc}$† | SaU 005‡ | DaG 476§ | ALH 77005# | LEW 88516# | Y-793605# |
| $SiO_2$ | 47.72 | 54.00 | 38.05 | 38.05–54.00 | 47.72–54.00 | 48.49 | 48.04–49.07 | 48.66 | 47.20 | 48.91 | 42.36 | 46.00 | 45.35 |
| $TiO_2$ | 0.34 | 0.14 | 0.02 | 0.03–0.45 | 0.14–0.45 | 0.41 | 0.36–0.44 | 0.26 | 0.42 | 0.42 | 0.39 | 0.39 | 0.35 |
| $Cr_2O_3$ | 1.01 | 0.56 | 0.04 | 0.04–1.65 | 0.56–1.65 | 1.03 | 0.73–1.03 | 0.99 | 0.78 | 0.83 | 0.97 | 0.86 | 1.01 |
| $Al_2O_3$ | 2.60 | 1.001 | 0.04 | 0.02–3.68 | 1.00–3.68 | 4.97 | 4.22–5.25 | 4.12 | 4.53 | 4.67 | 2.87 | 3.31 | 2.32 |
| $FeO_{tot}$ | 19.48 | 15.88 | 30.06 | 15.19–30.48 | 15.19–19.50 | 16.34 | 16.34–18.11 | 17.96 | 18.07 | 17.17 | 20.07 | 19.04 | 19.68 |
| MnO | 0.42 | 0.493 | 0.54 | 0.41–0.64 | 0.41–0.64 | 0.43 | 0.40–0.54 | 0.50 | 0.46 | 0.48 | 0.45 | 0.49 | 0.48 |
| MgO | 23.40 | 23.28 | 31.49 | 21.81–31.63 | 21.81–23.60 | 20.54 | 20.31–22.01 | 22.73 | 20.49 | 20.75 | 28.19 | 24.95 | 26.20 |
| NiO | b.d. | b.d. | b.d. | b.d.–0.13 | b.d.–0.13 | b.d. | b.d.–0.15 | – | – | – | – | – | – |
| CoO | – | b.d. | 0.05 | b.d.–0.08 | b.d.–0.08 | b.d. | b.d.–0.12 | – | – | – | – | – | – |
| CaO | 4.44 | 4.53 | 0.32 | 0.31–5.50 | 4.21–5.50 | 5.62 | 5.22–5.73 | 4.52 | 5.46 | 5.84 | 3.16 | 4.20 | 4.06 |
| $Na_2O$ | – | 0.11 | b.d. | b.d.–0.45 | 0.14–0.45 | 0.64 | 0.12–0.74 | 0.55 | 0.60 | 0.55 | 0.47 | 0.57 | 0.35 |
| $K_2O$ | – | – | – | – | – | – | – | b.d. | b.d. | 0.04 | 0.03 | 0.03 | 0.02 |
| $SO_2$ | 0.09 | b.d. | b.d. | b.d.–0.25 | b.d.–0.25 | 0.02 | b.d.–0.03 | – | – | – | – | – | – |
| Total | 99.50 | 99.99 | 100.61 | 99.13–101.45 | 99.13–100.81 | 98.49 | 98.76–100.18 | 100.29 | 98.01 | 99.66 | 98.96 | 99.84 | 99.82 |

*Analysis number.
†Calculated using mineral modes (Table 1) and average microprobe analyses.
‡Dreibus *et al.* (2000).
§Zipfel *et al.* (2000).
#Lodders (1998); recalculated as oxides.
Abbreviations: b.d. = below detection limit, – = not analyzed.

## MINERAL, SHOCK AND FUSION GLASS CHEMISTRY

Olivine has a restricted compositional range of $Fo_{65–69}$ (Table 3; Fig. 5a). The olivines average 0.56 wt% MnO, are relatively high in CaO (0.37 wt%) and contain little NiO (0.03 wt%) and $Cr_2O_3$ (0.06 wt%). The average FeO/MnO is 51.9 ± 3.4. Increasing shock oxidation is correlated with an increased ferrifayalite (laihunite component) of the olivine (Fleischer *et al.*, 1978; Ostertag *et al.*, 1984), manifested in reduced microprobe totals (Table 3) and darker brown color. The amount of ferric iron (laihunite component; $Fe^{3+}{}_2?_1Fe^{2+}{}_{-3}$-exchange) in the olivines was estimated by normalizing to 1 Si (pfu). Microprobe traverses (Fig. 6a,b) revealed zoning similar to the zoning described by Mikouchi *et al.* (2001) for DaG 476, but less pronounced.

Pigeonite ($En_{60–68}Fs_{20–27}Wo_{7–9}$) shows relatively restricted compositional variation (Table 3; Fig. 5b). No enstatite was detected. Augite ($En_{46–49}Fs_{15–16}Wo_{28–31}$) occurs rarely associated with the pigeonite and is listed in Table 3. In backscattered electron images weak pyroxene zoning is visible, and no exsolution of pigeonite into enstatite and augite was observed. Qualitative analyses show that pyroxene in melt inclusions has distinct higher Al values (4–5 wt% $Al_2O_3$) than the matrix pyroxene (average 1.21 ± 0.43). Pigeonite microprobe traverses (Fig. 6c,d) are characteristically flat and irregular due to shock deformation and possible exsolution.

The clear maskelynite glass filling the interstitial areas between olivine and pyroxene grains seems stoichiometric and has a labradoritic composition ($An_{50–64}Or_{0.3–0.9}$; Fig. 5c) with relatively high potassium contents (Table 3). In one case (Fig. 6f) anorthite content dropped to 50%. The maskelynite also contains measurable amounts of Fe, Mn and Mg (Table 3). Maskelynite microprobe traverses are generally flat (Fig. 6e) but in one case a continuous change towards one rim was detected (Fig. 6f).

Chromites to titanian magnesian chromites contain 0.1–0.3 wt% ZnO, 1.0–15.2 wt% $TiO_2$, 3.9–5.1 wt% MgO and 7.9–11.9 wt% $Al_2O_3$ (Table 4). They form subhedral grains and clusters occurring in association with all other minerals (*e.g.*, Fig. 3e). Chromites show considerable variation in Ti content. If the ulvöspinel vector, $M^{2+}Ti^{4+}\ M^{3+}{}_{-2}$, is plotted (Fig. 7a), a perfect relationship is obtained with Mg (magnesioulvöspinel) the most important divalent, and Cr the main trivalent cation ($Mg^{2+}Ti^{4+}\ Cr^{3+}{}_{-2}$ ). Two microprobe traverses (Fig. 6i,k) show ulvöspinel-enriched rims and asymmetric zoning.

Ilmenite ($Ilm_{80–86}$; 6% of dark opaques) contains up to 0.7 wt% MnO (pyrophanite component), up to 4.7 wt% MgO (geikielite) and up to 0.48 wt% $Cr_2O_3$ (eskolaite). Ilmenites are plotted together with the chromites in Fig. 7b, and an analysis listed in Table 4.

All phosphate grains found are merrillite $Ca_9Na(Mg,Fe)(PO_4)_7$ (Dowty, 1977). Similar to other martian meteorites (*e.g.*, Mikouchi *et al.*, 2001) merrillite contains considerable amounts of F (average 1.1 wt%), and traces of Cl

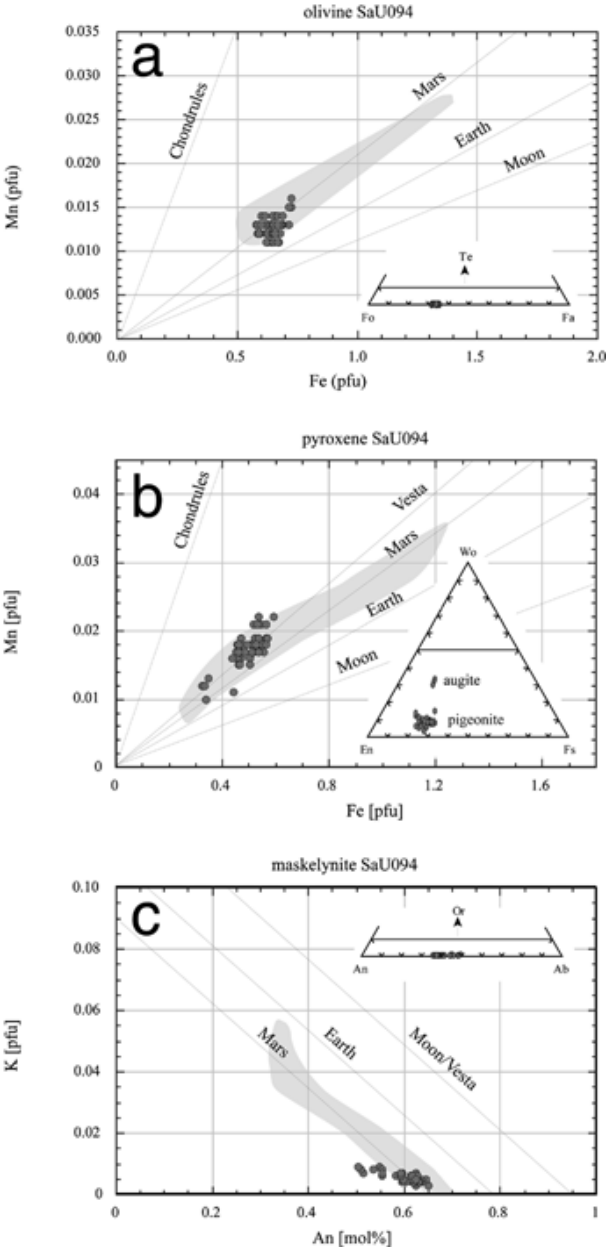


FIG. 5. Fe-Mn compositions of olivine and clinopyroxene and anorthite-K compositions of maskelynite in SaU 094 compared to compositional trends (lines and shaded areas) given by Papike (1998). Insets show compositions in the corresponding ternary diagrams. Te = tephroite.

(Table 5) which point to either solid-solution with a structurally similar "fluor whitlockite" or, as replacement of $PO_4$ by $SiO_4$ suggests, a solid-solution series with structurally similar silicate members (*e.g.*, Moore, 1983). Rare earth elements are only present in trace amount and at the limit of detection by

TABLE 3. Silicates in SaU 094B.

| | Olivine | | | | | Augite | Pigeonite | | | | Maskelynite | | | |
|---|---|---|---|---|---|---|---|---|---|---|---|---|---|---|
| Analysis | #1 | #6 | #13 | #18 | Range | #15 | #5 | #10 | #26 | Range | #1 | #2 | #4 | Range |
| $SiO_2$ | 37.77 | 37.41 | 37.06 | 37.47 | 36.68–37.97 | 53.22 | 54.18 | 54.19 | 52.56 | 52.06–54.39 | 54.99 | 53.00 | 52.73 | 52.35–54.99 |
| $TiO_2$ | b.d. | b.d. | b.d. | b.d. | b.d. | 0.32 | 0.12 | 0.06 | 0.23 | 0.06–0.91 | b.d. | b.d. | b.d. | b.d. |
| $Cr_2O_3$ | 0.04 | 0.08 | 0.07 | 0.03 | 0.02–0.60 | 0.83 | 0.51 | 0.47 | 0.55 | 0.25–1.29 | 0.03 | 0.03 | 0.03 | 0.03 |
| $Al_2O_3$ | 0.04 | 0.04 | 0.11 | 0.08 | 0.01–0.21 | 2.10 | 1.00 | 1.14 | 1.75 | 0.67–1.98 | 28.24 | 29.51 | 29.97 | 28.16–29.97 |
| $Fe_2O_3$ | – | – | – | – | – | 0.45 | 1.13 | 0.49 | 1.18 | 0.16–3.83 | 0.00 | 0.00 | 0.00 | 0.00–0.66 |
| FeO | 26.63 | 28.43 | 27.23 | 27.37 | 25.83–31.98 | 10.52 | 13.98 | 14.56 | 14.59 | 10.79–18.13 | 0.37 | 0.43 | 0.39 | 0.00–0.52 |
| Mn0 | 0.53 | 0.54 | 0.53 | 0.77 | 0.46–0.71 | 0.38 | 0.56 | 0.57 | 0.56 | 0.50–0.69 | 0.02 | 0.04 | 0.00 | 0.00–0.04 |
| MgO | 34.75 | 32.90 | 30.94 | 30.80 | 30.14–34.75 | 17.90 | 24.78 | 25.30 | 21.99 | 21.75–25.30 | 0.12 | 0.15 | 0.16 | 0.12–0.61 |
| NiO | b.d. | b.d. | b.d. | b.d. | b.d.–b.d. | 0.05 | b.d. | b.d. | b.d. | b.d.–0.04 | b.d. | b.d. | b.d. | b.d. |
| CaO | 0.42 | 0.34 | 0.57 | 0.79 | 0.29–0.88 | 15.72 | 4.49 | 3.48 | 6.46 | 3.48–6.89 | 11.32 | 12.85 | 13.14 | 11.32–13.14 |
| $Na_2O$ | b.d. | b.d. | b.d. | b.d. | b.d.–b.d. | 0.19 | 0.08 | 0.03 | 0.09 | b.d.–0.11 | 5.07 | 4.16 | 3.96 | 3.96–5.07 |
| $K_2O$ | b.d. | b.d. | b.d. | b.d. | b.d.–b.d. | b.d. | 0.02 | b.d. | b.d. | b.d.–0.04 | 0.15 | 0.09 | 0.09 | 0.06–0.15 |
| Total | 100.18 | 99.74 | 96.51 | 97.31 | 96.11–100.95 | 101.68 | 100.85 | 100.29 | 99.96 | 99.20–100.89 | 100.31 | 100.26 | 100.47 | 99.74–100.69 |
| Si | 1.000* | 1.000* | 1.000* | 1.000* | 1.000* | 1.935 | 1.956 | 1.962 | 1.935 | 1.900–1.970 | 2.478 | 2.401 | 2.386 | 2.384–2.550 |
| Ti | b.d. | b.d. | b.d. | b.d. | b.d. | 0.009 | 0.003 | 0.002 | 0.007 | 0.002–0.025 | b.d. | b.d. | b.d. | b.d.–0.004 |
| Cr | 0.001 | 0.002 | 0.001 | 0.001 | b.d.–0.013 | 0.024 | 0.015 | 0.014 | 0.016 | 0.007–0.037 | 0.001 | 0.001 | 0.001 | b.d.–0.002 |
| Al | 0.001 | 0.001 | 0.003 | 0.003 | b.d.–0.007 | 0.090 | 0.043 | 0.049 | 0.076 | 0.029–0.086 | 1.500 | 1.575 | 1.598 | 1.430–1.598 |
| $Fe^{III}$ | 0.026 | 0.058 | 0.213 | 0.239 | b.d.–0.243 | 0.012 | 0.031 | 0.013 | 0.033 | 0.005–0.105 | – | – | – | – |
| $Fe^{II}$ | 0.564 | 0.577 | 0.413 | 0.368 | 0.367–0.756 | 0.320 | 0.422 | 0.441 | 0.449 | 0.329–0.559 | 0.014 | 0.016 | 0.015 | b.d.–0.044 |
| Mn | 0.012 | 0.012 | 0.011 | 0.010 | 0.010–0.016 | 0.012 | 0.017 | 0.018 | 0.017 | 0.016–0.022 | 0.001 | 0.002 | b.d. | b.d.–0.002 |
| Mg | 1.371 | 1.311 | 1.245 | 1.227 | 1.214–1.371 | 0.970 | 1.333 | 1.365 | 1.207 | 1.190–1.367 | 0.008 | 0.010 | 0.011 | 0.007–0.096 |
| Ni | b.d. | b.d. | b.d. | b.d. | b.d. | 0.002 | b.d. | b.d. | b.d. | b.d.–0.001 | b.d. | b.d. | b.d. | b.d. |
| Ca | 0.012 | 0.010 | 0.016 | 0.025 | 0.008–0.025 | 0.612 | 0.174 | 0.135 | 0.255 | 0.135–0.269 | 0.547 | 0.624 | 0.637 | 0.500–0.637 |
| Na | b.d. | b.d. | b.d. | b.d. | b.d. | 0.014 | 0.006 | 0.002 | 0.007 | b.d.–0.008 | 0.443 | 0.365 | 0.347 | 0.347–0.485 |
| K | b.d. | b.d. | b.d. | b.d. | b.d. | 0.001 | 0.001 | b.d. | b.d. | b.d.–0.002 | 0.009 | 0.005 | 0.005 | 0.003–0.009 |
| Fo† | 0.695 | 0.670 | 0.662 | 0.666 | En | 0.507 | 0.680 | 0.699 | 0.621 | An | 0.548 | 0.628 | 0.644 | |
| Fa | 0.299 | 0.324 | 0.333 | 0.329 | Fs | 0.173 | 0.231 | 0.232 | 0.248 | Ab | 0.443 | 0.367 | 0.351 | |
| Te‡ | 0.006 | 0.006 | 0.006 | 0.005 | Wo | 0.320 | 0.089 | 0.069 | 0.131 | Or | 0.009 | 0.005 | 0.005 | |

Abbreviations: b.d. = below detection limit; – = not analyzed.

*Normalized to 1 Si per formula unit; $Fe^{3+}$ is calculated according to discussion in text.

†Fo = Mg/Mg + $Fe_{tot}$ + Mn.

‡Te = tephroite.

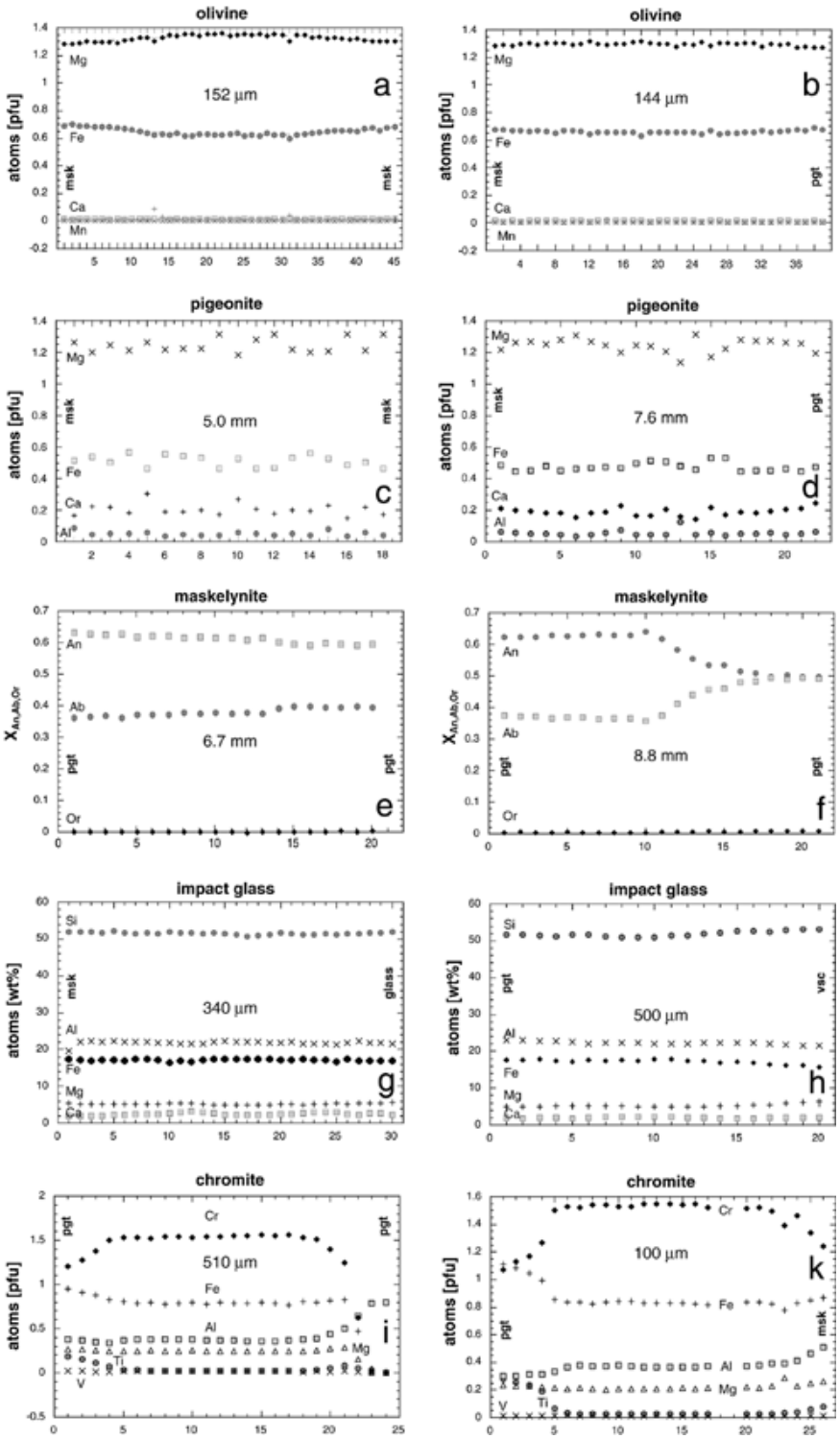


FIG. 6. Mineral transects displaying weak to absent chemical zoning; numbers indicate analysis spots. Abbreviation are phases in contact with the analyzed grain: msk = maskelynite; pgt = pigeonite; glass = recrystallized glass; vsc = vesicle.

TABLE 4. Oxides in SaU 094.

| | Chromite | | | | Ilmenite |
|---|---|---|---|---|---|
| Sample | SaU 094C | SaU 094C | SaU 094B | | SaU 094B |
| Analysis | #17 | #59 | #21 | Range | #43 |
| $SiO_2$ | 0.09 | 0.17 | 0.03 | 0.02–0.79 | 0.04 |
| $TiO_2$ | 0.70 | 1.03 | 15.22 | 0.46–15.22 | 53.31 |
| $Cr_2O_3$ | 60.58 | 56.58 | 31.03 | 31.03–61.05 | 0.48 |
| $V_2O_3$ | 0.52 | 0.73 | – | 0.29–0.82 | – |
| $Al_2O_3$ | 6.95 | 9.27 | 5.99 | 5.99–17.68 | b.d. |
| $Fe_2O_3$ | – | – | 2.17 | (b.d.–3.20) | 0.40 |
| $FeO_{tot}$ | 26.23 | 27.58 | 40.41 | 26.72–40.41 | 41.50 |
| MnO | b.d. | b.d. | b.d. | b.d. | 0.74 |
| MgO | 4.60 | 4.83 | 4.14 | 3.63–5.40 | 3.11 |
| ZnO | 0.27 | 0.11 | 0.14 | b.d.–0.33 | – |
| NiO | 0.08 | 0.13 | 0.12 | b.d.–0.19 | b.d. |
| CoO | b.d. | b.d. | b.d. | b.d.–0.11 | – |
| CaO | b.d. | b.d. | 0.09 | 0.01–0.32 | 0.15 |
| Total | 100.02 | 100.43 | 99.34 | 99.32–100.92 | 99.73 |
| Si | 0.003 | 0.006 | 0.001 | 0.001–0.021 | 0.001 |
| Ti | 0.018 | 0.027 | 0.408 | 0.021–0.408 | 0.991 |
| Cr | 1.665 | 1.533 | 0.874 | 0.874–1.604 | 0.009 |
| Al | 0.285 | 0.374 | 0.251 | 0.251–0.688 | b.d. |
| $Fe^{3+}$ | b.d. | 0.007 | 0.058 | 0.022–0.084 | 0.008 |
| $Fe^{2+}$ | 0.762 | 0.781 | 1.263 | 0.810–1.263 | 0.858 |
| Mn | b.d. | b.d. | b.d. | b.d. | 0.015 |
| Mg | 0.239 | 0.247 | 0.220 | 0.189–0.273 | 0.115 |
| Zn | 0.007 | 0.003 | 0.004 | b.d.–0.008 | – |
| Ni | 0.002 | 0.004 | 0.003 | b.d.–0.005 | b.d. |
| Co | b.d. | b.d. | b.d. | b.d. | – |
| Ca | 0.001 | 0.001 | 0.003 | b.d.–0.012 | 0.004 |

Abbreviations: – = not analyzed, b.d. = below detection limit.

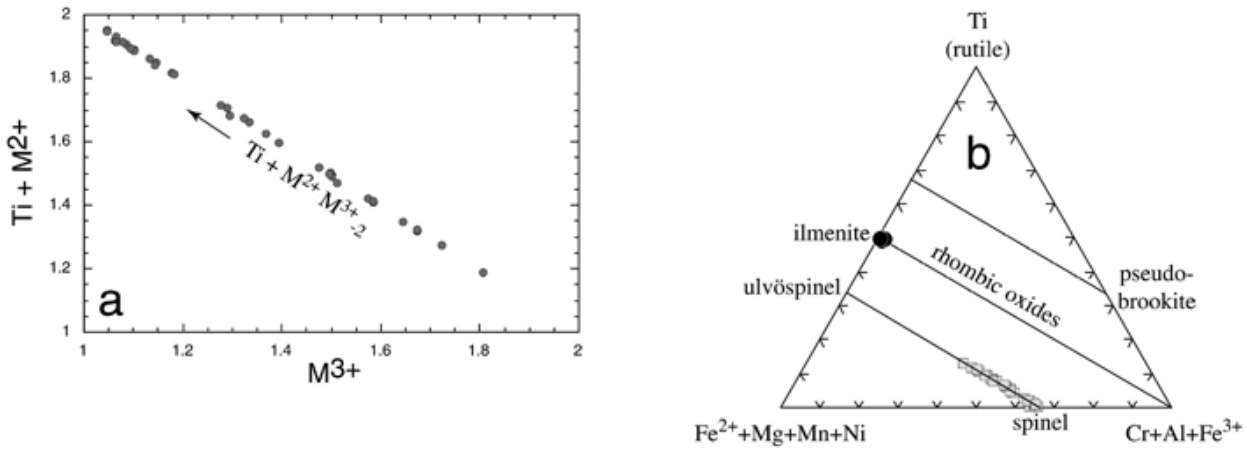


FIG. 7. Chromite (a, b) and ilmenite (b) compositions in SaU 094.

TABLE 5. Phosphates and sulfides in SaU 094.

| | Merrillite | | | | Pyrrhotite | | | Sulfide melt | Pentlandite |
|---|---|---|---|---|---|---|---|---|---|
| Sample | SaU 094B | SaU 094B | Range | | SaU 094C | SaU 094C | Range | SaU 094C | SaU 094C |
| Analysis | #9 | #20 | | | #2 | #28 | | #17 | #3 |
| $P_2O_5$ | 44.77 | 45.64 | 42.75–45.64 | Cr | b.d. | b.d. | b.d.0–0.54 | 0.07 | b.d. |
| $SiO_2$ | 1.38 | 0.36 | 0.36–1.64 | Fe | 60.47 | 55.85 | 55.37–63.04 | 63.04 | 37.21 |
| $Al_2O_3$ | 0.23 | 0.10 | 0.09–0.47 | Mn | 0.06 | b.d. | b.d.–0.07 | 0.10 | 0.03 |
| FeO | 1.17 | 1.10 | 0.85–1.28 | Zn | b.d. | 0.19 | b.d.–0.21 | b.d. | b.d. |
| MgO | 4.04 | 3.56 | 3.50–4.61 | Ni | 2.19 | 4.13 | 0.73–7.20† | 0.45 | 29.17 |
| CaO | 46.15 | 47.22 | 46.03–47.60 | Co | 0.03 | 0.10 | b.d.-0.10 | 0.14 | 0.66 |
| $Na_2O$ | 1.75 | 1.71 | 1.48–1.86 | Cu | b.d. | b.d. | b.d.–1.11 | b.d. | b.d. |
| $Ce_2O_3$ | b.d. | b.d. | b.d.–0.06 | Se | 0.05 | 0.03 | b.d.–0.08 | b.d. | 0.06 |
| $La_2O_3$ | b.d. | 0.04 | b.d.–0.07 | As | 0.04 | 0.04 | b.d.–0.09 | b.d. | 0.05 |
| $Nd_2O_3$ | 0.08 | b.d. | b.d.–0.08 | S | 37.01 | 37.22 | 36.44–38.09 | 36.08 | 33.42 |
| $Y_2O_3$ | 0.09 | 0.04 | 0.03–0.09 | | | | | | |
| F | 1.16 | 1.05 | 0.50–1.28 | | | | | | |
| Cl | 0.09 | b.d. | 0.02–0.10 | | | | | | |
| Total | 100.31* | 100.32* | 99.18–100.44* | Total | 99.85 | 99.56 | 99.03–100.92 | 99.88 | 100.60 |
| P | 6.795 | 6.933 | 6.575–6.933 | Cr | b.d. | b.d. | b.d.–0.009 | 0.001 | 0.004 |
| Si | 0.248 | 0.065 | 0.065–0.297 | Fe | 0.938 | 0.893 | 0.843–0.965 | 1.003 | 5.110 |
| Al | 0.048 | 0.021 | 0.020–0.100 | Mn | 0.001 | b.d. | b.d.–0.002 | 0.002 | 0.003 |
| Fe | 0.175 | 0.165 | 0.128–0.191 | Zn | b.d. | 0.003 | b.d.–0.003 | b.d. | b.d. |
| Mg | 1.080 | 0.953 | 0.949–1.243 | Ni | 0.032 | 0.061 | 0.011–0.108 | 0.007 | 3.812 |
| Ca | 8.865 | 9.077 | 8.826–9.317 | Co | b.d. | 0.001 | b.d.–0.001 | 0.002 | 0.086 |
| Na | 0.607 | 0.596 | 0.523–0.645 | Cu | b.d. | 0.008 | b.d.–0.008 | b.d. | b.d. |
| Ce | b.d. | 0.001 | b.d.–0.013 | Se | 0.001 | b.d. | b.d.-0.001 | b.d. | 0.006 |
| La | b.d. | 0.003 | b.d.–0.005 | As | b.d.‡ | 0.001‡ | b.d.–0.001‡ | b.d.‡ | 0.005‡ |
| Nd | 0.005 | b.d. | b.d.–0.014 | S | 1.000‡ | 0.999‡ | 0.999–1.000‡ | 1.000‡ | 7.995‡ |
| Y | 0.008 | 0.004 | 0.004–0.008 | | | | | | |
| F | 0.656 | 0.598 | 0.289–0.739 | | | | | | |
| Cl | 0.028 | 0.005 | 0.005–0.030 | | | | | | |

Abbreviations: b.d. = below detection limit. Detection limits at the $2\sigma$ level were derived in the following way: $(2\sigma)$ in ppm = $10^4 \times 2.241/(t_{tot} \times I_{pk} \times I_{pk}/I_{bdg})^{1/2}$ where $t_{tot}$ = total integration time in seconds, $I_{pk}$ = intensity on pure peak in counts per second, and $I_{bgd}$ = intensity on background in counts per second. Detection limits in ppm are: Ce, 200; La, 200; Nd, 450; Y, 250. Detection limits for Se and As in the sulfides are 250 ppm. Relative $1\sigma$ analytical uncertainties for these elements are 50–250%.
*Corrected for F, Cl = O.
†Maximum value where only small exsolutions occur.
‡Normalized to the elements marked with a star.

microprobe. Yttrium is dominating, pointing to a heavy REE enrichment.

The iron sulfide chemistry varies between FeS (troilite) and $Fe_{10}S_{11}$ (hexagonal non-magnetic pyrrhotite; Kissin, 1974) with Fe/S ratios between 0.92 to 1.00 (Table 5). Pyrrhotite also contains small amounts of Cr and Co (Table 5). Due to the presence of irregularly distributed pentlandite inclusions (Fig. 3; see also Fig. 9), pyrrhotite analyses show a wide range of NiS contents of 0.9–7.2 wt% (Table 5). Areas free of pentlandite exsolution typically contain 2.7–3 wt% Ni. Arsenic and selenium are found to be at the detection limit, but pentlandite (Table 5) seems to concentrate selenium.

The green shock glass pockets interpreted as shock-induced melts have, according to the TAS classification (Le Maitre *et al.*, 1989), mainly a basaltic to basaltic andesite composition (Fig. 8). Compared with a bulk analysis of SaU 005 (Dreibus *et al.*, 2000; Table 2), the shock glass is commonly enriched in $SiO_2$, possibly due to partial recrystallization to relatively Si-poor phases (*e.g.*, olivine). The glass composition of the largest pocket analyzed plots close to the SaU 005 bulk composition (Fig. 8). However, the compositions of a few small melt pockets strongly deviate from the bulk composition, reflecting local melting of minerals (Table 2). Microprobe profiles across two larger melt pockets (Fig. 6g,h) revealed no zoning in the

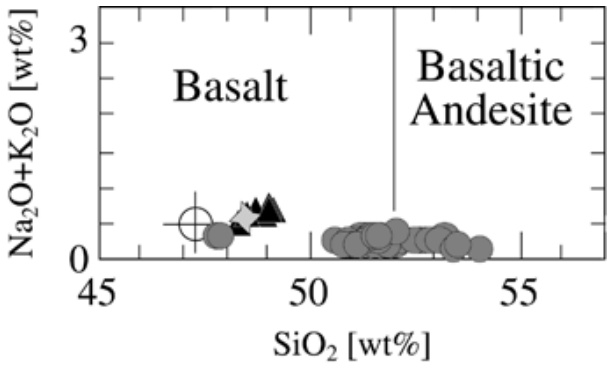


FIG. 8. Chemical compositions of impact glass (circles), fusion crust (triangles), bulk composition calculated from microprobe mineral averages and mode (star), and SaU 005 bulk composition (circle with cross; Dreibus *et al.*, 2000) plotted in the TAS classification diagram for volcanic rocks (Le Maitre *et al.*, 1989). Note the similarity of fusion glass, larger melt pockets and calculated bulk composition with SaU 005. Some analyzed melt pocket glasses plot outside the diagram boundaries near 38 wt% $SiO_2$ (see Table 4).

optically homogeneous green glass. The sulfur content is measurable but variable (Table 2).

Analyses of fusion crust glass are listed in Table 2 and shown in Fig. 8. Its composition is very similar to the bulk-rock chemistry of Dreibus *et al.* (2000). The brown color of the glass suggest the presence of ferric iron.

## SHOCK FEATURES AND METAMORPHISM

SaU 094 is an unbrecciated, shocked gabbroic rock displaying solid-state deformation features as well as finely grained recrystallized areas along grain boundaries, and pockets of shock-melted rock (Fig. 3c).

In pyroxene mechanical shock deformation produced deformation bands, polysynthetic twin lamellae and fracturing. Polysynthetic mechanical twinning subparallel to (001) with twin spacing of 2–40 $\mu$m dominates in such a way that pigeonite appears like twinned magmatic plagioclase (Fig. 9a). The twin boundaries are generally straight, sometimes slightly curved. All pyroxene grains are irregularly fractured but one set of fractures perpendicular to the prism is common. Sets of planar fractures are restricted to areas around melt pockets. Along pyroxene grain contacts and within the crystals fine-grained granular corridors produced by frictional melting and recrystallization are very common (Fig. 9b).

Based on experimental calibrations that relate refractive index to shock pressure (*e.g.*, Stöffler, 1984) the optically isotropic, labradoritic maskelynite can be used for estimating minimum shock pressure in SaU 094. Refractive indices obtained for three maskelynite grains are 1.540 and twice 1.542, indicating shock pressures in excess of 45 GPa (Fig. 10).

Olivine is characteristically yellow to dark brown (Fig. 9c) and patchy and shows several sets of planar fractures and strong mosaicism (Fig. 9d). Locally, the grains were melted, the melt now visible as small crystalline grains and a bleached zone (deformation-free, recrystallized olivine) separating the oxidized olivine from the melt pocket (Figs. 3c and 10c). Areas and veins of fine-grained recrystallized olivine are common and quenched glassy olivine is locally preserved along melt pockets where olivine crystals turn clear (recrystallization to $Fe^{2+}$-olivine). At the contact to melt pockets olivine shows characteristically rounded (resorbed) edges.

Chromites behave brittly during shock metamorphism and show several sets of parallel fractures. The same is observed in the few phosphate grains. Compared with spinels, ilmenite shows more intense shock fracturing and characteristic mechanical twinning (Fig. 3e). Chromite and ulvöspinel are ideomorphic as inclusions in olivine and pyroxene, but rounded (resorbed) in contact with shock melt.

The most obvious shock feature in sulfide grains adjacent to silicate shock melts is complete or partial melting (Fig. 9e), resulting in the formation of globular sulfide droplets enclosing silicate droplets (Fig. 9f). One large pyrrhotite grain (Fig. 9f) shows partial melting and a recrystallized (grain size 5–10 $\mu$m), polygonal, pentlandite-free transition zone (50 $\mu$m wide) towards unaffected, pentlandite-rich, coarse polygonal pyrrhotite (grain size 20–50 $\mu$m). Pyrrhotite in the compositional range observed is hexagonal

FIG. 9. (*right*) Shock features in SaU 094. (a) Shock-induced mechanical twinning in pigeonite leading to a plagioclase-like appearance. Crossed polarizers, section D, width of image 1 mm. (b) Shock-produced fine-grained polygonal granular bands of recrystallized pigeonite in pigeonite. These bands characteristically occur at grain boundaries and commonly as parallel (crystallographically oriented?) swarms within pigeonite grains. Crossed polarizers, section D, width of image 1 mm. (c) Shock-oxidized olivine. At its left end, in the extension of the melt pocket, the olivine turns dark brown (higher defect density) and at the direct contact to the melt pocket the olivine is reduced due to *in situ* recrystalliation of the vitrified olivine. Plain light, section D, width of image 2 mm. (d) Olivine grain showing strong mosaicism. Crossed polarizers, section D, width of image 1 mm. (e) Maskelynite quenched in a state of being injected by brownish melt from left to right. Note the flow structures suggesting fluidization of maskelynite. Plane polarized light, section D, width of image 0.11 mm. (f) Pyrrhotite showing transition from coarse polygonal crystals (with pentlandite exsolution lamellae; right) to finer polygonal crystals with small silicate inclusions (center, dark speckles) to globular sulfide melt droplets set in silicate shock melt (left). Reflected light, oil immersion, section D, width of image 0.11 mm. (g) Globular sulfide melt droplets in silicate melt. Note that the sulfide melt droplets show exsolutions of silicate melt, and the silicate melt tiny exsolutions of sulfides. This suggests that maximum mutual solubility was reached. Reflected light, oil immersion, section D, width of image 0.09 mm. (h) Grano-globular partly-melted sulfide inclusion in melt pocket. Note the grain boundary areas full of silicate melt inclusions, whereas pentlandite exsolutions remain unaffected by melting in the central part of the grains. The sulfide aggregate was subsequently crossed by a carbonate vein. Reflected light, oil immersion, section D, width of image 50 $\mu$m. Msk = maskelynite; Cpx = pigeonite; Ol = olivine.

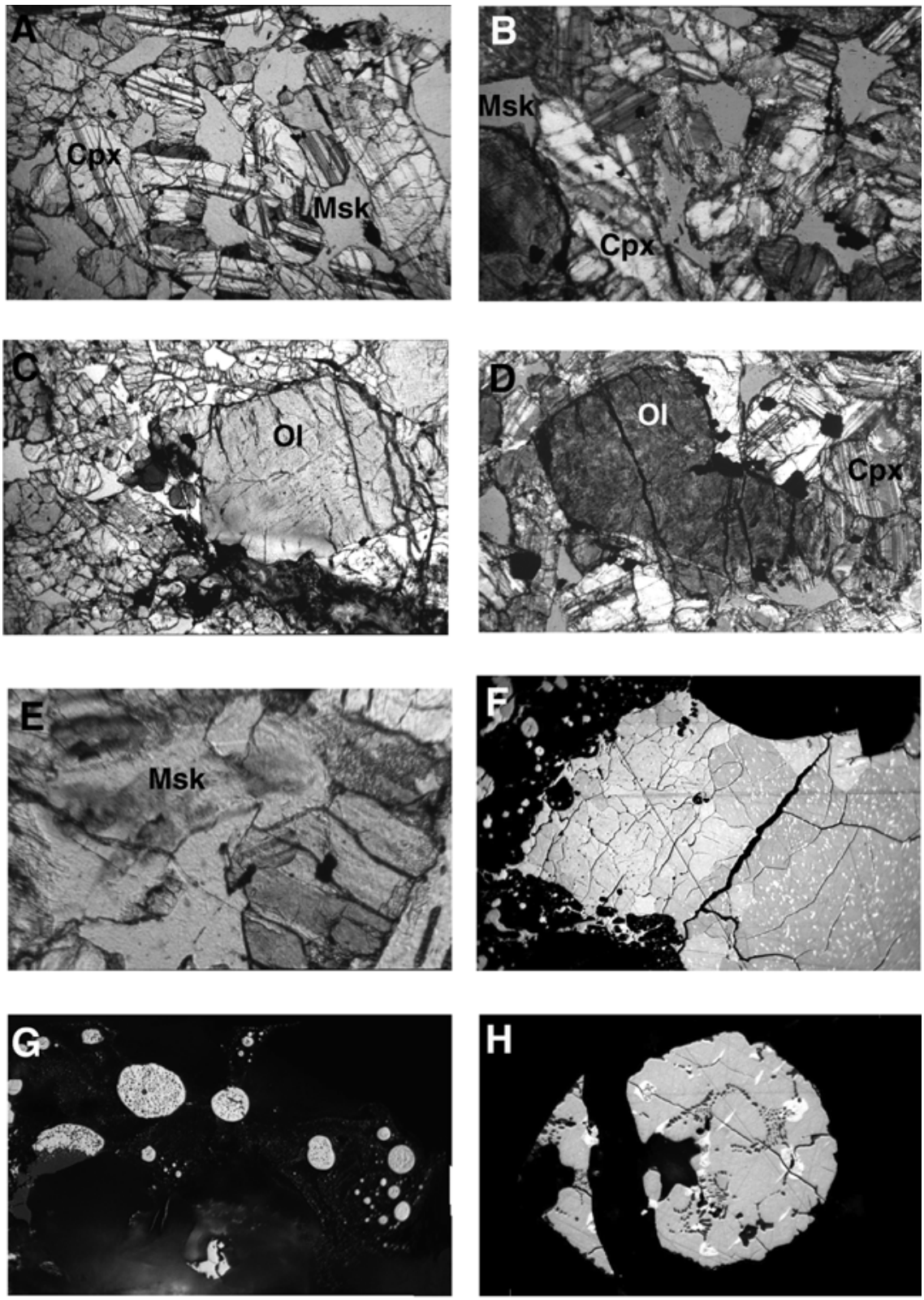
A
Cpx
Msk
B
Msk
Cpx
C
Ol
D
Ol
Cpx
E
Msk
F
G
H

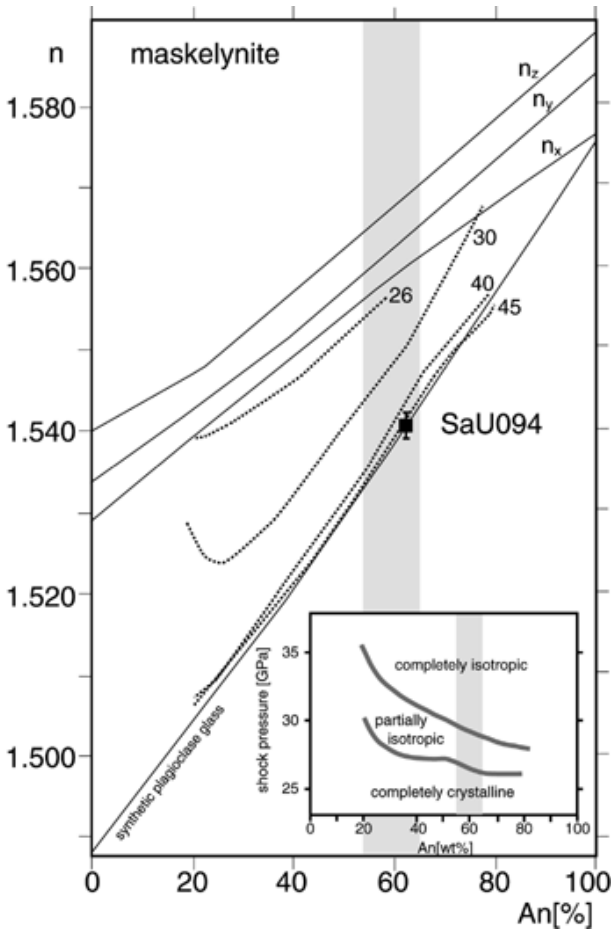


FIG. 10. Minimum shock pressure estimate based on maskelynite chemistry and optical refractive indices. The data indicate shock pressures in excess of 45 GPa throughout the rock. Isobars are from Stöffler (1984).

at room temperatures but no deformation were observed in reflected light, suggesting complete recrystallization. Even the least affected pyrrhotite grains are aggregates of polygonal grains.

Shock-wave and ultra-high pressure experiments on $Fe_{0.9}S$ and FeS compositions were conducted by Brown *et al.* (1984) and Williams and Jeanloz (1990). Their data indicate that shock temperatures of ~3000 K at >45 GPa are needed to melt pyrrhotite. This temperature drops below 2000 K at lower pressures (Fig. 11). Brown *et al.* (1984) noted phase transitions of $Fe_{0.9}S$ with increasing pressure before it melts. This suggests that the equigranular polygonal texture of the pyrrhotite grains in SaU 094 was acquired either during recrystallization after shock deformation (dislocation density too high and post-shock temperature high enough), recrystallization associated with a phase transition, or a combination of the two.

Shock melt pockets form up to 6.7 vol% of the rock. The central parts of larger pockets generally consist of a fresh green glass, locally containing sulfide melt droplets and vesicles (Fig. 3c). The glassy part is separated from the host rock minerals by a dark (macroscopically black) zone of a very fine-grained, polycrystalline silicates (Fig. 3c) also containing globular sulfide droplets and angular oxide fragments. Based on experimental work such melt pockets suggest local shock pressure as high as 80 GPa (*e.g.*, McSween and Stöffler, 1980) accompanied by heating to 1600–2000 °C. The oblate millimeter-sized vesicles are common in glassy and recrystallized shock melts in SaU 094 (Figs. 2 and 3c) and have a preferred orientation (Fig. 4).

Considering all shock features, the shock grade of SaU 094 is S6, according to the scale for chondrites proposed by Stöffler *et al.* (1991). In the original description of SaU 094 (Grossman *et al.*, 2001) which was based on small fragments lacking melt pockets only S5 was estimated (optically isotropic maskelynite).

## OXYGEN ISOTOPES

The oxygen isotopic composition of SaU 094 was initially determined on a 18 mg untreated sample recovered from the surface. Two oxygen isotope measurements on a surface chip yielded $\delta^{17}O$ 2.50/2.51‰, $\delta^{18}O$ 4.30/4.28‰, $\delta^{17}O$ 0.27/0.30‰. The low $\delta^{17}O$ value probably is influenced by the presence of terrestrial calcite. The $\delta^{18}O$ *vs.* $\delta^{17}O$ values plot close to the fractionation line defined by other Mars meteorites (Franchi *et al.*, 1999; Fig. 11). The O isotopic composition of SaU 094 is one of the lightest of the known Mars meteorites, similar to Chassigny.

## DISCUSSION

### Magmatic History

In comparison with similar shergottites like DaG 476/489/670/735 (*e.g.*, McSween and Treimann, 1998; Zipfel *et al.*, 2000; Folco *et al.*, 2000; Mikouchi *et al.*, 2001) the minerals and glasses in SaU 094 show little zonation (Fig. 6). This implies that the minerals had enough time to chemically reequilibrate during crystallization. Also, the grain size of the groundmass is larger than in typical terrestrial volcanic flows. Both criteria suggest crystallization in a plutonic to subvolcanic environment. Oxygen fugacity conditions were near the Fe/FeO buffer as indicated by the presence of chromite to titanian magnesian chromite and $Fe^{3+}$-poor ilmenite. Because of the shock oxidation and the weak zoning of olivine megacrysts in SaU 094 no attempts are made here to interpret them as phenocrysts or xenocrysts. However, Zipfel (2000) described the olivines in SaU 005, which we interpret as paired with SaU 094, as phenocrysts, and compared them with DaG 476 where the large olivines were interpreted as xenocrysts (Mikouchi *et al.*, 1999; Zipfel *et al.*, 2000).

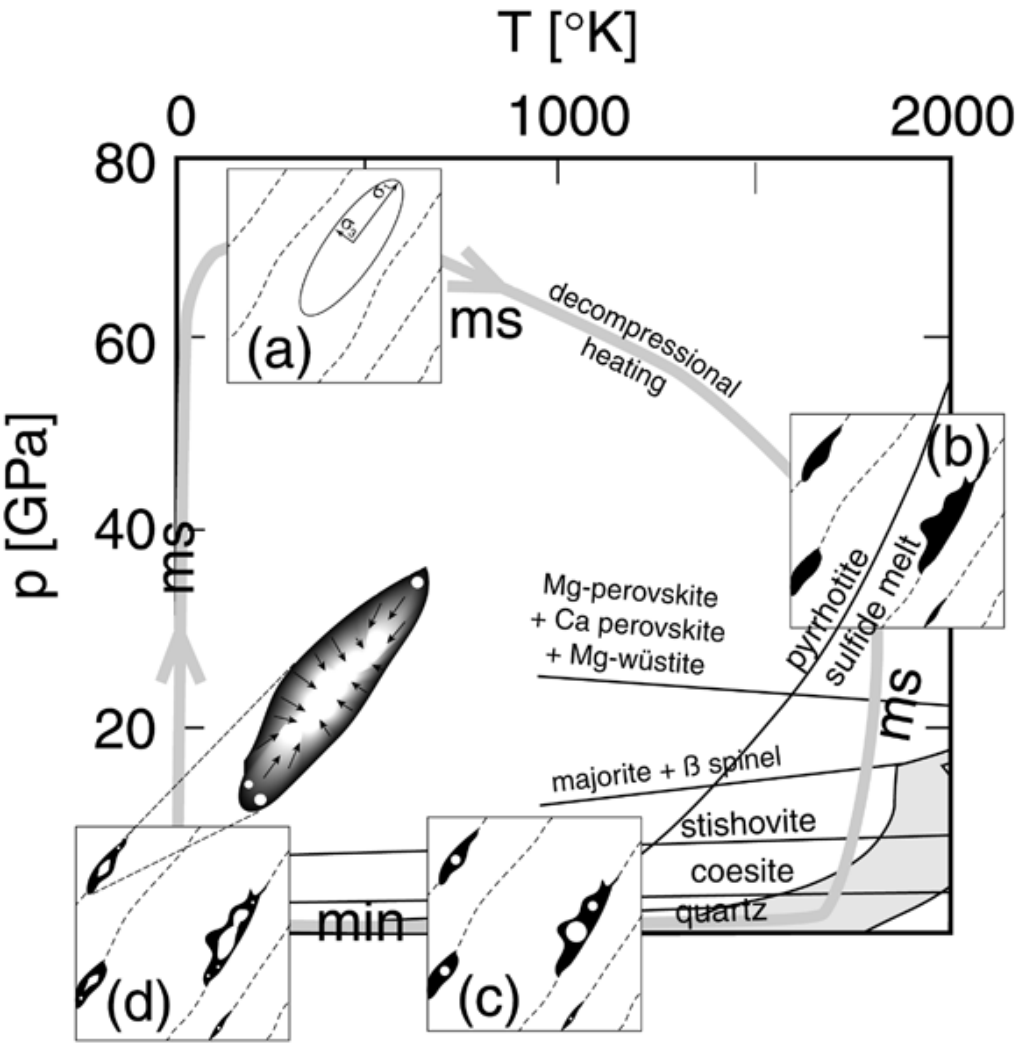


FIG. 11. Schematic diagram showing different steps in the formation of oriented vesicles in melt pockets. Note that not all parts of the rock reached melting conditions. Sulfide melting curve is from Williams and Jeanloz (1990), the $SiO_2$ polymorph boundaries from Hemley *et al.* (1994), all other phase boundaries from McDonough and Rudnick (1998). ms = milliseconds; min = minutes. For discussion see text.

Considering the trace element distribution, Zn and V are strongly fractionated into chromites, Mn is slightly fractionated into the oxides. Maskelynite concentrates K (and presumably Sr, Ba, Cs, Rb). Co and Ni concentrate in pentlandite and olivine. As, Se, and Cu fractionate mainly into pyrrhotite and pentlandite. REEs are fractionated into merrillite but occur probably also in the other Ca-phases clinopyroxene and plagioclase.

Based on a content of 0.3 wt% sulfides and an average pentlandite volume fraction of 0.085 in the sulfides (derived from image analysis), the NiS fraction in the sulfides averages 7.1 wt%. Using a total Ni of 310 ppm (SaU 005; Dreibus *et al.*, 2000) and KD values for sulfide/silicate partitioning of Ni from the compilation of Naldrett (1989), a range of 3.6–6.6% NiS in the sulfide is predicted. Given the uncertainties, this indicates that the Ni content of the sulfides corresponds to magmatic equilibrium values. The detectable arsenic in the sulfides in SaU 094 indicate that this phase probably is the most important As carrier in the meteorite.

**Shock Metamorphism**

The shock oxidation of olivines in SaU 094 is similarly strong as that in ALH 77005 (Osterdag *et al.*, 1984) and Lewis

Cliff (LEW) 88516 (Harvey *et al.*, 2001). This suggests a shock-imprint under oxygen fugacity conditions that were relatively high, probably near the martian surface or, alternatively, terrestrial oxidation of shocked olivines. It is evident that during the early stage of shock imprint on Mars some shock-deformed olivines along shock melt pockets melted and recrystallized as clear ($Fe^{3+}$-poor) olivine.

Interesting is the high amount, large size and the preferred orientation of vesicles in SaU 094, to our knowledge not reported from other shergottites. As the amount of shock melt is similar to other shergottites (*e.g.*, Dar al Gani in Table 1) this may, however, indicate that they have been overlooked. It remains to be confirmed that such oriented vesicles are additional evidence for very high shock pressures (near a fragmentation value).

A model as to how such oriented vesicles may have formed during shock deformation is shown in Fig. 11. An anisotropic shock wave produces oriented deformation bands and fractures in the bulk rock parallel to the main stress direction $\sigma_1$ (a). Olivine shock oxidation and crystal plastic, as well as brittle deformation occur during this very early stage. Decompressional heating induces melting in areas of highest dislocation densities (b), and these melt herds propagate along the prestructured rock upon decompression resulting in many cases in elongated melt pockets (b, c). Mineral grain contacts with appropriate minimum melting composition seem not important because melt formation is seen within olivine and pyroxene (see Table 2). The composition of the melt is controlled by the local mineralogy, and only larger pockets reach near bulk-rock composition. Although 2000 K may have been reached at peak pressures (*e.g.*, McSween and Stöffler, 1980), reaching such temperatures by decompression melting is probably more effective, and very likely in our case, where the pyrrhotite melting curve is crossed at lower pressures. During the cooling stage at low pressure silicate melt and fluid (vapor) exsolve to produce globular fluid droplets in a silicate melt (c). As cooling propagates from the walls of melt pockets to the interior, fluid (vapor) migrates and coalesces in the central part of the melt pockets (Fig. 3c). The interplay of diffusion and melt viscosity results in larger, elongated vesicles in the central part of the melt pockets which are recognizable on the tomographs (Fig. 2). Smaller globular droplets remain trapped in the melt pocket glass. We suggest that also the shock melt pockets have a preferred orientation. However, the tomographs do not allow to distinguish shock melt from the rest of the matrix. The elongated shock melt pockets with central, elongated hole are visible in thin section (Fig. 3c). The proposed p–T–t path suggest presence of ultra-high pressure phases like ringwoodite, majorite or $KAlSi_3O_8$ hollandite which were found in similarly strong shocked martian meteorites (Lagenhorst and Poirier, 2000).

**Low-Temperature Overprinting**

If we assume that shock metamorphism occurred during ejection from Mars, consequently, all oxidation products are of terrestrial origin and SaU 094 shows no obvious signs of pre-terrestrial aqueous alteration. This is also indicated by the absence of pyrite which is present in the majority of martian meteorites. Due to its maximum thermal stability of 743 °C pyrite is an indicator of fluid-driven alteration processes.

**Comparison with Dar al Gani 476**

Dar al Gani 476/489/670/735/876 and SaU 005/008/051/094 are similar in modal composition, mineralogy, grain size and texture. Direct comparison of SaU 094 and DaG 476 in backscattered images (Fig. 12) indicates that similar zoning in pigeonite is found in both. The chemical variation in DaG 476 is stronger, and even macroscopically visible (Folco *et al.*, 2000; Mikouchi *et al.*, 2001; Wadhwa *et al.*, 2001; Zipfel *et al.*, 2000). Although irregular zoning patterns can occur in magmatic pyroxenes (*e.g.*, by replacement) the zoning is unlike typical magmatic pyroxene growth zoning parallel to the crystal faces (compare Fig. 12b and 12c). The relatively narrow $X_{Mg}$ range of olivine in SaU 094 is similar to lherzolitic shergotties (*e.g.*, McSween and Treimann, 1998) and below the maximum of $Fo_{76}$ found in DaG 476 (Mikouchi *et al.*, 2001). Moreover, SaU 094 shows slight Mg enrichment towards olivine rims (Fig. 6), whereas olivine rims in DaG 476 are Fe-rich. As shock oxidation affects the Fe/Mg ratio of the olivines it is difficult to deduce a magmatic history from the zoning. The anorthite content of the maskelynite is also similar to lherzolitic shergottites and higher than the anorthite content in basaltic shergottites, except DaG. In SaU 005 (Zipfel, 2000; Goodrich and Zipfel, 2001) the observed compositional ranges are $Fo_{63–73}$ (olivine), $En_{70}Wo_6$ to $En_{61}Wo_{13}$ (pigeonite), $En_{47\ and\ 50}Wo_{32}$ (augite) and $An_{51–65}Or_{0.3–0.9}$ (maskelynite). The observed compositional ranges in SaU 094, and the mineral zoning further support that SaU 094 and SaU 005/008 are paired.

A comparison of the magnetic properties of pyrrhotite using the Bitter method (Soffel, 1991) showed that magnetic pyrrhotite in DaG is significantly more abundant, consistent with a stronger magnetization of DaG compared with SaU as reported by Rochette *et al.* (2001). Since rare magnetic pyrrhotite is associated with weathering products in SaU 094, and DaG is more strongly altered, the stronger bulk magnetism of the latter may be related to its degree of terrestrial alteration.

## CONCLUSIONS

SaU 094 is a strongly shocked gabbroic shergottitic meteorite with lherzolithic affinities. Its chemistry is very likely that of a basaltic shergottite. Low-temperature alteration products apparently are all of terrestrial origin and there is no obvious pre-terrestrial aqueous alteration. Besides the lower degree of terrestrial weathering, the similarity with DaG 476 and paired shergottites is extremely high.

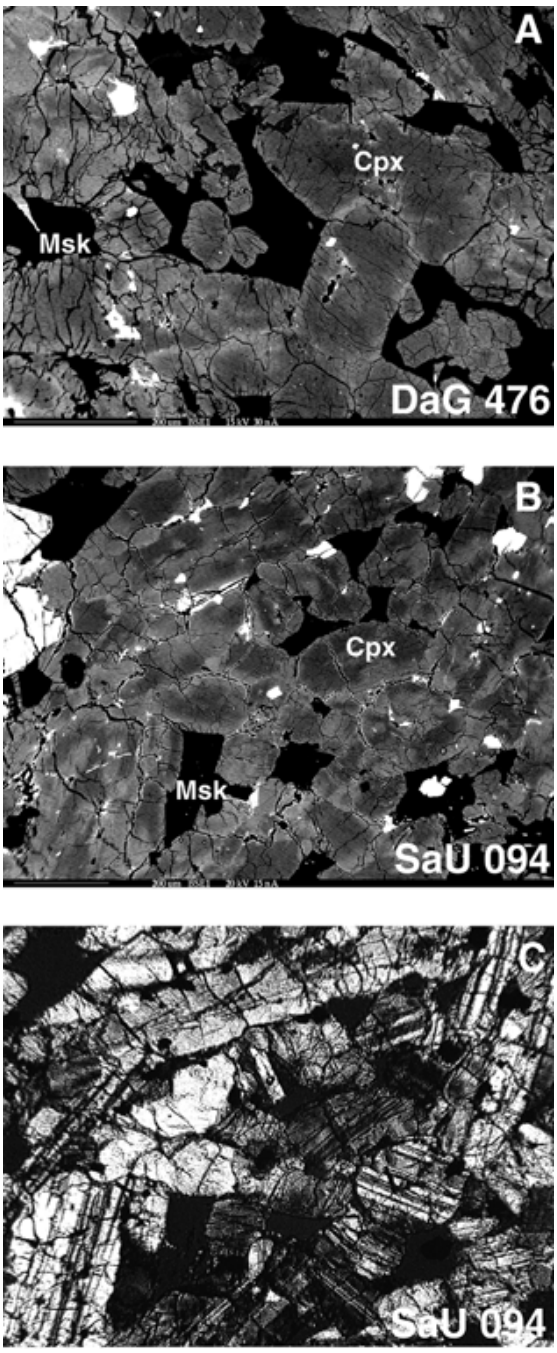


FIG. 12. Comparison of backscattered electron images of pigeonite zoning in DaG 476 (a) and SaU 094, obtained with the same detector. Both samples show similar chemical zoning although the chemical variation is larger in DaG 476. Note that the zoning in SaU 094 in (b) is irregular within a crystal. Grain boundaries are more visible in the optical microscope image (c). The chemical irregularities within one grain are also reflected in the pigeonite single crystal traverses in Fig. 6.

*Acknowledgments*–A. Flisch (EMPA, Dübendorf), is thanked for operating the x-ray tomograph. Dr. Hilal al Azri, Deputy Director General of Minerals, Ministry of Commerce and Industry is thanked for giving permission for the field work in Oman and logistic support. We thank Tj. Peters for his support during various stages of this project, R. Graf for his help with the photomicrographs, and K. Ramseyer for help on the kathode luminescence machine. Critical reviews by Gordon A. McKay and an anonymous reviewer are greatfully acknowledged**.**

*Editorial handling*: H. Nagahara

## REFERENCES

BOGARD D. D. AND JOHNSON P. (1983) Martian gases in an Antarctic meteorite. *Science* **221**, 651–654.

BROWN J. M., AHRENS T. J. AND SHAMPINE D. L. (1984) Hugeniot data for pyrrhotite and the Earth's core. *J. Geophys. Res.* **89**, 6041–6048.

CLAYTON R. N. AND MAYEDA T. K. (1996) Oxygen-isotope studies of achondrites. *Geochim. Cosmochim. Acta* **60**, 1999–2017.

DOWTY E. (1977) Phosphates in Agra Dos Reis: Structure and composition of the $Ca_3(PO_4)_2$ minerals. *Earth Planet. Sci. Lett.* **35**, 347–351.

DREIBUS G. AND WÄNKE H. (1987) Volatiles on Earth and Mars: A comparison. *Icarus* **60**, 225–240.

DREIBUS G., SPETTEL B., HAUBOLD R., JOCHUM K. P., PALME H., WOLF D. AND ZIPFEL J. (2000) Chemistry of a shergottite: Sayh al Uhaymir 005 (abstract). *Meteorit. Planet. Sci.* **35 (Suppl.)**, A49.

FLEISCHER M., CABRI L. J., CHAO G. Y. AND PABST A. (1978) New mineral names. Ferrifayalite (= laihunite). *Am. Mineral.* **63**, 424–425.

FOLCO L., FRANCHI I. A., D'ORAZIO M., ROCCHI S. AND SCHULTZ L. (2000) A new meteorite from the Sahara: The shergottite Dar al Gani 489. *Meteorit. Planet. Sci.* **35**, 827–839.

FRANCHI I. A., WRIGHT I. P., SEXTON A. S. AND PILLINGER C. T. (1999) The oxygen isotopic composition of Earth and Mars. *Meteorit. Planet. Sci.* **34**, 657–661.

GLEASON J. D., KRING D. A., HILL D. H. AND BOYNTON W. V. (1997) Petrography and bulk chemistry of martian lherzolite LEW 88516. *Geochim. Cosmochim. Acta* **61**, 4007–4014.

GOODRICH C. A. AND ZIPFEL J. (2001) Magmatic inclusions in olivine and chromite in basaltic shergottite Sayh al Uhaymir 005: Implications for petrogenesis and relationship to lherzolitic shergottites (abstract). *Lunar Planet. Sci.* **32**, # 1174, Lunar and Planetary Institute, Houston, Texas, USA (CD-ROM).

GROSSMAN J. N. (2000) The Meteoritical Bulletin, 84. *Meteorit. Planet. Sci.* **35 (Suppl.)**, A199–A225.

GROSSMAN J. N. AND ZIPFEL J. (2001) The Meteoritical Bulletin, 85. *Meteorit. Planet. Sci.* **36 (Suppl.)**, A293–A322.

HARVEY R. P., WADHWA M., MCSWEEN H. Y., JR. AND CROZAZ G. (1993) Petrography, mineral chemistry, and petrogenesis of Antarctic shergottite LEW 88516. *Geochim. Cosmochim. Acta* **57**, 4769–4783.

HEMLEY R. J., PREWIT C. T. AND KINGM K. J. (1994) High-pressure behavior of silica. *Rev. Mineral.* **29**, 41–73.

KISSIN S. A. (1974) Sulfide mineralogy. Reviews in Mineralogy **1,** Mineralogical Society of America, Washington, D.C., USA.

LAGENHORST F. AND POIRIER J-P. (2000) 'Eclogitic' minerals in a shocked basaltic meteorite. *Earth Planet. Sci. Lett.* **176**, 259–265.

LE MAITRE R. W. *ET AL.* (1989) *A Classification of Igneous Rocks and Glossary of Terms*. Blackwell, Oxford, U.K.

LE MÉTOUR J., MICHEL J. C., BÉCHENNEC F., PLATEL J. P. AND ROGER J. (1995) *Geology and Mineral Wealth of the Sultanate of Oman*. Ministry of Petroleum and Minerals, Directorate General Of Minerals, Sultanate of Oman, Muscat, Oman. 285 pp.

LODDERS K. (1998) A survey of shergottite, nakhlite and chassigny meteorites whole-rock compositions. *Meteorit. Planet. Sci.* **33 (Suppl.)**, A183–A190.

MCDONOUGH W. F. AND RUDNICK R. L. (1998) Mineralogy and composition of the upper mantle. *Rev. Mineral.* **37**, 139–159.

MCKAY D. S., GIBSON E. K. J., THOMAS-KEPRTRA K. L., VALI H., ROMANEK C. S., CLEMENT S. J., CHILLIER X. D. F., MAECHLING C. R. AND ZARE R. N. (1996) Search for past life on Mars: Possible relic biogenic activity in martian meteorite ALH 84001. *Science* **273**, 924–930.

MCSWEEN H. Y. AND JAROSEWICH E., JR. (1983) Petrogenesis of the Elephant Moraine A79001 meteorite: Multiple magma pulses on the shergottite parent body. *Geochim. Cosmochim. Acta* **47**, 1501–1513.

MCSWEEN H. Y. AND TREIMAN A. H. (1998) Martian meteorites. In *Planetary Materials* (ed. J. J. Papike), pp. 6–01 to 6–53. Mineralogical Society of America, Washington, D.C., USA.

MCSWEEN H. Y., JR. AND STÖFFLER D. (1980) Shock metamorphic features in Allan Hills 77005 meteorite (abstract). *Lunar Planet. Sci.* **11**, 717–719.

MIKOUCHI T., MIYAMOTO M. AND MCKAY G. A. (2001) Mineralogy and petrology of the Dar al Gani 476 martian meteorite: Implications for its cooling history and relationship to other shergottites. *Meteorit. Planet. Sci.* **36**, 531–548.

MILLER M. F., FRANCHI I. A., SEXTON A. S. AND PILLINGER C. T. (1999) High-precision $\delta^{17}O$ measurements of oxygen from silicates and other oxides: Method and applications. *Rapid Commun. Mass Spectrom.* **13**, 1211–1217.

NALDRETT A. J. (1989) *Magmatic Sulfide Deposits.* Clarendon Press, New York, New York, USA. 186 pp.

MOORE P. B. (1983) Cerite, $Re_9(Fe^{3+},Mg)(SiO_4)_6(SiO_4OH)(OH)_3$: Its crystal structure and relation to whitlockite. *Am. Mineral.* **68**, 996–1003

OSTERDAG R., AMTHAUER G., RAGER H. AND MCSWEEN, H. Y., JR. (1984) $Fe^{3+}$ in shocked olivine crystals of the ALHA77005 meteorite. *Earth Planet. Sci. Lett.* **67**, 162–166.

PAPIKE J. J. (1998) Comperative planetary mineralogy: Chemistry of melt-derived pyroxene, feldspar, and olivine. In *Planetary Materials* (ed. J. J. Papike), pp. 7–01 to 7–11. Mineralogical Society of America, Washington, D.C., USA.

ROCHETTE P., LORAND J-P., FILLION G. AND AUTTER V. (2001) Pyrrhotite and the remanent magnetization of SNC meteorites; a changing perspective on martian magnetism. *Earth Planet. Sci. Lett.* **190**, 1–12.

SCHERRER N. C., ENGI M., GNOS E., JAKOB V. AND LIECHTI A. (2000) Monazite analysis; from sample preparation to microprobe age dating and REE quantification. *Schweiz. Mineral. Petr. Mitt.* **80**, 93–105.

SOFFEL H. C. (1991) *Paläomagnetismus und Archäomagnetismus.* Springer, Berlin, Germany. 276 pp.

STEELE I. M. AND SMITH J. V. (1982) Petrography and mineralogy of two basalts and olivine-pyroxene-spinel fragments in achondrite EETA97001. *J. Geophys. Res.* **87**, A375–A384.

STÖFFLER D. (1984) Glasses formed by hypervelocity impact. *J. Non-Cryst. Solids* **67**, 465–502.

STÖFFLER D., KEIL K. AND SCOTT E. R. D. (1991) Shock metamorphism of ordinary chondrites. *Geochim. Cosmochim. Acta* **55**, 2845–3867.

STRECKEISEN A. (1976) To each plutonic rock its proper name. *Earth Sci. Rev.* **12**, 1–33.

TREIMAN A. H. (1990) Complex petrogenesis of the Nakhla (SNC) meteorite: Evidence from petrography and mineral chemistry. *Proc. Lunar Planet. Sci. Conf.* **20th**, 273–280.

WADHWA M., LENTZ, R. C. F., MCSWEEN H. Y., JR. AND CROZAZ G. (2001) A petrologic trace element study of Dar al Gani 476 and Dar al Gani 489: Twin meteorites with affinities to basaltic and lherzolitic shergottites. *Meteorit. Planet. Sci.* **36**, 195–208.

WÄNKE H. (1991) Chemistry, accretion and evolution of Mars. *Space Sci. Rev.* **56**, 1–8.

WILLIAMS Q. AND JEANLOZ R. (1990) Melting relations in the iron-sulfur system at ultra-high pressures: Implications for the thermal state of the Earth. *J. Geophys. Res.* **95**, 19 299–19 310.

ZIPFEL J. (2000) Sayh al Uhaymir 005/008 and its relationship to Dar al Gani 476/489 (abstract). *Meteorit. Planet. Sci.* **35 (Suppl.)**, A178.

ZIPFEL J., SCHERER P., SPETTEL B., DREIBUS G. AND SCHULTZ L. (2000) Petrology and chemistry of the new shergottite Dar al Gani 476. *Meteorit. Planet. Sci.* **35**, 95–106.

Appendix 1. Published meteorite finds recovered during Omani-Swiss meteorite search program.

| Name | Date found | Latitude (N) | Longitude (E) | Mass (g) | Pieces | Class | Shock | WG | Fa mol% | Fs mol% | Wo mol% | Comments | Type | Info |
|---|---|---|---|---|---|---|---|---|---|---|---|---|---|---|
| AH 003 | 22/10/2002 | 19° 30.417 | 57° 7.171 | 115.417 | 1 | L4 | S1/2 | W2 | 24.0 | 20.9 | 1.7 | | NHB | AB |
| AH 004 | 21/10/2002 | 19° 32.689 | 57° 5.884 | 260.220 | 1 | L5 | S3 | W2-3 | 25.7 | 21.3 | 1.5 | cpx | NHB | AB |
| AH 005 | 28/11/2002 | 19° 50.434 | 57° 0.509 | 763.291 | many | L6 | S4 | W4 | 24.9 | 21.7 | 1.5 | | NHB | AA |
| AH 006 | 28/11/2002 | 19° 50.440 | 57° 0.505 | 1861.211 | >7 | L6 | S3 | W3 | 24.9 | 21.0 | 1.5 | | NHB | AA |
| AH 007 | 28/11/2002 | 19° 50.477 | 57° 0.572 | 1042.700 | 1 | L5 | S3 | W3 | 24.5 | 20.9 | 1.5 | cpx | NHB | AA |
| AH 008 | 28/11/2002 | 19° 50.522 | 57° 0.448 | 1074.300 | 1 | L6 | S3 | W2 | 25.1 | 20.7 | 1.4 | | NHB | AA |
| AH 009 | 14/12/2002 | 19° 50.538 | 57° 0.008 | 39.832 | 1 | H4 | S2 | W4 | 19.2 | 17.0 | 1.0 | | NHB | AA |
| AH 010 | 1/27/02 | 19° 52.071 | 57° 0.168 | 41539.339 | 100 | L6 | S4 | W2 | 25.2 | 21.1 | 1.6 | pr 0201-788 | NHB | AE |
| AH 011 | 1/27/02 | 19° 51.964 | 57° 0.192 | 8056 | 1 | L6 | S4 | W2 | 25.5 | 22.0 | 1.6 | cpx; pr 0201-791 | NHB | AE |
| AH 012 | 01/13/2003 | 19° 48.151 | 57° 19.282 | 402.754 | 14 | L6 | S4 | W4 | 25.7 | 22.8 | 1.5 | | NHB | AI |
| Aybut 001 | 1/30/02 | 17° 45.476 | 53° 59.419 | 442.260 | 1 | H6 | S2 | W1 | 20.5 | 17.4 | 1.3 | cpx | NHB | AD |
| Dho 820 | 2/12/2001 | 19°2.752' | 54°29.671' | 49.304 | 1 | H4 | S4 | W3 | 17.8-20.9 | 15.9-18.1 | 1.0-1.3 | | NMB | AB |
| Dho 1000 | 1/7/02 | 18° 29.267 | 54° 10.851 | 527.346 | 16 | H4 | S1 | W4 | 18.1 | 16.8 | 1.2 | | NHB | AA |
| Dho 1001 | 1/8/02 | 18° 33.346 | 54° 0.046 | 606.968 | 1 | L6 | S4 | W3 | 23.9 | 20.2 | 1.5 | | NHB | AA |
| Dho 1002 | 1/31/01 | 18° 33.543 | 54° 5.895 | 61.818 | 1 | L6 | S4 | W4 | 24.7 | 21.2 | 1.4 | | NHB | AA |
| Dho 1003 | 1/29/01 | 18° 55.593 | 54° 15.744 | 7.605 | 1 | H5 | S2 | W3 | 21.6 | 19.2 | 1.3 | | NHB | AA |
| Dho 1004 | 1/28/01 | 19° 2.688 | 54° 30.443 | 113.682 | 2 | H3,4 | S4 | W4 | 19.3 | 16.5 | 1.2 | | NHB | AA |
| Dho 1005 | 1/28/01 | 19° 3.771 | 54° 29.825 | 35.369 | 1 | H3,4 | S4 | W4 | 19.1 | 15.8-17.9 | 1.3 | | NHB | AA |
| Dho 1006 | 19/12/2002 | 18° 32.576 | 54° 0.064 | 155.668 | 9 | L6 | S4 | W2 | 25.4 | 21.6 | 1.6 | | NHB | AG |
| Dho 1007 | 07/01/2003 | 18° 32.718 | 54° 1.21 | 87.767 | 1 | L4 | S3 | W4 | 24.3 | 22.6 | 1.6 | | NHB | AH |
| Dho 1008 | 21/12/2002 | 18° 32.923 | 54° 1.621 | 76.451 | 13 | L5 | S1 | W4 | 24.4 | 22.2 | 1.6 | | NHB | AG |
| Dho 1009 | 01/21/2003 | 18° 33.234 | 54° 0.789 | 334.226 | 1 | L4 | S1 | W4 | 24.8 | 23.7 | 1.6 | pr 0301-76 | NHB | AI |
| Dho 1010 | 21/12/2002 | 18° 33.250 | 54° 0.152 | 2298.400 | 1 | H4 | S1 | W3 | 17.4 | 15.7 | 1.4 | | NHB | AG |
| Dho 1011 | 21/12/2002 | 18° 33.287 | 54° 2.563 | 292.797 | 2 | L3.3/3.4 | S1 | W3 | 7.4-29.7 | 15.7-24.6 | 0.0-3.0 | cpx | NHB | AG |
| Dho 1012 | 21/12/2002 | 18° 33.295 | 54° 1.758 | 144.865 | 1 | L6 | S3 | W1 | 24.8 | 21.2 | 1.5 | | NHB | AG |
| Dho 1013 | 01/21/2003 | 18° 33.312 | 54° 0.943 | 194.046 | 13 | L4 | S1 | W4 | 24.4 | 21.8 | 1.5 | pr 0301-77 | NHB | AI |
| Dho 1014 | 21/12/2002 | 18° 33.404 | 54° 0.050 | 298.274 | 1 | L4 | S2 | W4 | 25.7 | 21.5 | 1.5 | | NHB | AG |
| Dho 1015 | 21/12/2002 | 18° 33.544 | 54° 4.897 | 63.526 | 1 | EH4 | S2 | W3 | 0.4-0.6 | 0.5-4.1 | 0.4-1.6 | Plag: An0.04 | NHB | AG |
| Dho 1016 | 07/01/2003 | 18° 33.565 | 54° 2.708 | 125.207 | 1 | L5 | S2 | W3 | 24.2 | 21.2 | 1.6 | | NHB | AH |
| Dho 1017 | 12/30/2002 | 19° 10.322 | 54° 47.677 | 273.299 | 1 | H4 | S2/3 | W3 | 19.9 | 15.8 | 0.7 | cpx | NHB | AH |
| Dho 785 | 01/26/2001 | 19°4.941' | 54°27.137' | 98.449 | 1 | H4/5 | S3 | W3 | 18.3-19.4 | 16.4-18.4 | 1.1-1.5 | | NMB | AA |
| Dho 786 | 1/26/2001 | 19°4.016' | 54°31.159' | 36.334 | 1 | H4/5 | S2/3 | W3 | 18.6-19.9 | 16.5-18.4 | 1.0-1.3 | | NMB | AA |
| Dho 787 | 1/27/2001 | 19°1.753' | 54°32.684' | 382.497 | 18 | H4 | S1/2 | W4 | 16.3-19.2 | 15.9-16.8 | 0.7-1.4 | di | NMB | AA |
| Dho 788 | 1/27/2001 | 19°1.769' | 54°32.662' | 274.38 | 1 | H4 | S4 | W3 | 17.4-19.5 | 15.4-16.9 | 0.8-1.1 | | NMB | AA |
| Dho 789 | 1/27/2001 | 19°2.275' | 54°32.222' | 430.539 | 6 | L6 | S5 | W4 | 24.6-25.6 | 20.6-21.6 | 1.1-1.8 | | NMB | AA |
| Dho 790 | 1/27/2001 | 19°3.979' | 54°31.318' | 20.445 | 1 | H6 | S3/4 | W4 | 18.4-21.8 | 15.6-16.8 | 1.1-1.4 | Paired: 32, 36,130,132,137,139,141,142 | NMB | AA |
| Dho 791 | 1/27/2001 | 19°4.166' | 54°31.281' | 146.519 | 1 | H6 | S3 | W3 | 18.9-20.8 | 17.7 | 1.4 | di; paired 30, 36,130,132,137,139,141,142 | NMB | AA |
| Dho 792 | 1/27/2001 | 19°4.106' | 54°32.101' | 519.016 | 1 | H5 | S3 | W3 | 18.3-19.9 | 16.3-17.0 | 1.2-1.4 | | NMB | AA |
| Dho 793 | 1/27/2001 | 19°2.510' | 54°33.388' | 151.132 | 1 | H6 | S3 | W4 | 18.5-19.6 | 15.6-18.5 | 1.1-1.5 | Paired: 30, 32,130,132,137,139,141,142 | NMB | AA |

| | | | | | | | | | | | | | |
|---|---|---|---|---|---|---|---|---|---|---|---|---|---|
| Dho 794 | 1/28/2001 | 19°3.097' | 54°27.803' | 431.811 | 1 | H6 | S1 | W4 | 17.8-18.6 | 15.6-16.2 | 1.0-1.4 | | NMB | AA |
| Dho 795 | 1/28/2001 | 19°2.922' | 54°31.746' | 32.182 | 1 | L6 | S4 | W3 | 24.8-26.6 | 20.8-21.2 | 1.4-1.7 | | NMB | AA |
| Dho 796 | 1/28/2001 | 19°3.544' | 54°32.216' | 246.377 | 1 | H4 | S3 | W4 | 17.4-17.6 | 15.1-17.3 | 0.8-1.2 | | NMB | AA |
| Dho 797 | 1/28/2001 | 19°3.624' | 54°32.203' | 132.189 | 1 | H6 | S3 | W2/3 | 18.7-20.1 | 15.8-18.3 | 0.8-1.2 | | NMB | AA |
| Dho 798 | 1/28/2001 | 19°3.630' | 54°32.206' | 18.425 | 1 | H6 | S3 | W4 | 19.4-20.8 | 16.8-17.5 | 1.2-1.5 | Paired: 30, 32, 36,130,137,139,141,142 | NMB | AA |
| Dho 799 | 1/28/2001 | 19°4.224' | 54°32.303' | 56.11 | 1 | H4 | S2 | W3 | 17.8-19.1 | 15.7-19.1 | 1.0-1.7 | | NMB | AA |
| Dho 800 | 1/28/2001 | 19°3.751' | 54°33.029' | 55.884 | 1 | L4 | S2 | W4 | 24.8-26.1 | 20.2-21.5 | 1.2-2.0 | | NMB | AA |
| Dho 801 | 1/28/2001 | 19°3.341' | 54°33.065' | 119.149 | 2 | H6 | S2 | W4 | 18.6-18.9 | 15.5-17.7 | 1.0-1.2 | Paired: 30, 32, 36,130,132,139,141,142 | NMB | AA |
| Dho 802 | 1/28/2001 | 19°3.140' | 54°32.517' | 199.433 | 1 | H6 | S3 | W2 | 19.5-20.0 | 17.2-19.1 | 1.0-1.7 | Paired: 30, 32, 36,130,132,137,141,142 | NMB | AA |
| Dho 803 | 1/28/2001 | 19°3.516' | 54°32.102' | 22.427 | 1 | H6 | S3 | W4 | 19.4-21.1 | 16.3-18.0 | 1.2-1.7 | di; 30, 32, 36,130,132,137,139,142 | NMB | AA |
| Dho 804 | 1/28/2001 | 19°3.693' | 54°32.077' | 44.404 | 2 | H6 | S3 | W4 | 19.0-19.9 | 15.9-17.1 | 1.1-1.5 | di; 30, 32, 36,130,132,137,139,141 | NMB | AA |
| Dho 805 | 1/29/2001 | 18°55.155' | 54°16.015' | 237.941 | 1 | L6 | S3 | W3/4 | 24.2-26.4 | 20.4-22.3 | 1.5-1.7 | di | NMB | AA |
| Dho 806 | 1/29/2001 | 18°33.917' | 54°4.842' | 117.237 | 1 | L5 | S3 | W4 | 23.1-24.2 | 19.3-20.2 | 1.4-1.5 | | NMB | AA |
| Dho 807 | 1/29/2001 | 18°30.257' | 54°5.154' | 1260 | 1 | H5 | S1 | W2 | 19.1-20.4 | 16.7-19.1 | 1.1-1.5 | | NMB | AA |
| Dho 808 | 1/30/2001 | 18°10.799' | 54°12.220' | 2.496 | 1 | L6 | S5 | W4 | 23.6-24.8 | 19.6-21.0 | 1.2-1.8 | di | NMB | AA |
| Dho 809 | 1/31/2001 | 18°33.870' | 54°5.776' | 25.424 | 1 | L4 | S2 | W3 | 23.6-24.7 | 19.9-20.3 | 1.4-1.7 | | NMB | AA |
| Dho 810 | 1/31/2001 | 18°33.657' | 54°5.990' | 82.573 | 1 | H4 | S2 | W4 | 18.4-20.9 | 15.7-16.4 | 1.0-1.3 | | NMB | AA |
| Dho 811 | 1/31/2001 | 18°33.486' | 54°6.234' | 19.324 | 1 | H5 | S2 | W2 | 18.1-19.6 | 15.8-16.2 | 1.0-1.6 | | NMB | AA |
| Dho 812 | 1/31/2001 | 18°33.744' | 54°6.537' | 24.867 | 1 | L5 | S4 | W4 | 23.8-24.9 | 20.1-22.1 | 1.5-1.8 | | NMB | AA |
| Dho 813 | 1/31/2001 | 18°32.982' | 54°7.214' | 75.869 | 1 | L5 | S4 | W3 | 23.3-23.6 | 20.0-20.4 | 1.5-1.8 | | NMB | AA |
| Dho 814 | 2/11/2001 | 18°57.732' | 54°35.407' | 99.805 | 1 | H5 | S2 | W2 | 16.7-17.6 | 14.6-15.0 | 1.1-1.5 | | NMB | AB |
| Dho 815 | 2/11/2001 | 18°57.732' | 54°35.407' | 89.451 | 1 | H5 | S1 | W2 | 17.7-17.9 | 16.8-17.0 | 1.0-1.2 | di | NMB | AB |
| Dho 816 | 2/12/2001 | 18°58.754' | 54°37.691' | 23.858 | 1 | H5 | S2 | W2 | 18.9-21.8 | 19.6-20.5 | 1.1-1.5 | | NMB | AB |
| Dho 817 | 2/12/2001 | 19°1.189' | 54°30.839' | 164.753 | 8 | H4 | S3 | W4 | 18.3-20.3 | 16.4-18.1 | 0.9-1.3 | | NMB | AB |
| Dho 818 | 2/12/2001 | 19°1.525' | 54°30.380' | 82.427 | 1 | H 6 | S1 | W3 | 18.5-19.5 | 16.1-16.6 | 1.5-1.8 | | NMB | AB |
| Dho 819 | 2/12/2001 | 19°2.417' | 54°29.632' | 72.135 | 1 | H4 | S2 | W3 | 18.4-19.9 | 15.7-16.9 | 0.8-1.7 | | NMB | AB |
| Dho 821 | 2/12/2001 | 19°2.736' | 54°29.640' | 133.216 | 5 | H4 | S4 | W4 | 17.6-20.0 | 16.0-17.0 | 1.1-1.4 | di | NMB | AB |
| Dho 822 | 2/12/2001 | 19°2.935' | 54°29.560' | 39.296 | 11 | L5 | S3 | W4 | 24.0-26.0 | 20.5-22.5 | 1.4-1.8 | | NMB | AB |
| Dho 823 | 2/12/2001 | 19°3.015' | 54°29.545' | 23.329 | 1 | H4 | S4 | W3 | 18.7-20.6 | 16.2-18.2 | 0.9-1.1 | | NMB | AB |
| Dho 824 | 2/12/2001 | 19°3.608' | 54°31.909' | 12.052 | 1 | H6 | S3 | W4 | 18.6-19.9 | 16.5-17.0 | 1.1-1.4 | | NMB | AB |
| Dho 825 | 2/12/2001 | 19°3.616' | 54°32.609' | 50.441 | 1 | H6 | S3 | W3 | 19.7-20.6 | 15.9-16.6 | 1.0-1.7 | di | NMB | AB |
| Dho 826 | 2/12/2001 | 19°3.627' | 54°32.620' | 63.975 | 1 | H6 | S2/3 | W3 | 18.2-19.5 | 16.0-16.7 | 0.9-1.4 | | NMB | AB |
| Dho 827 | 2/12/2001 | 19°3.526' | 54°32.843' | 134.987 | 1 | H6 | S2 | W3 | 18.5-19.7 | 12.1-13.7 | 1.1-1.4 | | NMB | AB |
| Dho 828 | 2/12/2001 | 19°3.587' | 54°33.761' | 225.861 | 1 | H5 | S2 | W3 | 17.2-18.9 | 15.4-17.4 | 1.2-1.3 | di | NMB | AB |
| Dho 829 | 2/12/2001 | 19°3.602' | 54°34.728' | 19.677 | 1 | H6 | S3 | W4 | 19.1-20.9 | 17.5-20.1 | 1.2-1.6 | | NMB | AB |
| Dho 830 | 2/13/2001 | 19°2.696' | 54°28.582' | 15.676 | 1 | H5 | S3 | W4 | 17.9-18.9 | 15.8-18.7 | 0.8-1.3 | | NMB | AB |
| Dho 831 | 2/13/2001 | 19°2.878' | 54°29.347' | 22.291 | 1 | H4 | S3 | W4 | 17.6-25.7 | 15.1-19.5 | 0.9-1.0 | di | NMB | AB |
| Dho 832 | 2/13/2001 | 19°3.024' | 54°29.436' | 7.839 | 1 | H4/5 | S3 | W4 | 18.1-20.0 | 15.2-16.9 | 1.0-1.6 | di | NMB | AB |
| Dho 833 | 2/13/2001 | 19°3.201' | 54°29.594' | 4.583 | 1 | H4/5 | S3 | W4 | 18.1-19.6 | 16.3-17.3 | 0.7-0.8 | di | NMB | AB |
| Dho 834 | 2/13/2001 | 19°3.737' | 54°29.841' | 4.036 | 1 | H4 | S4 | W4 | 17.3-19.4 | 15.4-16.7 | 1.0-1.4 | aug | NMB | AB |
| Dho 835 | 2/15/2001 | 18°38.689' | 54°0.236' | 160.091 | 1 | H5 | S1/2 | W4 | 17.5-18.0 | 15.2-15.7 | 1.1-1.8 | di | NMB | AB |
| Dho 999 | 1/30/01 | 18° 16.090 | 54° 9.040 | 20.894 | 1 | H5 | S1 | W4 | 16.5 | 13.4 | 1.3 | | NHB | AA |

| | | | | | | | | | | | | | |
|---|---|---|---|---|---|---|---|---|---|---|---|---|---|
| JaH 069 | 1/25/2001 | 19°20.751' | 56°9.940' | 250.948 | 10 | H5 | S1/2 | W4 | 19.0-20.5 | 17.3-18.0 | 1.9-2.1 | | NMB | AA |
| JaH 070 | 1/25/2001 | 19°20.802' | 56°8.947' | 79.841 | 2 | H5 | S3 | W3/4 | 18.5-19.3 | 16.8-18.1 | 1.4-1.6 | | NMB | AA |
| JaH 071 | 1/25/2001 | 19°19.996' | 56°10.494' | 415.134 | 1 | H6 | S1 | W3 | 17.9-18.8 | 15.6-18.8 | 1.1-1.7 | | NMB | AA |
| JaH 072 | 1/25/2001 | 19°20.705' | 56°19.988' | 254.507 | 1 | H5 | S2 | W3 | 17.4-18.5 | 16.2-16.9 | 0.9-1.6 | | NMB | AA |
| JaH 073 | 1/17/2002 | 19°42' | 55°44' | 550000 | 2768 | L6 | S4 | W2-4 | 24.2-26.5 | 20.6-24.1 | 0.9-1.6 | | NMB | AA |
| JaH 076 | 29/10/2002 | 19° 3.002 | 55° 26.661 | 300.557 | 3 | L6 | S5 | W4 | 25.4 | 22.0 | 1.7 | | NHB | AB |
| JaH 077 | 22/12/2002 | 19° 39.964 | 55° 39.100 | 307.802 | 1 | L4 | S1 | W2 | 24.8 | 20.9 | 1.1 | | NHB | AG |
| JaH 078 | 01/17/2003 | 19° 54.869 | 55° 39.767 | 882.700 | 1 | L6 | S4 | W2 | 25.0 | 21.3 | 1.6 | pr 0301-51 | NHB | AI |
| JaH 079 | 01/17/2003 | 19° 54.873 | 55° 39.868 | 3959.857 | 5 | L6 | S4 | W2 | 25.9 | 22.2 | 1.6 | pr0301-52 | NHB | AI |
| JaH 080 | 08/01/2003 | 19° 35.042 | 55° 40.788 | 23.410 | 1 | L6 | S2 | W4 | 25.1 | 21 | 1.7 | cpx | NHB | AH |
| JaH 081 | 01/17/2003 | 19° 57.299 | 55° 41.342 | 35.954 | 3 | H6 | S1-3 | W3-4 | 19.5 | 17.4 | 1.4 | | NHB | AI |
| JaH 082 | 08/01/2003 | 19° 33.936 | 55° 41.834 | 18.586 | 1 | H4 | S2 | W4 | 17.0 | 15.3 | 1.0 | | NHB | AH |
| JaH 084 | 05/12/2002 | 19° 39.311 | 55° 45.185 | 59.473 | 1 | CO3.0/3.2 | S1 | W1 | 3.2-39.2 | 1.1-4.9 | 0.9-2.7 | | NHB | AA |
| JaH 085 | 05/12/2002 | 19° 39.511 | 55° 45.186 | 51.895 | 1 | H4 | S2 | W3 | 19.0 | 17.2 | 1.3 | cpx | NHB | AA |
| JaH 086 | 1/17/02 | 19° 43.437 | 55° 47.634 | 123.344 | 1 | H6 | S3 | W4 | 19.3 | 18.0 | 1.3 | | NHB | AA |
| JaH 087 | 11/10/2002 | 19° 35.319 | 56° 10.553 | 1532.700 | 1 | H4-6 | S1/2 | W3 | 18.7 | 17.3 | 1.1 | | NHB | AB |
| JaH 088 | 21/10/2002 | 19° 21.426 | 56° 16.119 | 185.397 | 1 | L6 | S5 | W4 | 25.2 | 22.5 | 1.4 | | NHB | AB |
| JaH 089 | 1/13/02 | 19° 56.342 | 56° 25.685 | 170.69 | 1 | IMB | S3-4 | W2 | 25.2 | 19.7 | 2.3-6.9 | | NHB | AA |
| JaH 090 | 18/10/2002 | 19° 43.007 | 56° 36.372 | 92667.600 | 15 | L5 | S2 | W2/3 | 25.1 | 22.8 | 1.7 | pr 10-11 | NHB | AB |
| JaH 091 | 19/10/2002 | 19° 41.617 | 56° 39.259 | 123374.40 | >1000 | L5 | S2 | W3 | 25.0 | 21.3 | 1.6 | pr 10-10 | NHB | AB |
| JaH 092 | 1/12/02 | 19° 12.340 | 56° 43.833 | 204.552 | 5 | H4-5 | S1 | W4 | 18.4 | 16.2 | 1.2 | cpx | NHB | AA |
| JaH 093 | 11/10/2002 | 19° 57.753 | 56° 45.399 | 246.769 | 1 | L5 | S1 | W3 | 24.8 | 20.4 | 1.3 | cpx | NHB | AB |
| JaH 094 | 11/10/2002 | 19° 59.015 | 56° 46.379 | 3713.745 | 8 | L6 | S3 | W3 | 24.9 | 22.3 | 1.4 | pr 10-07 | NHB | AB |
| JaH 095 | 12/10/2002 | 19° 59.015 | 56° 46.379 | 1211.574 | 5 | L6 | S3 | W3 | 24.8 | 22.0 | 1.4 | pr 10-06 | NHB | AB |
| JaH 096 | 23/10/2002 | 19° 27.617 | 56° 49.676 | 1853.500 | 1 | L6 | S3 | W3 | 24.9 | 20.5 | 1.5 | | NHB | AB |
| JaH 097 | 23/10/2002 | 19° 27.697 | 56° 49.923 | 674.300 | 1 | L5 | S3 | W2-3 | 24.9 | 21.5 | 1.3 | cpx | NHB | AB |
| JaH 098 | 16/10/2002 | 19° 13.716 | 56° 5.539 | 7521.315 | 30 | H4 | S2 | W2/3 | 19.7 | 18.8 | 1.3 | | NHB | AB |
| JaH 099 | 25/10/2002 | 19° 31.613 | 56° 50.131 | 1595.377 | 5 | H4(-5) | S1 | W4 | 17.9 | 15.8 | 1.2 | | NHB | AB |
| JaH 100 | 24/10/2002 | 19° 30.851 | 56° 51.121 | 1362.500 | 1 | H4(-5) | S1 | W3 | 17.8 | 15.8 | 1.1 | | NHB | AB |
| JaH 101 | 01/13/2003 | 19° 45.044 | 56° 57.991 | 3563.000 | 1 | L6 | S2 | W3 | 25.5 | 23.5 | 1.6 | | NHB | AI |
| JaH 102 | 1/12/02 | 19° 30.711 | 56° 58.907 | 1007.329 | 67 | H5 | S2 | W4 | 19.1 | 16.5 | 1.3 | | NHB | AA |
| JaH 103 | 01/13/2003 | 19° 51.474 | 56° 59.984 | 2711.000 | 1 | L4 | S2 | W3 | 22.4 | 18.9 | 1.5 | | NHB | AI |
| JaH 104 | 01/13/2003 | 19° 54.835 | 56° 59.995 | 19.908 | 2 | H6 | S3 | W3 | 20.2 | 17.8 | 1.3 | | NHB | AI |
| JaH 105 | 16/10/2002 | 19° 10.761 | 56° 7.066 | 59.412 | 1 | H6 | S2 | W3 | 20.9 | 18.5 | 2.0 | | NHB | AB |
| JaH 106 | 11/10/2002 | 19° 35.669 | 56° 9.420 | 263.723 | 1 | H4 | S2 | W2 | 18.7 | 15.5 | 0.9 | | NHB | AB |
| JaH 107 | 10/10/2002 | 19° 34.794 | 56° 9.767 | 77.872 | 1 | H6 | S2 | W4 | 19.2 | 17.3 | 1.5 | | NHB | AB |
| JaH 108 | 1/17/02 | 19° 44.152 | 55° 49.732 | 817.2 | 1 | H6 | S1-S2 | W3 | 20.8 | 18.3 | 1.3 | cpx | NHB | AA |
| JaH 109 | 09/10/2002 | 19° 56.752 | 56° 55.628 | 729.700 | 1 | H4 | S2 | W4 | 18.3 | 15.2 | 1.8 | | NHB | AB |
| RaS 001 | 01/09/2003 | 20° 12.138 | 56° 22.001 | 97.533 | 3 | L6 | S4 | W3 | 24.5 | 21.3 | 1.5 | | NHB | AI |
| RaS 002 | 01/18/2003 | 20° 14.599 | 56° 27.099 | 200.511 | 1 | H6 | S1 | W4 | 18.1 | 16.1 | 1.7 | | NHB | AI |
| RaS 003 | 01/18/2003 | 20° 15.817 | 56° 27.843 | 39.814 | 1 | H5 | S1 | W3 | 19.2 | 17.1 | 1.5 | | NHB | AI |
| RaS 004 | 01/18/2003 | 20° 15.843 | 56° 27.789 | 475.964 | 4 | H4 | S2 | W4 | 18.8 | 18.2 | 1.1 | | NHB | AI |
| RaS 005 | 08/01/2003 | 20° 2.217 | 56° 17.326 | 275.278 | 1 | H5 | S3 | W3 | 18.9 | 17.3 | 1.2 | | NHB | AH |
| RaS 006 | 08/01/2003 | 20° 3.255 | 56° 18.528 | 17.946 | 1 | H5 | S2 | W3 | 18.9 | 16.6 | 1.3 | cpx | NHB | AH |

| | | | | | | | | | | | | | | |
|---|---|---|---|---|---|---|---|---|---|---|---|---|---|---|
| SaU 063 | 1/22/2001 | 21°2.222' | 57°19.611' | 1877.301 | 36 | H5 | S1/2 | W3/4 | 17.9-19.7 | 15.4-16.5 | 1.0-1.8 | | NMB | AA |
| SaU 164 | 1/22/2001 | 20°59.012' | 57°12.061' | 331.469 | 3 | H6 | S1/2 | W4 | 20.4 | 17.1-17.7 | 1.6-2.0 | | NMB | AA |
| SaU 165 | 1/23/2001 | 21°1.211' | 57°12.688' | 457.152 | 3 | L5 | S3 | W4 | 24.7-29.5 | 19.2-22.1 | 1.1-1.5 | | NMB | AA |
| SaU 166 | 1/23/2001 | 21°1.238' | 57°12.786' | 385.201 | 2 | H5 | S1/2 | W4 | 18.6-19.9 | 15.7-17.9 | 0.9-1.3 | | NMB | AA |
| SaU 167 | 2/10/2001 | 21°10.073' | 56°32.482' | 68.035 | 2 | L6 | S4 | W3/4 | 23.5-24.9 | 20.2-22.0 | 1.0-1.4 | | NMB | AB |
| SaU 168 | 2/10/2001 | 21°6.310' | 56°59.778' | 24.726 | 3 | H4 | S4 | W4 | 17.9-20.2 | 17.9-19.1 | 0.9-1.2 | di | NMB | AB |
| SaU 169 | 1/16/2002 | 20°34.391' | 57°19.4' | 206.454 | 1 | lunar | | | | | | | NMB | AA |
| SaU 184 | 1/16/02 | 20° 28.580 | 57° 21.608 | 226.219 | 1 | L6 | S3 | W3 | 25.5 | 20.6 | 1.5 | | NHB | AA |
| SaU 185 | 1/16/02 | 20° 30.891 | 57° 16.643 | 1575.3 | 1 | L/H4-5 | S1-S3 | W2 | 19.4-24.5 | 17.2-20.6 | 1.0-1.6 | br | NHB | AA |
| SaU 186 | 1/14/02 | 20° 33.873 | 57° 10.675 | 3166.736 | 1 | H4-6 | S2 | W4 | 19.4 | 16.3 | 1.5 | cpx, br | NHB | AA |
| SaU 187 | 1/16/02 | 20° 34.167 | 57° 19.300 | 4211 | 1 | L4-5 | S2 | W2 | 25.8 | 21.7 | 1.7 | | NHB | AA |
| SaU 188 | 1/16/02 | 20° 35.262 | 57° 5.851 | 127.915 | 1 | EL4 | S2 | W1-W3 | 26.8 | 0.5-4.4 | 0.2-0.8 | | NHB | AA |
| SaU 189 | 1/16/02 | 20° 36.145 | 57° 22.742 | 694.9 | 1 | LL7 | S5 | W4 | 27.3 | 22.2 | 1.5 | plg >200 $\mu$m | NHB | AA |
| SaU 190 | 12/2001 | 20° 51.800 | 56° 12.200 | 262.0000 | 1 | L5 | S4 | W2 | 24.0 | 20.4 | 1.4 | | NHB | AB |
| SaU 191 | 1/15/02 | 20° 57.957 | 57° 19.473 | 284.826 | 1 | H6 | S1 | W4 | 19.4 | 16.9 | 1.4 | | NHB | AA |
| SaU 192 | 1/15/02 | 20° 57.958 | 57° 19.542 | 349.28 | 1 | H6 | S1 | W4 | 19.3 | 17.7 | 1.5 | | NHB | AA |
| SaU 193 | 12/2001 | 20°51.810 | 56° 12.210 | 52 | 1 | L4 | S4 | W2 | 23.0 | 19.5 | 0.7 | | NHB | AB |
| SaU 194 | 2/9/01 | 21° 2.147 | 57° 19.695 | 198.357 | 1 | L6 | S2,3 | W4 | 25.5 | 21.1 | 1.1 | | NHB | AB |
| SaU 195 | 1/15/02 | 21° 2.378 | 57° 18.651 | 48.093 | 1 | H5 | S2 | W3 | 20.3 | 16.8 | 1.5 | | NHB | AA |
| SaU 196 | 1/15/02 | 21° 2.580 | 57° 20.584 | 407.77 | 1 | L6 | S2 | W4 | 24.9 | 21.0 | 1.5 | | NHB | AA |
| SaU 197 | 1/14/02 | 21° 3.757 | 57° 16.428 | 34.692 | 1 | L6 | S3 | W2 | 25.2 | 20.7 | 1.5 | cpx, br | NHB | AA |
| SaU 198 | 1/14/02 | 21° 3.757 | 57° 16.453 | 36.032 | 1 | L6 | S3 | W2 | 24.5 | 20.8 | 1.4 | | NHB | AA |
| SaU 199 | 1/14/02 | 21° 3.917 | 57° 16.824 | 75.134 | 1 | L6 | S3 | W2 | 24.5 | 21.3 | 1.3 | | NHB | AA |
| SaU 200 | 1/14/02 | 21° 4.033 | 57° 17.007 | 16.084 | 1 | L6 | S3 | W1 | 24.7 | 20.4 | 1.3 | | NHB | AA |
| SaU 201 | 1/14/02 | 21° 4.178 | 57° 17.474 | 44.708 | 1 | L6 | S3 | W2 | 25.3 | 20.9 | 1.5 | | NHB | AA |
| SaU 202 | 1/22/01 | 21° 4.252 | 57° 18.670 | 335.860 | 7 | CV3.2/3.3 | S2 | W2 | 1.8-8.5 | 1.8-6.3 | 1.1-1.4 | | NHB | AA |
| SaU 203 | 1/14/02 | 21° 4.261 | 57° 17.691 | 22.788 | 1 | L6 | S3 | W3 | 26.9 | 21.3 | 1.5 | | NHB | AA |
| SaU 204 | 1/3/02 | 21° 5.010 | 57° 15.165 | 139.957 | 1 | H5 | S3 | W3 | 19.4 | 16.7 | 1.5 | | NHB | AA |
| SaU 205 | 17/11/2002 | 20° 0.240 | 56° 45.721 | 137.796 | 1 | L6 | S5-6 | W3 | 25.4 | 21.1 | 1.5 | | NHB | AB |
| SaU 206 | 01/14/2003 | 20° 11.691 | 57° 12.132 | 76.044 | 1 | H4-5 | S1 | W4 | 19.5 | 17.4 | 1.2 | | NHB | AI |
| SaU 207 | 30/11/2002 | 20° 12.075 | 56° 57.686 | 606.922 | 1 | H4 | S1 | W3 | 17.7 | 15.5 | 0.8 | | NHB | AA |
| SaU 208 | 01/18/2003 | 20° 17.701 | 56° 30.453 | 48.645 | 1 | H4 | S1 | W4 | 18.9 | 17.3 | 1.5 | | NHB | AI |
| SaU 209 | 07/12/2002 | 20° 19.901 | 57° 14.844 | 5585.000 | 1 | H5 | S1 | W2 | 17.8 | 15.7 | 1.7 | | NHB (66.80g) | AF |
| SaU 210 | 01/14/2003 | 20° 2.146 | 57° 13.223 | 97.271 | 1 | L6 | S3 | W3 | 25.4 | 21.2 | 1.5 | | NHB | AI |
| SaU 211 | 19/11/2002 | 20° 22.115 | 56° 53.201 | 319.000 | 1 | H4 | S2 | W3 | 18.1 | 16.4 | 1.1 | | NHB | AB |
| SaU 212 | 31/10/2002 | 20° 24.166 | 57° 2.244 | 2027.064 | 3 | L5 | S4 | W3 | 24.4 | 22.5 | 1.3 | | NHB | AB |
| SaU 213 | 22/09/2002 | 20° 24.862 | 57° 3.947 | 187.503 | 1 | H4 | S1 | W3 | 17.6 | 15.8 | 1.0 | | NHB | AB |
| SaU 214 | 01/10/2003 | 20° 25.252 | 57° 21.556 | 1081.800 | 1 | L5 | S1 | W4 | 24.7 | 21.0 | 1.6 | | NHB | AI |
| SaU 215 | 01/09/2003 | 20° 25.453 | 56° 33.711 | 188.381 | 2 | H5 | S2 | W3 | 19.6 | 18.5 | 1.4 | | NHB | AI |
| SaU 216 | 23/09/2002 | 20° 25.645 | 57° 6.178 | 29.868 | 1 | H4 | S2 | W4 | 18.3 | 16.8 | 1.3 | | NHB | AB |
| SaU 217 | 01/09/2003 | 20° 26.005 | 56° 35.23 | 181.258 | 2 | H5 | S2 | W3 | 19.6 | 16.9 | 1.3 | | NHB | AI |
| SaU 218 | 12/11/2002 | 20° 26.548 | 57° 13.977 | 86.332 | 1 | L4 | S2 | W3 | 25.0 | 21.0 | 1.8 | | NHB | AB |
| SaU 219 | 22/09/2002 | 20° 29.044 | 56° 56.574 | 2934.000 | 1 | H4 | S1 | W3 | 18.2 | 16.1 | 1.2 | | NHB | AB |

| | | | | | | | | | | | | | | |
|---|---|---|---|---|---|---|---|---|---|---|---|---|---|---|
| SaU 220 | 11/11/2002 | 20° 29.118 | 57° 12.855 | 185.358 | 1 | H3.9 | S2 | W3 | 15.7-22.4 | 15.3-25.5 | 0.5-3.7 | cpx | NHB | AB |
| SaU 221 | 25/09/2002 | 20° 29.360 | 57° 24.038 | 1945.348 | 9 | L5 | S2 | W3 | 24.1 | 20.8 | 1.2 | | NHB | AB |
| SaU 222 | 25/09/2002 | 20° 29.425 | 57° 23.613 | 77.782 | 1 | L6 | S2 | W3 | 25.2 | 21.2 | 1.5 | | NHB | AB |
| SaU 223 | 20/09/2002 | 20° 29.480 | 57° 22.171 | 2309.195 | 10 | L5 | S3 | W4 | 24.0 | 20.2 | 1.3 | | NHB | AB |
| SaU 224 | 21/09/2002 | 20° 29.610 | 57° 15.112 | 688.100 | 1 | L5 | S2 | W2 | 24.5 | 20.9 | 1.9 | | NHB | AB |
| SaU 225 | 20/11/2002 | 20° 3.621 | 56° 56.951 | 306.690 | 1 | H4 | S2 | W4 | 18.8 | 16.5 | 1.7 | | NHB | AA |
| SaU 226 | 18/11/2002 | 20° 3.753 | 56° 57.196 | 93.473 | 2 | H6 | S2 | W4 | 19.3 | 16.8 | 1.5 | | NHB | AB |
| SaU 227 | 01/12/2002 | 20° 30.031 | 57° 16.231 | 646.100 | 1 | H5(4-6) | S1/2 | W3 | 18.0 | 16.1 | 1.5 | | NHB | AA |
| SaU 228 | 26/09/2002 | 20° 30.133 | 57° 22.423 | 450.932 | 1 | H6 | S1 | W2 | 18.7 | 16.4 | 1.5 | | NHB | AB |
| SaU 229 | 08/12/2002 | 20° 30.463 | 57° 9.076 | 149.000 | 1 | H6 | S1 | W3 | 18.9 | 17.1 | 1.4 | | NHB | AB |
| SaU 230 | 25/09/2002 | 20° 30.701 | 57° 19.106 | 711.200 | 1 | L6 | S3 | W3 | 25.3 | 20.9 | 1.7 | | NHB | AB |
| SaU 231 | 12/11/2002 | 20° 30.793 | 57° 22.054 | 307.277 | 3 | L4 | S3 | W3 | 24.3 | 20.3 | 1.7 | | NHB | AB |
| SaU 232 | 12/11/2002 | 20° 31.006 | 57° 21.906 | 60.919 | 1 | H5 | S3 | W4 | 19.8 | 17.4 | 1.4 | | NHB | AB |
| SaU 233 | 13/11/2002 | 20° 31.576 | 57° 23.159 | 74.760 | 1 | H4 | S2 | W4 | 20.8 | 19.1 | 1.2 | | NHB | AB |
| SaU 234 | 02/12/2002 | 20° 32.385 | 57° 18.405 | 647.700 | 1 | L6 | S4 | W2 | 25.5 | 21.6 | 1.4 | pr 0212-05, cpx | NHB | AA |
| SaU 235 | 16/12/2002 | 20° 32.509 | 57° 11.935 | 2370.062 | 80 | L6 | S4 | W4 | 25.5 | 21.3 | 1.6 | | NHB | AA |
| SaU 236 | 16/12/2002 | 20° 32.624 | 57° 7.710 | 210.492 | 1 | H6 | S2 | W3 | 18.2 | 17.0 | 1.6 | | NHB | AA |
| SaU 237 | 24/09/2002 | 20° 33.217 | 57° 19.460 | 431.900 | 1 | L5 | S3 | W4 | 25.6 | 22.1 | 1.3 | | NHB | AB |
| SaU 238 | 13/11/2002 | 20° 33.370 | 57° 18.600 | 3436.000 | 1 | L4 | S2 | W2 | 24.2 | 21.8 | 1.6 | | NHB | AB |
| SaU 239 | 01/09/2003 | 20° 33.41 | 56° 50.844 | 2094.800 | 1 | L4 | S2 | W2 | 29.8 | 18.6 | 1.2 | cpx | NHB | AI |
| SaU 240 | 26/09/2002 | 20° 33.656 | 57° 19.956 | 341.646 | 1 | H4,5 | S2 | W4 | 19.3 | 19.3 | 1.2 | | NHB | AB |
| SaU 241 | 02/12/2002 | 20° 33.740 | 57° 22.564 | 1391.800 | 1 | H5(4-6) | S2 | W3 | 18.4 | 16.6 | 1.4 | | NHB | AA |
| SaU 242 | 01/10/2003 | 20° 33.765 | 57° 17.142 | 2737.000 | 1 | L4 | S1 | W2 | 24.8 | 21.6 | 2.0 | | NHB | AI |
| SaU 243 | 25/09/2002 | 20° 33.939 | 57° 21.498 | 419.163 | 1 | H5 | S2 | W2 | 19.4 | 16.9 | 1.4 | | NHB | AB |
| SaU 244 | 02/12/2002 | 20° 34.080 | 57° 22.453 | 63.051 | 1 | H5(4-6) | S2 | W3 | 18.5 | 16.5 | 1.4 | | NHB | AA |
| SaU 245 | 02/12/2002 | 20° 34.361 | 57° 22.163 | 566.648 | 2 | L6 | S1 | W4 | 25.4 | 20.9 | 1.5 | | NHB | AA |
| SaU 246 | 16/12/2002 | 20° 34.761 | 57° 11.088 | 614.429 | 1 | H3.4 | S1/2 | W3 | 18.2-23.2 | 15.2-19.8 | 0.6-1.4 | cpx | NHB | AA |
| SaU 247 | 16/12/2002 | 20° 34.779 | 57° 11.090 | 183.080 | 1 | L6 | S3 | W3 | 25.1 | 21.2 | 1.5 | | NHB | AA |
| SaU 248 | 01/10/2003 | 20° 34.862 | 57° 24.177 | 773.900 | 1 | L6 | S4 | W3 | 24.7 | 20.8 | 1.7 | pr 0301-21, 23, 24, 25, 25 | NHB | AI |
| SaU 249 | 02/12/2002 | 20° 34.968 | 57° 21.640 | 486.212 | 2 | H5 | S1 | W4 | 18.1 | 15.9 | 1.3 | | NHB | AA |
| SaU 250 | 01/10/2003 | 20° 34.979 | 57° 18.99 | 16200.000 | 2 | H4-6 | S2 | W3 | 18.0 | 16.6 | 1.6 | cpx | NHB | AI |
| SaU 251 | 01/11/2003 | 20° 35.248 | 57° 21.175 | 485.923 | 1 | L6 | S4 | W3 | 25.6 | 21.7 | 1.6 | pr 0301-21, 22, 24, 25, 25 | NHB | AI |
| SaU 252 | 24/09/2002 | 20° 35.456 | 57° 11.852 | 22.559 | 1 | H4-(5) | S2 | W3 | 18.8 | 17.6 | 2.2 | | NHB | AB |
| SaU 253 | 27/09/2002 | 20° 35.782 | 57° 9.698 | 2128.900 | 1 | H5 | S2 | W3 | 18.1 | 16.2 | 1.5 | pr 09-16 | NHB | AB |
| SaU 254 | 20/09/2002 | 20° 35.934 | 57° 1.228 | 964.189 | 4 | L6 | S4 | W2 | 25.0 | 21.3 | 1.5 | | NHB | AB |
| SaU 255 | 01/10/2003 | 20° 35.975 | 57° 22.515 | 461.130 | 1 | L6 | S4 | W4 | 25.5 | 21.5 | 1.7 | pr 0301-22, 23, 24, 25, 25;cpx | NHB | AI |
| SaU 256 | 27/09/2002 | 20° 36.038 | 57° 9.555 | 392.500 | 1 | H5 | S2 | W3 | 18.9 | 17.3 | 1.5 | pr 09-15 | NHB | AB |
| SaU 257 | 01/10/2003 | 20° 36.303 | 57° 19.305 | 175.121 | 1 | H5 | S2 | W4 | 18.3 | 17.4 | 1.4 | | NHB | AI |
| SaU 258 | 02/12/2002 | 20° 36.796 | 57° 20.347 | 3864.213 | 1 | L6 | S4 | W3 | 25.5 | 21.1 | 1.3 | pr 0212-06 | NHB | AA |
| SaU 259 | 16/12/2002 | 20° 37.362 | 56° 56.875 | 1415.132 | 1 | H4 | S1 | W4 | 18.9 | 17.3 | 1.2 | | NHB | AA |
| SaU 260 | 01/12/2003 | 20° 38.166 | 57° 12.846 | 460.134 | 1 | L6 | S2 | W4 | 25.5 | 22.0 | 1.5 | pr 0301-26 | NHB | AI |
| SaU 261 | 14/11/2002 | 20° 40.106 | 57° 9.562 | 499.437 | 3 | L3.7/3.2 | S2 | W3 | 24.2-27.3 | 19.9-33.4 | .1-4.5 | | NHB | AB |
| SaU 262 | 01/11/2003 | 20° 38.185 | 57° 17.236 | 1069.500 | 1 | L6 | S4 | W3 | 25.0 | 20.9 | 1.8 | pr 0301-21, 22, 23, 25, 25 | NHB | AI |
| SaU 263 | 03/12/2002 | 20° 41.717 | 57° 10.994 | 400.803 | 7 | H5 | S3 | W3 | 19.0 | 16.7 | 1.6 | | NHB | AA |

| | | | | | | | | | | | | | |
|---|---|---|---|---|---|---|---|---|---|---|---|---|---|
| SaU 264 | 09/11/2002 | 20° 41.770 | 57° 11.694 | 3548.079 | 6 | LL6 | S1-2 | W4 | 31.0 | 25.2 | 3.3 | NHB | AB |
| SaU 265 | 12/28/2002 | 20° 42.392 | 57° 11.035 | 6289.877 | 37 | H4-6 | S1 | W3 | 18.3 | 16.8 | 1.5 | NHB | AH |
| SaU 266 | 12/28/2002 | 20° 42.428 | 57° 10.99 | 25013.960 | 1 | H5 | S3 | W3 | 18.3 | 16.4 | 1.4 | NHB | AH |
| SaU 267 | 09/11/2002 | 20° 43.323 | 57° 12.608 | 223.004 | 1 | L6 | S2 | W3 | 24.4 | 20.5 | 1.4 cpx | NHB | AB |
| SaU 268 | 03/12/2002 | 20° 43.577 | 57° 9.583 | 71.102 | 1 | H5(4-6) | S1 | W4 | 18.4 | 16.7 | 1.3 br | NHB | AB |
| SaU 269 | 01/12/2003 | 20° 43.666 | 57° 11.305 | 1033.000 | 1 | H4-5 | S1/2 | W3 | 18.5 | 16.1 | 1.5 pr 0301-29;cpx | NHB | AI |
| SaU 270 | 011/12/2003 | 20° 43.751 | 57° 11.34 | 43508.193 | 55 | H4-6 | S1/2 | W4 | 19.1 | 16.7 | 1.5 pr 0301-28; cpx | NHB | AI |
| SaU 271 | 09/11/2002 | 20° 46.131 | 57° 15.601 | 314.634 | 1 | H4 | S1 | W3 | 19.3 | 17.8 | 1.3 | NHB | AB |
| SaU 272 | 01/12/2003 | 20° 47.2 | 57° 12.843 | 7563.000 | 1 | H5 | S2 | W2 | 19.3 | 17.0 | 1.3 | NHB | AI |
| SaU 273 | 01/11/2003 | 20° 47.417 | 57° 11.645 | 97.454 | 1 | L6 | S4 | W4 | 25.3 | 21.4 | 1.7 pr 0301-21, 22, 23, 24;cpx | NHB | AI |
| SaU 274 | 10/11/2002 | 20° 48.786 | 57° 19.811 | 56.753 | 1 | L4 | S2 | W4 | 25.3 | 21.8 | 1.7 | NHB | AB |
| SaU 275 | 10/11/2002 | 20° 56.697 | 57° 21.351 | 303.227 | 1 | H6 | S1 | W3 | 19.5 | 17.2 | 1.3 | NHB | AB |
| SaU 276 | 31/10/2002 | 20° 6.010 | 56° 50.265 | 286.405 | 1 | H6 | S1 | W3 | 18.6 | 16.4 | 1.5 | NHB | AB |
| SaU 277 | 07/12/2002 | 20° 9.995 | 57° 4.527 | 11643.000 | 1 | H6 | S1 | W3 | 19.5 | 16.8 | 1.3 | NHB (50.80g) | AF |
| SaU 278 | 11/11/2002 | 21° 15.703 | 57° 10.732 | 27860.800 | 158 | L5 | S4 | W3 | 25.1 | 20.9 | 1.3 | NHB | AB |
| SaU 279 | 01/11/2003 | 21° 2.673 | 57° 16.41 | 79.557 | 1 | L6 | S2 | W3 | 24.7 | 21.2 | 1.5 pr 0301-27 | NHB | AI |
| SaU 280 | 10/11/2002 | 21° 3.756 | 57° 18.751 | 193.021 | 1 | H4 | S1 | W4 | 17.6 | 16.1 | 1.1 | NHB | AB |
| Shalim 003 | 3/21/2001 | 18°10.940' | 55°30.110' | 10350 | 50 | H5 | S1/2 | W3 | 18.1-19.1 | 16.2-17.1 | 1.2-1.5 | NMB | AC |
| Shalim 004 | 3/21/01 | 18° 10.940 | 55° 30.110 | 10350.000 | 5 | H5 | S1,2 | W3 | 18.6 | 16.6 | 1.3 | NHB | AC |
| Shalim 005 | 1/10/02 | 18° 12.859 | 55° 42.793 | 344.664 | 15 | H5 | 6 | W4 | 18.6 | 16.4 | 1.2 | NHB | AA |
| Shalim 006 | 1/11/02 | 18° 26.837 | 55° 55.298 | 374.419 | 1 | H6 | S2 | W3 | 19.3 | 16.6 | 1.5 cpx | NHB | AA |
| Shalim 007 | 1/11/02 | 18° 31.579 | 55° 55.979 | 323.85 | 1 | H6 | S1 | W3 | 18.9 | 16.3 | 1.4 | NHB | AA |
| Shisr 015 | 2/02/2001 | 18°32.945' | 53°55.374' | 3409.297 | 20 | L5 | S2 | W4 | 23.2-25.5 | 19.4-22.8 | 1.3-1.7 | NMB | AA |
| Shisr 016 | 2/02/2001 | 18°26.304' | 53°58.135' | 84.481 | 1 | H5 | S3 | W4 | 18.4-19.2 | 16.0-17.3 | 1.1-1.6 | NMB | AA |
| Shisr 017 | 2/14/2001 | 18°25.393' | 53°36.543' | 12.83 | 1 | H4 | S5 | W 4 | 17.8-20.2 | 16.0-17.3 | 1.0-1.4 di | NMB | AB |
| Shisr 018 | 2/15/2001 | 18°32.240' | 53°55.987' | 116.538 | 1 | L6 | S1 | W4 | 24.7-26.2 | 20.1-22.3 | 1.2-1.6 | NMB | AB |
| Shisr 019 | 2/15/2001 | 18°32.850' | 53°53.610' | 1332.725 | 4 | H4 | S3 | W3 | 18.2-21.2 | 15.8-18.2 | 1.0-1.6 | NMB | AB |
| Shisr 020 | 2/15/2001 | 18°33.556' | 53°53.493' | 2200.715 | 4 | H4-6 | S1 | W3 | 17.6-20.6 | 15.5-19.2 | 1.0-1.6 br; paired 257 | NMB | AB |
| Shisr 021 | 2/15/2001 | 18°36.272' | 53°53.254' | 135.226 | 1 | H4-6 | S1 | W4 | 16.4-20.9 | 15.1-17.0 | 0.8-1.4 br, di; paired 256 | NMB | AB |
| Shisr 023 | 1/8/02 | 18° 33.172 | 53° 59.246 | 841 | 1 | L5 | S4 | W3 | 23.9 | 20.4 | 1.5 | NHB | AA |
| Shisr 024 | 1/8/02 | 18° 33.284 | 53° 59.812 | 900.837 | 2 | L5 | S4 | W3 | 24.6 | 20.2 | 1.7 | NHB | AA |
| Shisr 025 | 1/8/02 | 18° 6.444 | 53° 49.914 | 7293.476 | 8 | L6 | S3 | W2 | 25.0 | 21.3 | 1.5 | NHB | AA |
| Shisr 026 | 1/8/02 | 18° 7.382 | 53° 45.287 | 396.555 | 1 | H4 | S2 | W3 | 18.5 | 15.8 | 1.3 | NHB | AA |
| Shisr 027 | 1/9/02 | 18° 8.478 | 53° 54.723 | 61.385 | 1 | H6 | S1 | W4 | 18.4 | 16.5 | 1.5 | NHB | AA |
| Shisr 028 | 1/8/02 | 18° 8.566 | 53° 48.452 | 818.106 | 10 | LL6 | S3 | W4 | 27.6 | 23.2 | 1.3 | NHB | AA |
| Shisr 029 | 1/9/02 | 18° 9.006 | 53° 48.028 | 204.706 | 1 | H5 | S1 | W2 | 18.9 | 17.5 | 1.2 | NHB | AA |
| Shisr 030 | 1/9/02 | 18° 9.216 | 53° 46.492 | 176.279 | 1 | H5 | S1-S2 | W2 | 19.2 | 16.8 | 1.3 | NHB | AA |
| Shisr 031 | 01/01/2003 | 18° 12.801 | 53° 50.805 | 503.757 | 2 | L6 | S3 | W4 | 26.4 | 22.2 | 1.6 | NHB | AH |
| Shisr 032 | 08/25/2003 | 18° 2.46 | 53° 41.56 | 69.516 | 1 | H5 | S2 | W1 | 18.7 | 17.2 | 1.3 | NHB | AC |
| Shisr 033 | 25/10/2002 | 18° 20.835 | 53° 44.862 | 1097.722 | 65 | CR3.0 | S2 | W2-3 | 2.0-7.9 | 1.2-12.1 | 0.4-3.5 | NHB | AB |
| Shisr 034 | 07/01/2003 | 18° 25.237 | 54° 3.035 | 73.652 | 1 | H4 | S3 | W2-3 | 19.3 | 15.8 | 1.2 | NHB | AH |
| Shisr 035 | 07/01/2003 | 18° 25.774 | 54° 2.476 | 355.055 | 1 | L6 | S5 | W4 | 25.6 | 22.3 | 1.6 | NHB | AH |
| Shisr 036 | 26/10/2002 | 18° 30.453 | 53° 59.595 | 10175.000 | 56 | H3.8/3.9 | S2 | W2-3 | 10.5-23.8 | 3.0-19.6 | 0.2-4.6 | NHB | AB |

| | | | | | | | | | | | | | |
|---|---|---|---|---|---|---|---|---|---|---|---|---|---|
| Shisr 037 | 26/10/2002 | 18° 32.521 | 53° 56.248 | 1508.600 | 1 | L5 | S2 | W4 | 25.2 | 20.9 | 1.6 | NHB | AB |
| Shisr 038 | 26/10/2002 | 18° 32.753 | 53° 56.027 | 379.853 | 1 | L5 | S2 | W4 | 25.0 | 22.7 | 1.5 | NHB | AB |
| Shisr 039 | 25/10/2002 | 18° 32.834 | 53° 57.422 | 2123.195 | 3 | L4-5 | S3 | W3 | 25.0 | 20.9 | 1.6 | NHB | AB |
| Shisr 040 | 25/10/2002 | 18° 32.866 | 53° 57.007 | 121.414 | 1 | L4-5 | S1 | W4 | 24.9 | 20.9 | 1.6 | NHB | AB |
| Shisr 041 | 25/10/2002 | 18° 33.169 | 53° 56.130 | 1400.200 | 1 | L5 | S3 | W2 | 24.5 | 20.5 | 1.7 | NHB | AB |
| Shisr 042 | 01/21/2003 | 18° 34.471 | 53° 48.966 | 393.857 | 11 | L6 | S2 | W4 | 24.5 | 22.7 | 1.5 | NHB | AI |
| Shisr 043 | 01/21/2003 | 18° 35.546 | 53° 48.748 | 8407.000 | 1 | IIIAB | | | | | | NHB | AI |
| Shisr 044 | 01/01/2003 | 18° 9.19 | 53° 50.517 | 88.478 | 2 | H4 | S2 | W4 | 20.2 | 17.0 | 1.6 | NHB | AH |
| Sisr 022 | 1/9/02 | 18° 10.032 | 53° 50.733 | 255.251 | 1 | L5 | S3 | W4 | 24.9 | 20.7 | 1.7 | NHB | AA |
| UaH 001 | 03/01/2003 | 18° 26.659 | 52° 58.683 | 2335.639 | 7 | LL5 | S2 | W2 | 29.2 | 23.7 | 1.4 | NHB | AH |
| UaH 002 | 1996 | 18° 30 | 52° 10 | 3700 | 1 | H3.8/3.9 | S1,2 | W1 | 14.2-20.3 | 11.9-21.2 | 0.4-1.7 | NHB (96.2 g) | AK |

NMB: All specimen at NMB
AA: Finder and classification: E. Gnos, B. Hofmann and A. Al-Kathiri; analyst E. Gnos and A. Al-Kathiri
AB: Finder: M. Hauser and L. Moser; classification: E. Gnos, B. Hofmann and A. Al-Kathiri; analyst E. Gnos and A. Al-Kathiri
AC: Finder: A. Al-Kathiri; classification: E. Gnos, B. Hofmann and A. Al-Kathiri; analyst E. Gnos and A. Al-Kathiri
AD: Finder: A. Al-Kathiri, E.Gnos, O. Eugster, S. Lorenzetti; classification: E. Gnos, B. Hofmann and A. Al-Kathiri; analyst E. Gnos and A. Al-Kathiri
AE: Finder: A. Al-Kathiri, E.Gnos, O. Eugster, S. Lorenzetti, M. Al-Batashi, S. Al-Busaidi, A. Al-Radshi; classification: E. Gnos, B. Hofmann and A. Al-Kathiri; analyst E. Gnos and A. Al-Kathiri
AF: Anonymous finder; classification: E. Gnos, B. Hofmann and A. Al-Kathiri; analysts E. Gnos and A. Al-Kathiri; main mass, with finder
AG: Finder and classification: E. Gnos, B. Hofmann, A. Al-Kathiri, M. Eggimann and S. Lorenzetti; analyst E. Gnos and A. Al-Kathiri
AH: Finder A. Al-Kathiri, M. Eggimann; classification: E. Gnos, B. Hofmann, A. Al-Kathiri; analyst E. Gnos and A. Al-Kathiri
AI: Finder A. Al-Kathiri, B. Hofmann, M. Eggimann, U. Krähenbühl; classification: E. Gnos, B. Hofmann, A. Al-Kathiri; analyst E. Gnos and A. Al-Kathiri
AK: Finder and classification: E. Gnos, B. Hofmann and A. Al-Kathiri; analyst E. Gnos and A. Al-Kathiri
DG: Weathering grade
Dho: Dhofar
JaH: Jiddat al Harasis
RaFa: Ramlat Fasad
SaU: Sayh al Uhaymir
AH: Al Huqf
br = breccia
IMB: Impact melt breccia
cpx = calcic clinopyroxene
di = diopside
aug = augite

Appendix 2. Chemical analysis of ordinary chondrites using combination of INAA, ICP-MS and ICP-OES methods.

| Elements | Li | Na | Mg | Al | P | S | K | Ca | Sc | Ti | V | Cr | Mn | Fe | Co | Ni | Cu | Zn | Ga | As | Se | Rb | Sr | Y | Zr | Nb | Cs | Ba | La | Ce | Pr | Nd | Sm | Eu | Gd | Dy | Er | Yb | Hf | Ir | Tl | Pb | Au | U | H2O |
|---|---|---|---|---|---|---|---|---|---|---|---|---|---|---|---|---|---|---|---|---|---|---|---|---|---|---|---|---|---|---|---|---|---|---|---|---|---|---|---|---|---|---|---|---|---|
| Methods | 2 | 1 | 3 | 3 | 3 | 3 | 3 | 3 | 1 | 3 | 2 | 1 | 3 | 1 | 1 | 1 | 2 | 3 | 2 | 1 | 2 | 2 | 2 | 2 | 2 | 2 | 2 | 3 | 2 | 2 | 2 | 2 | 2 | 2 | 2 | 2 | 2 | 2 | 1 | 2 | 2 | 1 | 2 | | |
| Units | ppm | % | % | % | % | % | % | % | ppm | % | ppm | ppm | ppm | % | ppm | ppm | ppm | ppm | ppm | ppm | ppm | ppm | ppm | ppm | ppm | ppm | ppm | ppm | ppm | ppm | ppm | ppm | ppm | ppm | ppm | ppm | ppm | ppm | ppm | ppb | ppm | ppm | ppb | ppm | % |
| Mean H chondrites | 1.7 | 0.6 | 14.20 | 1.01 | 0.097 | 2.000 | 0.08 | 1.20 | 8.0 | 0.06 | 61 | 3400 | 2260 | 28 | 834 | 16850 | 90 | 50* | 5.2 | 2.0 | 7.0 | 3.0 | 9.5 | 2.2 | 9.5 | 1.1 | 0.01* | 3.5 | 0.3 | 0.8 | 0.1 | 0.6 | 0.2 | 0.1 | 0.3 | 0.3 | 0.2 | 0.2 | 0.3 | 790* | 0.001 | 0.2 | 230 | 0.01 | | |
| Aybut 001 | 1.3 | 0.6 | 11.23 | 1.13 | 0.076 | 1.093 | 0.07 | 1.17 | 8.0 | 0.06 | 55 | 3870 | 1985 | 30 | 808 | 14600 | 92.6 | 73 | 5.3 | 4.8 | 7.9 | 2.0 | 20.2 | 1.5 | 6 | 0.5 | 0.07 | 5 | 0.4 | 0.9 | 0.1 | 0.6 | 0.2 | 0.07 | 0.3 | 0.3 | 0.2 | 0.2 | 0.2 | 570 | <0.05 | <0.5 | 247 | <0.1 | 1.78 |
| UaH 002 | 1.3 | 0.7 | 11.00 | 0.80 | 0.079 | 1.508 | 0.08 | 1.23 | 8.2 | 0.07 | 55 | 3860 | 2070 | 29 | 846 | 15600 | 91.0 | 78 | 5.4 | 3.8 | 7.3 | 2.1 | 61.4 | 1.5 | 6 | 0.4 | <0.05 | 8 | 0.4 | 0.9 | 0.1 | 0.7 | 0.2 | 0.08 | 0.3 | 0.3 | 0.2 | 0.2 | 0.2 | 530 | <0.05 | <0.5 | 275 | <0.1 | 2.04 |
| SaU 228 | 2.0 | 0.7 | 12.55 | 0.82 | 0.096 | 1.216 | 0.09 | 1.15 | 8.3 | 0.05 | 58 | 3210 | 1987 | 25 | 800 | 15000 | 83.1 | 83 | 5.4 | <0.5 | 7.8 | 3.3 | 13.3 | <0.1 | 6 | 0.5 | 0.06 | 6 | 0.7 | 1.5 | 0.2 | 1.0 | 0.3 | 0.09 | 0.4 | 0.4 | 0.2 | 0.2 | 0.1 | 560 | <0.05 | <0.5 | 213 | <0.1 | 0.72 |
| Dho 787 | 2.0 | 0.9 | 11.06 | 0.91 | 0.078 | 0.393 | 0.09 | 1.66 | 10 | 0.07 | 62 | 4930 | 2261 | 26 | 452 | 7520 | 83.1 | 71 | 5.1 | 2.8 | 7.3 | 2.5 | 173 | 1.6 | 6 | 0.5 | <0.05 | 35 | 0.4 | 0.9 | 0.1 | 0.7 | 0.2 | 0.08 | 0.3 | 0.4 | 0.2 | 0.2 | 0.2 | 410 | <0.05 | <0.5 | 174 | <0.1 | 2.22 |
| Dho 1005 | 1.7 | 0.70 | 10.34 | 0.85 | 0.081 | 0.570 | 0.10 | 1.39 | 8.7 | 0.07 | 63 | 4190 | 2047 | 26 | 590 | 12000 | 92.7 | 89 | 5.6 | 2.1 | 7.3 | 2.5 | 216 | 1.5 | 7 | 0.5 | 0.06 | 53 | 0.6 | 1.2 | 0.2 | 0.8 | 0.2 | 0.09 | 0.3 | 0.4 | 0.2 | 0.2 | 0.2 | 570 | <0.05 | <0.5 | 251 | 0.1 | 2.44 |
| Dho 020 | 2.5 | 0.7 | 10.18 | 0.86 | 0.082 | 0.401 | 0.10 | 1.43 | 9.4 | 0.07 | 61 | 4270 | 2032 | 26 | 608 | 11900 | 83.9 | 73 | 5.2 | 1.8 | 5.6 | 1.9 | 291 | 1.5 | 7 | 0.5 | 0.06 | 72 | 0.5 | 1.1 | 0.2 | 0.7 | 0.2 | 0.08 | 0.3 | 0.4 | 0.3 | 0.2 | 0.2 | 560 | <0.05 | <0.5 | 215 | 0.2 | 2.60 |
| Shalim 003 | 1.1 | 0.6 | 10.98 | 0.82 | 0.077 | 1.558 | 0.06 | 1.23 | 7.6 | 0.07 | 51 | 3500 | 2066 | 24 | 780 | 14500 | 84.9 | 76 | 4.9 | 2.8 | 7.2 | 1.8 | 19.4 | 1.5 | 6 | 0.4 | <0.05 | 5 | 0.4 | 0.8 | 0.1 | 0.6 | 0.2 | 0.07 | 0.3 | 0.3 | 0.2 | 0.2 | 0.1 | 460 | <0.05 | <0.5 | 231 | <0.1 | 2.01 |
| Dho 814 | 1.5 | 0.6 | 10.66 | 0.79 | 0.078 | 1.496 | 0.07 | 1.64 | 8.0 | 0.06 | 51 | 3800 | 1943 | 29 | 849 | 16600 | 98.4 | 66 | 3.9 | 2.7 | 8.0 | 1.3 | 80.2 | 1.4 | 6 | 0.4 | <0.05 | 11 | 0.4 | 0.9 | 0.1 | 0.6 | 0.2 | 0.07 | 0.3 | 0.3 | 0.2 | 0.2 | 0.1 | 580 | <0.05 | <0.5 | 241 | <0.1 | 1.80 |
| Dho 1010 | 1.6 | 0.6 | 11.93 | 0.71 | 0.093 | 1.350 | 0.08 | 1.61 | 7.4 | 0.05 | 57 | 3220 | 1932 | 24 | 745 | 16000 | 83.6 | 66 | 4.9 | <0.5 | 6.8 | 1.5 | 41.6 | <0.1 | 5 | 0.4 | <0.05 | 4 | 0.3 | 0.8 | 0.1 | 0.6 | 0.2 | 0.08 | 0.3 | 0.3 | 0.2 | 0.2 | 0.1 | 590 | <0.05 | <0.5 | 207 | <0.1 | 2.12 |
| SaU 219 | 3.9 | 0.5 | 12.09 | 0.76 | 0.106 | 1.425 | 0.08 | 1.35 | 7.2 | 0.05 | 57 | 3080 | 1976 | 23 | 728 | 14800 | 82.5 | 84 | 5.1 | 1.3 | 7.2 | 1.7 | 108 | <0.1 | 6 | 0.5 | <0.05 | 6 | 0.4 | 1.0 | 0.1 | 0.7 | 0.2 | 0.07 | 0.3 | 0.3 | 0.2 | 0.2 | 0.1 | 540 | <0.05 | <0.5 | 179 | <0.1 | 2.12 |
| Dho 794 | 1.1 | 0.8 | 10.20 | 0.79 | 0.079 | 1.365 | 0.08 | 1.21 | 8.5 | 0.06 | 55 | 4230 | 1993 | 26 | 780 | 14000 | 87.6 | 81 | 5.2 | 3.7 | 7.8 | 2.4 | 81.9 | 1.4 | 7 | 0.4 | <0.05 | 12 | 0.4 | 0.8 | 0.1 | 0.6 | 0.2 | 0.07 | 0.3 | 0.3 | 0.2 | 0.2 | 0.2 | 540 | <0.05 | <0.5 | 276 | <0.1 | 2.08 |
| Dho 819 | 1.8 | 0.6 | 10.01 | 0.79 | 0.074 | 1.504 | 0.08 | 1.52 | 8.4 | 0.07 | 53 | 3760 | 1913 | 26 | 744 | 14300 | 88.4 | 87 | 5.1 | 1.8 | 7.6 | 2.5 | 108 | 1.5 | 7 | 0.5 | 0.10 | 26 | 0.5 | 1.2 | 0.2 | 0.8 | 0.2 | 0.08 | 0.3 | 0.4 | 0.2 | 0.2 | 0.2 | 510 | <0.05 | <0.5 | 236 | <0.1 | 2.66 |
| Dho 802 | 2.3 | 0.7 | 10.74 | 0.80 | 0.079 | 1.288 | 0.09 | 1.43 | 8.3 | 0.07 | 56 | 4100 | 2050 | 26 | 702 | 13900 | 87.7 | 76 | 5.3 | 2.2 | 7.5 | 2.6 | 133 | 1.4 | 6 | 0.4 | 0.05 | 18 | 0.4 | 0.9 | 0.1 | 0.6 | 0.2 | 0.07 | 0.3 | 0.4 | 0.2 | 0.2 | 0.2 | 560 | <0.05 | <0.5 | 241 | <0.1 | 2.41 |
| Dho 835 | 2.1 | 0.6 | 9.80 | 0.79 | 0.074 | 0.702 | 0.08 | 2.06 | 8.3 | 0.06 | 52 | 3740 | 1847 | 27.0 | 662 | 12300 | 80.6 | 59 | 3.9 | 3.4 | 6.3 | 2.3 | 895 | 1.5 | 6 | 0.5 | <0.05 | 122 | 0.5 | 1.1 | 0.2 | 0.7 | 0.2 | 0.08 | 0.3 | 0.3 | 0.2 | 0.2 | 0.2 | 530 | 0.10 | 1.7 | 213 | 0.2 | 2.35 |
| SaU 259 | 2.8 | 0.7 | 12.17 | 0.81 | 0.088 | 0.312 | 0.12 | 1.44 | 8.0 | 0.06 | 59 | 3270 | 2068 | 22 | 533 | 10800 | 76.0 | 62 | 4.8 | 1.3 | 5.6 | 1.8 | 208 | <0.1 | 6 | 0.4 | <0.05 | 26 | 0.3 | 0.8 | 0.1 | 0.6 | 0.2 | 0.07 | 0.3 | 0.3 | 0.2 | 0.2 | 0.1 | 530 | <0.05 | <0.5 | 158 | <0.1 | 2.78 |
| JaH 069 | 2.1 | 0.8 | 9.76 | 0.85 | 0.077 | 0.403 | 0.10 | 1.48 | 9.4 | 0.07 | 56 | 4410 | 1974 | 30 | 750 | 13200 | 89.9 | 75 | 4.7 | 4.6 | 6.5 | 2.6 | 594 | 1.5 | 6 | 0.5 | 0.11 | 150 | 0.6 | 1.3 | 0.2 | 0.8 | 0.2 | 0.08 | 0.3 | 0.3 | 0.2 | 0.2 | 0.2 | 630 | 0.10 | 2.4 | 182 | 0.3 | 2.6 |
| Shisr 020 | 2.2 | 0.7 | 9.08 | 0.79 | 0.076 | 0.533 | 0.08 | 1.47 | 9.1 | 0.07 | 57 | 4160 | 1874 | 30 | 733 | 13200 | 79.8 | 79 | 3.4 | 3.9 | 6.3 | 1.8 | 938 | 1.5 | 7 | 0.4 | 0.06 | 265 | 0.4 | 1.0 | 0.2 | 0.6 | 0.2 | 0.07 | 0.3 | 0.3 | 0.2 | 0.2 | 0.1 | 620 | 0.11 | 2.3 | 180 | 0.2 | 2.83 |
| JaH 102 | 2.1 | 0.7 | 9.98 | 0.72 | 0.093 | 0.565 | 0.08 | 1.47 | 8.1 | 0.07 | 59 | 3670 | 2087 | 25 | 740 | 14500 | 83.3 | 69 | 4.7 | 1.9 | 5.5 | 2.1 | 399 | 1.7 | 7 | 0.5 | <0.05 | 95 | 0.7 | 1.5 | 0.2 | 0.9 | 0.3 | 0.08 | 0.3 | 0.4 | 0.3 | 0.2 | 0.2 | 550 | <0.05 | 1.6 | 267 | 0.3 | 3.37 |
| SaU 163 | 4.0 | 0.7 | 10.27 | 0.92 | 0.080 | 0.637 | 0.09 | 1.63 | 9.4 | 0.07 | 63 | 4290 | 1983 | 29 | 745 | 14100 | 95.7 | 69 | 5.4 | 0.5 | 6.4 | 1.8 | 228 | 1.5 | 8 | 0.7 | <0.05 | 101 | 0.5 | 1.0 | 0.1 | 0.7 | 0.2 | 0.07 | 0.3 | 0.4 | 0.2 | 0.3 | 0.3 | 670 | 0.09 | <0.5 | 230 | 0.1 | 3.32 |
| Dho 807 | 1.0 | 0.70 | 11.65 | 1.12 | 0.084 | 0.817 | 0.07 | 1.27 | 8.4 | 0.07 | 55 | 4200 | 2085 | 30 | 883 | 17600 | 95.4 | 125 | 5.1 | 1.4 | 8.0 | 2.8 | 28.5 | 1.5 | 5 | 0.5 | 0.20 | 6 | 0.6 | 1.2 | 0.2 | 0.8 | 0.2 | 0.08 | 0.3 | 0.4 | 0.2 | 0.2 | 0.1 | 590 | <0.05 | 1.4 | 285 | 0.1 | 1.03 |
| Mean L chondrites | 1.8 | 0.7 | 15.19 | 1.10 | 0.110 | 2.170 | 0.09 | 1.28 | 8.9 | 0.07 | 65 | 3800 | 2460 | 22 | 550 | 11530 | 86 | 50* | 5.2 | 1.5 | 8.9 | 2.8 | 10.8 | 2.1 | 8.9 | 0.4 | 0.01* | 4 | 0.3 | 0.8 | 0.1 | 0.6 | 0.2 | 0.1 | 0.3 | 0.3 | 0.2 | 0.2 | 0.2 | 565* | 0.004 | 0.3 | 160 | 0.01 | | |
| Ghubara (rim) | 1.4 | 0.8 | 12.30 | 0.90 | 0.075 | 0.455 | 0.09 | 1.27 | 8.4 | 0.07 | 60 | 3790 | 2324 | 22 | 580 | 12000 | 94.8 | 89 | 5.3 | <0.5 | 9.1 | 3.6 | 11.0 | 2.4 | 7 | 0.5 | 0.27 | 4 | 0.4 | 0.9 | 0.1 | 0.7 | 0.2 | 0.08 | 0.3 | 0.4 | 0.3 | 0.2 | 0.2 | 350 | <0.05 | <0.5 | 247 | <0.1 | | |
| Ghubara (inner) | 1.0 | 0.7 | 12.25 | 1.03 | 0.072 | 0.736 | 0.09 | 1.25 | 10 | 0.07 | 56 | 4060 | 2264 | 28 | 617 | 12200 | 92.2 | 79 | 4.9 | <0.5 | 9.2 | 3.4 | 10.2 | 1.9 | 6 | 0.5 | 0.25 | 4 | 0.4 | 0.9 | 0.1 | 0.7 | 0.2 | 0.08 | 0.3 | 0.4 | 0.2 | 0.2 | 0.2 | 380 | <0.05 | <0.5 | 159 | <0.1 | 0.2 |
| AH 011 | 2.6 | 0.8 | 11.06 | 0.82 | 0.067 | 1.557 | 0.08 | 1.25 | 9.0 | 0.07 | 55 | 4000 | 2151 | 23.0 | 571 | 10800 | 78.3 | 64 | 4.5 | <0.5 | 8.1 | 2.3 | 24.9 | 1.8 | 6 | 0.5 | <0.05 | 7 | 0.4 | 1.0 | 0.1 | 0.8 | 0.2 | 0.08 | 0.3 | 0.4 | 0.3 | 0.3 | 0.2 | 390 | <0.05 | <0.5 | 180 | <0.1 | 2.32 |
| AH 010 | 3.0 | 0.7 | 11.42 | 0.88 | 0.066 | 1.241 | 0.08 | 1.45 | 8.9 | 0.07 | 53 | 3930 | 2216 | 22 | 527 | 9610 | 79.2 | 95 | 4.6 | 2.5 | 7.5 | 2.4 | 103 | 1.7 | 6 | 0.4 | <0.05 | 11 | 0.4 | 1.0 | 0.2 | 0.8 | 0.2 | 0.08 | 0.3 | 0.4 | 0.2 | 0.2 | 0.2 | 340 | <0.05 | <0.5 | 143 | <0.1 | 1.97 |
| SaU 001 | 1.4 | 0.8 | 11.57 | 0.85 | 0.073 | 1.670 | 0.08 | 1.27 | 9.4 | 0.07 | 58 | 4460 | 2213 | 25 | 584 | 12100 | 87.6 | 85 | 5.2 | <0.5 | 8.4 | 2.4 | 25.2 | 1.6 | 6 | 0.4 | 0.25 | 5 | 0.4 | 1.0 | 0.1 | 0.7 | 0.2 | 0.08 | 0.3 | 0.4 | 0.2 | 0.2 | 0.2 | 450 | <0.05 | <0.5 | 200 | <0.1 | 1.5 |
| Dho 1012 | 1.6 | 0.7 | 13.83 | 0.80 | 0.085 | 0.471 | 0.09 | 1.44 | 8.3 | 0.06 | 60 | 3300 | 2300 | 23 | 775 | 15100 | 81.2 | 81 | 5.0 | <0.5 | 7.4 | 2.0 | 33.7 | <0.1 | 6 | 0.4 | <0.05 | 5 | 0.3 | 0.8 | 0.1 | 0.6 | 0.2 | 0.08 | 0.3 | 0.3 | 0.2 | 0.2 | 0.2 | 420 | <0.05 | 1.0 | 181 | <0.1 | 0.46 |
| Shisr 025 | 1.4 | 0.7 | 11.60 | 1.01 | 0.072 | 0.961 | 0.08 | 1.23 | 8.8 | 0.07 | 60 | 3870 | 2261 | 22 | 528 | 10300 | 78.9 | 84 | 3.9 | 2.5 | 7.3 | 2.4 | 50.5 | 1.7 | 6 | 0.5 | <0.05 | 115 | 0.4 | 1.0 | 0.2 | 0.7 | 0.2 | 0.07 | 0.3 | 0.4 | 0.3 | 0.2 | 0.2 | 350 | <0.05 | <0.5 | 183 | <0.1 | 2.56 |
| Zawliah | 3.0 | 0.7 | 11.98 | 0.74 | 0.074 | 1.664 | 0.08 | 1.19 | 9.0 | 0.06 | 56 | 3510 | 2018 | 22 | 560 | 12700 | 83.4 | 69 | 4.8 | <0.5 | 9.1 | 2.4 | 33.3 | 0.3 | 6 | 0.4 | <0.05 | 14 | 0.4 | 0.9 | 0.1 | 0.8 | 0.2 | 0.08 | 0.3 | 0.4 | 0.2 | 0.2 | 0.2 | 450 | <0.05 | <0.5 | 142 | <0.1 | 1.37 |
| Zawliah | 1.4 | 0.7 | 12.83 | 0.74 | 0.090 | 1.167 | 0.08 | 1.17 | 8.0 | 0.05 | 55 | 3500 | 2154 | 21 | 548 | 12400 | 76.3 | 66 | 4.6 | <0.5 | 7.5 | 1.6 | 16.9 | <0.1 | 5 | 0.4 | <0.05 | 4 | 0.3 | 0.9 | 0.1 | 0.6 | 0.2 | 0.08 | 0.3 | 0.3 | 0.2 | 0.2 | 0.1 | 410 | <0.05 | <0.5 | 158 | <0.1 | 1.42 |
| JaH 073-1 | 2.7 | 0.7 | 12.35 | 1.08 | 0.071 | 1.735 | 0.08 | 1.34 | 9.9 | 0.07 | 64 | 4190 | 2358 | 23 | 490 | 10800 | 84.0 | 81 | 4.5 | 2.6 | 8.6 | 2.2 | 92.7 | 1.7 | 7 | 0.5 | <0.05 | 89 | 0.4 | 1.0 | 0.1 | 0.7 | 0.2 | 0.08 | 0.3 | 0.4 | 0.3 | 0.2 | 0.2 | 420 | <0.05 | <0.5 | 180 | <0.1 | 2.26 |
| JaH 073-2 | 2.1 | 0.8 | 11.24 | 0.85 | 0.064 | 1.558 | 0.08 | 1.39 | 9.1 | 0.07 | 55 | 4070 | 2245 | 23 | 563 | 11300 | 82.9 | 73 | 4.5 | 2 | 8.7 | 2.4 | 95.0 | 1.6 | 6 | 0.4 | <0.05 | 40 | 0.4 | 0.9 | 0.1 | 0.6 | 0.2 | 0.08 | 0.3 | 0.4 | 0.2 | 0.2 | 0.2 | 400 | 0.07 | <0.5 | 212 | <0.1 | 2.26 |
| JaH 073-3 | 4.2 | 0.7 | 11.46 | 0.87 | 0.070 | 1.650 | 0.08 | 1.34 | 8.7 | 0.07 | 56 | 3880 | 2279 | 22 | 488 | 10500 | 81.3 | 71 | 4.7 | 1.4 | 8.3 | 2.1 | 67.2 | 1.5 | 6 | 0.4 | <0.05 | 18 | 0.4 | 0.9 | 0.1 | 0.6 | 0.2 | 0.08 | 0.3 | 0.3 | 0.2 | 0.2 | 0.2 | 420 | 0.06 | <0.5 | 179 | <0.1 | 2.52 |
| JaH 073-4 | 2.6 | 0.7 | 10.62 | 0.85 | 0.070 | 0.424 | 0.09 | 1.69 | 8.6 | 0.07 | 58 | 3960 | 2113 | 20 | 332 | 7230 | 73.7 | 58 | 4.3 | 2.5 | 7.5 | 2.4 | 179 | 1.6 | 6 | 0.5 | <0.05 | 41 | 0.4 | 0.9 | 0.1 | 0.7 | 0.2 | 0.08 | 0.3 | 0.4 | 0.2 | 0.2 | 0.2 | 390 | <0.05 | <0.5 | 115 | 0.1 | 1.77 |
| JaH 073-5 | 4.4 | 0.7 | 10.83 | 0.83 | 0.071 | 1.768 | 0.08 | 1.27 | 8.9 | 0.08 | 59 | 4060 | 2142 | 22 | 413 | 9680 | 87.6 | 85 | 4.6 | <0.5 | 9.8 | 2.4 | 114 | 1.8 | 8 | 1.2 | <0.05 | 27 | 0.4 | 1.0 | 0.2 | 0.7 | 0.2 | 0.08 | 0.3 | 0.4 | 0.3 | 0.3 | 0.2 | 360 | 0.05 | <0.5 | 152 | <0.1 | 2.67 |
| JaH 091 | 1.1 | 0.7 | 11.79 | 0.81 | 0.087 | 0.814 | 0.08 | 1.10 | 8.6 | 0.05 | 58 | 3360 | 1982 | 20 | 550 | 11900 | 75.3 | 75 | 4.9 | <0.5 | 7.1 | 1.9 | 13.5 | <0.1 | 6 | 0.4 | <0.05 | 3 | 0.3 | 0.8 | 0.1 | 0.6 | 0.2 | 0.08 | 0.3 | 0.3 | 0.2 | 0.2 | 0.1 | 400 | <0.05 | 0.6 | 161 | <0.1 | 2.29 |
| SaU 235 | 1.9 | 0.7 | 13.58 | 0.85 | 0.089 | 0.411 | 0.10 | 1.84 | 8.7 | 0.06 | 62 | 3250 | 2365 | 18 | 409 | 7950 | 58.7 | 77 | 4.6 | <0.5 | 4.3 | 1.8 | 33.6 | <0.1 | 6 | 0.5 | <0.05 | 4 | 0.3 | 0.8 | 0.1 | 0.6 | 0.2 | 0.07 | 0.3 | 0.3 | 0.2 | 0.2 | 0.1 | 340 | <0.05 | <0.5 | 125 | <0.1 | 2.15 |
| Zawliah | 2.8 | 0.7 | 11.62 | 0.83 | 0.106 | 0.524 | 0.14 | 1.45 | 7.9 | 0.06 | 61 | 3420 | 2028 | 22 | 465 | 9400 | 81.8 | 69 | 5.2 | <0.5 | 8.2 | 2.4 | 129 | <0.1 | 6 | 0.4 | <0.05 | 13 | 0.5 | 1.0 | 0.2 | 0.8 | 0.3 | 0.08 | 0.4 | 0.4 | 0.3 | 0.2 | 0.1 | 400 | <0.05 | <0.5 | 157 | <0.1 | 2.73 |
| Dho 805 | 2.2 | 0.8 | 11.34 | 0.89 | 0.080 | 0.547 | 0.11 | 1.41 | 10 | 0.07 | 62 | 4490 | 2280 | 25 | 541 | 9740 | 87.8 | 91 | 5.3 | 1.5 | 8.3 | 2.6 | 87.0 | 1.6 | 6 | 0.5 | <0.05 | 16 | 0.4 | 1.0 | 0.1 | 0.7 | 0.2 | 0.08 | 0.3 | 0.4 | 0.3 | 0.2 | 0.2 | 400 | <0.05 | <0.5 | 188 | <0.1 | 2.25 |
| SaU 165 | 1.2 | 0.8 | 10.50 | 0.97 | 0.077 | 0.232 | 0.11 | 1.37 | 10 | 0.08 | 65 | 4780 | 2224 | 27 | 571 | 10700 | 90.2 | 97 | 5.5 | 3.3 | 7.5 | 2.5 | 209 | 1.6 | 6 | 0.5 | <0.05 | 45 | 0.5 | 1.1 | 0.2 | 0.7 | 0.2 | 0.09 | 0.3 | 0.4 | 0.3 | 0.2 | 0.2 | 400 | <0.05 | <0.5 | 165 | <0.1 | 2.47 |
| SaU 194 | 13.8 | 0.6 | 10.65 | 1.05 | 0.080 | 0.824 | 0.10 | 1.37 | 8.0 | 0.07 | 56 | 3630 | 2001 | 24.0 | 644 | 13600 | 84.8 | 87 | 4.7 | 2.8 | 6.8 | 1.7 | 181 | 1.4 | 6 | 0.4 | 0.07 | 73 | 0.4 | 0.9 | 0.1 | 0.6 | 0.2 | 0.07 | 0.3 | 0.3 | 0.2 | 0.2 | 0.1 | 500 | <0.05 | <0.5 | 227 | 0.1 | 2.56 |
| Shisr 015 | 1.5 | 0.7 | 11.23 | 0.94 | 0.079 | 0.367 | 0.09 | 1.39 | 9.2 | 0.07 | 59 | 4060 | 2309 | 23 | 505 | 9760 | 77.5 | 217 | 5.5 | 1.3 | 7.1 | 3.2 | 133 | 1.7 | 8 | 0.4 | 0.25 | 12 | 0.5 | 1.1 | 0.2 | 0.8 | 0.2 | 0.08 | 0.3 | 0.4 | 0.3 | 0.3 | 0.2 | 460 | <0.05 | <0.5 | 165 | <0.1 | 2.51 |
| Zawliah | 1.5 | 0.8 | 10.99 | 0.77 | 0.090 | 0.340 | 0.11 | 1.39 | 8.9 | 0.06 | 56 | 3730 | 1992 | 21.0 | 352 | 7020 | 68.0 | 63 | 4.4 | <0.5 | 6.4 | 2.0 | 177 | <0.1 | 5 | 0.4 | <0.05 | 13 | 0.4 | 1.0 | 0.1 | 0.7 | 0.2 | 0.07 | 0.3 | 0.4 | 0.2 | 0.2 | 0.1 | 430 | <0.05 | <0.5 | 105 | <0.1 | 2.17 |
| Dho 806 | 2.1 | 0.8 | 11.31 | 0.79 | 0.082 | 0.401 | 0.11 | 1.57 | 11 | 0.07 | 62 | 4680 | 2327 | 26 | 559 | 10800 | 80.9 | 120 | 5.8 | 3.9 | 7.0 | 2.7 | 314 | 1.6 | 6 | 0.4 | 0.09 | 39 | 0.4 | 1.0 | 0.1 | 0.7 | 0.2 | 0.08 | 0.3 | 0.4 | 0.2 | 0.2 | 0.1 | 480 | <0.05 | <0.5 | 137 | 0.1 | 2.17 |
| Dho 005-1 | 3.4 | 0.8 | 11.43 | 1.01 | 0.082 | 0.364 | 0.12 | 1.79 | 9.8 | 0.08 | 60 | 4380 | 2334 | 24 | 380 | 6720 | 65.7 | 117 | 4.5 | 3.0 | 6.7 | 3.2 | 473 | 1.7 | 6 | 0.5 | <0.05 | 66 | 0.6 | 1.3 | 0.2 | 0.8 | 0.3 | 0.09 | 0.3 | 0.4 | 0.3 | 0.3 | 0.2 | 370 | 0.05 | 0.6 | 83 | 0.3 | 1.88 |
| Dho 005-2 | 0.7 | 0.7 | 12.65 | 0.98 | 0.075 | 0.243 | 0.11 | 1.59 | 10 | 0.07 | 63 | 4420 | 2243 | 25 | 392 | 6820 | 84.0 | 66 | 5.2 | 3.2 | 7.5 | 3.1 | 99.8 | 1.6 | 6 | 0.5 | <0.05 | 28 | 0.5 | 1.0 | 0.2 | 0.7 | 0.2 | 0.08 | 0.3 | 0.4 | 0.3 | 0.2 | 0.2 | 420 | <0.05 | <0.5 | 128 | <0.1 | 2.19 |
| Dho 005-3 | 3.1 | 0.7 | 11.01 | 0.90 | 0.078 | 0.368 | 0.11 | 1.63 | 9.2 | 0.07 | 59 | 4080 | 2236 | 24 | 393 | 7210 | 84.4 | 101 | 4.7 | 1.3 | 7.5 | 3.0 | 175 | 1.7 | 7 | 0.5 | <0.05 | 29 | 0.5 | 1.1 | 0.2 | 0.8 | 0.2 | 0.08 | 0.3 | 0.4 | 0.3 | 0.3 | 0.2 | 410 | <0.05 | <0.5 | 127 | 0.1 | 2 |
| Dho 813 | 2.4 | 0.70 | 11.60 | 1.17 | 0.069 | 0.831 | 0.11 | 1.62 | 9.0 | 0.07 | 62 | 4180 | 2295 | 24 | 601 | 10000 | 81.2 | 93 | 5.2 | 1.9 | 7.4 | 2.7 | 1140 | 1.6 | 6 | 0.5 | 0.11 | 150 | 0.5 | 1.1 | 0.2 | 0.8 | 0.2 | 0.08 | 0.3 | 0.4 | 0.3 | 0.2 | 0.1 | 450 | 0.11 | 1.8 | 156 | 0.4 | 2.36 |

Elements Below detection limit (0.1 ppm): Sb , Be , Cd , Tb , Ho , Tm , Lu , and Ta

Mean H and L chondritic values for most elements from mason 1970

* Man H and L chondritic values for Zn and Cs from Friedrich 2003

* Man H and L chondritic values for Ir from Friedrich 2003 and Kallemeyn 1989

Appendix 3. Bulk chemical analysis of reference soil samples using combination of INAA, ICP-MS and ICP-OES methods.

| Elements | Li | Na | Mg | Al | P | S | K | Ca | Sc | Ti | V | Cr | Mn | Fe | Co | Ni | Zn | Ga | As | Se | Rb | Sr | Y | Zr | Nb | Cs | Ba | La | Ce | Pr | Nd | Sm | Eu | Gd | Hf | Ta | Th | U |
|---|---|---|---|---|---|---|---|---|---|---|---|---|---|---|---|---|---|---|---|---|---|---|---|---|---|---|---|---|---|---|---|---|---|---|---|---|---|
| methods | 2 | 1 | 3 | 3 | 3 | 3 | 3 | 3 | 1 | 3 | 2 | 1 | 3 | 1 | 2 | 2 | 3 | 2 | 1 | 2 | 2 | 2 | 2 | 2 | 2 | 2 | 3 | 2 | 2 | 2 | 2 | 2 | 2 | 2 | 2 | 2 | 2 |
| Units | ppm | % | % | % | % | % | % | % | ppm | % | ppm | ppm | ppm | % | ppm | ppm | ppm | ppm | ppm | ppm | ppm | ppm | ppm | ppm | ppm | ppm | ppm | ppm | ppm | ppm | ppm | ppm | ppm | ppm | ppm | ppm | ppm | ppn |
| Mean Upper crust | 20 | 2.89 | 1.33 | 8.04 | 0.105 | 0.026 | 2.80 | 3 | 11 | 0.30 | 60 | 35 | 600 | 3.5 | 10 | 20 | 71 | 17 | 1.5 | 0.05 | 112 | 350 | 22 | 190 | 25 | 3.7 | 550 | 30 | 64 | 7.1 | 26 | 4.5 | 0.88 | 3.8 | 5.8 | 2.2 | 10.7 | 2.8 |
| 0101-4 | 6.2 | 0.87 | 1.83 | 2.37 | 0.016 | 0.040 | 0.92 | 15 | 6.3 | 0.43 | 43 | 2120 | 458 | 1.67 | 15.8 | 221 | 29 | 3.5 | 2.7 | 0.3 | 24.7 | 408 | 10.8 | 55 | 7.2 | 0.74 | 292 | 14.6 | 26.1 | 3.4 | 12.7 | 2.7 | 0.62 | 2.5 | 1.5 | 0.4 | 3.3 | 1.3 |
| 0101-5 | 6.8 | 0.72 | 1.54 | 2.24 | 0.018 | 0.040 | 0.89 | 17 | 5.5 | 0.30 | 44 | 1270 | 527 | 1.48 | 11.5 | 86.4 | 20 | 3.6 | 3.2 | 0.6 | 26.0 | 351 | 9.6 | 63 | 5.4 | 0.90 | 337 | 12.9 | 22.0 | 2.9 | 10.5 | 2.2 | 0.52 | 2.0 | 1.7 | 0.3 | 3.0 | 1.1 |
| 0101-10 | 10.1 | 0.87 | 1.93 | 2.63 | 0.023 | 0.062 | 0.97 | 16 | 8.8 | 0.61 | 60 | 1510 | 509 | 2.25 | 9.5 | 54.3 | 44 | 5.2 | 3.7 | 0.8 | 27.3 | 529 | 14.5 | 152 | 10.5 | 1.19 | 249 | 23.0 | 41.3 | 5.1 | 18.6 | 3.8 | 0.71 | 3.4 | 4.0 | 0.6 | 7.3 | 2.1 |
| 0101-51 | 7.9 | 1.11 | 1.53 | 2.60 | 0.018 | 0.040 | 1.00 | 13 | 8.6 | 0.58 | 55 | 1440 | 470 | 2.02 | 8.4 | 47.2 | 34 | 4.8 | 0.25 | 0.6 | 26.5 | 332 | 14.1 | 121 | 9.9 | 0.85 | 281 | 22.9 | 41.0 | 5.2 | 18.9 | 3.7 | 0.74 | 3.5 | 3.4 | 0.6 | 7.2 | 1.8 |
| 0102-199 | 8.4 | 0.98 | 1.40 | 2.65 | 0.016 | 0.031 | 1.01 | 15 | 7.7 | 0.52 | 52 | 1330 | 446 | 1.89 | 7.9 | 47.9 | 35 | 5.7 | 3.7 | 0.05 | 26.8 | 297 | 12.6 | 73 | 8.5 | 0.83 | 281 | 18.0 | 32.1 | 4.0 | 15.2 | 3.1 | 0.67 | 2.9 | 2.0 | 0.4 | 5.7 | 1.4 |
| 0102-216-II | 8.7 | 0.9 | 1.80 | 2.40 | 0.018 | 0.045 | 0.89 | 16 | 8 | 0.70 | 63 | 2310 | 560 | 2.18 | 9.7 | 50.9 | 42 | 5.2 | 3.9 | 0.7 | 24.2 | 397 | 14.6 | 103 | 11.2 | 0.82 | 245 | 24.0 | 42.9 | 5.3 | 19.8 | 3.9 | 0.74 | 3.6 | 2.9 | 0.6 | 7.9 | 1.8 |
| 0102-256-II | 8.1 | 2.24 | 1.36 | 2.38 | 0.013 | 0.037 | 0.97 | 17 | 6.8 | 0.44 | 42 | 1040 | 396 | 1.52 | 6.6 | 39.7 | 49 | 4.1 | 2.3 | 0.7 | 22.1 | 330 | 10.8 | 81 | 6.7 | 0.70 | 291 | 14.8 | 27.1 | 3.3 | 12.6 | 2.6 | 0.56 | 2.5 | 2.1 | 0.3 | 5.0 | 1.2 |
| 0103-262 | 11.0 | 0.63 | 1.38 | 2.03 | 0.015 | 0.105 | 0.77 | 20 | 6.1 | 0.28 | 40 | 548 | 287 | 1.58 | 7.4 | 51.5 | 17 | 4.2 | 5.6 | 0.8 | 24.6 | 520 | 8.9 | 74 | 6.0 | 1.21 | 291 | 12.3 | 21.8 | 2.7 | 10.1 | 2.0 | 0.49 | 2.1 | 1.9 | 0.4 | 3.5 | 1.4 |
| 0201-10 | 12.0 | 0.92 | 2.27 | 2.23 | 0.017 | 0.159 | 0.81 | 16 | 7.2 | 0.52 | 54 | 1600 | 434 | 1.96 | 8.1 | 52.1 | 40 | 4.6 | 4.4 | 0.6 | 23.6 | 527 | 12.2 | 87 | 9.0 | 0.91 | 242 | 18.6 | 34.1 | 4.2 | 16.1 | 3.2 | 0.63 | 3.0 | 2.4 | 0.5 | 5.5 | 1.6 |
| 0201-82 | 10.4 | 0.97 | 1.41 | 2.64 | 0.016 | 0.026 | 1.02 | 14 | 8.4 | 0.45 | 53 | 1050 | 407 | 2.19 | 8.6 | 53.1 | 23 | 5.6 | 3.8 | 0.8 | 30.8 | 295 | 12.1 | 85 | 8.1 | 1.18 | 277 | 18.2 | 33.1 | 4.1 | 15.5 | 3.2 | 0.65 | 2.9 | 2.4 | 0.4 | 5.4 | 1.5 |
| 0201-89 | 7.8 | 0.62 | 1.14 | 1.84 | 0.013 | 0.045 | 0.68 | 21 | 6.4 | 0.40 | 46 | 1000 | 361 | 1.7 | 7.1 | 43.8 | 20 | 3.8 | 4.1 | 0.5 | 19.9 | 419 | 10.6 | 106 | 7.7 | 0.83 | 309 | 15.7 | 28.5 | 3.5 | 13.1 | 2.6 | 0.54 | 2.6 | 2.9 | 0.4 | 4.8 | 1.3 |
| 0201-110 | 11.7 | 1.01 | 2.13 | 2.61 | 0.014 | 0.056 | 1.00 | 15 | 8.3 | 0.53 | 53 | 1380 | 446 | 2.13 | 8.7 | 51.4 | 31 | 6.1 | 2.6 | 0.7 | 27.6 | 366 | 12.5 | 124 | 9.3 | 1.13 | 253 | 19.6 | 35.3 | 4.3 | 15.8 | 3.2 | 0.64 | 2.9 | 3.4 | 0.5 | 6.1 | 1.7 |
| 0201-133 | 10.3 | 0.78 | 1.81 | 2.48 | 0.021 | 0.048 | 0.91 | 15 | 8 | 0.67 | 61 | 2070 | 561 | 2.08 | 10.4 | 62.4 | 29 | 5.5 | 3.8 | 0.2 | 25.6 | 374 | 13.5 | 100 | 11.0 | 1.10 | 244 | 19.9 | 36.1 | 4.5 | 16.8 | 3.5 | 0.71 | 3.3 | 2.7 | 0.6 | 9.0 | 1.8 |
| 0201-138 | 8.4 | 0.87 | 1.60 | 2.35 | 0.019 | 0.057 | 0.89 | 15 | 8.2 | 0.63 | 60 | 2720 | 563 | 2.22 | 11.0 | 62.6 | 107 | 4.9 | 3.5 | 0.2 | 25.1 | 374 | 13.7 | 136 | 10.8 | 0.96 | 261 | 20.6 | 37.4 | 4.6 | 17.0 | 3.4 | 0.69 | 3.1 | 3.6 | 0.6 | 6.6 | 1.7 |
| 0201-144 | 7.8 | 1.06 | 1.86 | 2.43 | 0.017 | 0.051 | 0.88 | 16 | 9.7 | 0.76 | 69 | 2520 | 562 | 2.59 | 9.5 | 45.9 | 37 | 5.4 | 5.9 | 0.2 | 23.4 | 374 | 16.6 | 196 | 12.9 | 0.73 | 255 | 28.7 | 51.8 | 6.2 | 22.9 | 4.5 | 0.81 | 4.2 | 5.3 | 0.7 | 10.4 | 2.2 |
| 0201-373 | 7.8 | 1.07 | 1.67 | 2.39 | 0.016 | 0.048 | 0.93 | 15 | 8.5 | 0.59 | 52 | 1880 | 466 | 2.22 | 7.9 | 41.4 | 33 | 5.3 | 3.9 | 0.6 | 23.8 | 338 | 13.0 | 98 | 9.4 | 0.74 | 263 | 22.1 | 40.6 | 5.1 | 18.7 | 3.7 | 0.69 | 3.4 | 2.8 | 0.5 | 8.2 | 1.7 |
| 0201-790 | 7.9 | 1.08 | 1.50 | 2.46 | 0.017 | 0.036 | 0.97 | 15 | 7.7 | 0.52 | 45 | 1470 | 437 | 1.91 | 7.7 | 46.5 | 31 | 5.1 | 1.4 | 0.5 | 25.9 | 365 | 12.8 | 137 | 9.6 | 0.81 | 267 | 18.4 | 32.2 | 4.0 | 15.1 | 3.0 | 0.67 | 3.0 | 3.6 | 0.6 | 5.3 | 1.6 |
| 0301-80 II | 9.1 | 0.84 | 1.45 | 2.36 | 0.019 | 0.031 | 1.06 | 14 | 8 | 0.63 | 65 | 1550 | 580 | 2.07 | 9.5 | 50.2 | 31 | 5.8 | 2.3 | 0.3 | 24.3 | 272 | 13.6 | 172 | 9.7 | 0.82 | 241 | 22.0 | 43.7 | 5.3 | 20.9 | 4.2 | 0.81 | 3.7 | 4.3 | 0.3 | 8.4 | 1.9 |

1= INAA
2= ICP-MS
3= ICP-OES

Appendix 4. Bulk chemical analysis of soil under meteorite samples using combination of INAA, ICP-MS and ICP-OES methods.

| Elements | As | Cr | Fe | Na | Sc | Li | V | Co | Ni | Ga | Se | Rb | Sr | Y | Zr | Nb | Cs | La | Ce | Pr | Nd | Sm | Eu | Gd | Hf | Ta | Th | U | Ba | Mn | Zn | Al | Ca | K | Mg | P | Ti | S |
|---|---|---|---|---|---|---|---|---|---|---|---|---|---|---|---|---|---|---|---|---|---|---|---|---|---|---|---|---|---|---|---|---|---|---|---|---|---|
| methods | 1 | 1 | 1 | 1 | 1 | 2 | 2 | 2 | 2 | 2 | 2 | 2 | 2 | 2 | 2 | 2 | 2 | 2 | 2 | 2 | 2 | 2 | 2 | 2 | 2 | 2 | 2 | 2 | 3 | 3 | 3 | 3 | 3 | 3 | 3 | 3.00 | 3 | 3.00 |
| Unit | ppm | ppm | % | % | ppm | ppm | ppm | ppm | ppm | ppm | ppm | ppm | ppm | ppm | ppm | ppm | ppm | ppm | ppm | ppm | ppm | ppm | ppm | ppm | ppm | ppm | ppm | ppm | ppm | ppm | ppm | % | % | % | % | % | % | % |
| Mean | | | | | | | | | | | | | | | | | | | | | | | | | | | | | | | | | | | | | | |
| Upper crust | 1.5 | 35 | 3.5 | 2.9 | 11 | 20 | 60 | 10 | 20 | 17 | 0.1 | 112 | 350 | 22 | 190 | 25 | 3.7 | 30 | 64 | 7.1 | 26 | 4.5 | 0.9 | 3.8 | 5.8 | 2.2 | 11 | 2.8 | 550 | 600 | 71 | 8.04 | 3 | 2.80 | 1.33 | 0.11 | 0.30 | 0.03 |
| 0101-9 | 4.2 | 1740 | 2.3 | 0.9 | 8.7 | 9.6 | 62 | 9.8 | 67.8 | 5.0 | 0.8 | 26.9 | 447 | 15.6 | 170 | 11.3 | 1.10 | 26.5 | 47.9 | 5.9 | 21.8 | 4.4 | 0.76 | 4.0 | 4.6 | 0.6 | 9.0 | 2.2 | 246 | 550 | 57 | 2.56 | 16 | 0.93 | 1.91 | 0.02 | 0.69 | 0.06 |
| 0102-198 | 2.3 | 828 | 1.6 | 1 | 6.7 | 7.8 | 41 | 7.0 | 44.6 | 4.8 | 0.8 | 26.2 | 283 | 11.2 | 95 | 7.9 | 0.88 | 14.7 | 26.0 | 3.4 | 12.7 | 2.6 | 0.60 | 2.4 | 2.6 | 0.4 | 4.0 | 1.3 | 295 | 367 | 33 | 2.56 | 14 | 1.05 | 1.21 | 0.01 | 0.42 | 0.03 |
| 0102-216-I | 2.3 | 925 | 1.3 | 0.8 | 5.3 | 8.7 | 34 | 5.8 | 40.4 | 4.2 | 0.4 | 26.5 | 358 | 9.4 | 84 | 6.4 | 0.79 | 12.9 | 22.3 | 2.9 | 10.7 | 2.3 | 0.54 | 2.2 | 2.2 | 0.3 | 3.3 | 1.1 | 280 | 309 | 20 | 2.20 | 14 | 0.99 | 1.54 | 0.01 | 0.35 | 0.05 |
| 0102-256-I | 2.1 | 823 | 1.6 | 1.1 | 6.7 | 7.3 | 40 | 11.3 | 264 | 4.7 | 0.5 | 27.6 | 259 | 9.7 | 84 | 6.9 | 0.78 | 13.3 | 23.5 | 3.0 | 11.1 | 2.3 | 0.53 | 2.2 | 2.3 | 0.4 | 4.0 | 1.2 | 361 | 378 | 27 | 2.82 | 14 | 1.22 | 1.25 | 0.01 | 0.43 | 0.05 |
| 0103-260 | 3 | 556 | 1.2 | 0.6 | 4.6 | 7.2 | 29 | 6.6 | 77.1 | 2.1 | 0.6 | 20.1 | 663 | 8.0 | 55 | 5.0 | 0.76 | 11.3 | 20.0 | 2.5 | 9.2 | 1.9 | 0.42 | 1.8 | 1.4 | 0.2 | 2.9 | 1.1 | 455 | 253 | 14 | 1.68 | 22 | 0.66 | 0.94 | 0.01 | 0.26 | 0.52 |
| 0201-86 | 2.5 | 765 | 1.6 | 1.1 | 6.7 | 8.7 | 36 | 7.4 | 68.8 | 5.6 | 0.5 | 29.9 | 267 | 9.7 | 52 | 6.3 | 0.90 | 14.5 | 25.8 | 3.3 | 12.1 | 2.5 | 0.57 | 2.5 | 1.5 | 0.4 | 3.8 | 1.1 | 359 | 331 | 22 | 2.76 | 13 | 1.22 | 1.18 | 0.01 | 0.36 | 0.02 |
| 0201-132 | 4.3 | 1870 | 2 | 0.9 | 7.4 | 8.6 | 47 | 14.8 | 250 | 5.3 | 0.4 | 27.3 | 336 | 11.4 | 73 | 8.9 | 0.94 | 17.1 | 30.1 | 3.7 | 13.6 | 2.7 | 0.62 | 2.7 | 2.1 | 0.5 | 4.5 | 1.3 | 302 | 503 | 33 | 2.58 | 14 | 1.07 | 1.52 | 0.02 | 0.57 | 0.04 |
| 0201-137 | 3.4 | 2700 | 2.2 | 1 | 7.7 | 7.9 | 56 | 9.7 | 52.7 | 5.1 | 0.2 | 25.5 | 328 | 13.2 | 121 | 10.5 | 0.74 | 19.9 | 35.3 | 4.3 | 15.7 | 3.3 | 0.68 | 3.0 | 3.3 | 0.7 | 5.8 | 1.6 | 289 | 541 | 58 | 2.43 | 13 | 0.99 | 1.39 | 0.02 | 0.68 | 0.03 |
| 0201-143 | 3.6 | 2110 | 2.2 | 1.1 | 8.9 | 7.9 | 60 | 8.9 | 55.3 | 5.1 | 0.2 | 24.8 | 362 | 14.3 | 133 | 12.0 | 0.74 | 23.7 | 42.3 | 5.2 | 19.1 | 3.8 | 0.74 | 3.7 | 3.6 | 0.7 | 8.0 | 1.9 | 257 | 492 | 56 | 2.34 | 15 | 0.89 | 1.67 | 0.02 | 0.64 | 0.05 |
| 0201-372 | 2.7 | 1010 | 1.4 | 1 | 5.9 | 6.4 | 36 | 16.2 | 428 | 4.6 | 0.2 | 27.3 | 296 | 10.4 | 106 | 7.5 | 0.75 | 15.0 | 26.4 | 3.3 | 12.5 | 2.5 | 0.56 | 2.6 | 2.8 | 0.4 | 4.6 | 1.3 | 314 | 360 | 27 | 2.50 | 15 | 1.07 | 1.41 | 0.01 | 0.42 | 0.04 |
| 0201-789 | 2.4 | 839 | 1.4 | 1.1 | 5.9 | 7.3 | 31 | 6.1 | 43.7 | 5.1 | 0.6 | 29.8 | 311 | 9.4 | 81 | 6.8 | 0.85 | 12.8 | 22.0 | 2.8 | 10.4 | 2.2 | 0.54 | 2.1 | 2.1 | 0.4 | 3.1 | 1.2 | 324 | 331 | 30 | 2.61 | 13 | 1.17 | 1.24 | 0.01 | 0.36 | 0.03 |
| 0301-80 I | 2.6 | 865 | 1.7 | 1 | 7 | 9.1 | 51 | 12.1 | 125 | 5.9 | 0.2 | 25.8 | 296 | 11.0 | 124 | 8.2 | 0.86 | 15.6 | 29.8 | 3.8 | 14.7 | 2.9 | 0.66 | 2.7 | 3.0 | 0.5 | 5.0 | 1.5 | 252 | 439 | 24 | 2.37 | 14 | 1.09 | 1.58 | 0.02 | 0.40 | 0.03 |

1= INAA
2= ICP-MS
3= ICP-OES

Appendix 5. Chemical analysis of reference soil samples using ICP-OES method following aqua regia extraction.

| Elements | Na | Mg | Al | P | S | K | Ca | Sc | Ti | V | Cr | Mn | Fe | Co | Ni | Zn | Sr | Zr | Ba | La | Pb |
|---|---|---|---|---|---|---|---|---|---|---|---|---|---|---|---|---|---|---|---|---|---|
| Units | % | % | % | % | % | % | % | ppm | % | ppm | ppm | ppm | % | ppm | ppm | ppm | ppm | ppm | ppm | ppm | ppm |
| Mean | | | | | | | | | | | | | | | | | | | | | |
| Upper crust | 2.9 | 1.3 | 8 | 0.1 | 0 | 2.8 | 3 | 11 | 0.3 | 60 | 35 | 600 | 3.5 | 10 | 20 | 71 | 350 | 190 | 550 | 30 | 20 |
| 0101-4 | 0.05 | 1.60 | 0.41 | 0.02 | 0.04 | 0.06 | 19 | 2.5 | 0.05 | 28 | 41 | 246 | 0.86 | 5 | 68 | 5 | 327 | 20 | 106 | 9 | 8 |
| 0101-5 | 0.05 | 1.24 | 0.48 | 0.02 | 0.04 | 0.08 | 20 | 2.3 | 0.04 | 37 | 44 | 392 | 0.84 | 9 | 73 | 4 | 280 | 18 | 191 | 8 | 9 |
| 0101-10 | 0.05 | 1.65 | 0.64 | 0.02 | 0.06 | 0.11 | 19 | 3.2 | 0.06 | 38 | 43 | 248 | 1.13 | 6 | 42 | 9 | 418 | 27 | 70 | 10 | 8 |
| 0101-16 | 0.05 | 1.45 | 0.60 | 0.02 | 0.03 | 0.10 | 19 | 3.0 | 0.06 | 34 | 40 | 237 | 1.06 | 5 | 40 | 9 | 265 | 20 | 73 | 10 | 7 |
| 0101-19 | 0.05 | 1.19 | 0.44 | 0.02 | 0.03 | 0.06 | 16 | 2.5 | 0.07 | 34 | 35 | 211 | 0.91 | 4 | 32 | 5 | 220 | 25 | 61 | 10 | 6 |
| 0101-22 | 0.03 | 1.10 | 0.32 | 0.01 | 0.03 | 0.04 | 15 | 1.8 | 0.03 | 25 | 25 | 181 | 0.71 | 4 | 30 | 5 | 208 | 21 | 58 | 6 | 7 |
| 0101-25 | 0.04 | 1.32 | 0.47 | 0.02 | 0.04 | 0.07 | 18 | 2.5 | 0.06 | 36 | 34 | 223 | 0.99 | 5 | 36 | 8 | 232 | 28 | 66 | 9 | 7 |
| 0101-27 | 0.04 | 1.08 | 0.44 | 0.01 | 0.02 | 0.07 | 16 | 2.4 | 0.06 | 29 | 30 | 190 | 0.81 | 4 | 40 | 6 | 180 | 26 | 70 | 9 | 6 |
| 0101-29 | 0.04 | 1.10 | 0.44 | 0.01 | 0.03 | 0.06 | 16 | 2.3 | 0.06 | 28 | 31 | 192 | 0.79 | 4 | 33 | 6 | 190 | 25 | 67 | 8 | 7 |
| 0101-38 | 0.04 | 1.20 | 0.43 | 0.02 | 0.03 | 0.06 | 16 | 2.4 | 0.06 | 33 | 32 | 206 | 0.89 | 4 | 33 | 6 | 208 | 26 | 66 | 9 | 7 |
| 0101-51 | 0.09 | 1.27 | 0.39 | 0.02 | 0.04 | 0.06 | 16 | 2.1 | 0.04 | 30 | 29 | 202 | 0.83 | 4 | 35 | 7 | 221 | 25 | 62 | 7 | 8 |
| 0101-146 | 0.04 | 1.47 | 0.59 | 0.02 | 0.04 | 0.09 | 18 | 2.8 | 0.05 | 36 | 35 | 237 | 1.10 | 6 | 42 | 10 | 256 | 32 | 73 | 9 | 8 |
| 0101-150 | 0.04 | 1.12 | 0.43 | 0.01 | 0.03 | 0.06 | 15 | 2.2 | 0.05 | 27 | 28 | 190 | 0.79 | 4 | 34 | 6 | 203 | 25 | 59 | 7 | 8 |
| 0101-157 | 0.04 | 1.17 | 0.45 | 0.01 | 0.03 | 0.06 | 16 | 2.3 | 0.05 | 29 | 31 | 204 | 0.87 | 5 | 36 | 8 | 200 | 27 | 61 | 8 | 7 |
| 0102-169 | 0.35 | 1.17 | 0.45 | 0.01 | 0.06 | 0.07 | 16 | 2.4 | 0.06 | 33 | 32 | 209 | 0.91 | 4 | 36 | 7 | 279 | 27 | 85 | 8 | 7 |
| 0102-175 | 0.03 | 1.09 | 0.43 | 0.01 | 0.02 | 0.06 | 17 | 2.4 | 0.06 | 31 | 31 | 196 | 0.86 | 4 | 33 | 6 | 185 | 26 | 55 | 8 | 6 |
| 0102-199 | 0.05 | 1.13 | 0.47 | 0.01 | 0.02 | 0.07 | 17 | 2.5 | 0.06 | 30 | 31 | 198 | 0.85 | 4 | 34 | 5 | 190 | 27 | 62 | 9 | 6 |
| 0102-213 II | 0.58 | 1.66 | 0.41 | 0.02 | 0.09 | 0.07 | 17 | 2.6 | 0.07 | 37 | 38 | 234 | 0.97 | 4 | 33 | 5 | 273 | 26 | 56 | 10 | 6 |
| 0102-214 II | 0.07 | 1.55 | 0.40 | 0.02 | 0.05 | 0.06 | 18 | 2.2 | 0.04 | 28 | 31 | 206 | 0.81 | 4 | 34 | 4 | 305 | 22 | 58 | 8 | 7 |
| 0102-215 II | 0.16 | 2.14 | 0.48 | 0.02 | 0.07 | 0.07 | 21 | 2.6 | 0.06 | 38 | 39 | 214 | 0.92 | 4 | 33 | 3 | 325 | 13 | 188 | 10 | 7 |
| 0102-216 II | 0.08 | 1.60 | 0.47 | 0.02 | 0.04 | 0.07 | 19 | 2.8 | 0.07 | 35 | 40 | 241 | 0.97 | 4 | 34 | 4 | 297 | 16 | 76 | 10 | 8 |
| 0102-217 II | 0.40 | 1.65 | 0.46 | 0.02 | 0.05 | 0.07 | 18 | 2.8 | 0.08 | 45 | 47 | 250 | 1.18 | 4 | 34 | 5 | 286 | 20 | 64 | 13 | 6 |
| 0102-227 II | 0.04 | 1.53 | 0.49 | 0.01 | 0.03 | 0.07 | 21 | 2.5 | 0.05 | 36 | 44 | 284 | 0.87 | 7 | 67 | 18 | 342 | 18 | 118 | 9 | 9 |
| 0102-232 II | 0.04 | 1.18 | 0.55 | 0.02 | 0.05 | 0.09 | 18 | 2.5 | 0.05 | 31 | 35 | 194 | 0.90 | 5 | 34 | 7 | 488 | 27 | 80 | 8 | 7 |
| 0102-235 II | 0.04 | 1.29 | 0.56 | 0.02 | 0.03 | 0.09 | 19 | 2.8 | 0.06 | 36 | 33 | 236 | 0.99 | 5 | 36 | 7 | 208 | 29 | 106 | 9 | 8 |
| 0102-237 II | 0.05 | 1.24 | 0.49 | 0.02 | 0.03 | 0.07 | 16 | 2.7 | 0.07 | 34 | 33 | 219 | 0.92 | 4 | 34 | 6 | 214 | 27 | 80 | 10 | 6 |
| 0102-239 II | 0.11 | 1.36 | 0.59 | 0.02 | 0.04 | 0.10 | 18 | 3.0 | 0.07 | 38 | 37 | 227 | 1.05 | 5 | 37 | 8 | 196 | 30 | 71 | 10 | 8 |
| 0102-240 II | 0.05 | 1.42 | 0.55 | 0.02 | 0.06 | 0.09 | 18 | 3.0 | 0.08 | 42 | 38 | 239 | 1.07 | 5 | 37 | 8 | 224 | 31 | 69 | 11 | 7 |
| 0102-245 II | 0.03 | 1.42 | 0.58 | 0.02 | 0.03 | 0.09 | 17 | 2.9 | 0.07 | 37 | 36 | 232 | 1.10 | 5 | 39 | 9 | 212 | 32 | 73 | 10 | 6 |
| 0102-255 II | 0.04 | 1.11 | 0.54 | 0.02 | 0.03 | 0.08 | 20 | 2.6 | 0.06 | 37 | 33 | 226 | 1.00 | 5 | 35 | 6 | 263 | 28 | 166 | 9 | 8 |
| 0102-256 II | 1.17 | 1.05 | 0.42 | 0.01 | 0.03 | 0.09 | 19 | 2.2 | 0.07 | 29 | 30 | 189 | 0.78 | 4 | 28 | 3 | 260 | 24 | 101 | 8 | 7 |
| 0102-258 II | 0.30 | 1.00 | 0.46 | 0.01 | 0.16 | 0.07 | 21 | 2.2 | 0.06 | 29 | 28 | 182 | 0.73 | 4 | 27 | 2 | 294 | 24 | 73 | 8 | 8 |
| 0103-262 | 0.03 | 1.16 | 0.56 | 0.01 | 0.10 | 0.09 | 23 | 2.3 | 0.04 | 28 | 37 | 178 | 0.85 | 5 | 34 | 6 | 390 | 23 | 195 | 7 | 11 |
| 0201-10 | 0.18 | 2.06 | 0.57 | 0.02 | 0.17 | 0.08 | 19 | 2.7 | 0.06 | 36 | 54 | 200 | 0.89 | 4 | 35 | 4 | 369 | 27 | 93 | 9 | 9 |
| 0201-79 | 0.03 | 1.03 | 0.52 | 0.01 | 0.02 | 0.08 | 16 | 2.6 | 0.07 | 34 | 33 | 206 | 0.96 | 5 | 35 | 6 | 179 | 28 | 107 | 9 | 7 |
| 0201-82 | 0.03 | 1.40 | 0.59 | 0.02 | 0.03 | 0.09 | 17 | 2.7 | 0.05 | 36 | 35 | 224 | 0.96 | 10 | 153 | 8 | 213 | 28 | 175 | 8 | 7 |
| 0201-89 | 0.03 | 0.87 | 0.44 | 0.01 | 0.03 | 0.07 | 25 | 2.0 | 0.06 | 34 | 30 | 194 | 0.78 | 4 | 26 | 1 | 324 | 23 | 240 | 9 | 8 |
| 0201-101 | 0.04 | 1.05 | 0.58 | 0.01 | 0.02 | 0.09 | 17 | 2.9 | 0.07 | 35 | 37 | 216 | 0.99 | 5 | 37 | 8 | 238 | 29 | 99 | 9 | 7 |
| 0201-110 | 0.10 | 1.80 | 0.57 | 0.01 | 0.05 | 0.10 | 17 | 2.7 | 0.06 | 33 | 42 | 212 | 0.94 | 5 | 37 | 6 | 257 | 25 | 50 | 9 | 8 |
| 0201-133 | 0.05 | 1.60 | 0.63 | 0.02 | 0.05 | 0.10 | 18 | 3.2 | 0.07 | 41 | 44 | 270 | 1.13 | 6 | 49 | 7 | 277 | 24 | 80 | 11 | 8 |
| 0201-138 | 0.05 | 1.35 | 0.54 | 0.02 | 0.05 | 0.08 | 18 | 2.8 | 0.07 | 36 | 40 | 290 | 1.00 | 6 | 46 | 5 | 266 | 17 | 97 | 10 | 8 |
| 0201-144 | 0.05 | 1.73 | 0.48 | 0.02 | 0.05 | 0.07 | 20 | 2.8 | 0.08 | 41 | 41 | 251 | 1.07 | 4 | 32 | 5 | 263 | 17 | 80 | 12 | 8 |
| 0201-373 | 0.05 | 1.43 | 0.42 | 0.01 | 0.05 | 0.06 | 18 | 2.3 | 0.06 | 31 | 32 | 200 | 0.83 | 4 | 28 | 3 | 229 | 19 | 69 | 9 | 5 |
| 0201-790 | 0.04 | 1.35 | 0.46 | 0.02 | 0.03 | 0.07 | 18 | 2.6 | 0.07 | 29 | 33 | 225 | 0.82 | 4 | 33 | 4 | 242 | 24 | 65 | 9 | 7 |
| 0301-80 II | 0.03 | 0.78 | 0.44 | 0.01 | 0.03 | 0.06 | 15 | 2.2 | 0.06 | 25 | 26 | 193 | 0.80 | 4 | 29 | 28 | 202 | 7 | 35 | 5 | 12 |
| 0301-69 II | 0.12 | 1.05 | 0.52 | 0.01 | 0.06 | 0.10 | 16 | 2.2 | 0.04 | 26 | 29 | 200 | 0.79 | 4 | 36 | 27 | 248 | 6 | 51 | 5 | 14 |

Appendix 6. Chemical analysis of soil under meteorite samples using ICP-OES method following aqua regia extraction.

| Element | Na | Mg | Al | P | S | K | Ca | Sc | Ti | V | Cr | Mn | Fe | Co | Ni | Zn | Sr | Zr | Ba | La | Pb |
|---|---|---|---|---|---|---|---|---|---|---|---|---|---|---|---|---|---|---|---|---|---|
| Units | % | % | % | % | % | % | % | ppm | % | ppm | ppm | ppm | % | ppm | ppm | ppm | ppm | ppm | ppm | ppm | ppm |
| Mean | 2.89 | 1.33 | 8.04 | 0.11 | 0.03 | 2.8 | 3 | 11 | 0.03 | 60 | 35 | 600 | 3.5 | 10 | 20 | 71 | 350 | 190 | 550 | 30 | 20 |
| Upper crust | | | | | | | | | | | | | | | | | | | | | |
| 0101-9 | 0.06 | 1.66 | 0.61 | 0.02 | 0.06 | 0.10 | 19.3 | 3.1 | 0.07 | 39 | 43 | 254 | 1.13 | 5 | 52 | 9 | 348 | 27 | 78 | 11 | 10 |
| 0101-13 | 0.05 | 1.56 | 0.53 | 0.02 | 0.12 | 0.08 | 18.7 | 2.7 | 0.06 | 33 | 37 | 224 | 0.94 | 4 | 36 | 6 | 483 | 22 | 85 | 9 | 8 |
| 0101-15 | 0.05 | 1.42 | 0.61 | 0.02 | 0.03 | 0.10 | 18.8 | 3.0 | 0.06 | 35 | 41 | 242 | 1.09 | 6 | 41 | 9 | 254 | 21 | 70 | 10 | 10 |
| 0101-18 | 0.05 | 1.23 | 0.47 | 0.02 | 0.03 | 0.07 | 16.5 | 2.7 | 0.07 | 35 | 35 | 218 | 0.94 | 5 | 40 | 6 | 233 | 25 | 67 | 10 | 6 |
| 0101-21 | 0.05 | 1.09 | 0.42 | 0.01 | 0.03 | 0.06 | 15.5 | 2.3 | 0.06 | 29 | 29 | 189 | 0.79 | 4 | 31 | 5 | 216 | 23 | 63 | 8 | 6 |
| 0101-24 | 0.03 | 1.24 | 0.43 | 0.02 | 0.04 | 0.07 | 16.9 | 2.3 | 0.04 | 31 | 30 | 204 | 0.88 | 4 | 36 | 8 | 203 | 26 | 56 | 7 | 8 |
| 0101-31 | 0.04 | 1.32 | 0.49 | 0.02 | 0.03 | 0.07 | 16.5 | 2.7 | 0.07 | 36 | 37 | 222 | 1.01 | 4 | 36 | 7 | 211 | 28 | 73 | 10 | 7 |
| 0101-33 | 0.03 | 1.03 | 0.42 | 0.01 | 0.02 | 0.06 | 15.9 | 2.2 | 0.05 | 26 | 28 | 173 | 0.72 | 4 | 32 | 5 | 185 | 23 | 78 | 8 | 6 |
| 0101-35 | 0.04 | 1.04 | 0.42 | 0.01 | 0.03 | 0.06 | 14.6 | 2.2 | 0.05 | 26 | 27 | 186 | 0.73 | 4 | 31 | 5 | 177 | 24 | 70 | 7 | 6 |
| 0101-37 | 0.04 | 1.04 | 0.40 | 0.01 | 0.03 | 0.06 | 15.1 | 2.2 | 0.06 | 26 | 27 | 178 | 0.73 | 4 | 30 | 5 | 185 | 23 | 64 | 8 | 7 |
| 0101-40 | 0.08 | 1.52 | 0.61 | 0.02 | 0.04 | 0.10 | 15.6 | 2.9 | 0.05 | 37 | 35 | 232 | 1.07 | 11 | 268 | 11 | 201 | 31 | 49 | 8 | 5 |
| 0101-50 | 0.13 | 1.11 | 0.35 | 0.01 | 0.03 | 0.05 | 14.7 | 1.8 | 0.03 | 26 | 24 | 174 | 0.69 | 4 | 35 | 5 | 191 | 22 | 66 | 6 | 7 |
| 0101-53 | 0.03 | 1.13 | 0.41 | 0.01 | 0.03 | 0.06 | 17.2 | 2.1 | 0.05 | 29 | 28 | 186 | 0.78 | 5 | 49 | 6 | 195 | 24 | 57 | 7 | 6 |
| 0101-56 | 0.04 | 1.26 | 0.44 | 0.02 | 0.03 | 0.06 | 16.2 | 2.4 | 0.05 | 31 | 31 | 208 | 0.87 | 5 | 61 | 7 | 210 | 27 | 55 | 8 | 7 |
| 0101-129 | 0.04 | 1.05 | 0.40 | 0.01 | 0.03 | 0.06 | 15.3 | 2.1 | 0.05 | 26 | 27 | 173 | 0.71 | 4 | 43 | 5 | 182 | 24 | 57 | 7 | 7 |
| 0101-131 | 0.03 | 1.05 | 0.44 | 0.01 | 0.05 | 0.07 | 17.4 | 2.2 | 0.05 | 30 | 32 | 176 | 0.77 | 4 | 38 | 5 | 237 | 25 | 140 | 7 | 6 |
| 0101-134 | 0.06 | 1.21 | 0.44 | 0.01 | 0.03 | 0.07 | 15.9 | 2.3 | 0.05 | 29 | 30 | 193 | 0.82 | 4 | 36 | 7 | 211 | 25 | 61 | 8 | 6 |
| 0101-136 | 0.03 | 1.01 | 0.46 | 0.01 | 0.03 | 0.07 | 17.1 | 2.3 | 0.05 | 29 | 29 | 192 | 0.82 | 4 | 33 | 6 | 193 | 25 | 85 | 7 | 7 |
| 0101-138 | 0.03 | 1.11 | 0.45 | 0.01 | 0.02 | 0.07 | 15.4 | 2.3 | 0.05 | 28 | 30 | 194 | 0.82 | 5 | 35 | 7 | 199 | 26 | 80 | 8 | 7 |
| 0101-140 | 0.03 | 1.18 | 0.53 | 0.02 | 0.03 | 0.08 | 18.1 | 2.4 | 0.04 | 35 | 33 | 203 | 0.93 | 6 | 61 | 7 | 203 | 28 | 95 | 8 | 9 |
| 0101-143 | 0.03 | 1.23 | 0.41 | 0.02 | 0.03 | 0.06 | 16.0 | 2.1 | 0.03 | 26 | 27 | 191 | 0.82 | 4 | 36 | 6 | 204 | 24 | 68 | 7 | 6 |
| 0101-145 | 0.02 | 1.05 | 0.40 | 0.01 | 0.05 | 0.07 | 16.3 | 1.9 | 0.03 | 26 | 26 | 172 | 0.72 | 5 | 73 | 7 | 186 | 23 | 88 | 6 | 7 |
| 0101-149 | 0.03 | 1.08 | 0.43 | 0.01 | 0.03 | 0.06 | 15.0 | 2.2 | 0.05 | 28 | 29 | 187 | 0.81 | 4 | 34 | 7 | 203 | 25 | 57 | 7 | 7 |
| 0101-152 | 0.02 | 1.10 | 0.53 | 0.01 | 0.02 | 0.08 | 16.0 | 2.5 | 0.05 | 31 | 33 | 204 | 0.92 | 5 | 41 | 8 | 189 | 29 | 68 | 8 | 7 |
| 0101-156 | 0.02 | 0.94 | 0.48 | 0.01 | 0.02 | 0.07 | 17.0 | 2.2 | 0.05 | 26 | 29 | 195 | 0.82 | 4 | 35 | 6 | 196 | 26 | 54 | 8 | 8 |
| 0101-160 | 0.10 | 1.10 | 0.42 | 0.01 | 0.03 | 0.06 | 15.4 | 2.1 | 0.05 | 28 | 28 | 187 | 0.82 | 4 | 37 | 7 | 183 | 25 | 53 | 7 | 7 |
| 0101-164 | 0.03 | 1.13 | 0.42 | 0.01 | 0.03 | 0.06 | 15.4 | 2.2 | 0.05 | 28 | 29 | 192 | 0.83 | 4 | 34 | 7 | 195 | 26 | 61 | 7 | 6 |
| 0102-166 | 0.03 | 0.97 | 0.38 | 0.01 | 0.06 | 0.05 | 14.7 | 1.9 | 0.04 | 25 | 25 | 162 | 0.71 | 4 | 59 | 5 | 205 | 23 | 68 | 6 | 5 |
| 0102-167 | 0.03 | 0.92 | 0.37 | 0.01 | 0.05 | 0.05 | 15.2 | 1.8 | 0.03 | 23 | 23 | 153 | 0.66 | 4 | 34 | 5 | 191 | 21 | 73 | 6 | 7 |
| 0102-168 | 0.46 | 1.06 | 0.42 | 0.01 | 0.09 | 0.07 | 16.3 | 2.1 | 0.04 | 28 | 29 | 181 | 0.78 | 4 | 34 | 6 | 314 | 25 | 89 | 7 | 8 |
| 0102-171 | 0.04 | 1.15 | 0.49 | 0.01 | 0.02 | 0.07 | 15.8 | 2.6 | 0.06 | 32 | 33 | 204 | 0.91 | 5 | 40 | 8 | 187 | 29 | 75 | 9 | 7 |
| 0102-173 | 0.03 | 0.95 | 0.42 | 0.01 | 0.02 | 0.06 | 16.6 | 2.1 | 0.05 | 25 | 26 | 167 | 0.72 | 4 | 31 | 4 | 164 | 24 | 54 | 7 | 6 |
| 0102-174 | 0.03 | 1.03 | 0.43 | 0.01 | 0.02 | 0.06 | 16.9 | 2.4 | 0.06 | 30 | 31 | 195 | 0.84 | 4 | 32 | 6 | 178 | 26 | 56 | 8 | 7 |
| 0102-177 | 0.03 | 0.98 | 0.39 | 0.01 | 0.02 | 0.05 | 16.7 | 2.1 | 0.05 | 26 | 27 | 184 | 0.74 | 4 | 32 | 6 | 169 | 24 | 55 | 7 | 8 |
| 0102-178 | 0.02 | 1.11 | 0.44 | 0.01 | 0.02 | 0.06 | 16.8 | 2.2 | 0.05 | 28 | 29 | 195 | 0.84 | 4 | 34 | 7 | 182 | 26 | 66 | 8 | 7 |
| 0102-183 | 0.03 | 1.09 | 0.44 | 0.01 | 0.02 | 0.06 | 16.6 | 2.1 | 0.04 | 26 | 27 | 182 | 0.78 | 4 | 35 | 7 | 183 | 25 | 58 | 7 | 7 |
| 0102-188 | 0.03 | 1.19 | 0.46 | 0.02 | 0.02 | 0.06 | 17.5 | 2.3 | 0.04 | 28 | 29 | 201 | 0.85 | 7 | 82 | 7 | 190 | 27 | 64 | 7 | 7 |
| 0102-190 | 0.03 | 1.08 | 0.40 | 0.01 | 0.02 | 0.05 | 17.8 | 2.1 | 0.05 | 28 | 28 | 193 | 0.81 | 4 | 33 | 5 | 185 | 25 | 57 | 7 | 9 |
| 0102-195 | 0.05 | 1.20 | 0.52 | 0.02 | 0.03 | 0.08 | 17.9 | 2.6 | 0.05 | 31 | 32 | 204 | 0.93 | 5 | 38 | 8 | 193 | 27 | 65 | 9 | 7 |
| 0102-198 | 0.04 | 1.07 | 0.47 | 0.01 | 0.02 | 0.07 | 17.3 | 2.4 | 0.06 | 28 | 29 | 185 | 0.81 | 4 | 34 | 5 | 179 | 26 | 61 | 8 | 7 |
| 0102-201 | 0.04 | 0.98 | 0.46 | 0.01 | 0.02 | 0.07 | 16.7 | 2.4 | 0.06 | 29 | 31 | 190 | 0.83 | 4 | 32 | 5 | 168 | 24 | 67 | 8 | 7 |
| 0102-204 | 0.04 | 1.09 | 0.52 | 0.01 | 0.02 | 0.08 | 15.9 | 2.6 | 0.06 | 31 | 32 | 195 | 0.90 | 5 | 35 | 7 | 173 | 26 | 60 | 8 | 7 |
| 0102-206 | 0.04 | 1.02 | 0.46 | 0.01 | 0.02 | 0.06 | 15.8 | 2.4 | 0.06 | 27 | 29 | 182 | 0.79 | 4 | 32 | 5 | 171 | 24 | 61 | 8 | 7 |
| 0102-213 I | 0.12 | 1.42 | 0.39 | 0.01 | 0.04 | 0.06 | 15.9 | 2.1 | 0.05 | 25 | 31 | 177 | 0.68 | 4 | 31 | 4 | 258 | 21 | 59 | 7 | 7 |
| 0102-214 I | 0.06 | 1.38 | 0.37 | 0.01 | 0.04 | 0.05 | 16.1 | 2.1 | 0.05 | 27 | 31 | 200 | 0.74 | 4 | 39 | 4 | 242 | 22 | 59 | 8 | 6 |
| 0102-215 I | 0.09 | 1.56 | 0.44 | 0.01 | 0.04 | 0.07 | 18.9 | 2.5 | 0.06 | 28 | 32 | 218 | 0.80 | 6 | 71 | 4 | 270 | 19 | 63 | 9 | 6 |
| 0102-216 I | 0.05 | 1.52 | 0.45 | 0.01 | 0.05 | 0.07 | 17.8 | 2.2 | 0.05 | 26 | 43 | 164 | 0.68 | 3 | 31 | 2 | 280 | 15 | 62 | 8 | 7 |
| 0102-217 I | 0.06 | 1.41 | 0.44 | 0.01 | 0.03 | 0.07 | 16.5 | 2.4 | 0.05 | 26 | 33 | 192 | 0.76 | 4 | 30 | 4 | 237 | 11 | 61 | 8 | 6 |
| 0102-227 I | 0.05 | 1.72 | 0.55 | 0.01 | 0.03 | 0.08 | 18.7 | 2.9 | 0.05 | 31 | 47 | 264 | 0.98 | 6 | 73 | 6 | 311 | 18 | 101 | 9 | 7 |
| 0102-232 I | 0.03 | 1.27 | 0.65 | 0.02 | 0.03 | 0.11 | 16.6 | 3.1 | 0.07 | 40 | 39 | 234 | 1.17 | 7 | 63 | 10 | 203 | 31 | 74 | 11 | 7 |
| 0102-235 I | 0.04 | 1.33 | 0.51 | 0.02 | 0.03 | 0.07 | 16.8 | 2.6 | 0.06 | 34 | 33 | 221 | 0.98 | 5 | 37 | 7 | 209 | 28 | 76 | 9 | 8 |
| 0102-237 I | 0.05 | 1.35 | 0.63 | 0.02 | 0.03 | 0.09 | 17.2 | 3.2 | 0.07 | 39 | 40 | 256 | 1.15 | 6 | 44 | 10 | 214 | 33 | 113 | 11 | 8 |
| 0102-239 I | 0.05 | 1.24 | 0.53 | 0.02 | 0.18 | 0.08 | 19.1 | 2.7 | 0.07 | 37 | 38 | 222 | 1.00 | 5 | 34 | 6 | 342 | 28 | 97 | 10 | 8 |
| 0102-240 I | 0.05 | 1.37 | 0.54 | 0.02 | 0.04 | 0.08 | 16.1 | 2.9 | 0.07 | 38 | 36 | 230 | 1.04 | 8 | 120 | 7 | 210 | 30 | 59 | 10 | 6 |
| 0102-245 I | 0.03 | 1.16 | 0.50 | 0.01 | 0.03 | 0.07 | 17.1 | 2.6 | 0.07 | 32 | 33 | 206 | 0.90 | 4 | 33 | 6 | 198 | 28 | 84 | 9 | 6 |
| 0102-246 I | 0.03 | 1.25 | 0.55 | 0.02 | 0.03 | 0.08 | 16.8 | 2.7 | 0.05 | 35 | 34 | 232 | 1.00 | 6 | 65 | 8 | 205 | 29 | 184 | 8 | 7 |
| 0102-255 I | 0.04 | 0.96 | 0.45 | 0.01 | 0.03 | 0.07 | 17.8 | 2.2 | 0.05 | 31 | 28 | 190 | 0.78 | 5 | 84 | 4 | 235 | 24 | 112 | 7 | 6 |
| 0102-256 I | 0.05 | 1.09 | 0.49 | 0.01 | 0.05 | 0.07 | 16.8 | 2.5 | 0.07 | 35 | 30 | 206 | 0.84 | 10 | 282 | 7 | 187 | 26 | 89 | 8 | 7 |
| 0102-258 I | 0.04 | 1.06 | 0.48 | 0.01 | 0.12 | 0.07 | 15.7 | 2.4 | 0.06 | 29 | 29 | 193 | 0.80 | 4 | 31 | 5 | 202 | 25 | 98 | 8 | 6 |
| 0103-260 | 0.03 | 0.74 | 0.35 | 0.01 | 0.51 | 0.06 | 24.9 | 1.6 | 0.04 | 21 | 24 | 137 | 0.58 | 4 | 56 | 0.5 | 519 | 17 | 223 | 6 | 8 |
| 0103-261 | 0.03 | 0.97 | 0.43 | 0.01 | 0.12 | 0.06 | 22.8 | 2.2 | 0.06 | 26 | 28 | 184 | 0.75 | 4 | 31 | 3 | 271 | 21 | 118 | 8 | 7 |
| 0201-8 | 0.04 | 1.64 | 0.50 | 0.01 | 0.04 | 0.06 | 17.1 | 2.4 | 0.06 | 30 | 40 | 187 | 0.78 | 4 | 66 | 3 | 315 | 24 | 178 | 8 | 8 |
| 0201-78 | 0.03 | 1.02 | 0.46 | 0.01 | 0.02 | 0.06 | 14.4 | 2.4 | 0.06 | 27 | 28 | 188 | 0.77 | 10 | 195 | 6 | 152 | 25 | 62 | 8 | 6 |
| 0201-81 | 0.03 | 1.22 | 0.64 | 0.01 | 0.02 | 0.10 | 17.0 | 3.0 | 0.07 | 38 | 39 | 236 | 1.10 | 6 | 41 | 10 | 196 | 32 | 86 | 10 | 7 |
| 0201-84 | 0.03 | 1.17 | 0.53 | 0.01 | 0.02 | 0.07 | 15.5 | 2.6 | 0.06 | 32 | 35 | 206 | 0.95 | 7 | 105 | 9 | 180 | 28 | 73 | 8 | 7 |
| 0201-86 | 0.02 | 0.97 | 0.44 | 0.01 | 0.02 | 0.06 | 14.5 | 2.1 | 0.04 | 25 | 27 | 173 | 0.74 | 5 | 57 | 5 | 149 | 24 | 81 | 6 | 5 |
| 0201-88 | 0.07 | 1.00 | 0.44 | 0.01 | 0.02 | 0.06 | 14.4 | 2.2 | 0.06 | 28 | 29 | 176 | 0.78 | 4 | 35 | 5 | 156 | 25 | 70 | 8 | 5 |
| 0201-91 | 0.03 | 1.06 | 0.52 | 0.01 | 0.02 | 0.07 | 15.1 | 2.7 | 0.08 | 35 | 36 | 212 | 0.97 | 4 | 39 | 7 | 180 | 29 | 109 | 9 | 7 |
| 0201-93 | 0.04 | 1.09 | 0.57 | 0.01 | 0.03 | 0.09 | 16.7 | 2.7 | 0.06 | 33 | 38 | 218 | 0.92 | 5 | 42 | 7 | 218 | 28 | 95 | 9 | 7 |
| 0201-96 | 0.03 | 1.06 | 0.50 | 0.01 | 0.02 | 0.07 | 14.9 | 2.6 | 0.08 | 32 | 31 | 200 | 0.90 | 5 | 34 | 18 | 164 | 28 | 62 | 9 | 39 |
| 0201-98 | 0.04 | 1.21 | 0.61 | 0.02 | 0.02 | 0.09 | 15.3 | 3.1 | 0.08 | 35 | 37 | 230 | 1.06 | 5 | 42 | 9 | 173 | 32 | 75 | 11 | 7 |
| 0201-100 | 0.04 | 1.12 | 0.54 | 0.01 | 0.02 | 0.08 | 15.0 | 2.8 | 0.07 | 34 | 34 | 210 | 0.97 | 4 | 35 | 7 | 178 | 29 | 73 | 10 | 7 |
| 0201-105 | 0.05 | 1.18 | 0.47 | 0.02 | 0.04 | 0.08 | 19.8 | 2.3 | 0.05 | 26 | 29 | 196 | 0.77 | 4 | 33 | 4 | 237 | 21 | 77 | 8 | 8 |
| 0201-132 | 0.05 | 1.35 | 0.51 | 0.02 | 0.04 | 0.08 | 16.9 | 2.6 | 0.07 | 31 | 36 | 235 | 0.92 | 11 | 239 | 6 | 244 | 23 | 78 | 9 | 6 |
| 0201-137 | 0.04 | 1.23 | 0.43 | 0.01 | 0.03 | 0.06 | 15.5 | 2.5 | 0.08 | 31 | 41 | 230 | 0.87 | 4 | 39 | 4 | 230 | 19 | 66 | 10 | 6 |
| 0201-140 | 0.04 | 1.17 | 0.45 | 0.01 | 0.02 | 0.06 | 14.6 | 2.4 | 0.06 | 25 | 32 | 209 | 0.73 | 4 | 40 | 3 | 196 | 14 | 76 | 8 | 7 |
| 0201-143 | 0.05 | 1.49 | 0.43 | 0.01 | 0.04 | 0.06 | 17.8 | 2.5 | 0.07 | 34 | 35 | 221 | 0.90 | 4 | 39 | 3 | 236 | 15 | 72 | 11 | 6 |
| 0201-372 | 0.05 | 1.23 | 0.38 | 0.01 | 0.03 | 0.06 | 17.9 | 2.0 | 0.05 | 24 | 26 | 170 | 0.63 | 13 | 407 | 1 | 189 | 13 | 73 | 7 | 7 |
| 0201-375 | 0.04 | 1.38 | 0.41 | 0.01 | 0.06 | 0.06 | 17.1 | 2.1 | 0.05 | 28 | 32 | 178 | 0.73 | 6 | 90 | 2 | 212 | 21 | 63 | 7 | 7 |
| 0201-379 | 0.04 | 1.33 | 0.38 | 0.01 | 0.04 | 0.06 | 17.6 | 2.0 | 0.05 | 25 | 26 | 167 | 0.67 | 7 | 146 | 2 | 199 | 21 | 72 | 8 | 6 |

| | | | | | | | | | | | | | | | | | | | | |
|---|---|---|---|---|---|---|---|---|---|---|---|---|---|---|---|---|---|---|---|---|
| 0201-384 | 0.03 | 1.21 | 0.39 | 0.01 | 0.04 | 0.06 | 17.9 | 2.0 | 0.05 | 26 | 27 | 166 | 0.69 | 7 | 137 | 2 | 186 | 20 | 85 | 8 | 7 |
| 0201-389 | 0.03 | 1.05 | 0.32 | 0.01 | 0.03 | 0.05 | 18.3 | 1.6 | 0.03 | 20 | 19 | 124 | 0.49 | 10 | 285 | 0.5 | 172 | 16 | 63 | 6 | 5 |
| 0201-504 | 0.03 | 1.16 | 0.34 | 0.01 | 0.04 | 0.05 | 15.9 | 1.8 | 0.04 | 20 | 22 | 139 | 0.53 | 4 | 69 | 0.5 | 173 | 18 | 61 | 6 | 6 |
| 0201-512 | 0.04 | 1.20 | 0.34 | 0.01 | 0.03 | 0.05 | 15.4 | 1.7 | 0.04 | 19 | 21 | 136 | 0.54 | 4 | 47 | 0.5 | 171 | 17 | 60 | 6 | 6 |
| 0201-522 | 0.04 | 1.26 | 0.37 | 0.01 | 0.03 | 0.06 | 15.3 | 1.8 | 0.04 | 22 | 23 | 137 | 0.57 | 4 | 37 | 0.5 | 194 | 18 | 55 | 6 | 6 |
| 0201-569 | 0.03 | 1.17 | 0.34 | 0.01 | 0.03 | 0.05 | 17.3 | 1.7 | 0.04 | 19 | 20 | 131 | 0.50 | 4 | 65 | 0.5 | 161 | 17 | 64 | 6 | 6 |
| 0201-579 | 0.03 | 1.07 | 0.31 | 0.01 | 0.06 | 0.05 | 16.7 | 1.6 | 0.04 | 18 | 20 | 136 | 0.49 | 6 | 155 | 0.5 | 172 | 16 | 75 | 6 | 6 |
| 0201-589 | 0.06 | 1.27 | 0.32 | 0.01 | 0.04 | 0.05 | 15.9 | 1.6 | 0.03 | 19 | 20 | 126 | 0.49 | 7 | 183 | 0.5 | 294 | 16 | 59 | 5 | 6 |
| 0201-593 | 0.20 | 1.40 | 0.40 | 0.01 | 0.03 | 0.07 | 14.3 | 2.0 | 0.04 | 24 | 28 | 187 | 0.79 | 9 | 255 | 4 | 184 | 21 | 51 | 6 | 6 |
| 0201-597 | 0.02 | 1.09 | 0.29 | 0.01 | 0.02 | 0.05 | 15.2 | 1.4 | 0.03 | 17 | 18 | 118 | 0.43 | 3 | 27 | 0.5 | 189 | 15 | 64 | 5 | 5 |
| 0201-599 | 0.05 | 1.20 | 0.32 | 0.01 | 0.08 | 0.05 | 14.9 | 1.6 | 0.04 | 19 | 20 | 129 | 0.50 | 4 | 63 | 0.5 | 216 | 16 | 55 | 5 | 4 |
| 0201-614 | 0.03 | 1.39 | 0.42 | 0.01 | 0.14 | 0.07 | 16.7 | 2.2 | 0.06 | 30 | 31 | 190 | 0.79 | 8 | 164 | 4 | 422 | 22 | 52 | 8 | 7 |
| 0201-622 | 0.06 | 1.95 | 0.36 | 0.01 | 0.09 | 0.05 | 17.3 | 1.9 | 0.05 | 28 | 28 | 164 | 0.66 | 15 | 856 | 3 | 347 | 20 | 55 | 7 | 6 |
| 0201-688 | 0.08 | 2.75 | 0.38 | 0.01 | 0.08 | 0.05 | 15.8 | 1.8 | 0.04 | 25 | 27 | 280 | 0.68 | 216 | 6752 | 16 | 174 | 19 | 88 | 6 | 1 |
| 0201-789 | 0.03 | 1.16 | 0.45 | 0.01 | 0.03 | 0.07 | 15.8 | 2.3 | 0.05 | 24 | 28 | 188 | 0.71 | 4 | 38 | 4 | 208 | 20 | 62 | 7 | 7 |
| 0201-1133 | 0.04 | 1.28 | 0.39 | 0.01 | 0.04 | 0.06 | 17.1 | 1.8 | 0.04 | 21 | 25 | 142 | 0.59 | 5 | 77 | 0.5 | 187 | 19 | 83 | 6 | 7 |
| 0301-80 | 0.04 | 0.90 | 0.48 | 0.01 | 0.03 | 0.07 | 15.5 | 2.3 | 0.05 | 24 | 26 | 230 | 0.83 | 8 | 110 | 26 | 241 | 7 | 48 | 6 | 15 |

# Brief CV of Ali Al-Kathiri

| | |
|---|---|
| 1st January 1967 | Born in Salalah, Sultanate of Oman |
| 1975 - 1981 | Primary school in Salalah, Oman |
| 1981 - 1984 | Preparatory school in Salalah, Oman |
| 1984 - 1992 | Employed by Raysut Cement Company as a B-shift (3-11 PM) production helper, Salalah, Oman (study leave was granted during my bachelor of Science study period) |
| 1984 - 1987 | Secondary school in Salalah, Oman |
| 1987 - 1992 | Bachelor of Science, Sultan Qaboos University, Muscat, Sultanate of Oman |
| 1993 - 1996 | Geologist at the Ministry of Commerce and Industry, Salalah, Oman |
| 1996 - 1998 | Master of Science, University of Bern, Switzerland |
| 1998 - 2002 | Head of Mineral Exploration Section at the Ministry of Commerce and Industry, Salalah, Oman |
| 1st March 2002 | Start of my PhD work at the University of Bern, Switzerland |